DESIGN AND DEVELOPMENT OF PHASE CHANGE MATERIAL BASED MILKING CUM COOLING PAIL

THESIS SUBMITTED TO THE

ICAR-NATIONAL DAIRY RESEARCH INSTITUTE

(DEEMED UNIVERSITY)

IN PARTIAL FULFILLMENT OF THE REQUIREMENTS

FOR THE AWARD OF THE DEGREE OF

DOCTOR OF PHILOSOPHY

IN

DAIRY ENGINEERING

BY

RAVI PRAKASH

M. TECH. (DAIRY ENGINEERING)

DAIRY ENGINEERING SECTION
SOUTHERN REGIONAL STATION
ICAR-NATIONAL DAIRY RESEARCH INSTITUTE

BENGALURU-560 030, INDIA

2022

Reg. No. 16-P-DE-01

DESIGN AND DEVELOPMENT OF PHASE CHANGE MATERIAL BASED MILKING CUM COOLING PAIL

By

RAVI PRAKASH

Thesis submitted to the

ICAR-NATIONAL DAIRY RESEARCH INSTITUTE

(Deemed University)

In partial fulfillment of the requirements for the award of the degree of

DOCTOR OF PHILOSOPHY

IN

DAIRY ENGINEERING

APPROVED BY

Dr. P. Sudheer Babu
(External Examiner)

Dr. Menon Rekha Ravindra
(Major Advisor)

Members of Advisory Committee

1. **Dr. P. Heartwin Amaladhas**
   (Principal Scientist, Dairy Engineering)
2. **Dr. F. Magdaline E. E.**
   (Principal Scientist, Dairy Engineering)
3. **Dr. Sivaram M.**
   (Principal Scientist, Agri. Statistics)
4. **Dr. S. Jeyakumar**
   (Principal Scientist, VGO)
5. **Dr. K. Jayaraj Rao** (Director's Nominee)
   (Principal Scientist, Dairy Technology)

Dedicated to

The Lotus Feet of My Beloved Spiritual Master

H.H. SUBHAG SWAMI MAHARAJ

&

My Lord

LORD SRI SRI RADHA-KRISHNACHANDRA

SOUTHERN REGIONAL STATION
ICAR-NATIONAL DAIRY RESEARCH INSTITUTE
(DEEMED UNIVERSITY)
(INDIAN COUNCIL OF AGRICULTURAL RESEARCH)
BENGALURU-560 030, KARNATAKA, INDIA

Dr. Menon Rekha Ravindra, Ph.D.
Principal Scientist
Dairy Engineering Section
ICAR-National Dairy Research Institute
Southern Regional Station
Bengaluru-560 030

CERTIFICATE

This is to certify that the thesis entitled, **"DESIGN AND DEVELOPMENT OF PHASE CHANGE MATERIAL BASED MILKING CUM COOLING PAIL"**, submitted by **RAVI PRAKASH** towards the partial fulfillment for the award of the degree of **DOCTOR OF PHILOSOPHY** in **DAIRY ENGINEERING** of the **ICAR-NATIONAL DAIRY RESEARCH INSTITUTE (DEEMED UNIVERSITY), KARNAL (HARYANA), INDIA,** is a bonafide research work carried out by him under my guidance, and no part of the thesis has been submitted for any other degree or diploma.

Menon Rekha Ravindra
Major Advisor

ACKNOWLEDGEMENT

Before opening my heart, I would like to thank ***The Supreme Personality of Godhead "Lord Sri Krishna"*** *who is the dearmost friend, highest benefactor and ultimate beneficiary of each and every activity in this world. Out of His causeless mercy and natural affection for the creatures, He is readily supplying all the necessities without expecting any thanks.*

I do not find suitable words in my memory to express gratitude to my dearest Mother, Srimati Arundhati Devi; Father, Sri. Arvind Kumar Dwivedi; for not only bringing me in this world but also imparting good human values. From the beginning of my humble life, they taught me: how to lead very simple and happy life even in scarcity. Sincere thanks to Sri Ramchandra Dwivedi, my grandfather, now 94, a building block of my spiritual life and purity. With all blessings, I am here.

I wish to endow my sincere thanks to the Hon'ble Dr. A.K. Srivastava, Ex-Director & Vice Chancellor, ICAR-NDRI, Karnal, Dr. M. S. Chauhan, Director & Vice Chancellor, ICAR-NDRI, Karnal, Dr. Dheer Singh, JD(R), ICAR-NDRI, Karnal, Dr. R.R.B. Singh, JD(A), ICAR-NDRI, Karnal, Dr. K.P. Ramesha, Head, SRS of ICAR-NDRI, Bengaluru for providing the required facilities.

I feel, my words are insufficient to thank Dr. Menon Rekha Ravindra: a guide of scientific rigor, mentor, gentle personality and motherly affectionate upon me. Though, I am very small; understand or not; but, yes; I can recall some difficult moments… and, at once get rejuvenated simply by hearing from you. Thank you mam, for accepting me as a student and constantly providing all supports and encouragements throughout my PhD work.

I sincerely thank my Advisory Committee Members Dr. B. Surendra Nath (Ex-Member), Dr. M. Manjunatha (Ex-Member), Dr. P. Heartwin Amaladhas, Dr. M. Sivaram, Dr. K. Jayaraj Rao, Dr. F. Magdaline E.E., Dr. S. Jeyakumar for their cordial treatment, valuable suggestions and practical help throughout my research work. I would like to thank Dr. Mukund A. K. (Incharge, Education and Training) and the supporting staff in the section for helping me tirelessly.

I acknowledge the help and support extended by Late Prof. Sudipto Ghosh (our beloved Sitanath Prabhu), IIT-Kharagpur, in planning the simulation work of this project. I also acknowledge the valuable inputs extended by Prof. Milind V. Rane, IIT-Bombay and Dr. Devaraj, Scientist, DT-Section, SRS, ICAR-NDRI.

Funding also plays crucial role in accomplishing a project's milestones within stipulated timeframe. I would sincerely acknowledge the supports extended by SRISTI and BIRAC under Gandhian Young Technological Innovation (GYTI) Award-Scheme. I also thank DST, Govt. of India for supporting me

under IUSSTF-Lockheed Martin and Tata Trust-IIGP scheme. For fabrication work involved in this project, I sincerely thank the services extended by M/s Gajanan Refrigeration, Pune; M/s Yeshraj Enterprises, Pune and M/s VPE Systems and Solutions, Bengaluru.

I would further like to thank Micro and Nano Characterization Facility-Indian Institute of Science (MNCF-IISc.) and SID-IISc., Bengaluru for facilitating characterizations of nanofluids and phase change materials.

I would like to extend thanks to my batch-mates Dr. B. Manjunatha, Mr. Adarsh M. Kalla, Mrs. Priyanka, for their ready cooperation and help whenever needed. My beloved colleagues and fellows, not able to collect all names but all are in my core of heart, just to call upon few Dr. Rajshekhar, Dr. Preeti, Naveen, Digvijay, Karan, Adarsh, Soumyadeep, Rahul, Prateek, Pramod, Partha, Saurabh, Rupesh, Gajanan, Amarik, Rajesh, Banashree and just to add many…I miss you all; pray for your all good.

It gives me immense pleasure to thank Dr. P.K. Dixit, Principal Scientist, DEM Section, Dr. Chitranayak sinha, Senior Scientist, Dairy Engineering Section, Dr. B.C. Ghosh, Ex-Head, Dairy Technology Section, Dr. Satish Kumar M.H., Scientist, Dairy Technology, Dr. Laxman Naik, Scientist, Dairy Chemistry and all the scientists of SRS of ICAR-NDRI for their kind support and co-operation.

I take this opportunity to thank all the technical and supporting staff of the Institute for their generous support, encouragement and affection, showered onto me.

I thank all the seen and unseen hands in my life for their love, compassion, support and contributions.

I would like to thank all the members of Bhaktivedanta Institute, Bengaluru, particularly HG Paramkaruna Prabhu for providing spiritual supports and platforms to serve the Divine.

Finally I bow down myself onto the lotus feet of my most worshipable Lord Jagannath (The Lord of the Universe) and beg for his mercy to use my limited capabilities in His Divine services.

RAVI PRAKASH

Reg. No. 16-P-DE-01

ABSTRACT

It is essential to immediately chill fresh raw milk from its milking temperature (37°C) to below the critical point (10°C) to preserve its safety and quality as well as derived products. In developed and large-scale commercial dairy enterprise, this critical step in post-harvest processing of milk is achieved by integrating the milking machine with chilling unit accessorized with suitable piping and storage tanks. However, in a country like India where most of the dairy farmers belong to a class of millions of scattered small scale producers (0.5-10L per head), such sophistication remain impractical and uneconomical at the field level. Hence, this project was aimed at addressing the issue by developing a nano-particle enhanced phase change material (NePCM) based milking cum cooling pail, so that cooling as well as milking can be achieved simultaneously, even if the farmer has only one animal. NePCMs were developed by dispersing nano-particles (TiO_2, CeO_2 and Si_3N_4) into different base-fluids viz., distilled water (DW), distilled water+propylene glycol (DW+PG), distilled water+ethylene glycol (DW+EG) and distilled water+silver nano-ionic solution (DW+AgNP) @ 0.00, 0.05, 0.25, 0.50, 0.75 and 1.00%. The NePCMs were characterized for thermal, nano-structural and milk cooling behaviour in the milking pail. Prior to fabrication, the charging and discharging of NePCMs into the pail were simulated in ANSYS-fluent-19 software. Finally, a milking pail made of SS-304 assimilating the developed NePCM was fabricated and coupled with a matching capacity charger to pre-store the thermal energy prior to milking. The units were tested in lab as well as at farm (LRC of SRS, ICAR-NDRI, Bengaluru). The maximum enhancement of 'thermal conductivity (k)' of NePCM was observed using TiO_2 nanoparticles at 1.00% weight fraction, between 30-40°C, in DW+AgNP base fluid. Milk cooling as well as discharging of NePCM were influenced by nanoparticle concentration and agitator speed. The total energy exchange time for milk cooling was accelerated by 8.00, 18.67, 25.33 and 30.67%, respectively at 30, 50, 70 and 100 rpm, as compared to control (0 rpm) at 1.00% of TiO_2 nanoparticles in NePCM. Experimental validations of the simulated results indicated a close agreement confirming the robustness of the simulation. Thus, a milking cum cooling pail based on developed PCM was successfully designed, fabricated and tested to cool milk from 37 to below 10°C in 30-40 min. The PCM in the developed pail maintained the chilled temperature of the raw milk for at least 4h when exposed to an environmental temperature of 40°C. The PCM formulated with enhanced thermal performances assimilated into the pail efficiently cooled fresh raw milk from the point of production to below the critical temperature, which could help preserve the quality of the raw milk in the primary tier of the supply chain.

सारांश

कच्चे दूध तथा इसके द्वारा बने उत्पादों की गुणवत्ता व सुरक्षा के लिए, दूध को उत्पादन के तुरंत बाद ३७ डिग्री सेंटीग्रेड से क्रांतिक ताप १० डिग्री सेंटीग्रेड तापमान तक ठंडा किया जाना चाहिये। विकसित व बड़े डेरी उद्योगों में यह क्रांतिक कदम मिल्किंग मशीन के साथ उपयुक्त पाइप व भण्डारण टैंकों के उपयोग द्वारा सम्पादित किया जाता है। जबकि, भारत जैसे एक विकासशील देश में, जहाँ लाखों किसान मुख्यतः छोटे व सीमांत श्रेणी के हैं, जिनकी दूध उत्पादन क्षमता आधा से कुछ १० लीटर तक है, वहां ये यांत्रिक चिलर न तो उपयुक्त हो पाते हैं ना ही लाभप्रद। अतः, इन समस्याओं को ध्यान में रखते हुए, यह परियोजना, जो नैनोपार्टिकल संवर्धित फेज चेंज मटेरिअल पर आधारित, दुहने के साथ ठंडा करने वाले एक ऐसी पात्र के निर्माण पर केंद्रित है, जिसका उपयोग सभी किसान कर सकते है, यहाँ तक कि जिनके पास एक भी जानवर है। इस संवर्धित मटेरिअल का निर्माण टाइटेनियम डाई ऑक्साइड, सेरियम ऑक्साइड व सिलिकॉन नाइट्राइड नैनोपार्टिकल्स, जिन्हें अलग–अलग आधारी–द्रवों जैसे–आसुत जल, आसुत जल+प्रोपाइलिन ग्लाइकोल, आसुत जल+ईथीलीन ग्लाइकोल, व आसुत जल+चांदी के नैनो–आयनिक घोलों में ०.००, ०.०५, ०.२५, ०.५०, ०.७५, १.०० प्रतिशत की दर से डाला गया। इस मटेरिअल की उष्मीय, नैनो–संरचनात्मक, व विकाश किये गए पात्र में दुग्ध शीतलन सम्बंधित क्षमता व गुणों का अध्ययन किया गया। इस पात्र के निर्माण से पहले, एनसीस–फ्लूएंट–१६ सॉफ्टवेयर में इसके चार्जिंग व ऊर्जा डिस्चार्जिंग को सिमुलेट कर प्रायोगिक आकङो से मिलान किया गया। इस प्रकार, स्टेनलेस स्टील से बना एक दूध ठंडा करने का पात्र बनकर तैयार हुआ, जिसमें उष्मीय ऊर्जा का भण्डारण दूध दुहने से पहले किया जा सकता है। यह पात्र एक समायोजित चार्जर से भी युक्त था। विकसित इकाईओं की जाँच प्रयोगशाला व फार्म (एल आर सी, एस आर एस, राष्ट्रीय डेरी अनुसन्धान संस्थान, बेंगलुरु) में किया गया। उष्मीय चालकता में सबसे अधिक बढ़ोतरी टाइटेनियम डाई ऑक्साइड के १.00 प्रतिशत भार फ्रैक्शन के साथ आसुत जल+चांदी के नैनो–आयनिक घोलों में ३० से ४० डिग्री तापमान के बीच पाया गया। दूध शीतलन व उष्मीय ऊर्जा का डिस्चार्ज नैनोपार्टिकल्स के सांद्रण व मिस्रक के वेग पर आधारित था। ऊर्जा स्थानांतरण का समय ८.००, १८.६७, २५.३३ तथा ३०.६७ प्रतिशत, ३०, ५०, ७० व १०० आरपीएम पर कंट्रोल (0 आरपीएम) की तुलना में १.00 प्रतिशत टाइटेनियम डाई ऑक्साइड नैनोपार्टिकल के साथ पाया गया। प्रायोगिक व अनुमानित आकङो की तुलना से यह पता चला कि सिमुलेशन मॉडल काफी पुष्ट थे। इस प्रकार दुहने के साथ ठंडा करने वाला पात्र की संरचना, निर्माण व परीक्षण संपन्न हुआ जो दूध को ३७ डिग्री सेन्ट्रीग्रेड से १० डिग्री से नीचे ३०–४० मिनट में ठंडा कर सकता है। फेज चेंज मटेरियल इस प्रकार ठन्डे दूध के तापमान को कम से कम ४ घंटे तक पात्र में रख सकता है, जब वातावरण का तापमान लगभग ४० डिग्री सेल्सियस था। अतः विकसित मटेरियल कच्चे दूध को क्रांतिक ताप से नीचे इस पात्र में दूध उत्पादन विंदु से ही ठंडा करने में समर्थ है, जो ग्रामीण शीतलन प्रणाली को सुदृढ़ करने में सहायक सिद्ध हो सकता है।

CONTENTS

LIST OF TABLES

LIST OF FIGURES

LIST OF ABBREVIATIONS

Al_2O_3	Aluminium Oxide
BMCs	Bulk Milk Chillers
CeO_2	Cerium di-Oxide
cfu	Colony Forming Unit
CNTs	Carbon Nanotubes
C_p	Specific Heat Capacity
CTAB	Cetyl Trimethyl Ammonium Bromide
CuO	Copper Oxide
DCS	Dairy Cooperative Society
deg	Degree
dia	Diameter
DLS	Dynamic Light Scattering
DSC	Differential Scanning Calorimeter
DW	Distilled water
EDS	Energy Dispersive Spectroscopy
EG	Ethylene Glycol
FAO	Food and Agricultural Organization
Fig.	Figure
FSSAI	Food Safety and Standards Authority of India
g	Gram
h	Hour
IDF	International Dairy Federation
IS	Indian standards
J	Joules
k	Thermal conductivity
K	Kelvin temperature
kV	Kilovolt
L	Litre

LA	Lactic acid
mA	milliampere
MA	Milk agar
MBRT	Methylene Blue Dye Reduction Time
MCC	Milk Chilling Centre
MDSC	Modulated Differential Scanning Calorimeter
mg	Milligram
min	Minute
mL	Milliliter
MT	Million tonnes
mV	Millivolt
N	Normality
NaOH	Sodium Hydroxide
NDDB	National Dairy Development Board
nm	Nanometer
PCMs	Phase change materials
PG	Propylene Glycol
SEM	Scanning Electron Microscope
Si_3N_4	Silicon Nitride
SS	Stainless Steel
TA	Titratable Acidity
TBC	Total Bacterial Count
TEM	Transmission Electron Microscopy
TIG	Tungsten Inert Gas
TiO_2	Titanium Oxide
vol.	Volume
w/v	weight per volume
wt.	Weight
XRD	X-ray diffractometer
ζ	Zeta potential
ρ_m	Density of milk

%	Percent
°C	degree Celsius
µm	Micrometer

CHAPTER-1
INTRODUCTION

Milk is complete, first and foremost food for all mammalian offspring just after their humble ingress into the creation. For milk being equally important for all age groups, humans invented numerous ways and means of rearing, domesticating and caring animals which included cows, buffaloes, sheep, goats, camels etc. Indian ancient Vedic text also witness dairying as an integral element of agriculture and a foremost source of livelihood of millions of farmers since the olden era. For its value addition and prolong use, various preservation techniques were also devised in due course of traditional breakthroughs which included heating, cooling, boiling followed by cooling, concentration by slow heat, desiccation etc. Out of these techniques, milk cooling immediately after milking is one of the widespread and well-established scientific method for maintaining the quality of fresh raw milk with negligible change in physico-chemical characteristics.

Milk at its drawing temperature (37°C) serves as ideal substrate for microbial growth and chemical deterioration. Such deteriorative reactions follow first order kinetics, in which rate of reaction depends directly on total microbial count at a particular instant, which increases logarithmically above the critical temperature (10°C). Therefore, it is imperative to immediately cool milk from 37°C to below 10°C in order to preserve the safety and quality of fresh raw milk and thereby, its derived products. In developed and large-scale commercial dairy enterprises, this critical step to bring down temperature below the limit in post-production processing of milk is achieved by integrating the milking machine with chilling unit accessorized with suitable piping and storage tanks. However, in a country like India, where most of the dairy farmers belongs to a class of millions of scattered small scale producers (0.5-10L per head; ≈ 17 million registered dairy farmers across 1,90,516 dairy cooperative societies in India (NDDB, 2019-20)), such sophistications remained impractical and uneconomical at the field level. It is to be emphasized that it is the major contribution of these small to marginal dairy farmers (70-80%) whose pooled efforts brought India to achieve its status as the world leading producer of milk (198.4 MT; NDDB, 2020).

Presently, the individual farmers pool their milk at a village or society level wherein it is cooled using chilling units or bulk milk coolers. Such interventions are useful for larger volumes of milk (minimum of 500L) and takes at least 3-4h to cool the raw milk below critical limit. The dairy industry faces huge loss in terms of product quality and almost 3% of total milk pooled at various dairies across the country wasted annually (IBEF, 2019), particularly due to poor cold-chain facilities and larger time gap (practically 5-6h) between the point of production and cooling of milk below critical limit. Over the years, several approaches and cooling systems viz., hydro-vac cooler, surface cooler, sprinkler cooler, tub cooler, mechanical cooler, ice bank coolers, bulk milk coolers, refrigerated tank cooling, cooling rings, ice cones, instant chillers, churn cooling, direct expansion cooling and rural-air-cum-milk-can-cooler have been developed to cool and/or chill fresh raw milk, but they are not very practical and economical for small and scattered production of milk.

Therefore, a need to develop a system/device that could instantly cool small volumes of milk at the on-farm level, preferably simultaneous to the milking process, was realized. This work was aimed at addressing the issue by developing a phase change material (PCM) based milking cum cooling pail to be used at the farm level/by an individual farmer to cool milk from its drawing temperature to below 10°C immediately after milking. Considering the gap between demand and supply of electricity in rural areas, a suitable PCM with higher cooling energy storage capacity was primarily designed based on thermal characterization and preliminary milk cooling data.

Nano-solid materials viz., nanoparticles (at least one dimension ≤ 100nm) of metal oxides, carbides, nitrides, nanofibers, nanotubes, nanowires, nano-rods and nano-sheet dispersed into the conventional energy storage fluids such as engine and mineral oils, water, glycols and their eutectic mixtures, bio-fuels, slurries and molten salts were reported to possess higher energy storage competencies as compared to traditional PCM (Lundqvist, 2000; Conde 2004; Arias and Lundqvist 2005; Fedele *et al.*, 2012; Cabaliero *et al.*, 2015, Prakash 2016). Therefore, nano-particle and base fluid combinations (referred as 'nanofluids') were selected based on thermal performance as well as cost. The selected nanofluids were used for developing nanoparticle enhanced PCM (NePCM) for rapid cooling of milk. NePCM, thus developed was assimilated into the jacketed walls of the milking pail to facilitate pre-storage of thermal energy by charging and use it during milk cooling. The contemplated and

developed design of the pail consisted of an outer insulated housing, jacketed bucket type pail, filled with the developed NePCM in the jacketed space, accessorized with a detachable charger (a hermetically sealed well-matched refrigeration unit), handle to lift, cover lid and temperature sensors at appropriate places.

This technology was devised to minimize the time gap between milk production and milk cooling below critical limit even if a farmer has only one animal. It is envisaged to have high socio-economic utility by helping large number of small scale dairy farmers in developing countries like India in maintaining and supplying better quality raw milk to dairy plants for preparation of quality and value added market milk as well as dairy products and hence, contributing to the overall economy of dairy farmers, industry and the country as a whole. Under these considerations, the present study was proposed with the following objectives:

1. To evaluate and select suitable phase change material for rapid cooling of milk
2. To design and fabricate a milking cum cooling pail based on selected phase change material
3. To evaluate the performance of the developed pail

CHAPTER-2

REVIEW OF LITERATURE

Over the decades, number of technological breakthroughs have been reported in milk cooling equipment in order to arrive suitable, energy efficient, convenient, cost-effective and reliable devices/systems for dairy industry. For fulfilling the gap between demand and supply of electricity, energy storing materials generally termed as phase change materials (PCM) were developed and reported to be used as "thermal batteries" in variety of applications which included refrigeration, air-conditioning, space, textile, defense, bio-medical, reefer transports, buildings etc. The performance of these thermal batteries were further enhanced by number of techniques such as micro/nano encapsulation, nanoparticle dispersion, confinement, surface-coating, nano-inclusion and so on. Selection or development of a PCM of suitable working temperature range and ensuring its thermal compliance plays a crucial role in arriving desired cooled temperature of the commodity being stored. Thereafter, assimilation of a selected/developed PCM in apt and accurate measurement at a suitable place in an energy storage/exchange device determines its efficacy, cost and weight (important for a handy and portable device).

Therefore, focusing on all these considerations and the intended objectives of the present work, this chapter is focused on up to date and closely related published work in the following areas outlined as follows:

2.1 Current pattern of milk production and procurement in India

2.2 Existing on farm milk cooling methods and systems

2.3 Energy storing coolants

2.4 Developments in PCM, their properties and characterization methods

2.5 Existing applications of PCM in cooling

2.6 Numerical simulation of PCM

2.7 Suitable material of construction and insulating materials for fabricating dairy equipment

2.8 Methods of evaluating the performance of a cooling system

2.1 Current pattern of milk production and procurement in India

India is leading milk producer in the world with an annual output of 198.4 MT and annual growth rate around 6.27% (NDDB, 2020). Milk production, collection and procurement pattern followed in villages of a developing country like India is pigeonholed by high fragmentation. This vital and scattered network of the Indian dairy supply chain is dominated (70-80%) by an unorganized sector comprising of millions of small to marginal scale and dispersed rural milk producers contributing 0.5 to tens of litres (L) per day per farmer who possesses one to tens of dairy animals in their premises.

At present, there are around 50 million small to marginal dairy farmers in India, out of which almost 17 million are registered with 1,90,516 Dairy Co-operative Societies (DCS) in India (NDDB, 2019-20). The growth rate depicting total number of DCS in India (Fig.2.1), registered dairy farmers, milk collection via DCS (Fig.2.2) are promising factors worthy for this project.

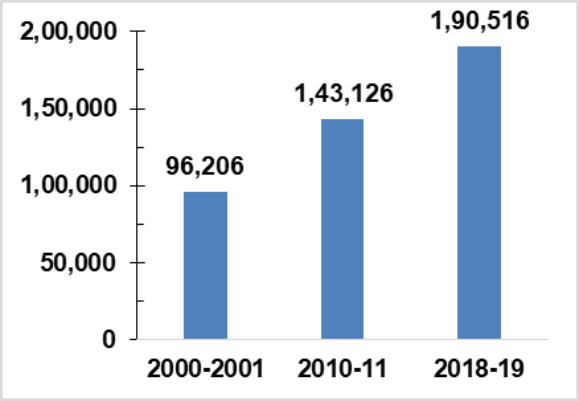

Fig. 2.1 Number of dairy co-operative societies (DCS) in India

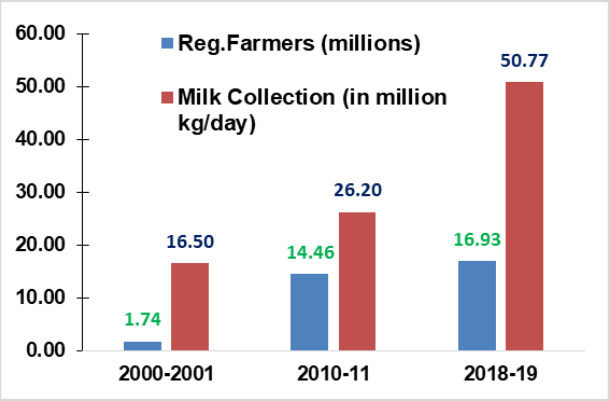

Fig. 2.2 Registered dairy farmers and milk collection

As a general practice, after milking animals into an ordinary container (pail), a dairy farmer transports milk (0.5- few litres) either to DCS at the village level or a milk collection cum chilling centre facilitated in some villages. Top five states in India procuring milk via DCS are presented in Fig. 2.3, which handles 80% of total milk procured in the country (FICCI, 2020). It is usually performed either on foot or by bicycle

or mechanized trollies in some cases to reach collection centres located at DCS. The common transit time between production point and its collection point in villages is normally 1-2h. Milk collection in queue is accomplished in about 1h.

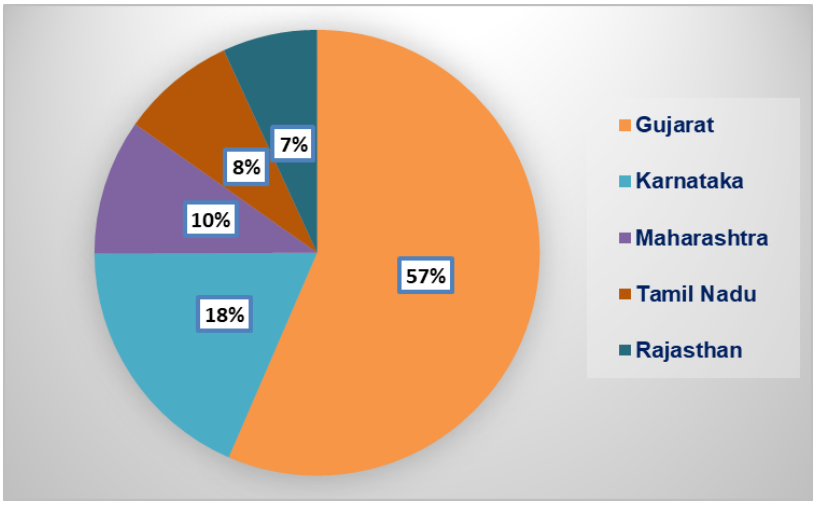

Fig. 2.3 Top five states procuring milk via DCS in India

Thereafter, collected milk is transported either to bulk milk chillers (BMC) for preservation by chilling or to milk chilling centres (MCC) in case the milk processing plant is substantially distant or otherwise it is mostly delivered directly to milk processing plant after filling into cans. Mostly, once milk is collected at DCS, it is transported in 40L cans either to milk chilling centre or directly to milk processing plant at ambient temperature in a normal transit time 1-2h. At any chilling centre/bulk chiller, chilling process is commenced only after a minimum collection of 500L, since bulk chillers are not economical below this capacity. Collection process of this minimum bulk (500L or more) takes normally 1-2h. Milk chilling commenced thereafter takes at least 3-4h (if continuous power back up is facilitated) to chill pooled milk from the ambient (sometimes elevated during summer) to below 10°C.

Therefore, the total transit time from the point of production at individual farmer level to milk chilling below the critical limit approaches around minimum 5-6h in the exiting pattern. These entire practices from the point of production to chilling raw milk below the critical limit of microbial growth and chemical deterioration (below 10°C) are performed almost in ambient conditions which goes up to 40-45°C in summer. The long exposure of raw milk to its field heat sufficiently deteriorates its quality and safety.

Therefore, following pain points were noted from the existing milk production, procurement and collection pattern in a country like India which invoked the idea and rationale behind this project:

a. Occasional milk rejection from dairy companies or paid lower price (on reduced axis, only based on fat) for quality, led to a lower income gained by farmers from dairy business.
b. Reduced quality of raw milk received at milk companies affects quality, safety, shelf-life of the milk products derived out of it, thereby affects net revenue earned by milk processors.

2.2 Existing on farm milk cooling methods and systems

Number of technological and design interventions have been reported in literature on milk cooling systems and equipment; the same are presented below in brief:

Kumar and Dodeja (2005) discussed the refrigerated transport of milk and milk products as well as different milk chilling systems being used at the village level. It was concluded that the vapor absorption refrigeration technology may offer viable option for the dairy industry. In the same study, experimental trials carried out for chilling raw milk at farm level using an intermittent vapor absorption refrigeration system faced problems of water carryover, as well as poor coefficient of performance.

The various methods and systems reported for milk cooling include:

- Hydro-vac cooler
- Surface cooler
- Sprinkler cooler
- Tub cooler
- Mechanical cooler
- Ice bank coolers
- Bulk milk coolers
- Refrigerated tank cooling
- Cooling rings
- Ice cones
- Instant chillers

- Churn cooling
- Direct expansion cooling
- Rural-air-cum-milk-can-cooler

Amongst the earliest reports on milk cooling systems, a report by Gamble (1918) described the cooling in milk cans placed in a wooden tank containing 545.5L of water at 12.2ºC with 45.35kg of ice. It was reported that the time taken to reduce 37.8L of milk from 32.7 to 10ºC was 90 min.

A comparative evaluation of cooling performance of on-farm system (hydro-vac cooler, surface cooler, sprinkler cooler and tub cooler) was reported by Wilster *et al.,* (1934). They reported as a better performance of hydro-vac coolers (15 min) than sprinkler cooler (80 min) and tub cooler (90 min) to reduce raw milk temperature from 32.7 to 14.4ºC. It was also observed that cooled milk using hydro-vac cooler obtained highest sensory scores while lowest bacterial count was reported with surface cooler and higher cream volume was found with tub cooling system.

Various farm level cooling techniques (air cooling, cooling milk with well water, cooling milk with mechanical cooler, ice bank cooling system and dry box coolers) were evaluated at farm level for best cooling practice to meet the legal requirements of United States public health service milk ordinance (Robberts and Larson, 1941) and it was deduced that cooling of milk using ice bank system was the best method among all. But, it was also suggested that to enhance cooling efficiency at farm level, well water with continuous agitation may be applied to reduce the temperature of raw milk from its drawing temperature to 17.7ºC.

Application of refrigerated milk cooling at farm (Jamotte, 1968) using immersion cooler and bulk milk cooler containing tanks integrated with direct expansion or ice-bank refrigeration systems have also been reported.

Must (1969) studied and compared the effect of cooling and handling milk on the farm on its microflora by four cooling methods viz., (i) Refrigerated tank cooling, (ii) Churn cooling, (iii) On-pasteur milking with subsequent refrigerated farm tank cooling and (iv) On-pasteur milking with direct transfer to dairy. Based on microbiological evaluation of nearly 2000 samples, it was recommended that milk with total bacterial counts ranged from 5 lakh to 1 million/mL, would have to be cooled to 8ºC or below; milk with

bacterial count ranged between 1 and 5 million/mL would have to be cooled instantly on the spot.

Vogelauer (1969) reported the use of an immersion cooler, consisting of a hollow cylinder type cooling element, for cooling milk from 35 to 4°C in 400L insulated tank. A major drawback of this system was that it was not suitable for small milk producers.

Vegter *et al.* (1969) also studied an on-farm tank of capacity 1500L with indirect cooling tested using water instead of milk. Four batches of 325L water was cooled from 35°C and the time required for cooling to 4°C was 2.33h after first filling and 3.03h after fourth filling. Two major drawbacks of this system were highlighted, i.e. (i) it was not economical for small quantity of milk and (ii) cooling was not rapid to chill milk below critical limit.

It was also reported that refrigerated tanks on the dairy farms in open as well as in vacuum tanks with automatic agitation and cooling by ice bank or direct expansion were being successfully used on Danish farms. Bulk milk collection was introduced in Denmark in 1960 and 75% of farm milk collected and cooled (Andersen, 1970).

Stenson (1970) developed a cooler for milk cooling, with a coil immersed in water in a cylindrical container which was mounted on the milk can. The milk was filtered, and then passed through the coil into the can; thereby facilitating filtering cum cooling. The system was found to be successful in reducing temperature, however, it faced problems of cleaning and sanitization.

Two Patents granted in U.S. discussed designs of bulk milk coolers. U.S. Patent. No. 4,130,996, issued Dec. 26, 1978 to G. M. Sult, disclosed bulk-milk cooling reservoir with an evaporation unit inside the reservoir and a condenser for recycling water to the evaporation unit to cool milk in a bulk quantity. But this kind of set up was found to be economical with minimum 500L of milk and took minimum of 3h to cool bulk quantity of milk from 37ºC to below 10ºC. U.S. Patent No. 4, 351,271, issued Sep. 28, 1982 to Mueller *et al.*, discloses a refrigerated receiver integrated with an automatic milking system having an improved plate type heat exchanger inside the receiver for pre-cooling the milk. This system was also suitable more for commercialized dairy farms. Moreover, it required skilled manpower and was not very handy to dairy farmers.

Upon reviewing the existing milk cooling methods in terms of their applicability for small to marginal and scattered milk producers, following limitations were deduced (Table 2.1):

Table 2.1 Milk cooling methods/systems and their limitation for small and scattered producers

Features	**Bulk Milk Chiller**	**Milking Machine cum Cooler**	**Milking Station with Cooler Vat**	**Can Immersion Cooler**	**Plate Chiller**
Cooling ≤ 10 °C	✓	✓	✓	×	✓
Rapid Cooling	× 3-4 h	× 2-3 h	× 5-6 h	× 6-8 h	✓ Continuous
Low Volume Milk Chilling	× 500 L	× 100 L	× 100 L	✓ 20-40 L	× 1000 L
Portability	×	×	×	✓	×
Quality Preservation	Medium	Medium	Low	**Poor**	**High**
Suitability	Commercial	Medium, Commercial	Small, Marginal	Small, Marginal	Commercial

Some of the latest interventions happened in the last decade into development of on farm and portable cooling devices includes:

Spoorthy (2010) revealed the development of an air cum milk can cooler wherein the milk was cooled to temperature below the wet bulb temperature of ambient air and the unit was tested for cooling of milk under rural conditions. But, the cooling process was very slow and net drop in temperature were not below the critical/safe limit.

Hegde *et al.* (2014) reported the concept, design and estimated cost of mobile raw milk cooling unit for rural areas, in which milk cans containing raw milk could be cooled during transportation from villages to chilling centers/milk processing plants in a refrigerated van. The method involve cooling cans into a refrigerated space, therefore cooling process was slow. The chilling cost for milk was estimated to be ₹2.25-3.19 per litre, which was reasonably high.

Darshan (2015) designed and developed a stainless steel module containing a eutectic solution as secondary refrigerant to store cooling energy inside the module that could be used in cans or milking pails by immersing the module inside the pool of milk. The module could cool 5L of raw milk from 37ºC to 18-19ºC in about 1h, but not below the critical limit.

Prakash (2016) developed a nanofluid based cooling module to cool raw milk from the point of production (37ºC) to below 10ºC. The developed module evaluated nanofluids, eutectic salt and glycol mixtures as secondary refrigerants to store cooling energy and the stored energy was subsequently used for milk cooling. It was noted that immersing pre-charged modules into milk could raise hygiene related issues in post-harvest handling of fresh raw milk.

Based on the review, it was deduced that rapid cooling of small volumes of milk at the farm level particularly from the production point presents a technical and economic problem.

2.3 Energy storing coolants

Aqueous solutions have been used as single phase (liquid) secondary refrigerants for cooling application in supermarkets, ice rinks, heat recovery systems, heat pumps and other applications. They have also been increasingly used in freezers in supermarkets and other applications in low temperature refrigeration. These solutions are also used in sorption based air conditioning equipment for the dehumidification of air (Lundqvist, 2000; Conde, 2004; Arias and Lundqvist, 2005; Kruse, 2005).

The classical definition for eutectic point was presented by Gunther (1957) as when one or more substances acting as solutes are mixed with one or more solvents in such proportions as to obtain the lowest possible freezing point for the combination, the resulting solution is called as eutectic solution. The lowest possible freezing temperature is called as eutectic point. Also, a reduction in specific heat value of the eutectic solution upon increasing the concentrations of salts. For example, a reduction of about 2.5% in heat transfer value takes place by each 1% increase in $CaCl_2$ concentration.

Melinder (1998) reviewed thermo-physical properties of liquid secondary refrigerants and concluded that indirect systems in supermarkets work well for cooling cabinets and have

an interesting challenge for low temperature freezers. From the cooling cabinet example presented, it can be deduced that salt solutions give turbulent flow, while propylene glycol and ethyl alcohol give laminar flow, resulting in lower heat transfer coefficients and larger temperature differences.

Hillerns (2001) presented an extensive review on thermo-physical properties and corrosion behavior of secondary coolants. It was suggested that traditional brines consisting of potassium carbonate or calcium chloride possess favorable thermo-physical properties, are non-toxic and inexpensive and provide efficient freezing-point depression (29.9% w/w $CaCl_2$ lowers the freezing point to –55°C). However, uncontrollable corrosivity at temperatures below 0°C restricts their application to industrial cooling systems with a relatively simple technical design (no mixing installation, any defrosting cycles possible). It was also presented that despite higher costs and inferior thermal transport properties i.e., a very high viscosity; non-toxic food grade propylene glycol is used exclusively for food cooling applications instead of ethylene glycol, which is classified as “injurious-to-health". Therefore, in this project propylene glycol as one of the base fluid for PCM was selected and results were compared with ethylene glycol.

Granryd and Melinder (2005) reported that the aqueous solutions do not usually freeze to solid ice when ice crystals begin to form and mix with the liquid. Total freezing takes place first only when the temperature drops to the eutectic point of the mixture.

Based on thorough consideration of both thermo-physical properties and other general characteristics such as flow regime and corrosively etc. presented in literature, it was concluded that secondary refrigerants possess limited cooling capacity because of inherently lower energy storage competencies and may not be suitable for extensive refrigeration capacity requirements. Therefore, coolants with better thermo-physical properties and their suitability in food related applications were identified and selected as base fluids for PCM preparation.

2.4 Developments in PCM, their properties and characterization methods

2.4.1 Principle

PCMs are contemporary class of energy storing materials to store heating as well as cooling energy in the form of sensible, structural and latent heat, particularly to use the stored energy when open accessibility of energy-supply is cut off.

The basic steps involved in any thermal energy storage arrangement are: thermal charging, thermal storing (maintaining) and finally thermal discharging (Cabeza *et al.* 2015). It is attained by either chilling, warming, solidification, melting or vaporizing a substance (called charging) when sufficient supply of energy is available, then stockpiled energy is kept on hold for later use (called thermal storing) and thereafter, stored energy is made available by reversing the charging process (called discharging).

Any material holds energy predominantly in four fundamental ways: sensible heat thermal energy storage (SHTS), latent heat thermal energy storage (LHTS), energy stored due to structural changes (transition) and last by chemical energy storage (Hesaraki *et al.* 2015, Pintaldi *et al.* 2015). SHTS, LHTS, chemical and structural energy storage are schematically presented in Fig.2.4.

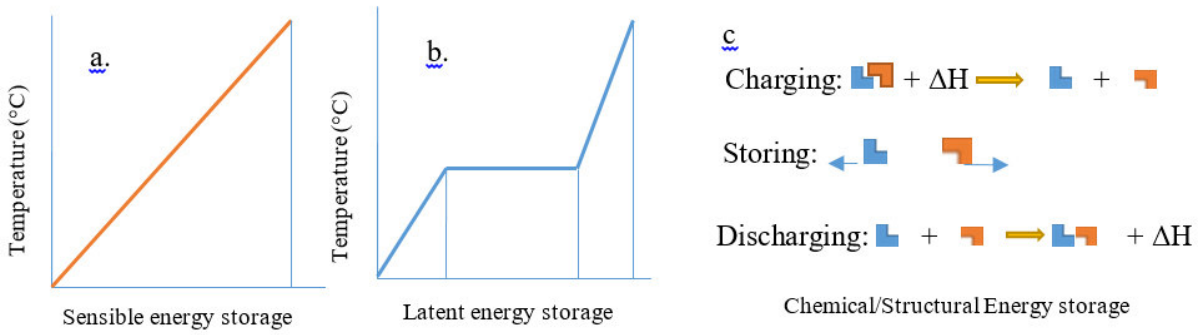

Fig. 2.4 Schematic diagram of (a) sensible energy (b) latent energy (c) chemical energy storage system

In SHTS, the temperature of material storing energy (heating or cooling) either increases or decreases during energy charging/discharging process. The effectiveness of SHTS storage system depends upon mass density, specific heat capacity and temperature difference from initial to final states, which could be achieved by any of the conventional

heat transfer methods such as conduction, convection or radiation and may be represented as:

$$Q=\int_{T_i}^{T_f} mCp\Delta T = mCp_{ave}(T_i-T_f) \quad \ldots(2.1)$$

Where Q: amount of energy being stored (J), T_i: starting temperature (°C), T_f: end temperature (°C), m: unit mass of the energy storing media (kg), Cp: specific heat capacity (J/kg-°C), Cp_{ave}: mean specific heat capacity from T_i to T_f (J/kg-°C).

The practical example of the SHTS in our daily life could be active space heating or cooling, water heating by solar collectors. Water is reported to be the best SHTS media due to its ample availability, low cost and high Cp (Demirbas, 2006). Moreover, working temperature range, melting and freezing characteristics, amount of energy stored per kg of water to cool milk below the critical temperature are also suitable and matching with cooling requirements of milk. Therefore, keeping these considerations into account, water as a base fluid for PCM preparation was selected in this work.

In LHTS, the material stores energy (heating or cooling) isothermally at/nearby melting/solidification or vaporization/condensation temperature, which imparts minimum temperature difference between storage and discharge of energy while reversing the onward process, thereby contributing to lower size and weight to stored energy ratio of energy storage heat exchanger units (El-Dessouky *et al.* 1997).

LHTS is accepted as the most capable method of thermal energy storage, which works on principle of charging (absorbing) and discharging (releasing) of energy by phase-change of a material from solid to solid, solid to liquid, or molten to gas or vice versa, therefore PCM work on the principle which could be numerically represented as:

$$Q=\int_{T_i}^{T_m} mC_{pf}\Delta T_f + mv_0 L_f + \int_{T_m}^{T_f} mC_{pl}\Delta T_l \quad \ldots(2.2)$$

Where Q: amount of energy been stowed (J), T_i: opening temperature of PCM (°C), T_m: melting/solidification temperatures of PCM (°C), m: mass of the energy storing media (PCM) (kg), C_{pf}: specific heat capacity of PCM before melting (J/kg-°C), v_o: volume fraction of PCM melted, L_f: Latent heat per unit mass, T_f: final temperature of PCM (°C),

C_{pl}: specific heat capacity of PCM after complete melting (J/kg-°C), ΔT: temperature difference.

2.4.2 Selection criteria for PCM

Commercial acceptance for a PCM rely on number of factors derived out of various thermo-physical, kinetic and chemical characteristics tabulated below (Table 2.2) as summarized by Khudhair and Farid (2004), and Sharma *et al.* (2009). Moreover, PCMs should be abundantly available at low cost. Practically no PCM or combination of PCMs meet all the requirements discussed below, however, a PCM meeting the requirements closely, is recognized as a better choice than others.

Table 2.2 List of characteristics of a Model PCM

Thermal characteristics	Physical characteristics	Dynamic characteristics	Chemical characteristics
• Temperature of phase-change should be within working/operation limit • higher enthalpies of fusion (latent energy absorbed for unit volume) • specific heat should be higher • thermal conductivity should be higher in both the phases	• a minor volume change during phase-transition • lower vapour pressure at working temperature • good equilibrium between phases before and after melting • sharp melting point of the PCM • higher mass density • lower volume to energy storage ratio	• lower degree of super-cooling • high nucleation rate to facilitate quick solidification • faster rate of crystallization • irreversibility against phase-separation of constituents during solidification and melting cycle	• chemically stable with time • freezing and melting cycle entirely reversible • compatibility with materials of construction • no corrosiveness, no toxicity, no in-flammability, un-explosive, safe

2.4.3 Developments in PCM

2.4.3.1 Salt and salt hydrates based PCM

The properties of common salt hydrate based PCM are listed in table 2.3. The enticing features of salt hydrate based PCM are higher energy storage per unit volume (340-360 MJ/m^3), quite more thermal conductivity (0.45 W/m-K) at low prices as compared to the organic PCMs (Iten and Liu (2014); Tatsidjodoung *et al.* (2013)). But, the widespread acceptability of these PCM faced limitations due to corrosion.

Table 2.3. Common salt hydrate based PCM

PCM	Melting Points (°C)	Latent heats (J/g)	Thermal conductivities (W/m-K)		Density (10^3 kg/m^3, Solid phase)	Ref.
			Solid	*Liquid*		
$KF.4H_2O$	18.4	232	-	-	1.45	Khudhair and Farid, (2004)
$CaCl_2.6H_2O$	28	195	0.541	1.087	1.80	Paris *et al.* (1993)
$CaCl_2.12H_2O$	29.8	174	-	-	-	
$CaBr_2.6H_2O$	35	115.4	-	-	2.18	
$Na_2HPO_4.12H_2O$	40	279.5	0.476	0.514	1.53	
$Zn(NO_3)_2.6H_2O$	36.5	146.7	0.465	-	-	Dincer and Rosen (2002)
$Na_2S_2O_3.5H_2O$	52.5	200	-	-	1.76	Paris *et al.* (1993)
$Na(CH_3COO).3H_2O$	57.5	225	-	-	1.44	Heckenkamp and Baumann (1997)

2.4.3.2 Paraffin based PCM

Paraffins are basically straight chain saturated hydrocarbons (C_nH_{2n+2}, alkane or mixture of alkanes), which store significantly higher thermal energy (128 to 198 kJ/kg) with melting point varying from -12 to 71°C (Peng *et al.* 2004) . The characteristics of paraffin based PCM are listed in Table 2.4.

These are the most common solid–liquid PCM, accepted all-inclusively, since they are non-corrosive, non-toxic, biologically harmless, low sub-cooling, safe, steadfast and economic, less volume expansion upon melting, chemically stable and inert at ≤ 500°C. Few drawbacks of these PCMs are inflammable, non-compatibility with plastics (causes permeations and softening to plastic containers due to chemical similarity and affinity

(e.g. polyolefin)) and relatively lower thermal conductivity (0.20-0.25 W/m-K) as compared to salt hydrates.

Table 2.4. Characteristics of paraffin based PCM

Paraffin	No. of C-atoms in chain	Fusion Point (°C)	Fusion Heat (J/g)	Density (g/cm^3)	Ref
n-Tetradecane ($C_{14}H_{30}$)	14	5.7-6.0	228	-	Nagano *et al.* (2003)
n-Pentadecane ($C_{15}H_{32}$)	15	9.8-10	206	-	He *et al.* (1999)
n-Hexadecane ($C_{16}H_{34}$)	16	19.5-20	231	0.773	Paris *et al.* (1993)
n-Heptadecane ($C_{17}H_{36}$)	17	22.5	165-214	0.777	
n-Oktadecane ($C_{18}H_{38}$)	18	28	200-245	0.776	
n-Nonadecane ($C_{19}H_{40}$)	19	32	222	0.785	
n-Eicozane ($C_{20}H_{42}$)	20	36.5	246	0.788	
n-Pentacozane ($C_{25}H_{52}$)	25	53	238	0.802	
n-Triacontane ($C_{30}H_{62}$)	30	65.5	252	0.775	

2.4.3.3 Fatty acid based PCM

Fatty acid based PCMs are becoming more popular for low temperature energy storing (≤ 15°C) because of appropriate thermal and kinetic characteristics in this temperature range. Moreover, they possess negligible degree of super-cooling, relatively higher phase-transition heat as compared to paraffins and consistent phase-change behavior during subsequent thermal cycles. However, the major shortcomings of these PCM are inflammability, corrosiveness, unpleasant odor, expensive as compared to paraffins, sensitivity towards high temperature and oxidizing agents (Sharma *et al.* 2009). Various features of fatty acid based PCM are listed in Table 2.5.

Table 2.5 Properties of Fatty acid based PCM

Fatty acid based PCMs	No. of C-atoms in chain	Fusion point (°C)	Fusion Heat (J/g)	Ref.
CA ($CH_3(CH_2)_6COOH$)	8	16.3	148	Bailey (1950)
CpA, ($CH_3(CH_2)_8COOH$)	10	31.5	163	Feldman *et al.* (1989)
LA, ($CH_3(CH_2)_{10}COOH$)	12	42	183-212	Sari and Kaygusuz (2002 A)
MA, ($CH_3(CH_2)_{12}COOH$)	14	52.5	190-205	Bailey (1950)
PA, ($CH_3(CH_2)_{14}COOH$)	16	62	204-212	Feldman *et al.* (1989)
SA, ($CH_3(CH_2)_{16}COOH$)	18	70	222	
AA, ($CH_3(CH_2)_{18}COOH$)	20	74	227	Bailey (1950)

CA: Caprylic acid, CpA: Capric acid, LA: Lauric acid, MA: Myristic acid, PA: Palmitic acid, SA: Stearic acid, AA: Arachidic acid

2.4.3.4 Eutectic PCM

Eutectic PCM generally encompass mixture of two or more PCMs in such a proportion that finishing mixture exposes lower melting point as compared to the individual PCMs. The properties of eutectic PCM are listed in Table 2.6.

Table 2.6. Properties of Eutectic PCM

Eutectic PCMs	Proportion	Fusion point (°C)	Fusion Heat (J/g)	Ref
a) *Fatty acid based eutectic PCMs*:				
CpA + LA	45:55	18-20	142	Khudhair and Farid (2004)
CpA + PA	76.5:23.5	21.7	171.1	Sari and Karaipekli (2008)
LA + MA	66:34	34.2	166.8	Keles *et al.* (2005)
LA + PA	69:31	35.1	166.2	Sari (2005)
LA + SA	75.5:24.5	36.9	182.6	Sari and Kaygusuz (2002b)
MA + PA	58:42	42.5	168	Sari (2003)
MA + SA	64:36	44.2	182.2	Sari (2005)
1. *Polyethylene oxide (PEO)+fatty acid blends of PCMs*:				
PEO3400+CpA	50:50	33.5-41	169	Pielichowski and Flejtuch (2003a)
PEO3400+LA	50:50	47.1	188	
PEO10000+CpA	75:25	33.5-43.5	174	Pielichowski and Flejtuch (2003b)
PEO10000+LA	25:75	46.8	195	Flejtuch (2004)
PEO10000+MA	25:75	57.2	190	
PEO10000+PA	75:25	61.5	192	
PEO10000+SA	75:25	63.8	203	Pielichowski and Flejtuch (2005)
2. *Other eutectic PCMs*:				
$CaCl_2$+$MgCl_2.6H_2O$	-	25	95	Ferrer *et al.* (2015); Waqas & Ud-Din Z (2013)
Triethylolethane + Urea	-	29.5	217	
$Ca(NO_3).4H_2O$+$Mg(NO_3)_3.6H_2O$	-	31	135	
$CH_3COONa.3H_2O$+Urea	-	31	201	
$CaCl_2$+NaCl+KCl+H_2O	-	27	188	

2.4.3.5 Nanoparticle enhanced phase change materials (NePCM)

In last two decades, nanofluids composed of dispersed nanoparticles (≤100 nm) in base fluids have evolved as the next generation PCM with a wide spectrum of thermo-physical properties. The attractive features of nanoparticles into base fluids (termed as

'nanofluids') are summarized as follow (Kim *et al.* 2001, Chieruzzi *et al.* 2013, Chew *et al.* 2015):

1. Greater available surface area for heat exchange due to higher surface area to volume ratio (i.e. with minimum volume, high available surface area of heat transfer) of nanoparticles into base fluids and hence enhanced rate of heat transfer in nanofluids. For example, a 1 nm spherical particle has a surface area-to-volume ratio 1000 times greater than that of a 1 μm particle.
2. Reduced degree of super cooling of base fluid because of early nucleation.
3. Reduced freezing and melting time and enhanced energy storage capabilities, thereby less energy consumption during thermal energy storage.
4. High mobility due to light weight, and hence faster Brownian motion and greater rate of micro-convection in liquid phase, thus enhanced heat transport properties.
5. Unlike micro-suspensions, dependency of thermal conductivity enhancement not only on particle concentration but also on particle size. As size of dispersed nanoparticle decreased, rate of thermal conductivity enhancement was found to be increased.

2.4.4 Selection of nanoparticles for PCM

Out of various nanoparticles as dispersing materials, metal oxides are considered to be cheap, abundant and more resistant to chemical reactions. Out of metal oxides, TiO_2 is a universally recognized safe material with least toxicity for humans, chemically stable, resistant to acid, alkali and other solvents, economical and stable in suspension for a prolong duration without any surfactant (Yang and Hu, 2017).

One of the earliest studies on the TiO_2 enhanced PCM carried out by Liu *et al.* (2009), reported a significant improvement in the thermal performance with total reduction in charging and discharging time by 30.3 and 28.2%, respectively, by dispersing 1.00% volume fraction of TiO_2 nanoparticles into saturated aqua-$BaCl_2$ salt blend. In another study, the thermal storage behavior of TiO_2 nanoparticles at 0.05, 0.10, 0.15, 0.20, 0.25, 0.30 weight % assimilated into stearic acid for solar heating elucidated the reduction in melting and freezing time by 7.03, 12.56, 19.59, 28.64, 35.17, 43.72% and 6.62, 13.57, 20.53, 26.82, 34.11, 41.39%; respectively (Harikrishnan *et al.* 2013).

Prakash (2016), reported relatively better thermo-physical characteristics and milk cooling performance by TiO_2 nanoparticles in aqua-glycol base fluids as compared to Al_2O_3 and CuO nanoparticles.

Żyła *et al.* (2018), reported a linear correlation between thermal conductivity and nanoparticle volume fraction with Si_3N_4/ethylene glycol nanofluids. It was found that thermal conductivity of nanofluid was increased with increasing volume fraction of nanoparticles.

CeO_2 nanoparticles were reported noteworthy because of their physicochemical properties, and functionality (Karakoti *et al*. 2012). CeO_2 nanoparticles were recognized for their suitability in catalysts, fuel cells and antioxidants. Basically, Ce exists in multiple oxidation states as Ce^{3+} and Ce^{4+} ions. Therefore in nano range, CeO_2 nano-crystal exhibit a three dimensional fluorite structure in which both ionic phases coexist at the surface. This leads to an apparent electron affinity and oxygen deficit in the crystal network, helps in improving redox characteristics and functionality (Perullini *et al.* 2013, Charbgoo *et al.* 2017). Recently in another study, Keyvani *et al.* (2018), also reported an experimental study on thermal conductivity of CeO_2/ethylene glycol nanofluid, indicated about 22% enhancement in thermal conductivity at 2.5% volume fraction of nanoparticles.

Therefore, in the present work a comparative study was conducted to examine the effects of TiO_2, CeO_2 and Si_3N_4 nanoparticles dispersion into aqua-glycol base fluids on milk cooling performance.

2.4.5 Thermal properties of PCM and characterization methods

2.4.5.1 Specific Heat

Specific heat play decisive role during selection of a PCM for energy storage. It signifies the thermal energy storage competency of a PCM in terms of sensible heat. Moreover, it plays remarkable role in engineering design in calculating dynamic thermal conductivity, convective heat transfer coefficient, Nusselt number and thermal diffusivity. It is also required in energy balance design calculations during estimating the amount of heat transferred in a unit operation. The specific heat of nanofluids depends on the specific heat capacity of nanoparticles and base fluid, the particle volume fraction and

temperature. Specific heat of nanoparticle depends on particle size: with decrease in particle size, specific surface area as well as effective surface energy increases and hence the effective specific heat (Wang *et al.,*2006). The dependency of specific heat on nanoparticle volume concentration was experimentally shown by Zhou *et al.* (2010) and it was validated by following correlations based on law of mixtures:

$$c_{pn} = \frac{(1-\emptyset)(\rho c_p)_f + \emptyset(\rho c_p)_p}{(1-\emptyset)\rho_f + \emptyset\rho_p} \quad \ldots (2.3)$$

$$c_{pn} = \emptyset c_p + (1-\emptyset)c_f \quad \ldots (2.4)$$

Where, c_{pn}: Specific heat of nanofluid, c_p : Specific heat of nanoparticle, c_f : Specific heat of base fluid, Ø: volume fraction of nanoparticles, ρ: density.

It was also reported that specific heat decreased from 2550 to 2450 kJ/kg-K as Ø varied from 0.10 to 0.60%. However, the experimentally measured values of specific heats were greater than the theoretically calculated values using the above relations.

Zhou and Ni (2008) measured specific heat of Al_2O_3/water (45nm) nanofluid with a differential scanning calorimeter (DSC) at 33°C and reported that the specific heat of nanofluid decreased gradually as the nanoparticle Ø increased from 0.00 to 21.70%. In similar line, Zhou *et al.* (2010) studied the specific heat of CuO/ethylene glycol nanofluid at Ø varying from 0.10 to 0.60% at incremental interval of 0.10%. The results indicated that specific heat capacity of CuO nanofluids decreased gradually with increasing Ø of nanoparticles. In another study, Vajjha and Das (2009) measured specific heat of Al_2O_3 (44nm)/60:40 ethylene glycol-water, ZnO (77nm)/60:40 ethylene glycol-water and SiO_2 (20nm)/water from 42-90K up to Ø = 10% and proposed the best fitted equation with experimental data of these nanofluids as follow:

$$c_{pn} = \left[\frac{(A\times T) + \left\{\frac{c_p}{c_f}\right\}}{C+\emptyset}\right] c_f \quad \ldots (2.5)$$

where; A, B, C are constants and their values for nanoparticles as follows:

Al_2O_3 : A = 0.0008911; B = 0.5719; C = 0.4250

SiO_2 : A = 0.001769; B = 1.1937; C = 0.8021

ZnO : A = 0.0004604; B = 0.9855; C = 0.2990

In contrast to the above citations, there are also reports indicating enhancement in specific heat and thermal storage capacity with increase of Ø. For example, Chieruzzi *et al.* (2013) developed different nanofluids with phase change behavior by mixing a molten salt base fluid ($NaNO_3$-KNO_3 (60:40 ratio) binary salt) with nanoparticles (silica (SiO_2), alumina (Al_2O_3), titania (TiO_2) and a mixture of silica-alumina (SiO_2-Al_2O_3)) at three weight fractions 0.50, 1.00, and 1.50 wt.%, using the direct-synthesis method. Specific heat was measured by DSC and the results obtained indicated that the addition of 1.00 *wt. %* of nanoparticles to the base salt increased the specific heat by 15 to 57% in the solid phase and 1 to 22% in the liquid phase. It was concluded that the addition of silica-alumina nanoparticles has a significant potential for enhancing the thermal storage characteristics of the $NaNO_3$-KNO_3 binary salt.

Lu and Huang (2013) reported that the specific heat capacity of the molten salt-based alumina nanofluid decreased with reducing particle size and increasing particle concentration. The nanoparticle size-dependent specific heat resulted from an augmentation of the nanolayer effect as the particle size reduced. They further suggested that the developed fluid could be used for evaluating the application of nanofluids in thermal storage for solar-thermal power plants.

In another study, Shin and Banerjee (2010) measured the specific heat capacity of neat chloride eutectics and their nanofluids obtained by doping with SiO_2 nanoparticles (20-30 nm diameter) at 1.00% weight concentration and reported that the SiO_2 nanofluid enhanced the specific heat capacity by 14.50% compared with that of the chloride salt eutectic. They further explained that this abnormal enhancement in the specific heat capacity contradicts the previous studies reported in the literature but it happened probably due to agglomeration/precipitation of the nanoparticles from the solution.

Chew *et al.* (2015) prepared dodecyl benzene sulfonic acid-doped polyaniline particles (DBSA-PANI)—water based nanofluid by chemical oxidative polymerization of aniline in the presence of dodecyl benzene sulfonic acid (DBSA) as a dopant in which size range of DBSA-PANI nanoparticles were 15 to 50nm. They measured the specific heat capacity of the nanofluids by DSC and reported that the specific heat capacity of water-based nanofluids decreased with increasing amount of DBSA-PANI nanoparticles. They further explained that reduction in specific heat was due to solid–liquid interface formed between DBSA-doped PANI nanoparticles and water molecules which could change the specific

heat capacity of water by establishing hydrogen bonding between doped DBSA and water. Hence, less thermal energy was stored when more DBSA-doped PANI nanoparticles dispersed in water.

2.4.5.2 Latent Heat

Latent heat storage in a PCM is one of the most efficient ways of storing thermal energy as discussed earlier. Wu *et al.* (2010) tested the potential of aqueous Al_2O_3 nanofluids as a PCM for cooling systems. The thermal response test indicated that the addition of Al_2O_3 nanoparticles considerably decreased the super cooling degree of water, advanced the onset of freezing time and reduced the total freezing time. At only 0.20% of Al_2O_3 nanoparticles, the total freezing time of nanofluids was reduced by 20.50%.

Liu *et al.* (2015) prepared NePCM using graphene oxide nanosheets in de-ionized water, and reported the reduction in super cooling degree by 69.10%, thereby facilitating early onset of nucleation and reducing the total freezing time by 90.70%. But, usually these nanoparticles are very costly and may not be affordable for milk cooling devices.

2.5 Existing applications of PCM in cooling

Energy stored by a PCM may be used for domestic and industrial heating/cooling applications. In upkeep of the discussed methods of energy storage by PCM, a study related to the performance evaluation of encapsulated salt-hydrates for latent heat storage in a household hot water vat was reported, in which a significant reduction in time required to solidify the small capsules of sphere confining PCM was observed (Barba and Spiga, 2003).

Lu *et al.* (2010) engineered a refrigerated cabinet ledge assimilated with a PCM to cool stored foods during thawing and informed the improved uniformity in temperature distribution. Application of PCM in food transportation was also reported by Johnston *et al.* (2008), who used a nano-calcium silicate infused composite paraffin PCM to supply sufficient thermal shielding for paper-board based packages used during the shipping and storing of chilled perishables. It was recognized that the PCM assimilated could retain the inside temperature at about 10°C/5h while ambient surrounding temperature was 23°C.

For dairy products, Leducq *et al.* (2015) comparatively studied the effect of PCM based packaging for ice-cream storage and during its transportation inside the polystyrene materials. It was found that the PCM based packaging upgraded the efficiency of refrigeration system and up kept better temperature control as compared to the insulated packaging during storage as well as transportations. Other advances in this area were a PCM based package for commercial ice-cream vessels reported by Oró *et al.* (2012), which showed better thermal performance over insulated packages during ambient storage as well as intermittent cycle of the compressor, door opening and power cut. A refrigeration cabinet based on PCM for storing ice-cold foods (0–5°C) tested by Lu and Tassou (2013), reported the significant reduction in the degree of super-cooling by addition of nucleating agents.

Commercially, PCM based containers are also reported for temperature sensitive foods. Generally, these containers are placed in either refrigerator or deep freezer for charging of PCM before being used. For example: SOFRIGRAM commercialized such containers having PCMs of melting temperatures 0, -15 and -20°C. The variety of such containers varied from rigid to soft. PCM pads for any common container of suitable size and shape were commercialized by TCP RELIABLE, Inc., PCM Thermal Solutions; PCM Products. For catering applications, PCM based containers were applied to maintain cold chain during carriage of pre-cooked foods, smoked salmon, milk derivatives, ice-creams and many others. The leading enterprises that commercialized these products are Rubitherm, Climator and Teap PCM.

NePCM have been studied for its suitability in chillers (as rapid coolant to enhance COP up to 5.15%), domestic as well as industrial refrigeration and air conditioning systems (Saidur *et al.,* 2011; Jiang *et al.* 2009) reported on the higher thermal conductivity of CNTs nano-refrigerants as compared to that of CNTs–water nanofluids or spherical nanoparticle-R113 nano-refrigerants. It was also suggested that the reduced diameter and greater aspect ratio of CNTs may further enhance the thermal conductivity of CNTs-nano-refrigerant. In order to compare the refrigerator performance by energy ingestion and freezer capacity tests, Bi *et al.* (2008) studied the HFC134a and mineral oil with and without TiO_2 and Al_2O_3 nanoparticles and reported improved performance with both nano-refrigerants (it was less in case of Al_2O_3 as compare to TiO_2) and 26.1% energy

saving when used with Ø = 0.1% of TiO_2 nanoparticles. The normal and safe working of these nano-refrigerants was also recommended in this study.

2.6 Numerical simulation of PCM

Numerical modelling and simulation is basically a mathematical exemplification and subsequent computation of a physical phenomenon or conduct of a system based on governing equations (generally Navier–Stokes equations), appropriate hypothesis and binding assumptions. In case of PCM, generally charging (solidification) and discharging (melting) behavior is modelled for a particular application within a suitable geometry such as spherical, cylindrical, rectangular, annular or any other simple to intricate geometry of interest. A typical simulation of phase-change phenomena may be modelled as reported by Prakash *et al.* (2021), as follows:

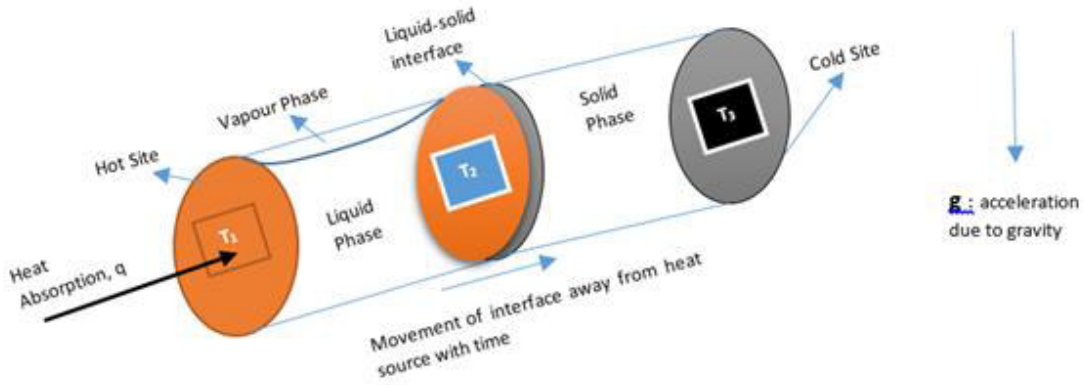

Fig. 2.5 Schematic diagram of melting of a PCM in an arbitrary container

Fig. 2.5 depicts an arbitrary container with all adiabatic boundaries (expect heat absorption site, which supplies a constant heat flux (q) for isothermal heating (melting) of PCM) containing PCM initially (at time, t = 0) in solid phase at temperature T_3. Upon heat exchange, PCM begins to melt at a point adjacent to hot site at temperature T_2 (melting point) and a solid-liquid interface (at T_2) between two phases built up, which migrates away from the heat source as time progresses resulting increase of liquid phase and diminishing of solid phase. Therefore, the temperature of liquid phase at any instant (t = t') varies from T_1 to T_2 whereas that of solid phase varies from T_2 to T_3. With time, the amount of liquid phase increases (with round about vapor phase) which dominates the convective heat exchange over conductive in the system driven by buoyancy and gravity forces.

The liquid fraction (β) of PCM remains zero (entirely solid) initially (at t = 0), varies from 0 to 1 at any instant (t = t') and finally reaches 1 at the end of melting (entirely liquid). In case of charging (solidification) in the same arbitrary container the entire process is reversed. Therefore, the transient solidification/melting of PCM convoyed by buoyancy and gravity driven convection heat transfer is governed by a dimensionless relation (called *Rayleigh number*) which qualified significance of the buoyancy force with the diffusion force in convection.

$$\text{Ra (Rayleigh number)} = \frac{g\beta(T_1-T_3)l^3}{\alpha\, v} \qquad \ldots(2.6)$$

Where *l*: length of diffusion zone (liquid zone), *α*: thermal diffusivity, *v*: kinematic viscosity

Another important dimensionless relation for PCMs simulation is *Stefan number*, which is quotient of sensible heat ($c_p\,\Delta T$) to latent heat (L_f).

$$S_{te} = \frac{c_p \Delta T}{L_f} \qquad \ldots(2.7)$$

Where $\Delta T = T_1 - T_3$; for constant temperature heating,

$= \frac{ql}{k}$; for constant flux heating,

k=thermal conductivity of PCM

As T_1 (heat source temperature) increases, the value of *Stefan number* also increases which results into quick melting of PCMs during discharge.

One of the earliest reports on the melting of a free solid enclosed inside a sphere influenced by sub-cooling by Roy and Sengupta (1989), showed a numerical solution of temperature ramp surrounded by a solid by an altered heat transfer mechanism solving the transient heat conduction equation at every time step by means of a toroidal coordinate comprising a seemly halt of the migrating boundary to transmute the infinite domain into a finite one. In continuation another study was reported by Roy and Sengupta (1990), in which the outcomes of the natural convection on gravity-assisted melting was further explored, which indicated the melting time and heat transfer coefficient varied directly with the physical and thermal properties of the PCM.

The phase-transition of PCM were modelled in various types of enclosures such as sphere, cylinder, square cavity and so on. A constrained and uncontained melting of n-octadecane PCM restrained on the vertical thermocouples inside a sphere were reported

by Tan (2008), which indicated that the temperature profile of the melting PCM recorded over the various vertical points centrally located inside the capsule were different from top to bottom.

Wang *et al.* (2021), studied the heat transfer performances and phase change behaviors of different shapes (spherical, cylindrical (short and long), pyramidal, tetrahedral, and a biomimetic red blood cell shape) of capsules having same volumes of tetra-n-butylammonium bromide as PCM. It was reported that freezing and melting times were function of surface area to volume ratios as well as the distance from centroid to the inner surface of the capsule confining PCM. The red blood cell shape (biconcave discoid) capsule performed most favorably and produced the most rapid freezing and melting process.

As already stated in the preceding sections, one of the main limitations of the PCM based heat transfer systems is its reasonably low thermal conductivity. It would be fascinating to explore if splitting the bulk PCM required for effectively chilling a given volume of milk in to multiple spherical PCM modules addresses this concern, by augmenting the surface area to volume ratio of the PCM bulk. Hence, in order to gain an understanding of the thermal behavior of PCM and subsequent milk chilling performance inside a sphere shaped module, the developed PCM in this study were primarily tested in a spherical module.

In general, the immediate container to hold milk after milking at farm premises resembles a cylinder either in household or at organized dairies. Therefore, in order to achieve minimum distance from the centroid of PCM volume (sink) to the closest convective surface of heat source (milk), as well as to cover maximum contact area between them, a jacketed cylindrical module containing milk at the central portion and the PCM in jackets, was taken as a test-rig for investigation in this project.

Another consideration during passive milk chilling by a PCM inside a container is slow speed agitation. In general, milk chilling in a tank or vat, particularly in a batch, is recommended with slow and gentle agitation. It helps in avoiding the separation of its constituents due to density differences, without incorporating surrounding air into it, at minimum rupturing the shear sensitive components such as milk fat globules membranes. It also facilitate uniform cooling, thereby avoid local bacterial growth at warmer sites inside the tank. Milk agitation at higher speed and vigorous mixing, causes leaching out of reactive components like free fats and fatty acids, which activate deteriorating enzymes

and generate off-flavors. A controlled agitation along with chilling eases uniform temperature distribution, less shear among constituents and delays activation of deteriorating enzymes, particularly lipases (Deeth *et al.* 1977; Bhavadasan *et al.* 1982).

Considering the above points, developing an energy efficient, portable and handy milk container with provision of passive cooling and agitation to handle small volumes, would help to preserve milk quality from production points as well as link the gap between demand and supply of electricity in the rural areas. Along with this, provision of slow speed agitation would help in speeding the cooling process, delaying the stratification of milk constituents and ease the sampling process at milk reception points for pricing and quality evaluations.

For modeling the phase-transition inside a container, Zeneli *et al.* (2021), critically reviewed the various methods of numerical simulations for solidification and melting processes, inferred that the enthalpy-porosity model was simple, effective, fast conversing and accurate for latent heat thermal storage systems. It was also suggested that the 'volume of fluid' (VOF) method with this model was most popular and suitable for tracking moving fronts of solid-liquid interface effectively.

For modelling the mixing of milk at slow agitation, which involve interactions of one or more moving (rotational/transitional) zones in a physical domain, e.g. mixing with a rotor inside a tank, the multiple reference frame (MRF) method, was reported as the simplest and effective method of approximation, in which the individual cell zones are assigned different speeds (zero for stationary and non-zero for moving). In this approach, at the boundary of two zones (i.e. interface), the diffusion equations are solved for relative velocity formulations to compute the velocities in each subdomain (Luo *et al.* 1994; ANSYS, 2013). Slow agitation of milk (nearly a Newtonian fluid) at low speed generally falls under higher than laminar to transitional regimes of flow. Transition Shear-Stress-Transport (SST) models are more suitable for these regimes, which solves transport equations for turbulent kinetic energy (k) with specific dissipation rates (ω) with two more factors viz. intermittency and transition onset criteria in terms of momentum-thickness Reynolds number via blending functions including eddy viscosities based shear-stresses ranged between the fully-turbulent models (standard k-ε model) to the wall-proximity (k-ω models) (Menter *et al.* 2006; Langtry *et al.* 2006).

2.7 Suitable material of construction and insulating materials for fabricating dairy equipment

2.7.1 Material of construction

Lancaster (1983) suggested the grade of stainless steel (SS) commonly used and recommended SS 304 type for mildly corrosive conditions whereas SS 316 type for more severe environments. Mahajani and Joshi (2003) reported the methods used in fabrication of various components based on material of construction and concluded that Tungsten Inert Gas (TIG) welding was most suitable for carbon steels, stainless steel and other exotic metals. Baddoo (2008) reported that apart from being a food grade material, stainless steel also offers exceptional advantages for certain applications in construction, combining intrinsic durability with aesthetics, strength, ductility and formability. International Stainless Steel Forum report (2010) suggested SS as most suitable food grade materials for following reasons: chemical, bacteriological and organoleptic neutrality with food products, its ability to be easily cleaned and hence hygienic, durability including resistance to corrosion and aging. Further, the recommended grades of SS for specific application in dairy industry were also summarized in Table 2.7:

Table 2.7 Common dairy equipment and material of construction

S. No.	Equipment	End Use	Grades
1	Refrigerated storage tank	All dairy products	304
2	Centrifuge, Pasteurizer	Milk, Yoghurt, Cream, Butter	304, 316
3	Plate and tubular heat exchanger	Milk, Cheese, Cream, Butter, Yoghurt	316
4	Packaging machine	Milk, Cream, Yoghurt	316
5	Ultra-filtration set up	Cheese	316
6	Maturation tank	Cheese, Ice-cream, Cream, Butter	304, 316
7	Cheese racks	Cheese	304
8	Other Equipment	All dairy products	304, 316

2.7.2 Insulation material

According to FAO, 1989, Polyurethane foam (PUF) is one of most suitable and commercially available choices of insulation material for fishing vessels, possessing good thermal insulating properties (thermal conductivity = 0.026 W/m-K), low moisture-vapour permeability, high resistance to water absorption, relatively high mechanical strength, low density, relatively easy and economical to install. Moreover, it adheres very well with SS surfaces. Expanded polystyrene foams (EPSF) are good insulating materials

but faced number of technical limitations such as flammable, gradual break down upon exposure to direct sunlight, tendency to react with solvents used in the installation of fibreglass-reinforced plastic (such as styrene-formulated polyesters) as well as with other organic solvents (petrol, kerosene, acetone, etc.).

Cork was possibly one of the firstborn insulation materials used commercially in the past especially in the refrigeration industry (112 kg/m^3 density and a thermal conductivity of 0.038 W/mK, a service temperature range of -180 to 100°C, water vapour transmission rate 20 to 40 µgm/Nh and a very less compressive strength compared to other materials) but at present, due to the shortage of cork-producing plants (Oak wood), it is relatively costly as compared to other insulating materials. These are available in slabs and pipe insulation form with available thickness of 13 to 305 mm (Anonymous, 2009).

Fibreglass or glass wool matting could be used as insulating material possessing following advantages such as high resistance to fire and bacteriological attack, good resistance to most of the chemicals, high heat resistance and thermal shock, commercially available in a variety of expositions (e.g. blankets, mats, loose fill and boards), low thermal conductivity (k = 0.036 W/m-K). It is generally employed for high temperature insulations popular in dairy and food industry for steam pipeline insulation. The density of the insulation material ranges from 10 to 80 kg/m^3 with service temperature range of -200 to 450°C. The compressive strength of the glass mineral wool is 1 to 8 kN/m^2, the water vapour transmission is 346 to 417 µgm/Nh and it is non-combustible by nature, which is acceptable for high temperature applications. However, the major technical limitations of glass wool matting as insulation material are: poor structural strength and compression resistance, sometimes possess a propensity to settle upon installation if not appropriately installed, high permeability to water vapour (Volovirta and Vinha, 2004).

Perrella *et al.* (2017) studied the effectiveness of common methods of cold-holding on the temperature of milk and determined that vacuum-insulated thermal carafes display excellent insulation properties and were therefore the most effective at keeping milk cold for an extended period of time. Based on this study it was recommended that public health inspectors should encourage their food premises operators to use these containers wherever appropriate. It was also reported that milk boxes permitted under the Regulation had poor insulation properties and bared milk to a higher risk of consumer contamination. Thus, it was suggested that the Regulation in Canada may need to be amended to forbid

the use of milk boxes while additionally needful the usage of specific vacuum-insulated thermal carafes.

Based on the review, it was deduced that

1. Stainless steel is the recommended metal of construction for milk holders
2. PUF or vacuum insulations are viable options for insulation during cold refrigeration

2.8 Methods of evaluating performance of a cooling system

2.8.1 Evaluation of refrigeration performance

Stinson (1987) conducted a series of experiments on a refrigeration heat recovery unit tested with two condensers (air and water) at four condenser pressures (6.5 bar, 7.5 bar, 10 bar and 12 bar) for two milk inlet temperatures (23°C and 18°C) and milk outlet temperatures (4°C and 7°C), receiver pressure and suction superheat degree to determine their effect on the overall system performance. It was reported that increasing condenser pressure resulted increase in gross heat recovery from 15.1 MJ (4.2 kWh)/d/m^3 to 29.2 MJ (8.1 kWh)/d/m^3 of milk for the water cooled system, while water outlet temperatures was increased from 45 to 64°C. Similarly, the corresponding ranges for the air cooled condenser were reported to be 13.7 MJ (3.8 kWh)/d/m^3 to 23.8 MJ (6.6 kWh)/d/m^3, and 38 to 55°C. Altering milk inlet and outlet temperatures gave a proportional change in cooling times and total heat recovery, but had no effect on co-efficient of performance (COP) or heat recovery rates. It was also observed that suction superheating augmented the total heat recovery by approximately 3.2 MJ (0.9 kWh)/d/m^3 and water outlet temperatures by 5°C.

Dabas *et al.* (2011) studied the performance parameters of a simple vapour compression refrigeration system under transient conditions during cooling of a fixed mass of brine from initial room temperature to sub-zero refrigeration temperature. It was reported that constant falling temperature of evaporator and refilling of capillary tube with more and more liquid refrigerant caused multifold increase in heat transfer coefficient which helped in maintaining refrigeration rate even at sinking temperature. Larger capillary tubes decreased the tendency of refilling of evaporator but offered less 'evaporator temperature'

effective in lower range of refrigeration temperature. Shorter capillary tube ensured higher COP initially but which declined at a sooner rate in lower temperature ranges.

2.8.2 On-farm milk cooling performance *vs* raw milk quality

The milk cooled using hydro-vac cooler was found to be of higher sensory scores (Wilster *et al.,* 1934) as compared to milk not cooled. Another study on the effect of milk cooling at farm level on bacteriological quality indicated that milk with initial bacterial count of ~105/mL upon cooling to 3-5ºC and 10-15ºC, immediately or after holding at 20ºC for 3-5h and 4-5h, respectively; the quality deteriorated significantly. In all cases, after 12h, the samples kept at 3-5ºC disclosed an increment of bacterial count by at least 3-5 times, while it was at least 8-11 times upon storing at 10-15ºC (Rasic *et al.,* 1968).

Majewski (1975) reported that the immediate cooling of milk to 4ºC reduced the psychrotrophic count even after 24h storage. At 15ºC, mesophilic, psychrotrophic and lipolytic bacterial counts were lower in milk cooled immediately after milking as compared to the milk that was not cooled after milking.

Darshan (2015) found that raw milk cooled by the eutectic module reported the bacterial counts much lower than the milk with no cooling up to 4h after milking (in the range of 4.51×10^5 to 5.34×10^5 cfu/mL). MBRT time recorded was 3h and 30 min to 3h and 45 min for milk cooled by the module, while MBRT time of 45 min was recorded for milk not cooled for 4 h after milking.

Prakash (2016) reported significant improvement in chemical quality (pH and acidity) as well as microbiological quality (difference in Total Bacterial Count by 2 log cycles and improvement in MBRT up to 5h) of raw milk cooled immediately after milking by nanofluid based cooling module for raw milk as compared to the milk not cooled for 4 h after milking.

CHAPTER-3

MATERIALS AND METHODS

The present research work was aimed at developing a phase change material (PCM) based milking cum cooling pail to be used by small to marginal and distantly located dairy farmers in rural areas. The developed unit intended for milk cooling is in the shape of an ordinary milking pail commonly used by farmers, a jacketed vessel design made of stainless steel 304 (SS 304), filled with developed PCM into the jacket adequately and appropriately. The entire unit is housed by a detachable and matching shape insulated container to avoid heat gain from surrounding. A de-attachable refrigeration cum charger unit for re-charging the milking pails was also design and developed. Different base fluids viz., distilled water (DW), distilled water+propylene glycol (DW+PG), distilled water+ethylene glycol (DW+EG) and distilled water+silver nano-ionic solution (DW+AgNP) were used as dispersing media for TiO_2, CeO_2 and Si_3N_4 nanoparticles during PCM formulation. The developed base fluids and PCMs were tested for thermo-physical, charging, discharging and milk cooling behavior to arrive best base fluids and nanoparticle combination and composition. The selected nanoparticle enhanced PCM (NePCM) were preliminary tested in a spherical shaped enclosure and then filled into the jackets of the cylindrical container. The developed units were tested for on farm milk cooling performance at Livestock Research Centre (LRC) of SRS, ICAR-NDRI, Bengaluru. The milk cooling performance was reported in terms of net temperature drop, rapidity of milk cooling, methylene blue dye reduction time (MBRT), total bacterial counts (TBC), pH and titratable acidity.

This chapter elaborate the various materials, fabrication techniques, developmental techniques, experimental procedures and methodologies employed during the investigation.

3.1 Materials

3.1.1 Chemicals and reagents

The analytical grade chemicals and reagents used for experimental investigation were bought from standard and authorized chemical suppliers. The chemicals used for the study were DW (prepared in the laboratory), PG, EG, Silver nano-ionic solution (prepared in laboratory), 0.1N sodium hydroxide (NaOH), 0.5% phenolphthalein. For all analytical purposes, freshly prepared reagents were used adopting standard procedures.

3.1.2 Glassware

Glassware of Borosil and Schott Duran brands procured from the authorized suppliers were used for the study. All glassware used during the study were sterilized prior to experimentation.

3.1.3 Microbiological media

Microbiological media required for microbial analysis of milk samples were procured from Hi Media Laboratories Pvt. Ltd., Mumbai.

3.1.4 Raw milk

Fresh raw milk was received immediately after milking from LRC of SRS, ICAR-NDRI, Bengaluru. The milk collected was from the pooled raw milk of different cow breeds.

3.1.5 Test modules of Milk Pails and the Charger

Milking pails of common shape and size used by dairy farmers were fabricated by SS-304 materials (Fig. 3.1a). The pails consisted jacketed space enough to contain requisite amount of PCM to chill milk from its drawing temperature to below the critical limit and hold within it for set durations. The various dimensions of milking pail were arrived based on engineering calculations.

A refrigeration cum charger unit having charging slot matching to the shape and size of the milking pail was also fabricated and used for studying the energy storage behavior of the PCM experimentally (Fig. 3.1b-c).

Fig. 3.1a Milking pail (prototype)

Fig. 3.1b Charger unit (prototype)

Fig. 3.1c Charger unit with milking pail

3.1.6 Insulated housing of pails

Insulated housing, filled with Polyurethane Foam (PUF), made of SS-304 material resembles like carriage containers of matching shape and size corresponding to the milking pails were fabricated and used for surrounding the charged milking pails to protect it from gaining heat from atmosphere (Fig. 3.2).

Fig. 3.2 Insulated housing for milking pail

3.1.7 Base Fluids and Nanoparticles

Different base fluids and nanoparticles were used for PCM formulation and used in the experimental trials (Table 3.1).

Table 3.1 Different base fluids and nanoparticles used for the study

S. No.	Base Fluid (BF)	Nano-Particles (NP)	Concentration of NP in BF (%)	Total Number of Combinations
1.	Distilled water (DW)	TiO_2 , CeO_2 , Si_3N_4 (15-80 nm) (Procured from Sigma Aldrich and Alfa Aser, USA	0, 0.05, 0.25, 0.50, 0.75, 1.00	4 BF × 3 NP × 6 Levels × 3 Replications (216)
2.	90% DW + 10% Propylene glycol (DW+PG)			
3.	90% DW + 10 % Ethylene glycol (DW+EG)			
4.	DW+ Silver nano-ionic solution (DW+AgNP)			
	Note: Abbreviations cited as nomenclature used throughout			

3.1.8 Instruments

Different instruments used for experiments during the study are listed in Table 3.2.

Table 3.2 Instruments used for experiments during the study

S. No.	Instrument	Purpose	Specification
1	Data logger	To record the temperature profile of PCM and milk with time	Model: CENTER 374. Instrument was equipped with a microprocessor, temperature sensor, 4 channels, desktop interface and inbuilt memory.
2	Thermocouple	To sense and measure temperature of milk and PCM	K-type (chromel+alumel). Temperature range: -200°C to +1350 °C
3	Deep Freezer	To freeze the base fluids and PCM during preliminary trials	Brand: LG, Model: GL-478G5X5. Temperature range: -18°C to -27°C
4	BOD Incubator	To conduct milk cooling trials under controlled conditions	Make: M/s M.K. Scientific Instruments, Capacity: 112L, Type: BOD cooling Incubator
5	X-ray diffractometer	To characterize nanoparticles for phase identification and purity	Make: RigakuSmartLab, High intensity XRD
6	Magnetic Stirrer	Mixing and dispersing nanoparticles into base fluids	Make: REMI Model: 5 MLH plus

7	Ultrasonicator	For ultrasonication of nano-dispersions to break agglomerates into fine and evenly distributed	Make: Grant Instruments (Cambridge) Ltd, Model: XUBA1 (35 W/33-38 kHz)
8	Zeta Potential analyzer	To determine zeta potential value of nanofluids and particle size of nanoparticles in the dispersion	Zeta PALS (Make: Malvern Instruments). Signal Processing: Phase Analysis Light Scattering, PALS
9	Scanning electron microscope (SEM)	For morphological analyses of dry nanoparticles and nanoparticles in PCM	Ultra-high resolution SEM with EDS (Model: Ultra 55), GEMINI technology
10	Energy dispersive spectroscopy (EDS) on SEM	For elemental analysis and their relative proportions in PCM	Ultra-high resolution SEM with EDS (Model: Ultra 55) based on latest GEMINI technology
11	KD2-pro thermal property analyzer	To measure thermal conductivities of nanoparticles and nanofluids at different temperatures.	Make: Decagon devices, Inc., USA. For liquid samples: Single needle KS-1 (1.3-mm diameter × 60-mm long) For dry nanoparticles: Dual needle SH-1 (Size: 1.3 mm diameter x 3 cm long, 6 mm spacing)
12	Modulated differential scanning calorimetry (MDSC)	To record heat flow v/s temperature profile and estimating heat capacities at different temperatures.	Model: METTLER TOLEDO MDSC1
13	pH-meter	To measure pH of milk	Model: EUTECH INSTRUMENTS
14	Energy Meter	To record electricity consumed by the charger during charging of milking pails	Brand: HTC, Model: PM03, Current : 0-400 A, Voltage : 0-600V
15	Constant temperature water bath	To control temperature of nanofluid based PCM samples during analysis	Make: Excel Scientific, Volume: 32 L, Temperature range: room temperature to 99°C. Precision: ± 0.5 °C.

3.2 Methods

3.2.1 Characterization of nanoparticles

3.2.1.1 X-ray diffraction (XRD)

The procured nanoparticles (TiO_2, CeO_2, Si_3N_4) were characterized by X-ray diffraction (XRD) method for phase identification and the obtained patterns of nanomaterials were compared with the standard database. The analysis was carried out by XRD machine (Fig. 3.3) installed at Micro and nano-characterization facility (MNCF) at Centre of Nanoscience and Engineering (CeNSE), Indian Institute of Science, Bangalore. In this method, X-rays generated from a cathode ray tube, filtered to produce monochromatic radiation, collimated to concentrate to a desired intensity and directed towards the nanoparticle sample. By continuously varying the incident angle of the X-ray beam, a spectrum of diffraction intensity versus the angle between incident and diffracted beam (2θ) was recorded.

Following protocols for phase identification of nanoparticles by XRD were followed:

1. 1 g of nanoparticle sample was duly placed on the sample holder surface and thinly smeared uniformly onto a glass slide to ensure a flat upper surface.
2. The smear packed inside a sample container and sprinkled on double sticky tape.
3. The intensities of diffracted X-rays were continuously recorded as the sample and detector rotated through their respective angles
4. The XRD-pattern of nanoparticles were presented as peak positions at 2θ (X-axis) and X-rays counts (intensity, Y-axis). The data obtained were compared with the standard database.

Fig. 3.3 X-Ray Diffractometer

3.2.1.2 Scanning electron microscopy (SEM) and the Energy dispersive spectroscopy (EDS) of nanoparticles

Energy dispersive spectroscopy (EDS) was carried out for nanoparticle powder samples to determine the elemental composition to ensure the purity. It was performed by capturing scanning electron microscopic images and the selected zones were characterized through EDS. In this process, the corresponding X-ray spectra generated from the entire scan area showed the counts (number of X-rays received and processed by the detector) on Y-axis; and the X-axis showed the energy level of these counts. Thereafter, obtained data was compared with the standard database of primarily known elements to arrive the elemental composition.

3.2.2 Preparation of base fluids and nanofluid based PCM

The base fluids of different compositions at various nanoparticles concentrations were prepared using distilled water, propylene glycol, ethylene glycol and silver nano-ionic solution. The experimental design of base fluids and nanoparticle concentrations were planned as presented in Table 3.1. The nanofluid (by two-step method) based PCM were prepare by following protocols (Fig. 3.3):

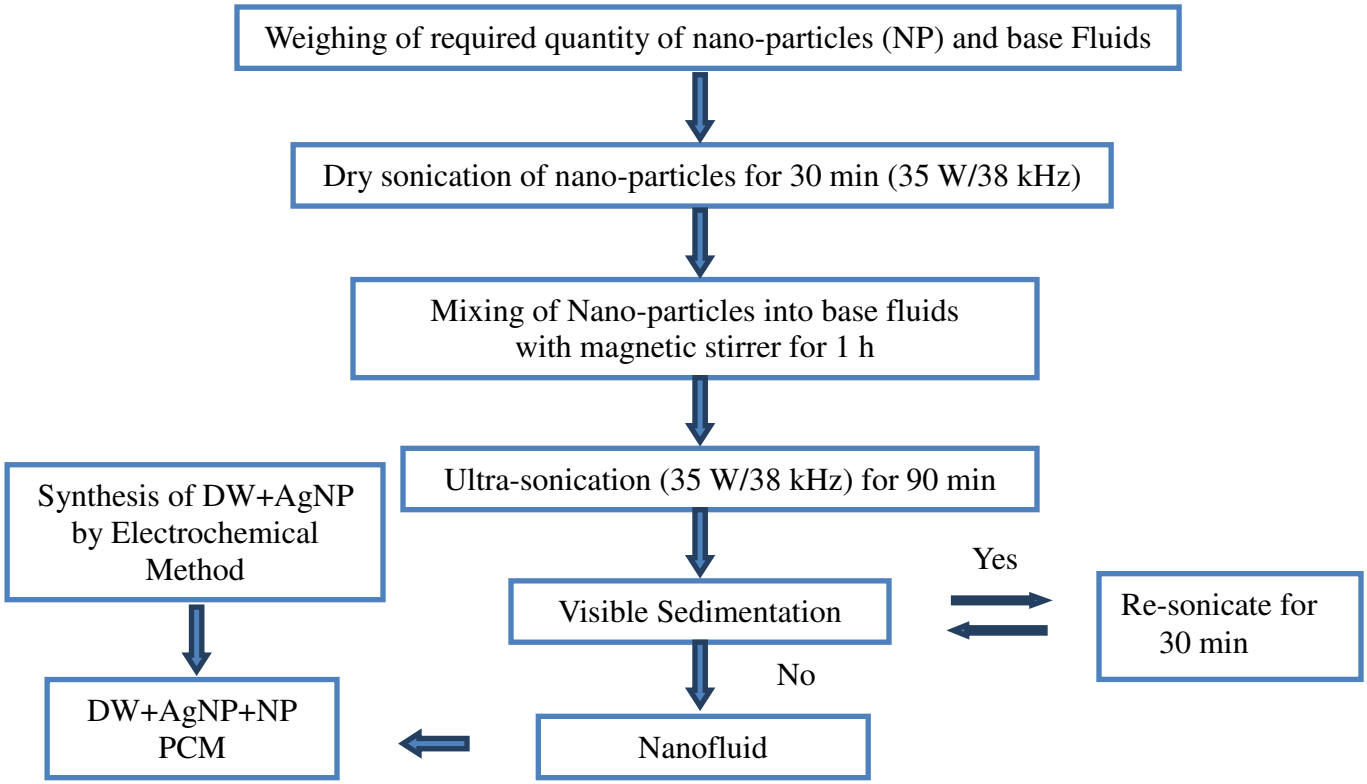

Fig. 3.3 Preparation of Nanofluid based PCM

3.2.3 Characterization of PCM

3.2.3.1 Thermal Conductivity

Thermal conductivities (k) of dry nanoparticle (powder form) were measured (±1% accuracy) by dual needle SH-1 (Size: 1.3 mm diameter x 3 cm long, 6 mm spacing) sensor installed with KD2-pro thermal property analyzer. For PCM in liquid form, 'k' values were measured by single needle KS-1 (1.3-mm diameter × 60-mm long) sensor of the same instrument (Fig. 3.4a). The temperatures of samples during measurements were kept constant by placing them into a constant temperature water bath for at least 10 min to reach an equilibrium temperature (Fig. 3.4b). A temperature sensor (thermocouple) was placed inside the sample and connected with a data logger. Equilibrium temperature of a sample was monitored on data logger screen. Once a constant value was reached, then respective sensor for measurement of 'k' was inserted into the samples up to the prescribed depth. The 'k values were recorded by KD2-pro analyzer using working principle of a transient hot wire

method. Prior to measurement, each sensors were calibrated by standard glycerin sample supplied with the instrument.

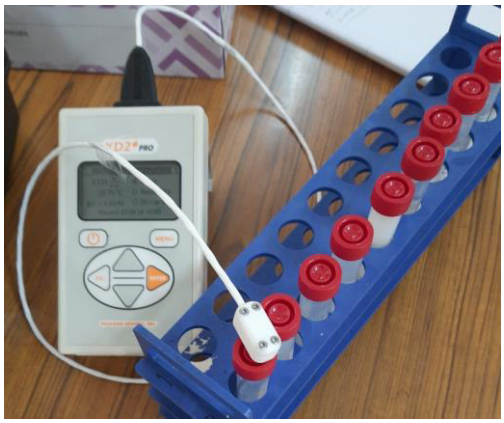

Fig. 3.4a Thermal conductivity measurement using KD2-pro thermal property analyzer

Fig. 3.4b Temperature control during thermal conductivity measurement of PCM

3.2.3.2 Scanning Electron Microscopy (SEM)

SEM characterization of liquid PCM were carried to understand the morphology and distribution patterns of the nanoparticles into the base fluid matrix. Liquid samples of PCM were drop-casted on suitable substrate and placed on sample holder of the SEM. All samples were metalized with a thin layer of gold (15 nm, 99.99% of gold, 2×10^{-6}Torr) in a thermal evaporator before capturing images. SEM images were captured at 10, 25, 50 and 100 kX magnifications. The analysis was carried out by SEM instrument (Fig. 3.5) installed at Micro and nano-characterization facility (MNCF) at Centre of Nanoscience and Engineering (CeNSE), Indian Institute of Science, Bangalore.

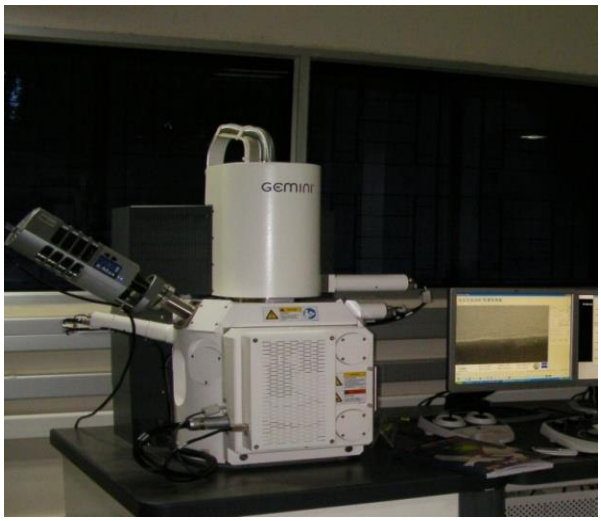

Fig. 3.5 Scanning Electron Microscope

3.2.3.3 Differential Scanning Calorimetry

Temperature modulated differential scanning calorimeter (MDSC) was used to determine heat flow vs temperatures of the PCM. It recorded the instantaneous difference in heat flows between the PCM sample and an inert reference sample placed within the instrument, when both are subjected to a simultaneous linear and sinusoidal temperature program. The temporal heat flow rate were used for calculating specific heat capacity (C_p) using Universal Analysis 2000 software (V3.7A) of the TA instruments. The measurements were carried out for a PCM sample mass of 23 to 26 mg from -10 to 40°C with a scanning step size of 5°C/min.

3.2.3.4 Zeta potential analysis

The dispersion stability and particle size distributions of the PCM prepared in this study were analyzed by a Zeta potential meter and Zeta particle size analyzer, respectively (Fig. 3.6). For calculating values of Zeta Potential (ζ) of a nano-dispersion, the surface charges of nanoparticles were used for predicting difference in potential of fixed and diffused layers by phase analysis light scattering (PLS) method to quantify the stability of nanoparticles dispersed in a base fluid. Particle size distributions of the PCM samples were measured by Zeta particle size analyzer by dynamic light scattering (DLS) method.

Fig. 3.6 Zeta potential analyzer

3.2.3.5 Transmission Electron Microscopy (TEM)

TEM characterization of the selected PCM of enhanced thermal properties (based on earlier characterization reports) were carried out to understand the particle size (in nanometer), their distribution, shape, morphology, agglomerations patterns and possible interactions among dispersed nanoparticles with base fluids or silver metal ions. The analysis was carried out by TEM instrument (Fig. 3.7) installed at Micro and nano-characterization facility (MNCF) at Centre of Nanoscience and Engineering (CeNSE), Indian Institute of Science, Bangalore.

3.2.4 Engineering design and fabrication of the milking pail and charger unit

The engineering designs for the milking pails and a matching refrigeration cum charger unit to charge the pails were calculated by heat transfer and energy balance calculations. At first, based on measured values of thermal properties of the PCM, the required amount of PCM to chill milk from its drawing temperature 37°C to below 10°C (assuming 80% heat utilization efficiency) was calculated. Then, the shape, size, dimensions and orientations of the milking pail were finalized based on number of constraints such as an average height of milking teats of a dairy animal from the ground/plinth level or milking platform, convenience of a dairy farmer during handling and transportation, average volume of milk occasionally produced at the premises of a small to marginal dairy farmer per milking, spare volume for accommodating the foaming and spillage of milk during milking and the expansion of PCM during phase-transition (charging) when assimilated into the

jacketed walls of the pail. The critical thickness of insulating housing was also calculated for the cylindrical geometry of matching shape and size with the milking pail to uphold the chilled milk temperature for at least 5-6h. The refrigeration capacity, compressor and condenser size, dimensions of evaporator cum charging slots (matching with the outer diameter of the pail), length of copper coiling of the refrigeration cum charger unit were calculated based on energy demand of the PCM for charging in about 1h. In order to prevent the phase-separation of milk-constituents at low temperature, a top mounted agitator at slow rpm (30-40) was installed along with the lid of milking pail. Thus, the various specifications of the milking pail and the charger arrived are presented in Table 3.3.

Fig. 3.7 Transmission Electron Microscope

Table 3.3 Engineering design specifications of the milking pail and the charger unit

A. **Milking Pail**	B. **Refrigeration cum Charger Unit**
• Working capacity : 0.5-6L • Total capacity : 8 L • Size of the pail : (outer dia. (ϕ_o) = 205 mm, height (h) = 360 mm, inner dia (ϕ_i) = 160 mm) • Thickness of PUF in insulating housing : 20 mm • Shape: Jacketed cylindrical • PCM : Assimilated into jackets • Agitator : Top mounted (0-100 rpm) • Quantity of PCM : 1.30-1.88 kg	• Volume of refrigeration space : 12L • Size of charging slot : (inner dia., ϕ = 250 mm; h = 380 mm • Refrigeration capacity: 0.1 TR • Compressor : 0.5 HP (R-600a) • Accessories and mountings : matching capacity • Shape of charging slot : cylindrical (to fit the pail) • Charging time: 1-1.25h

Based on above specifications, the virtual models representing different components of the milking pail and the charger unit were drawn in Pro-Engineering software (Fig. 3.8 a-c) and fabrications were done accordingly.

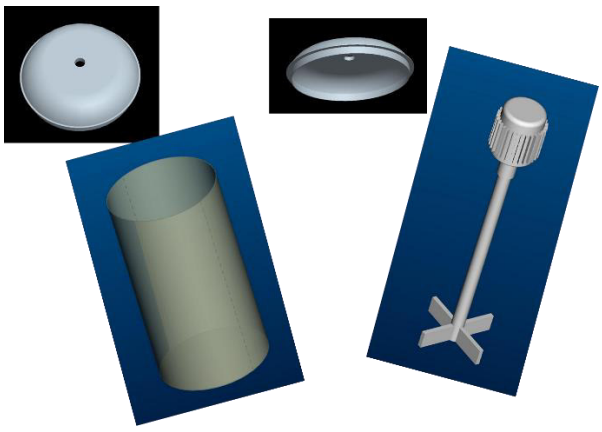

Fig. 3.8a 3-D models of the customized dismantled parts of the Pail

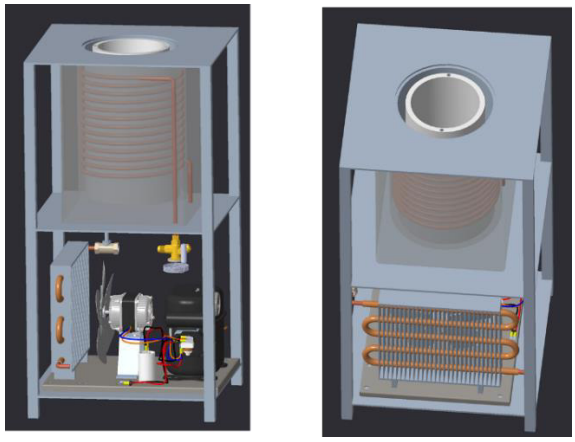

Fig. 3.8 3D-model of the **b. side view**; **c. isometric view** of the charger unit

Following steps were followed during fabrication of the jacketed cylindrical module:

Engineering calculations for design parameters (shape, size) of the pail

↓

Forming hemi-cylindrical halves of SS 304 sheet by hydraulic press and joined by TIG welding

↓

Formation of Double Jacketed Cylindrical Pail

↓

Embedding provision to insert thermocouples and agitators

↓

Fitting of Ferrule lock and

↓

Finishing the module surface to avoid fouling

↓

Hydrostatic testing for leak proofness

3.2.5 Computational Fluid Dynamics (CFD) simulation of PCM for charging and discharging in the proposed design

CFD simulation studies with experimental validations were preliminary carried out in a spherical enclosure containing NePCM and then the selected PCM were tested in the jacketed cylindrical modules.

3.2.5.1 Physical model for simulation

3.2.5.1.1 Spherical module

Two separate 3-dimensional (3D) physical models were developed and tetra-meshed in Ansys ICEM-CFD 19.0 software as explained below.

The physical domain of the module housing the PCM was considered to be a spherical shell made of stainless steel material (k = 16.2 W/m-K) of an inner diameter and a wall thickness of 150 and 1.2 mm, respectively. The module was initially (at time, t = 0s) filled with a liquid PCM at a temperature greater than the $T_{liquidus}$ of PCM. Fig. 3.9a, schematically represents a cut plan at centre of the 3D domain for modelling charging process. At any instant, t > 0s, the module filled with the PCM was considered to be placed inside a freezing chamber (196.5×196.5 mm^2) enclosed within adiabatic walls and a fixed refrigeration space temperature lower than $T_{solidus}$. Therefore, the energy storing (charging) process of the PCM

inside the module commenced as a result of sensible and latent heat exchange of the PCM with its surroundings.

An already charged spherical module of same specification as listed in the previous paragraph, was considered the physical domain for the discharging process. Initially (at time, t = 0s) the spherical module contained the solidified PCM, at an initial temperature corresponding to that of the freezing chamber (lower than $T_{solidus}$). Fig. 3.9b, schematically represents a cut plan at center of 3D domain simulating discharging of the PCM during chilling of milk.

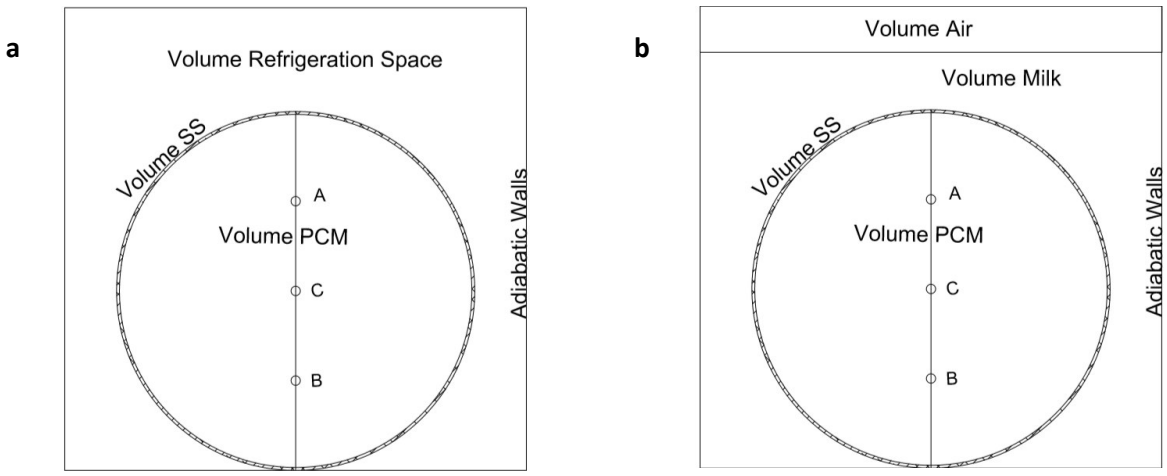

Fig. 3.9. Physical model for simulating **(a)** charging process of the PCM **(b)** discharging of the PCM during milk chilling

At any instant, t > 0s, during the milk chilling operation, the charged module containing the frozen PCM was assumed to be completely immersed inside a pool of 5L milk (at an initial temperature 37°C or 310.15 K, the milking temperature), contained in an ordinary milking vessel (rectangular dimension of 196.5 ×196.5 mm^2). The boundary of the milk vessel was assumed to be well insulated and hence modeled as adiabatic walls. The milk being chilled along with the immersed module was assumed to occupy 90% of total volume of the vessel, while the remaining 10% empty head space (practically provided to prevent splashing and spilling of milk during handling) was modeled as air fluid. Thus, at any given instant (t > 0s), the milk temperature (37°C or 310.15K, at t = 0s) is imposed on the surface of the charged module. Hence, the simulation considered that the cooling energy stored in the PCM would

now slowly discharge into the surrounding pool of milk due to latent and sensible heat exchange, resulting in the chilling of the milk. The thermo-physical properties of the PCM experimentally determined in the study, were used as input parameters as user defined function for the simulation, while the properties of milk used were the values reported by Fox *et al.* (2015).

3.2.5.1.2 Jacketed Cylindrical Module

The physical model of the module depicting charging of the NePCM was considered as a jacketed hollow cylindrical module made of stainless steel (SS) material (k = 16.2 W/m-K) comprising inner diameter, depth, wall thickness of SS, jacket clearance and outer diameter of 160, 360, 1.2, 20 and 205 mm respectively as shown in the Fig. 3.10a.

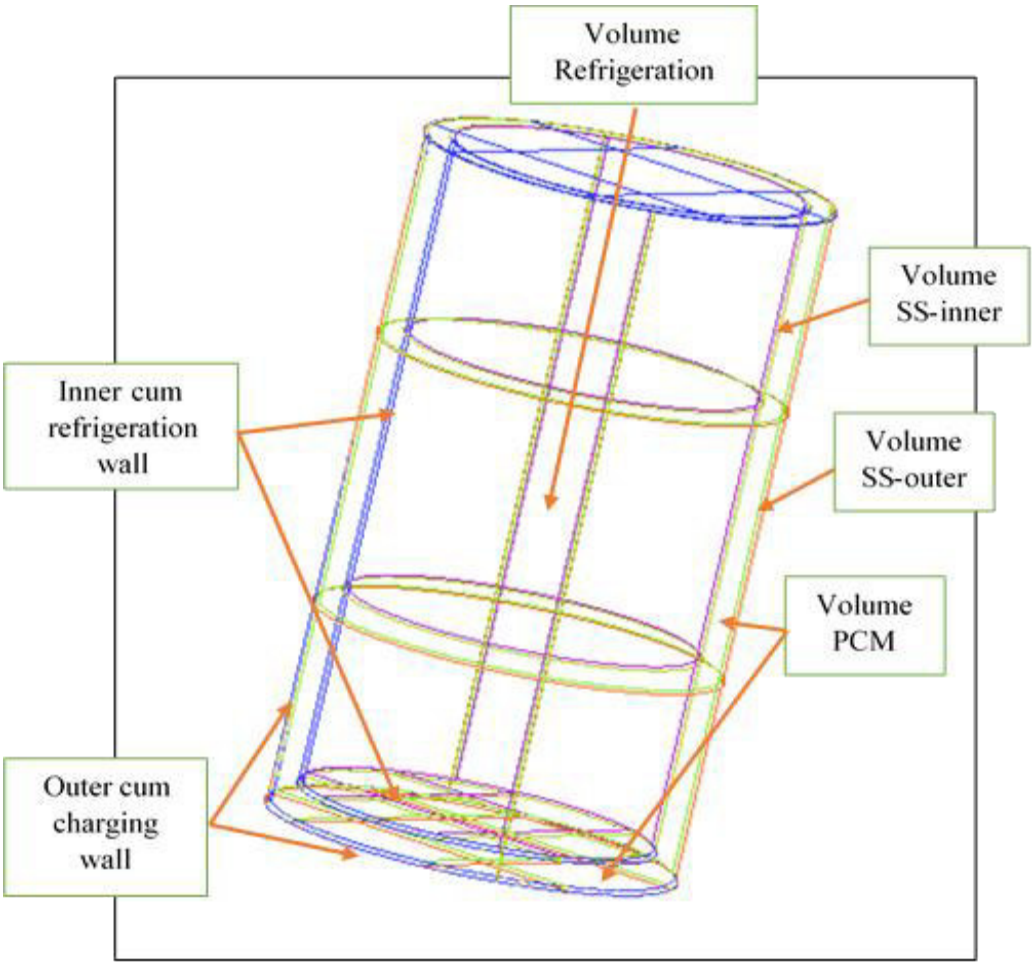

(a)

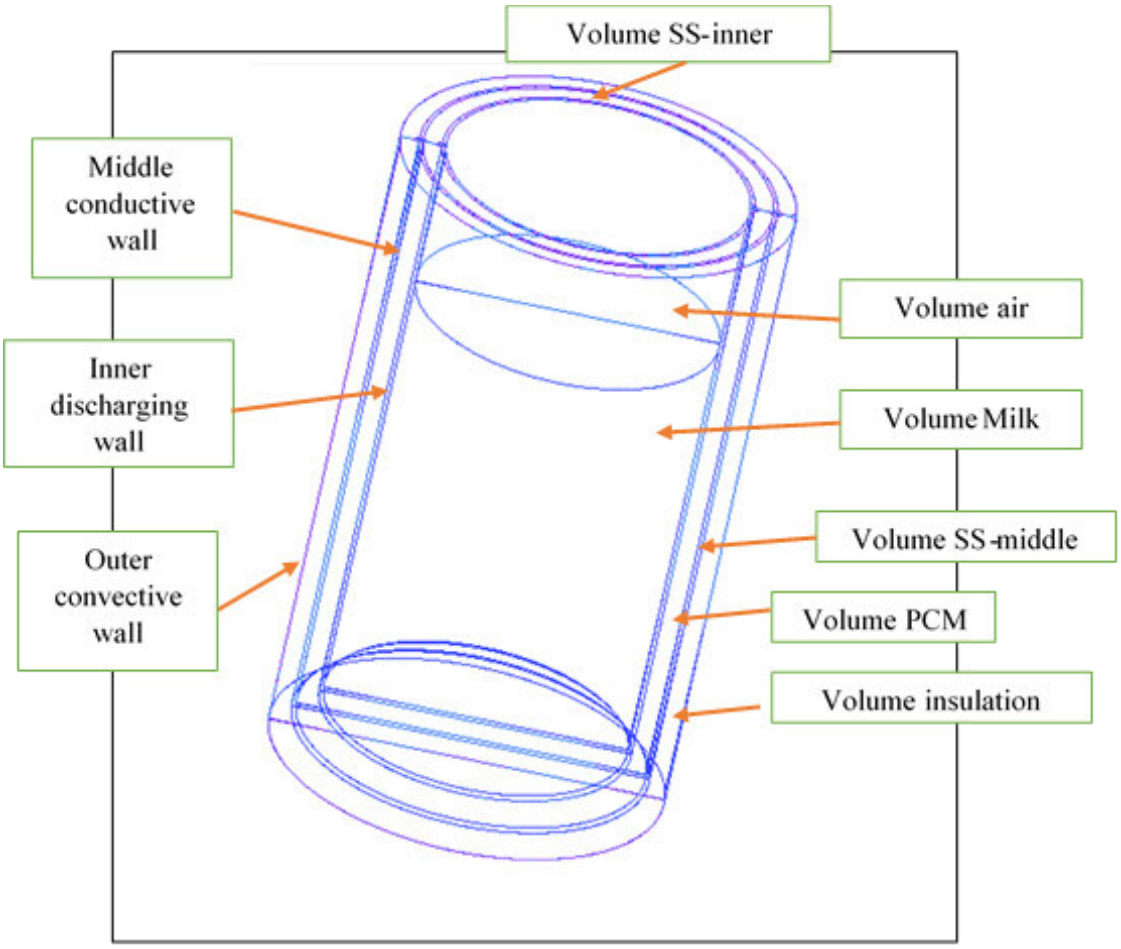

(b)

Fig. 3.10. Physical model for simulating **(a)** charging process of the NePCM in the jacketed cylindrical module; **(b)** discharging process of the NePCM during passive milk chilling

The model was initially (at an instant, t = 0 min) filled with a liquid NePCM (modelled as volume PCM), situated between jacketed space of the inner and outer walls of the cylindrical model, at a temperature greater than the liquidus temperature of the NePCM. Fig. 3.10a, schematically represents a cut plan at centre of the 3D domain for modelling the charging process. At any instant, t > 0 min, the outermost charging wall of the emptied module, (the emptied central space was to receive milk after charging) containing NePCM in the jackets, was imposed a fixed charging temperature lower than the solidus temperature of NePCM. The cooled energy was virtually exchanged through the charging walls into the NePCM. The empty hollow space at the centre was assumed as volume air (modelled as volume

refrigeration) and imposed at fixed temperature equal to the temperature of charging wall. It was assumed that the air volume confined in the empty portion already achieved the thermal equilibrium with the inner walls of the module at t = 0 min. The cooled energy was transferred into NePCM via inner wall also, therefore modelled as refrigeration wall. The volume of SS material of the inner and outer walls were modelled as 'volume SS-inner' and 'volume SS-outer'. Therefore, the energy storing (charging) process of the NePCM inside the module was commenced due to sensible and latent heat exchange.

It was considered that a charged cylindrical module, used for simulating passive milk chilling and consequent discharging of the NePCM, had similar specifications as mentioned in the previous para. Initially (at an instant, t = 0 min), the module contained solid NePCM (modelled as 'volume PCM') at an initial temperature lower than its solidus temperature. Fig. 3.10b, schematically presents a cut plan at the center of 3D domain simulating discharging of the NePCM during milk chilling. At any instant, t > 0 min, the module containing charged NePCM was filled with raw milk at 37°C (around the milking temperature), occupying 90% of its total empty volume (remaining 10% was modelled as 'volume air' to accommodate milk spillage and foaming during real time operations), modelled as 'volume milk'. The module containing milk was housed in a polyurethane foam (PUF) insulated container (thickness: 28 mm, k = 0.021 W/m-K), modelled as 'volume insulation'. The outer wall of the insulated housing was modelled as 'convective wall' thermally interacting with the surroundings at ambient temperature patched at free stream air temperature 40°C. The SS middle (volume SS-middle) wall acted as conductive partition between NePCM and insulation layer, modelled as coupled boundaries. Innermost walls (volume SS-inner) acted as 'discharging wall', exchanged heat from milk into NePCM, therefore the exchange of cooling energy into the pooled milk as latent and sensible heats was modelled as transient phenomena.

3.2.5.1.3 Jacketed Cylindrical Module with agitator

Two separate 3-dimensional (3D) physical models with and without agitation, depicting release of pre-stored cooling energy from the NePCM during passive milk cooling

inside a jacketed cylindrical container module, were developed and tetra-meshed in Ansys ICEM-CFD 19.0 software as explained below.

The physical model without agitation, consisted a jacketed hollow cylinder made of stainless steel (SS) material (k = 16.2 W/m-K) comprising inner diameter, depth, wall thickness of SS, jacket clearance and outer diameter of 160, 360, 1.2, 20 and 205 mm respectively as shown in the Fig. 3.11a.

At an instant, t = 0 min, the module was assumed to be filled with a pre-charged NePCM (modelled as volume PCM), inside the jackets of inner and outer walls, covering bottom and sides of the container. The initial temperatures of NePCM patched during simulations were less than its solidus temperature. The pre-charged module was used for simulating the passive milk chilling and consequent discharging of the NePCM. Fig. 3.11a, schematically represents the 3D domain simulating discharging of the NePCM during milk chilling. At any instant, t > 0 min, the module containing pre-charged NePCM was filled with raw milk at 37°C (around the milking temperature), occupying 90% of its total empty volume (remaining 10% was modelled as 'volume air' to accommodate milk spillage and foaming during real time operations), modelled as 'volume milk'. The module containing milk was housed in a polyurethane foam (PUF) insulated container (thickness: 28 mm, k = 0.021 W/m-K), modelled as 'volume insulation'. The outer wall of the insulated housing was modelled as 'convective wall' thermally interacting with the surroundings at ambient temperature patched at free stream air temperature 40°C. The SS middle (volume SS-middle) wall acted as conductive partition between NePCM and insulation layer, modelled as coupled boundaries. Innermost walls (volume SS-inner) acted as 'discharging wall', exchanged heat from milk into NePCM, therefore the exchange of cooling energy into the pooled milk as latent and sensible heats was modelled as unsteady state transient phenomena.

Fig. 3.11b, represents a model of same specifications as described in Fig. 3.11a, along with a paddle agitator with 4 flat blades. Considering sanitary designs and gentle handling of milk during agitation, pitched blades and baffles in the container were avoided. The ratio of impeller dia. (D_I) to milk container's inner dia. (D_T) was 1:3, the height of impeller base (C_I) from bottom of the container was one-third of the milk level (Z), and thickness of blades was

10 mm. At t >0 min, the agitator was rotated gently inside milk being chilled between 30-100 rpm with Reynold number (Re) ranging 700-3000. Volume average liquid fractions of the melted NePCM and corresponding temperature variations of NePCM as well as milk with time were recorded during computational analysis.

For defining multiple reference frame (MRF) in the 3-D model with agitator, separate domains were sketched viz. stationary zone ('volume milk' and 'container: volume PCM, volume insulation') and the rotational moving zone ('volume rotor'). Both domains were meshed separately and appended with an interface, depicting interaction between moving and stationary zones. The movement of rotor simulated herewith created a virtual motion in the stationary zone, which gradually progressed with time and persisted throughout milk volume.

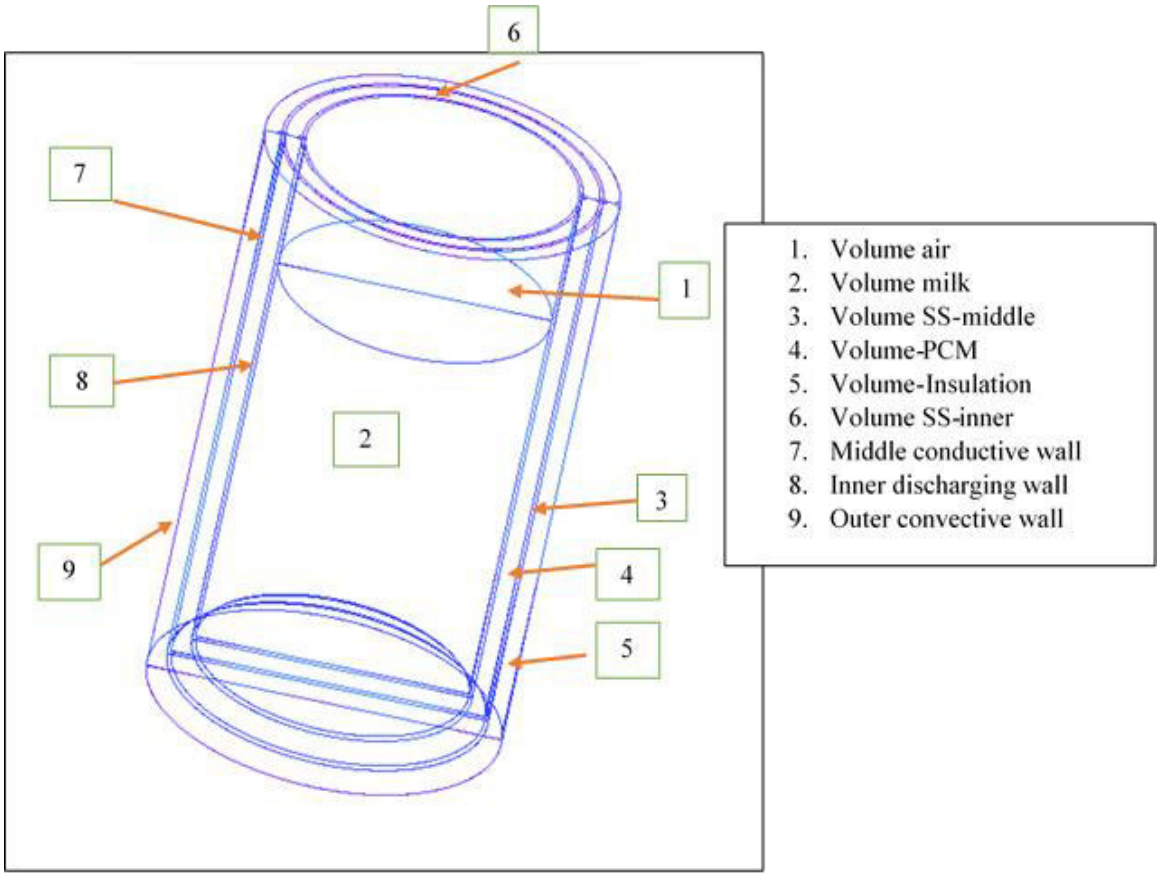

(a)

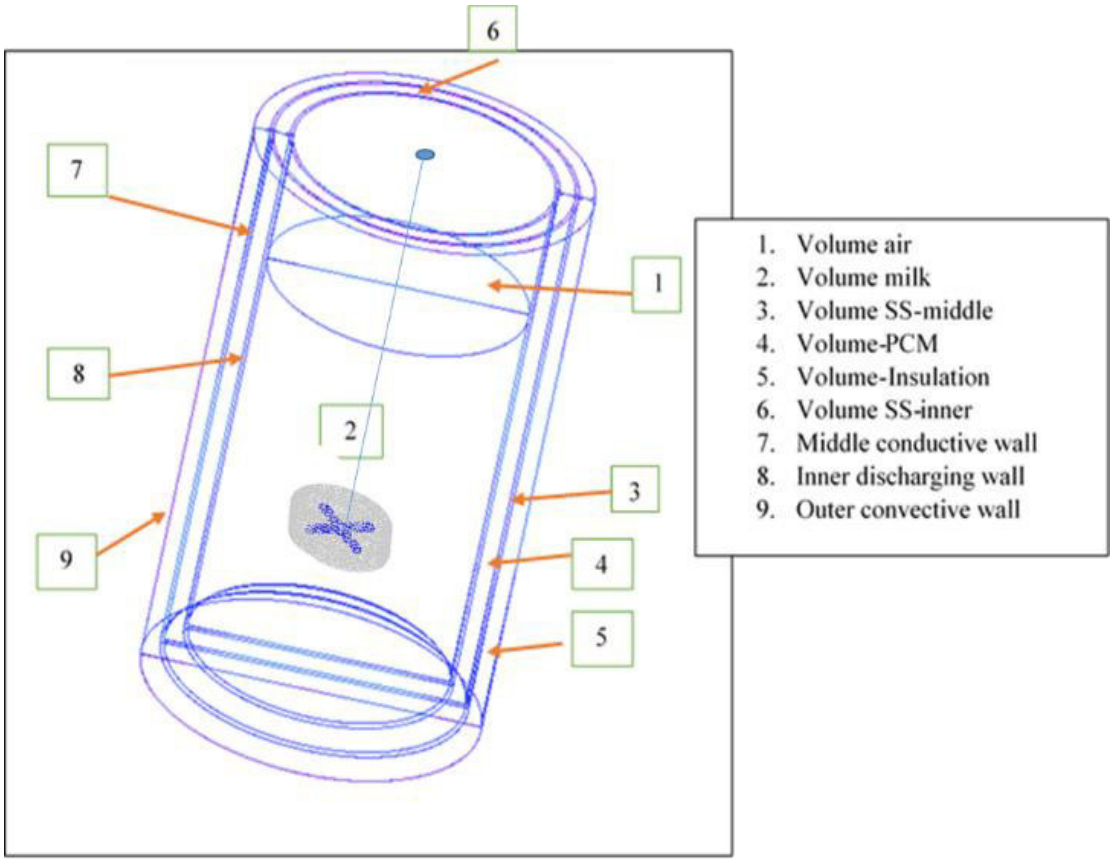

(b)

Fig. 3.11 Physical model for simulating discharging and passive milk chilling by the NePCM (a) without agitation; (b) with agitation

3.2.5.2 CFD simulation

The 3D physical models, as described in preceding paragraphs, were meshed and imported into ANSYS-Fluent-19 software. The pressure based solver was opted to solve transient, gravity-enabled, laminar, incompressible and three-dimensional multiphase (volume of fluid, VOF-model) flow of the PCM inside spherical module as well as the pail.

For simulating agitation, the pressure based solver was opted to solve transient, gravity-enabled, laminar (≤ 30 rpm) and transition SST (≥ 50 rpm), incompressible and three-dimensional multiphase (volume of fluid, VOF-model) flow of the NePCM inside the module.

3.2.5.2.1 Assumptions

The simulations were carried out considering following assumptions:

- The TiO_2 nanoparticles were homogeneously distributed throughout the PCM matrix.
- The charging and discharging of the PCM, mixing regime development, milk chilling were time-dependent, unsteady, incompressible, Newtonian and three dimensional.
- The modes of heat transport involved were only conduction and convection; the effects due to thermal radiations were neglected.
- Both the phases (liquid as well as solid) of PCM were isotropic, homogeneous and persisted in thermal-equilibrium at the solid-liquid interface.

3.2.5.2.2 Governing Equations

Based on above assumptions, the governing equations for solidification and melting (Zeneli *et al.* 2021; ANSYS, 2015) of the PCM inside the modules for charging (energy storage) and discharging during milk chilling included continuity, energy, momentum conservation and other phase-transition equations:

$$\text{Continuity : } \frac{\partial \rho}{\partial t} + \nabla.(\rho V) = 0 \quad \ldots (3.1)$$

$$\text{Momentum : } \frac{\partial (\rho V)}{\partial t} + \nabla.(\rho V) = - \nabla P + \mu \nabla^2 V + \rho g + S \quad \ldots (3.2)$$

$$\text{Energy : } \frac{\partial}{\partial t}(\rho H) + \nabla.(\rho V H) = \nabla.(k \nabla T) + S \quad \ldots (3.3)$$

$$\text{Enthalpy : } H = h + \Delta H \quad \ldots (3.4)$$

$$\text{where, } h = h_{ref} + \int_{T_{ref}}^{T} c_p \partial T \quad \ldots (3.5)$$

$$\text{and, } \Delta H = \beta L \quad \ldots (3.6)$$

where, V : fluid velocity vector (m/s), ρ : mass density (kg/m^3), μ : dynamic viscosity of the NePCM (kg/m-s), P : pressure (N/m^2), g : acceleration due to gravity (9.81 m/s^2), k : thermal conductivity (W/m-K), H : specific enthalpy (J/kg), t : time (s), h : sensible enthalpy (J), ΔH:

latent heat of the PCM at liquid fraction β (J), h_{ref} : reference enthalpy (J), c_p : specific heat at constant pressure (J/kg-K), T : absolute temperature (K) at instant 't', T_{ref} = 298.15K, S = source term, β = liquid fraction (ranges between 0 (for completely solid) to 1 (for completely liquid)), L : total latent heat content (J).

$\beta = 0$; if Temperature (T) of the PCM < $T_{solidus}$ … (3.7)

$\beta = 1$; if Temperature (T) of the PCM > $T_{liquidus}$ … (3.8)

$\beta = \frac{T - T_{solidus}}{T_{liquidus} - T_{solidus}}$, if $T_{solidus} < T < T_{liquidus}$, for mushy zone … (3.9)

S=Source term= $\frac{C(1-\beta)^2 V}{\beta^3}$, C=mushy zone constant $\left(10^4 \text{ to } 10^7\right)$ … (3.10)

$T_{solidus}$: the maximum temperature below which the PCM remained entirely in solid phase,

$T_{liquidus}$: the minimum temperature above which the PCM remained entirely in liquid phase.

For modelling the agitation of chilled milk, additional set of equations are as follows (Menter *et al.* 2006; Langtry *et al.* 2006):

The interface treatment of relative velocity formulations in multiple reference frame of rotor movement inside stationary milk contained in stationary container were as follows:

$$\vec{v} = \overrightarrow{v_r} + (\vec{\omega} \times \vec{r}) + \overrightarrow{v_t} \quad \text{… (3.11)}$$

$$\nabla\vec{v} = \nabla\overrightarrow{v_r} + \nabla(\vec{\omega} \times \vec{r}) \quad \text{… (3.12)}$$

Where, $\vec{v}$: absolute velocity; $\overrightarrow{v_r}$: relative velocity; $\overrightarrow{v_t}$: translational velocity; $\vec{\omega}$: angular velocity, $\vec{r}$: position vector

Transition SST model for milk agitation solved following transport equation for the intermittency 'γ' as follows:

$$\frac{\partial(\rho\gamma)}{\partial t} + \frac{\partial(\rho U_j \gamma)}{\partial x_j} = P_{\gamma 1} - E_{\gamma 1} + P_{\gamma 2} - E_{\gamma 2} + \frac{\partial}{\partial x_j}\left[\left(\mu + \frac{\mu_t}{\sigma_\gamma}\right)\frac{\partial \gamma}{\partial x_j}\right] \quad \text{… (3.13)}$$

Where $P_{\gamma 1}$ and $E_{\gamma 1}$ are transition sources, can be expressed as:

$$P_{\gamma_1}=C_{a1}F_1\rho S[\gamma F_o]^{c_{\gamma 3}} \quad \dots (3.14)$$

$$E_{\gamma 1} = C_{e1}P_{\gamma 1}\gamma \quad \dots (3.15)$$

Where S: strain rate magnitude, F_1 : empirical constant controlling the length of transition region, $C_{a1} = 2$, $C_{e1} = 1$, $c_{\gamma 3} = 0.5$,

And, $P_{\gamma 2}$ and $E_{\gamma 2}$ are destruction/re-laminarization sources, may be expressed as:

$$P_{\gamma_2}= C_{a2}\rho\Omega\gamma F_{turb} \quad \dots (3.16)$$

$$E_{\gamma 2} = C_{e2}P_{\gamma 2}\gamma \quad \dots (3.17)$$

Where Ω : vorticity constant, $C_{a2} = 0.06$, $C_{e2} = 50$,

Following functions controlled the transition onset:

$$Re_V= \frac{\rho\gamma^2 S}{\mu} \quad \dots (3.18)$$

$$R_T= \frac{\rho k}{\mu\omega} \quad \dots (3.19)$$

$$F_{onset1}= \frac{Re_v}{2.193Re_{\theta c}} \quad \dots (3.20)$$

$$F_{onset2}= \min\left(\max\left(F_{onset1}, \ F_{onset1}^{\ 4}\right), 2\right) \quad \dots (3.21)$$

$$F_{onset3}= \max\left(1 - \left(\frac{R_T}{2.5}\right)^3, 0\right) \quad \dots (3.22)$$

$$F_{onset}= \max\left(F_{onset2}-F_{onset3}, 0\right) \quad \dots (3.23)$$

$$F_{turb}=e^{-\left(\frac{R_T}{4}\right)^4} \quad \dots (3.24)$$

Where y: wall distance, $Re_{\theta c}$: critical Reynolds number where the intermittency begins to develop near the boundary layer.

$Re_{\theta t}$: transition momentum thickness Reynold number = f (Tu, ƛ)

$$Tu=\frac{100}{U}\sqrt{\frac{2}{3}k} \quad \ldots (3.25)$$

Where, k: turbulent energy; and $ƛ=\left(\theta^2/v\right)dU/ds$ … (3.26)

Where dU/ds: acceleration in stream-wise direction.

3.2.5.2.3 Computational procedure

An enthalpy-porosity method (Younsi and Naji, 2017) was applied for modeling the phase-transition of the NePCM, where instead of tracing the solid-liquid interface explicitly, the liquid-fraction (representing portion of the liquid volume associated with each cell in the domain) was computed at every iteration based on enthalpy balance equation. The temperatures of the mushy zones lies between solidus and liquidus range. The base fluid (distilled water) studied in this work was considered as a pure substance, whose solidus as well as liquidus temperatures were same (273.16K). The liquid-solid mushy zone (the transition region, where β lies between 0 and 1) was modeled by a fixed grid numerical modeling (Voller and Prakash, 1987), as a quasi-porous region having porosity equal to the instantaneous liquid fraction. The porosity of this zone was presumed to be reducing from 1 to 0 during solidification and reversed during melting. Once the PCM in a cell totally solidified, then porosity left was nil and all velocities fell to zero, therefore in order to account for the pressure drop due to solidification, suitable source terms (S) were added to momentum equation and reversed was the case during melting. The mushy zone constant (C) referred to the extent of damping due to the phase-transition effect which ultimately computed the rate of velocity transition of the PCM to zero as it solidified. The solution methods comprised SIMPLE (semi-implicit method for pressure-linked equations) algorithm (Patankar, 1980) for pressure-velocity coupling, least square cell based for gradient, PRESTO for pressure tuning, second order upwind for momentum and energy discretization and the Geo-reconstruct scheme for liquid fraction. The transient formulation comprised first order implicit method. The solution control under-relaxation factors for the pressure tuning,

density, body forces, momentum, liquid fraction update and energy were 0.3, 0.8, 0.8, 0.7, 0.9 and 0.8 respectively.

3.2.5.2.4 Grid independence studies

Sensitivity studies for the spherical models for grid independence were also conducted at varying grid densities. Accordingly, the CFD simulated volume average liquid fraction (β) of the PCM obtained for simulation using 7,72,888, 24,87,008 and 32,89,288 elements is presented in Fig. 3.12(a). Upon comparing the mesh densities, it was observed that the difference in two consequent β values reached ≤ 0.01 with 24,87,008 and 3289288 elements. Therefore, considering the accuracy of results as well as computation time, the mesh comprising of 24,87,008 elements was accepted for grid independency.

Values of β during charging at different mushy zones were also recorded and is shown in Fig. 3.12(b). Considering refinement of the model, the value for the mushy zone constant C_m = 10^7 was taken for final simulations. Fig. 3.12(c-d), represents the meshed 3D physical domain under study. Upon applying absolute and relative tolerance, time step size of 0.1s was found to be enough to satisfy time-step independency in the set transient problem.

Sensitivity studies for the jacketed cylindrical module meshed models for grid independence were also conducted at varying grid densities 2,77,382, 8,37,347 and 12,09,187 elements as presented in Fig. 3.13. Upon comparing the mesh densities, it was observed that the difference in β values reached ≤ 1 per cent with 8,37,347 and 12,09,187 elements, therefore considering the accuracy of results as well as computation time; 8,37,347 elements mesh was accepted for grid independency. Values of β during charging at different mushy zones were also recorded. Considering refinement of the model, 10^7 was taken for final simulations. Fig. 3.14(a-b), represents the meshed and unmeshed 3D models under study. Upon applying absolute and relative tolerance, time step size of 0.1 s was found to be enough for time-step independency in the set transient problem.

Grid independent studies for testing the sensitivity of meshing for the jacketed cylindrical module with agitator (fine mesh to capture the flow accurately) physical models were also

conducted at varying grid densities 15,33,222; 21,42,729 and 28,35,342 elements as plotted in Fig. 3.15a.

Upon comparing the mesh densities, it was observed that the difference in β values reached ≤ 1 per cent with 21,42,729 and 28,35,342 elements, therefore considering the accuracy of results as well as computation time, 21,42,729 elements mesh was accepted for grid independency. Values of β during charging at different mushy zones were also recorded. Considering refinement of the model, 10^7 was taken for final simulations. Fig. 3.15(b-c), represents the meshed 3D models of the container module with rotor and surrounding interface coupling the rotating and stationary domains using MRF. Upon applying absolute and relative tolerance, time step size of 0.1 s was found to be enough for time-step independency in the set transient problem.

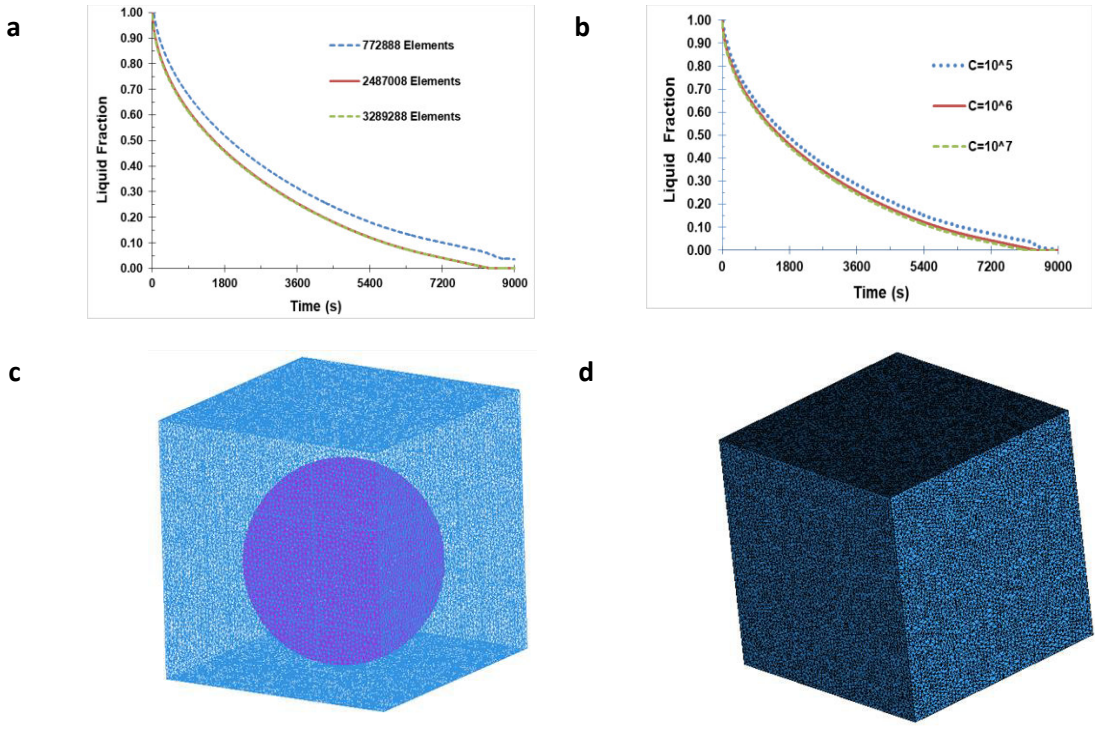

Fig. 3.12. Variation of CFD simulated volume average liquid fraction of the PCM vs time during charging at different **(a)** grid sizes **(b)** mushy zones; and meshed 3D models representing **(c)** surface mesh **(d)** volume mesh

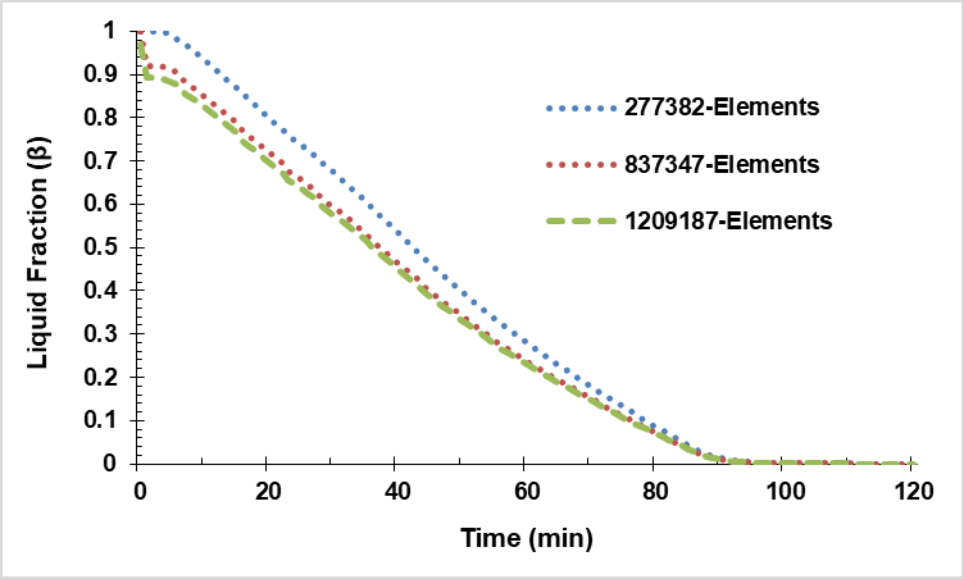

Fig. 3.13 Variation of CFD simulated volume average liquid fraction of the base fluid vs time during charging at different grid sizes of the physical model of the milking pail

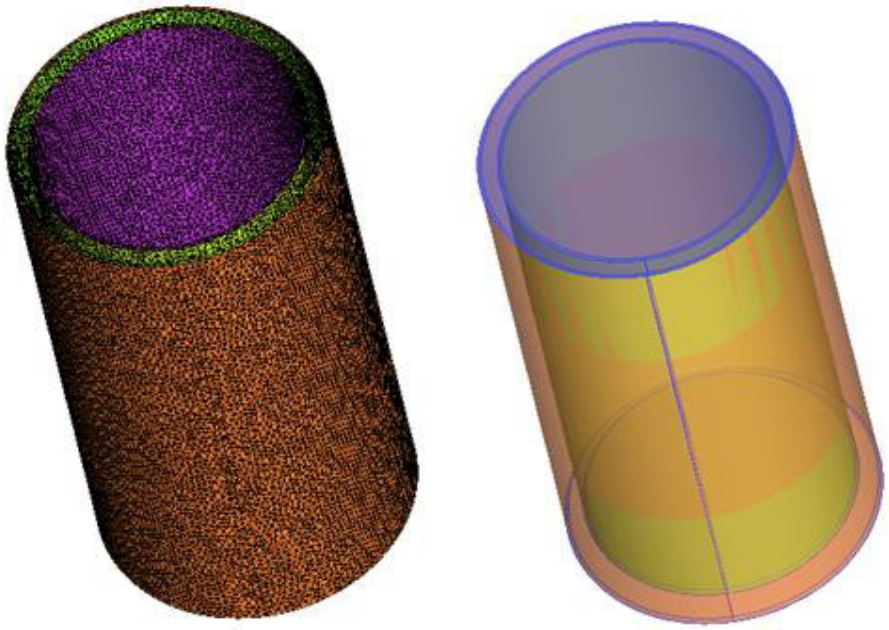

(a) **(b)**

Fig. 3.14 (a) Meshed 3D models representing surface and volume mesh (b) Unmeshed physical model of the milking pail

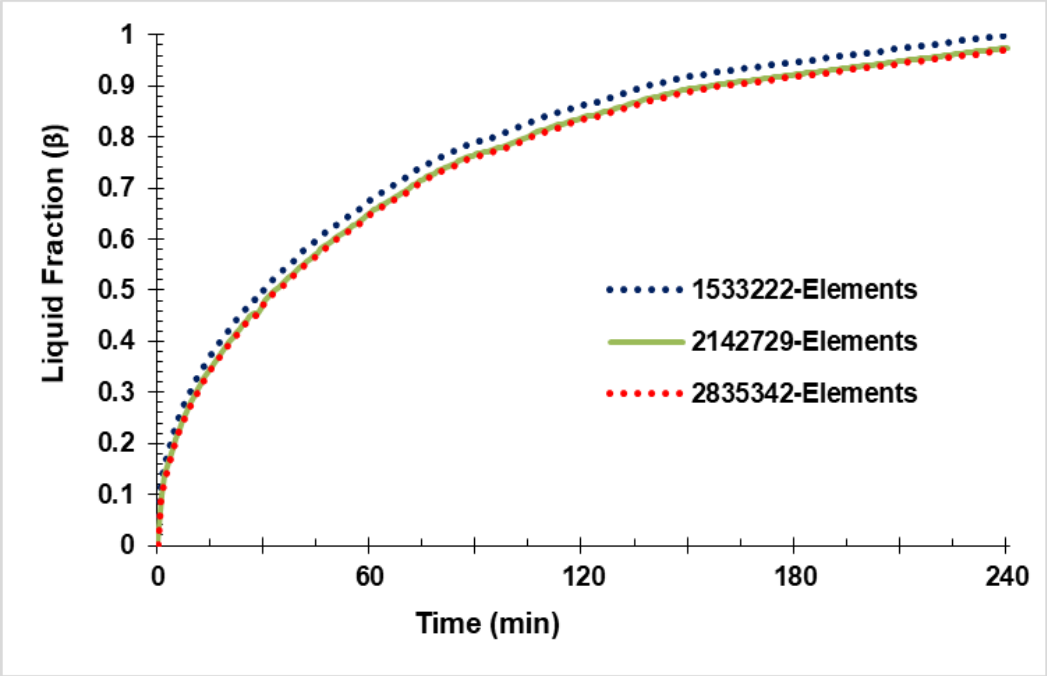

(a)

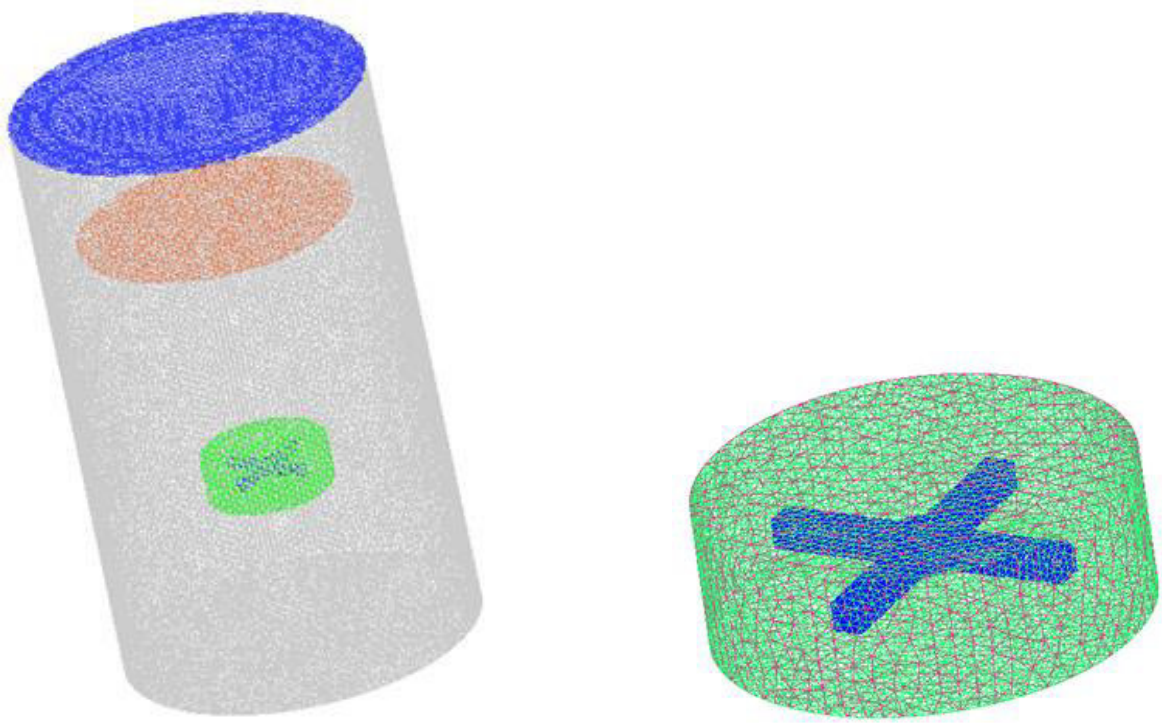

Fig. 3.15 (a) Volume average liquid fraction of the base fluid vs time during discharging at different grid sizes; **(b)** Meshed 3D model representing shell mesh of the container with rotor **(c)** rotor part with interface.

3.2.5.2.5 Initial and Boundary Conditions

For spherical module:

(a) *Charging*

At t = 0s; β of the PCM = 1, Temperature of the PCM = 300.15K, Refrigeration space temperature (fixed value) = 253.15K, Inner boundaries: coupled, Outer boundaries: adiabatic.

(b) *Discharging*

At t = 0s; β of the PCM = 0, Temperature of the PCM = ≤ $T_{solidus}$ (minimum temperature in K reached at the end of charging), Temperature of milk = 310.15K, Inner boundaries: coupled, Outer boundaries: adiabatic.

For Jacketed Cylindrical Module:

(a) Charging

At t = 0s; β of the PCM = 1, temperature of the PCM = 300.15K, volume refrigeration and charging wall (fixed value) = 253.15K, refrigeration wall: coupled, inner boundaries: coupled.

(b) *Discharging*

At t = 0s; β of the PCM = 0, temperature of the PCM = minimum value of temperature (K) reached during charging of a particular PCM, Temperature of milk = 310.15K, Inner boundaries: coupled, Outermost boundaries: convective with free stream temperature 313.15K.

For Jacketed Cylindrical Module with agitator:

At t = 0 min; β of the NePCM = 0, temperature of the NePCM = minimum value of temperature reached after charging the NePCM for a fixed duration, Temperature of milk = 37°C or 310.15K, Inner boundaries: coupled, Outermost boundaries: convective with free stream air temperature 40°C or 313.15K., rotor rotational velocity = 0, 30, 50, 70, 100 rpm.

3.2.6 Experimental set up and procedure

3.2.6.1 Charging of the PCM

For Spherical Module:

The experimental set up for charging of PCM comprised of an insulated deep freeze chamber (196.5×196.5 mm^2), coupled with a Proportional-Integral-Derivative (PID) controller to maintain a set temperature inside the chamber. The PCM was confined within a spherical shape stainless steel module (inner diameter: 150 mm and thickness of stainless steel material: 1.2 mm). Initially, all the PCM for trials were at 27°C (ambient temperature). The module containing a PCM was firmly kept at center of the deep freeze chamber maintained at a constant temperature of -20°C (Fig. 3.16a).

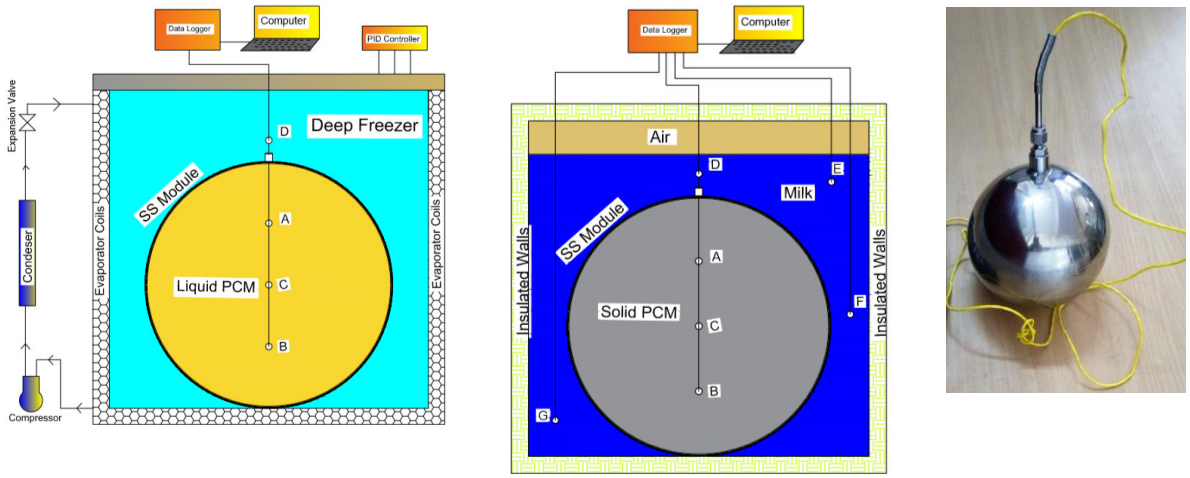

Fig. 3.16. Schematic diagram of the experimental set up for **(a)** charging of the PCM (left), **(b)** discharging of the PCM during milk chilling (middle); **(c)** Fabricated stainless steel module (right)

An adjustable thermocouple centered in a ferrule-lock design was provided on the module, as shown in Fig. 3.16(c), to record instantaneous temperature of the PCM. All thermocouples were linked to a data logger to record the temperature profile continuously at every second at the points (‘A’, ‘B’ and ‘C’) inside the module (Fig. 3.16(c)). The charging trials were carried out in triplicate to ensure the accuracy and repeatability and average of the three readings were plotted. Since the module containing the PCM were opaque, only computationally predicted values of ‘β’ were reported during for the charging process.

For Jacketed Cylindrical Module:

The experimental set up for charging of the NePCM comprised of an empty (i.e. empty central part for receiving milk) jacketed cylinder in the shape of an ordinary milking container (outer: inner dia. :: 205 : 160 mm) having NePCM filled inside the jacketed space (20 mm). The module filled with NePCM was inserted into the charging slot (i.e. evaporator part) of a matching capacity refrigeration cum charger unit developed for charging the modular unit for passive milk chilling (Fig. 3.17a). The slot was designed so as to exactly fit the empty container with minimum gap between outer wall of the container and the evaporator wall of charger. The air gap between outer wall of the container and the charger was filled with a conducting liquid (k = 0.65 W/m-K) to improve the heat transfer rates. The charger unit was coupled with a proportional-integral-derivative (PID) controller to maintain a set desired constant temperature (-20°C) inside the slot. At, t = 0 min, NePCM was at around 27°C (ambient temperature) and cooled first sensibly, till solidus temperature, and latently thereafter.

The PT-100 thermocouples probes with adjustable depths, centered on a ferrule-lock system, were inserted inside the NePCM to reach the points 'A' and 'B' (Fig. 3.17a), to record the instantaneous temperatures. All the thermocouples were linked to a multichannel data logger (coupled with a computer and data storage unit) to record the transient temperature profile continuously at every minute. The charging trials were carried out in triplicate to ensure the accuracy and repeatability and average of the three readings were plotted. Since the container unit having NePCM was opaque, therefore it was difficult to predict experimental transient values of liquid fraction (β) by image analysis, hence only computationally predicted values of β were taken into consideration during the charging process.

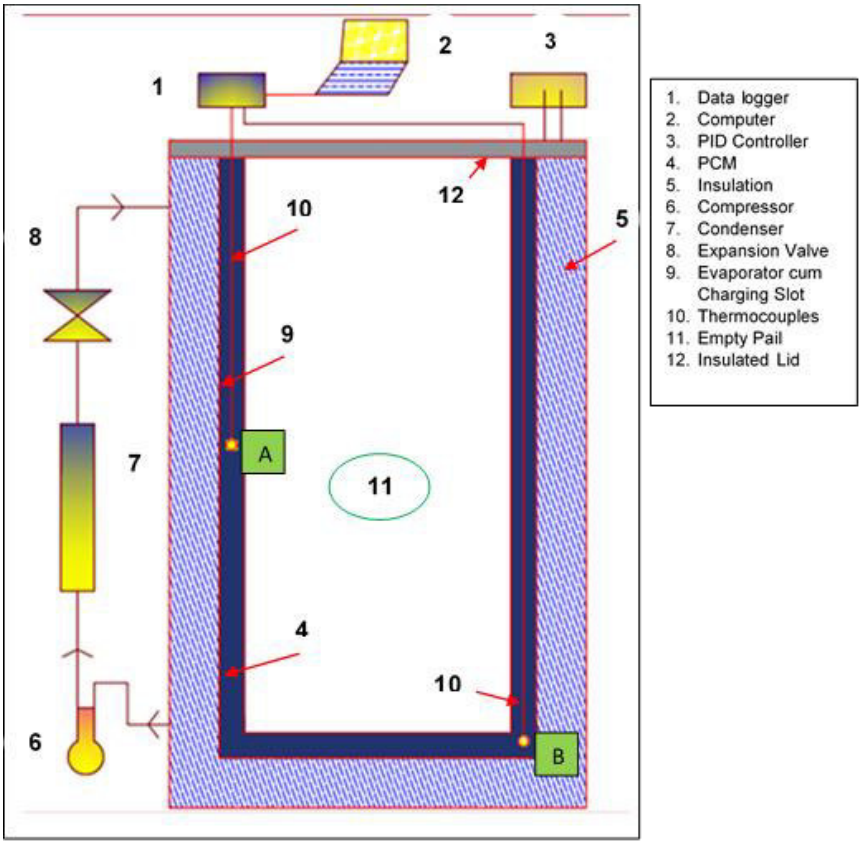
1
2
3
4
5
6
7
8
9
10
10
11
12
A
B
1. Data logger
2. Computer
3. PID Controller
4. PCM
5. Insulation
6. Compressor
7. Condenser
8. Expansion Valve
9. Evaporator cum Charging Slot
10. Thermocouples
11. Empty Pail
12. Insulated Lid

(a)

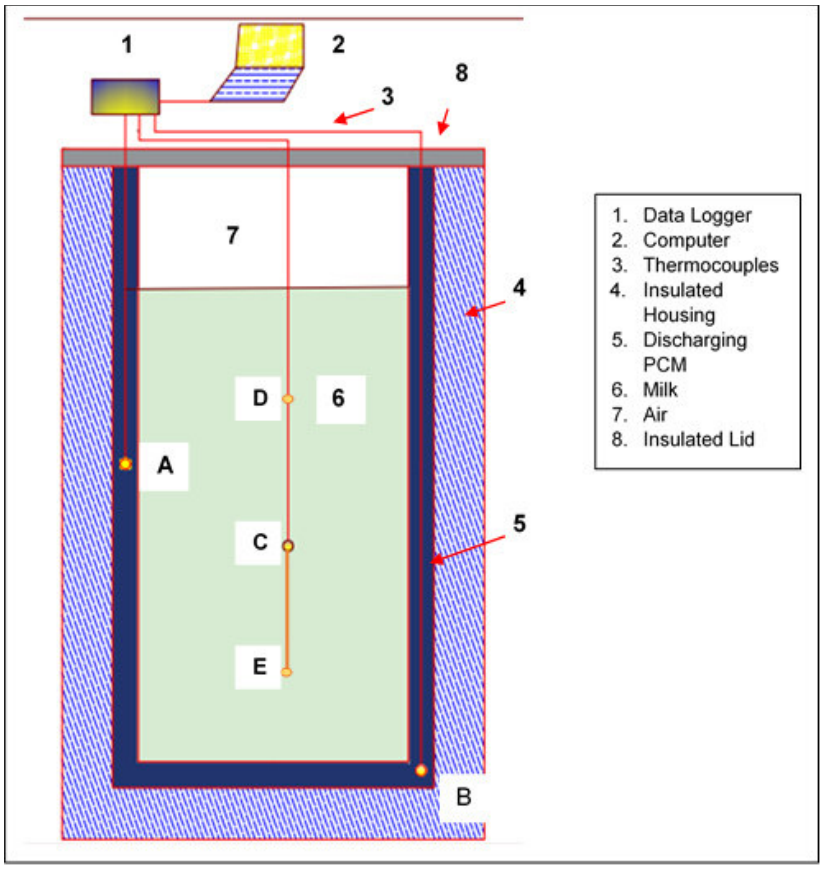

(b)

Fig. 3.17 Schematic diagram of the experimental set up during **(a)** charging of the NePCM; **(b)** discharging of the NePCM during passive milk chilling

3.2.6.2 Discharging of the PCM and milk chilling

For Spherical Module:

The experimental set up for discharging comprised of an insulated ordinary milk vessel (196.5 mm × 196.5 mm) holding the spherical module of said specifications and containing the charged PCM. The charged module was placed at center of the vessel, completely submerged inside a pool of 5L of raw milk (initially at 37°C, the normal milk drawing temperature). The thermocouples were plugged to a computer linked data logger to record the temperature profiles of discharging PCM within the module and the surrounding milk being chilled, The temperature was continuously recorded at an interval of every second at set locations (points 'A', 'B', 'C' inside the module and 'D', 'E', 'F', 'G' within the milk bath), as shown in the Fig. 3.16 (b). The discharging trials for the PCM (at different concentration)

for the chilling of milk were carried out in triplicate to ensure the accuracy and repeatability, and the average values were plotted.

Finally, the data generated during the CFD simulation were validated by comparing with corresponding real time experimental results. During discharging and consequent milk chilling, it was not practical to determine exact transient values of β. Therefore, in order to estimate comparable values of β, the charged modules were firmly placed in an inverted position inside a Bio-Oxygen Demand (BOD) incubator (at fixed temperature of 37°C) and the drips of the melted PCM were collected in a measuring flask. The instantaneous transient values of β, thus obtained, were assumed to be comparable to the liquid fraction inside the module during discharging, and used to compare with computed predictions.

For Jacketed Cylindrical Module:

The experimental set-up for discharging of the charged NePCM by exchanging heat with milk, comprised of a cylindrical shape container of similar dimensions as discussed during charging (Fig. 3.17b). The central empty part of the container was filled with 5-6L of milk (at t = 0 min, 37°C) covering up to 80-90% of total volume and leaving around 10% as air space and foams. The container filled with milk was housed inside an insulated container (fabricated matching with the container's dimensions) to avoid heat gain from surroundings.

The container was connected with PT-100 thermocouples centered inside a ferrule lock system, coupled with a computer and data logger, to record the transient temperature profiles of milk at points 'C', 'D' and 'E' along centerline of the pail and that of NePCM at points 'A' and 'B' (Fig. 3.17b).

For Jacketed Cylindrical Module with agitator:

The experimental set up for energy discharging of the pre-charged NePCM due to milk chilling comprised of an empty (i.e. empty central part for receiving milk) jacketed cylinder in the shape of an ordinary milking container (outer: inner dia. :: 205 : 160 mm) having an agitator (centrally oriented and top mounted; design aspects same as discussed in the simulation model) and NePCM was filled inside the jacketed space (20 mm). The stored cooling energy in the NePCM exchanged heat from milk, and thereby cooled it. The agitator

was coupled with a DC-motor of fixed power supply and speed control mechanisms (Fig. 3.18a-c). The central empty part of the container was filled with 5-6L of milk (at t =0 min, 37°C) covering up to 80-90% of total volume and leaving around 10% as air space and foams. The container filled with milk was housed inside an insulated container (fabricated matching with the container's dimensions) to avoid heat gain from surroundings.

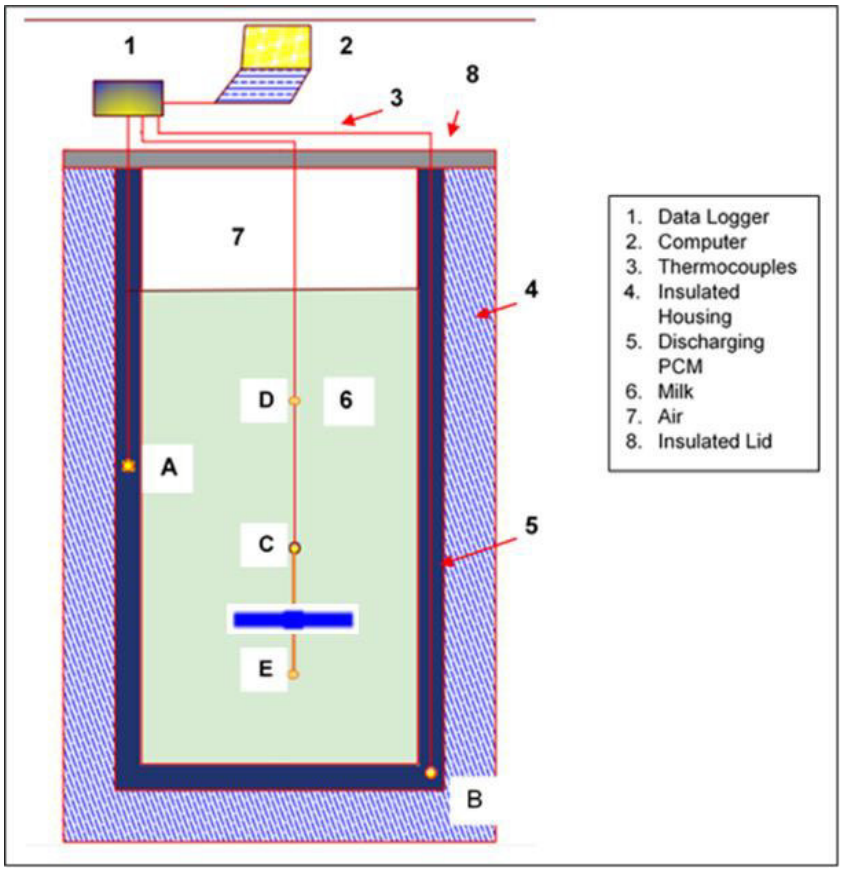

(a)

(b) **(c)**

Fig. 3.18 Schematic diagram of the experimental set up during **(a)** energy discharging from the NePCM due to passive milk chilling; **(b & c)** fabricated milk chilling module.

The container was connected with PT-100 thermocouples centered inside a ferrule lock system, coupled with a computer and data logger, to record the transient temperature profiles of milk at points 'C', 'D' and 'E' along centerline of the pail and that of NePCM at points 'A' and 'B' (Fig. 3.18a).

The discharging trials with NePCM during milk chilling were carried out in triplicate to ensure the accuracy and repeatability, and the average values were plotted. The experimental results obtained were compared with the CFD simulated data. During discharging and consequent passive milk chilling, it was not practical to determine exact transient values of β, therefore in order to arrive the comparable values, the charged container was firmly placed in an inverted position inside a BOD incubator (at fixed temperature 37°C) and the drips of the melted NePCM were collected in a measuring flask, thereby instantaneous transient values of β were calculated and compared with the CFD computed predictions.

3.2.7 Quality Evaluation of Chilled Milk

3.2.7.1 Milk Methylene blue reduction time (MBRT) analysis

The MBRT analysis of raw milk cooled by the developed milking pail modules (in the shape of jacketed cylinder) and of control (raw milk kept in an ordinary milk pail for 6h at ambient temperature after milking) was carried out.

Methylene blue tri-hydrate, powder purchased from HiMedia Laboratories Pvt. Ltd., Mumbai was used for MB solution. Exactly 0.0033g of MB powder was dissolved in 100 mL of distilled water, mixed well, heated till boiling and sterilized. The methylene blue reduction time test of milk was determined as per the standard procedure. The procedure for methylene blue test of milk is as follows

Procedure for MBRT analysis

1. Milk sample (10 mL) was transferred into a sterile test tube.
2. Added 1 mL of methylene blue dye to the test tube.
3. The methylene blue dye solution and milk were mixed by inverting the test tube.
4. The tubes were placed in the water bath maintained at constant temperature of 37°C.
5. The test tubes were observed every 30 min for the reduction of colour.
6. The observation was continued until complete reduction of the dye occurred and the time taken for complete discoloration was noted.

3.2.7.2 Total bacterial count (TBC)

The TBC analysis of raw milk cooled by the developed milking pail modules (in the shape of jacketed cylinder) and of control (raw milk kept in an ordinary milk pail for 6h at ambient temperature after milking) was carried out using following procedure.

Preparation of diluent physiological saline solution

Exactly 8.5g of sodium chloride (NaCl) was weighed and added to 1000mL of distilled water and mixed well. The aliquots of (99mL and 9mL) solution were transferred to the dilution bottle and test tubes of required numbers. Then the diluent was sterilized by

placing the dilution bottle and tubes in an autoclave at 1.05 kg/cm^2 steam pressure (at 121ºC) for 20min.

Preparation of media–milk agar (MA)

Exactly 24g of readily available milk agar (MA) was weighed. It was added to 1000mL of distilled water and mixed well. After dissolving the powder by heating it to boiling, the media was sterilized at 121ºC in an autoclave at 1.05 kg/cm^2 steam pressure for 20 min.

The standard plate count test of milk samples was determined by using serial dilution technique. The procedure for total bacterial count test of milk is as follows

Procedure

1. All the materials were sterilized before the start of experiment.
2. The bottle containing the sample of milk was shaken well. Milk (1 mL) was transferred with a sterile pipette to the tube of dilution (9 mL of saline solution) and rotated for the complete mixing. This made a dilution of 1:10.
3. From the first dilution, 1 mL was transferred (1:10) to another 9 mL dilution blank to make 1:100 or to a 99 mL dilution blank to make 1:1000 dilution.
4. Thus serial dilution technique was employed to prepare 3rd, 4th and 5th dilutions.

Preparation and incubation of plates

- One mL of the diluted sample was transferred into sterile petriplate using a fresh and sterile pipette.
- To each plate 10-15 mL of MA was added which was previously melted and cooled to 45ºC.
- The contents were mixed thoroughly while the medium was still liquid, by gently rotating and tilting the petriplate then the agar was allowed to cool and set.
- The plates were inverted and incubated at 37ºC for 48h.
- The plates were removed after 48h of incubation and the plates were counted having colonies 30 and 300.

- The average of the counts in the 3 plates was determined and this was multiplied by the dilution factor.
- The results were expressed as standard plate count per mL of milk.

3.2.7.3 Determination of pH and titratable acidity (TA)

The pH and TA analysis of raw milk cooled by the developed milking pail modules (in the shape of jacketed cylinder) and of control (raw milk kept in an ordinary milk pail for 6h at ambient temperature after milking) was carried out and compared. The pH was measured by using digital electronic pH-meter. Before pH measurement, the pH meter was calibrated by distilled water at pH =7.0. Titratable acidity (TA) of milk was measured by titrating 10 mL of milk against a standard alkali solution (0.1N NaOH) in the presence of 1 mL 0.5% phenolphthalein as an indicator till pink color as end point appeared.

Per cent acidity was determined by following calculation.

$$\% \text{ acidity} = \frac{9AN}{V} \text{ expressed as \% of lactic acid.} \qquad \ldots(3.27)$$

Where, A : Volume of 0.1N NaOH used for titration till end point

V : Quantity of milk taken for analysis (10 mL)

N : Normality of NaOH solution (0.1N)

3.2.8 Evaluation of cooling performance of the developed pail modules on farm level

The developed milking pail modules were tested on farm under real-time environs at Livestock Research Centre of SRS of ICAR-NDRI, Bengaluru (Fig 3.19). After charging, the developed pails were carried to the Livestock Research Centre in the insulated housing. The milking was done directly into the charged pails and the transient temperature profiles were recorded. Raw milk was chilled inside the module during milking as well as its conveyance to the Dairy Engineering Laboratory. The quality parameters of milk thus chilled were compared with the control.

Fig. 3.19. On-Farm Testing of the Module

3.2.9 Thermal Cyclic Performance of the NePCM

Thermal cyclic tests of the final NePCM (which performed best) was carried out in subsequent charging and discharging cycles for evaluating its effect on milk cooling performance. Moreover, a representative sample of the NePCM was frozen and melted in controlled conditions similar to that of charger inside a deep freezing chamber as shown in Fig. 3.20. The temperature profiles during subsequent cycles were recorded and compared up to 1000 cycles.

Fig. 3.20 Thermal Cyclic test of NePCM

3.2.10 Co-efficient of performance (COP) of the charger unit for the developed milking pail unit

COP of the refrigeration cum charger unit was evaluated as follows:

$$COP = \frac{\text{Net Refrigeration Effect Produced}}{\text{Work Done}} = \frac{\text{Amount of energy stored in PCM by charging}}{\text{Power Consumed}} \quad \ldots(3.28)$$

3.2.11 Statistical and Error Analysis

The effects of level of nanoparticles and the temperature on 'k' values as well as milk temperature drop, were analyzed using the univariate analysis of variance by asymmetric factorial design. The statistical model employed was as follows:

$$Y_{ijk}=\mu+\alpha_i+\beta_j+\alpha\beta_{ij}+e_{ijk} \quad \ldots(3.29)$$

(Where, i = 1, 2, 3; j =1, 2, 3, 4, 5; k = 1 to n); μ: Overall mean effect, α_i : the effect of i^{th} level of nanoparticle concentration, β_j : effect of j^{th} level of temperature, $(\alpha\beta)_{ij}$: the effect of interaction between the two factors, e_{ijk} : a random error component having a normal distribution with mean zero and variance 1.

The probability (p) ≤ 0.05 was considered as statistically significant. Statistical significance of the differences across the different treatments was analyzed by Post-hoc Tukey's test using the Statistical Package for Social Sciences (SPSS 20.00 Software for Windows).

The errors associated with the instrumental results of the various properties were quantified to understand the extent of uncertainty (e_{Ri}) of the experimental parameter (R) for an independent variable (x_i), by equations 3.30 and 3.31 as suggested in the literature (Holman, 1989).

$$e_{Ri}= \frac{x_i}{R}\frac{\partial R}{\partial x_i}e_{x_i} \qquad \ldots(3.30)$$

$$\max.e_R= \pm\sqrt{\left[\left(\frac{x_1}{R}\ \frac{\partial R}{\partial x_1}e_{x_1}\right)^2+\left(\frac{x_2}{R}\ \frac{\partial R}{\partial x_2}e_{x_2}\right)^2+\left(\frac{x_3}{R}\ \frac{\partial R}{\partial x_3}e_{x_3}\right)^2+\ldots+\left(\frac{x_n}{R}\ \frac{\partial R}{\partial x_n}e_{x_n}\right)^2\right]} \qquad \ldots(3.31)$$

Mean absolute percentage errors (MAPE) were estimated to quantify the difference between the numerically simulated and experimental results using following relations:

$$MAPE=\left(\frac{100}{n}\right)\sum_{i=1}^{n}\left|\frac{(y_i-\hat{y}}{y_i}\right| \qquad \ldots(3.32)$$

Where, y_i : the experimental value, $y^{\wedge}$: the corresponding simulated value, n: number of fitted points.

3.2.12 Empirical relations for properties of mixture

Density (ρ) and dynamic viscosity (μ) of the base fluid and PCM at average room temperature were calculated using the following empirical relations (Equations 3.33 and 3.34) suggested for nanoparticle-liquid mixture (Pantzali *et al.* 2009):

$$\rho_{nf}=\varphi\rho_{np}+(1-\varphi)\rho_{bf} \qquad \ldots(3.33)$$

$$\mu_{nf}=(1+2.5\varphi)\mu_{bf} \qquad \ldots(3.34)$$

where, ϕ: fraction of nanoparticles dispersed, subscripts viz., *nf*: nanofluid, *bf*: base fluid and *np*: nanoparticle.

CHAPTER-4

RESULTS AND DISCUSSION

This chapter deals the results and discussion part of the present investigation on design and development phase change material (PCM) based milking cum cooling pail. As per the engineering design calculations, the milk pails modules were developed and fabricated for an average capacity of milk generally handled by a small to marginal farmer per head per milking. For developing energy storage fluids (viz. PCM), different base fluids viz., distilled water (DW), distilled water+propylene glycol (DW+PG), distilled water+ethylene glycol (DW+EG) and distilled water+silver nano-ionic solution (DW+AgNP) were used as dispersing media for TiO_2, CeO_2 and Si_3N_4 nanoparticles. The developed base fluids and PCMs were characterized for thermo-physical, charging, discharging and milk cooling behavior to arrive best base fluids and nanoparticle combination and composition. The selected nanoparticle enhanced PCM (NePCM) were preliminary tested in a spherical shaped enclosure and then filled into the jackets of the cylindrical container module resembling a milk pail.

The transient phenomena involved in charging (energy storage) and discharging (energy release) of NePCM during milk cooling were first simulated and then validated with the experiments in spherical as well as actual pail module. Trials conducted to determine the energy storage behavior of base fluids and NePCM inside the developed modules. Performance evaluation of the customized charger unit in terms of co-efficient of performance (COP) were also investigated. Effect of cooling fresh raw milk on its microbiological parameters (total bacterial count and methylene blue reduction time) and chemical parameters (pH and titratable acidity) are also presented and discussed in this chapter. Thus, Results and discussion of the experiments are presented under the following headings:

4.1 Characterization of nanoparticles, base fluids and NePCM

4.2 Numerical and experimental study on thermal behavior of NePCM inside the spherical module

4.3 Numerical and experimental study on thermal behavior of NePCM inside the jacketed cylindrical milking pail module

4.4 Numerical and experimental study on thermal behavior of NePCM inside the jacketed cylindrical milking pail module with and without agitator

4.5 On-farm testing of performance of the milking pail module

4.1 Characterization of nanoparticles, base fluids and NePCM

Based on preliminary trials it was observed that addition of glycol (either PG or EG) more than 10% level, reduced the energy storage capacity in the latent heat energy storage system significantly. Though it increased the depression in freezing points of final mixture, thereby net temperature difference (ΔT) between coolant and milk also during cooling process, but parallelly it decreased latent heats (ΔH) also. Latent heats are considered as major energy storage tools by phase-change. Increasing ΔT, could be helpful in system like a plate heat exchanger (consisting flow of a coolant), but seemed less important in the present designs of cooling modules taken up in this study. In the present design, a batch-wise storage of cooling energy inside the milking pails was theorized, to maintain milk-cold longer after harvesting or milking, therefore rather than increasing ΔT, protecting ΔH appeared more important. Therefore, distilled water (DW), distilled water + 10% propylene glycol (DW+PG), distilled water + 10% ethylene glycol (DW+EG) and distilled water + silver nano-ionic solution (DW+AgNP), were selected as base fluids for developing NePCM. TiO_2, CeO_2 and Si_3N_4 nanoparticles were selected based on cost, availability, thermal stability and chemical reactivity, reported in literature.

4.1.1 Characterization of nanoparticles

Nanoparticles, prior to dispersion into the base fluids for NePCM preparations, were characterized by X-ray diffractometer (XRD) for phase-identification and purity. Fig. 4.1(a-c) indicate the XRD-patterns of the TiO_2, CeO_2 and Si_3N_4 nanoparticles. The peaks observed and phases identified were matched with the standard database to ensure purity of nano-materials.

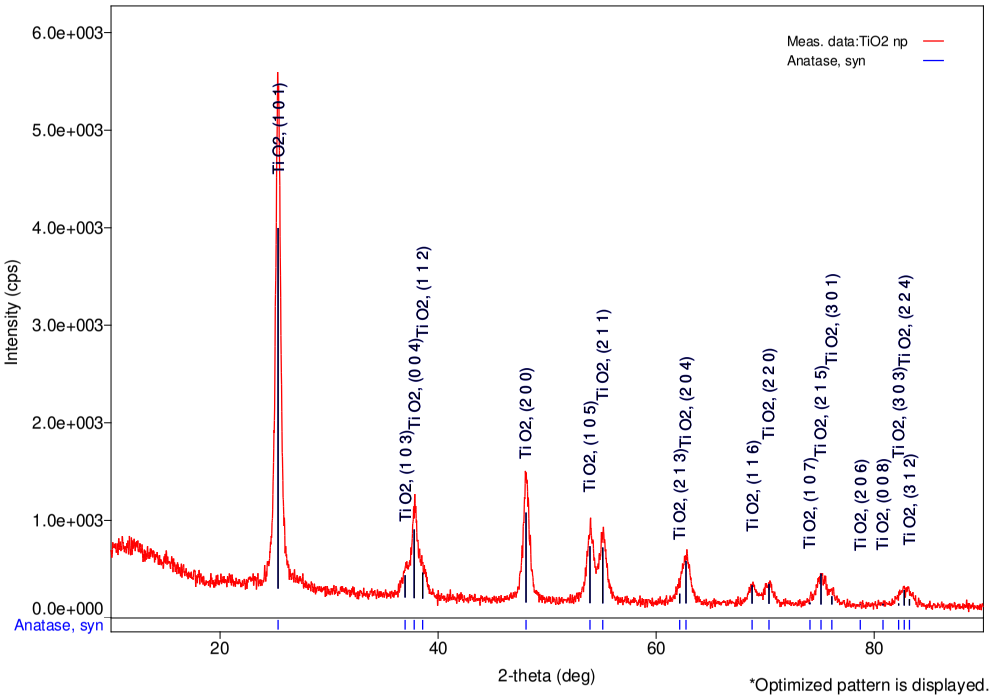

Fig. 4.1a XRD Pattern of TiO_2 Nano-particles

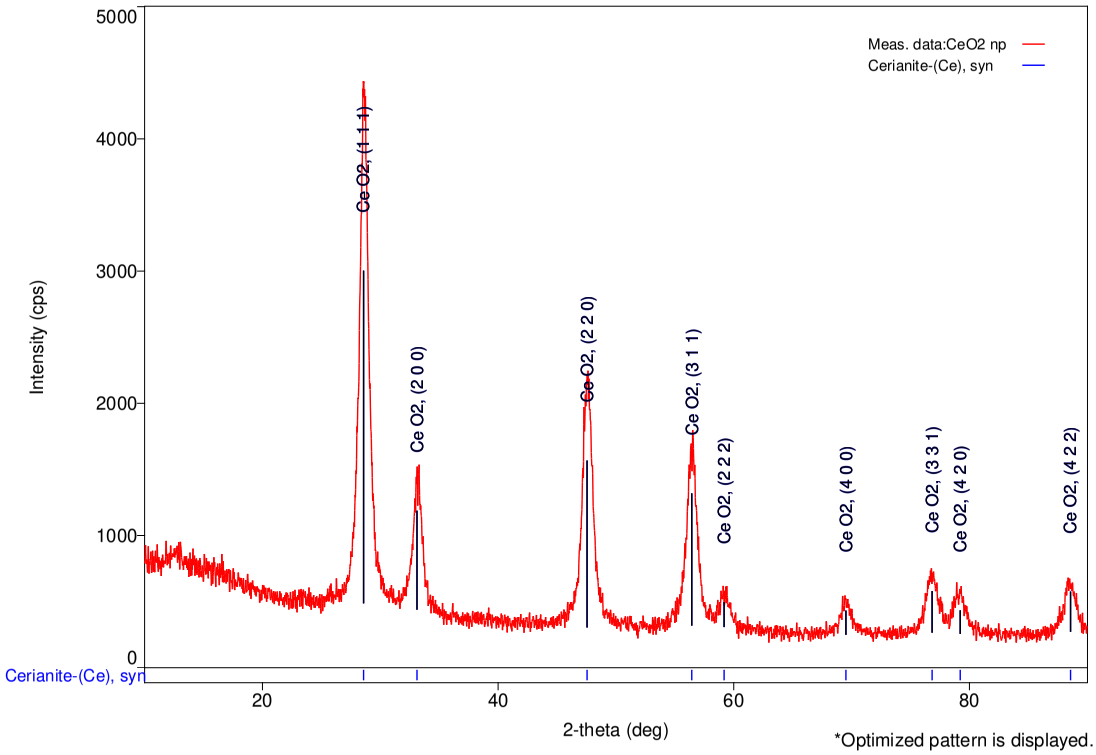

Fig. 4.1b XRD Pattern of CeO_2 Nano-particles

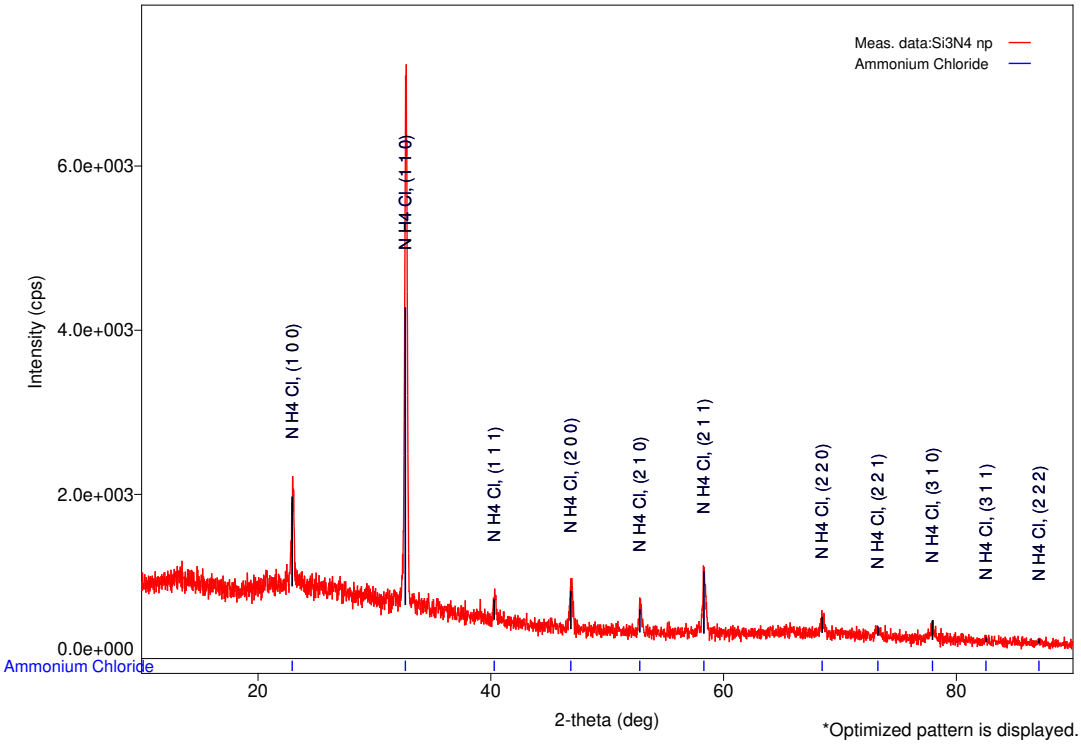

Fig. 4.1c XRD Pattern of Si_3N_4 Nano-particles

4.1.2 Thermal conductivity of NePCM

Thermal conductivities (k) of the base fluid 'DW' (at 0.00% nanoparticle) and NePCM prepared in DW, measured at different nanoparticle concentrations (0.00 to 1.00%) and different temperatures (0 to 40 °C), were shown in Fig. 4.2 (a-c).

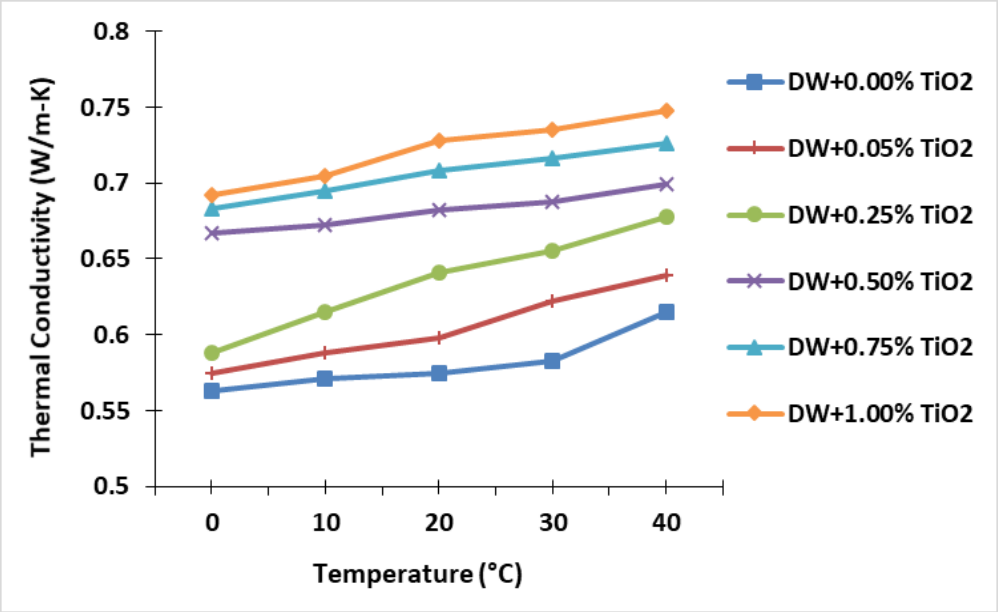

Fig. 4.2a Thermal Conductivity (W/m-k) vs temperature (°C) of TiO_2-DW-NePCM

Fig. 4.2a, indicates estimated marginal mean values of 'k' (dependent variable) of TiO_2-DW-NePCM as function of nanoparticle concentrations and temperatures at $p \leq 0.05$. The 'k' values in replications were analyzed at 0.00, 0.05, 0.25, 0.50, 0.75 and 1.00% of TiO_2 nanoparticle at 0, 10, 20, 30 and 40°C. It was observed that 'k' values were continuously increasing with increase of TiO_2 concentrations in the NePCM as well the temperature from 0 to 40°C. It was also evident that enhancement rates in 'k' values (indicated by slope of curves) with temperature rise were more at lower concentrations (up to 0.25% TiO_2), however it was saturated (slops turned flattened) and less in magnitude at 0.50, 0.75 and 1.00% level of TiO_2 nanoparticles in the NePCM.

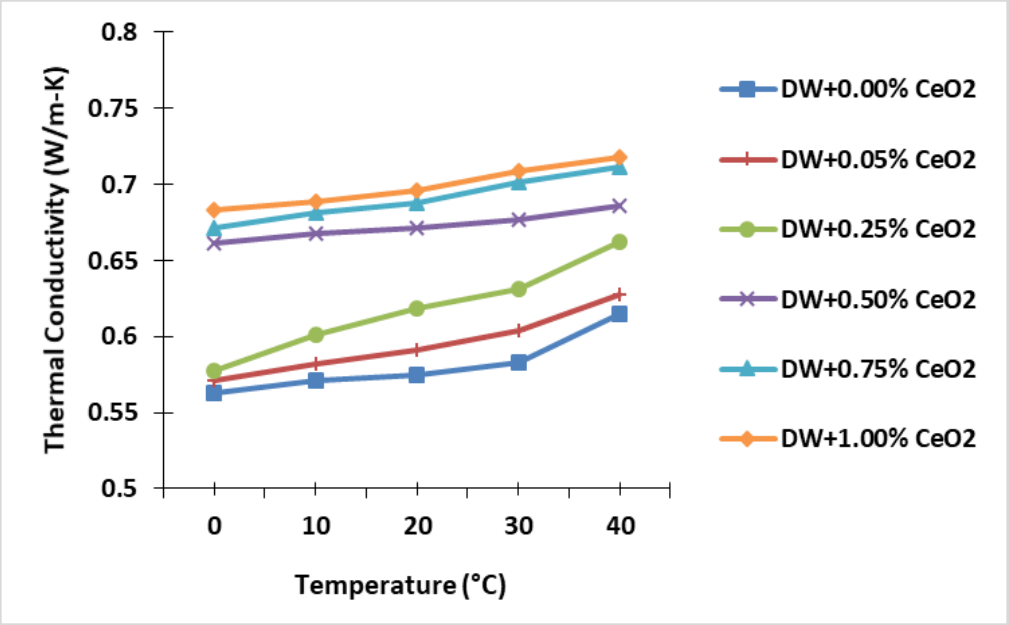

Fig. 4.2b Thermal Conductivity (W/m-k) vs temperature (°C) of CeO_2-DW-NePCM

Fig. 4.2b, indicates estimated marginal mean values of 'k' (dependent variable) of CeO_2-DW-NePCM as function of nanoparticle concentrations and temperatures at $p \leq 0.05$. The 'k' values in replications were reported at 0.00, 0.05, 0.25, 0.50, 0.75 and 1.00% of CeO_2 nanoparticles at 0, 10, 20, 30 and 40 °C. Similar trends of 'k' enhancements rates were observed in this case, as observed with TiO_2 nanoparticles, however the magnitude of these enhancements were less (restricted below 0.7 W/m-K) with CeO_2 nanoparticles in DW even at 1.00% weight fraction. Therefore, it was inferred that 'k' enhancements with CeO_2 nanoparticles in DW was saturated earlier than TiO_2 nanoparticles.

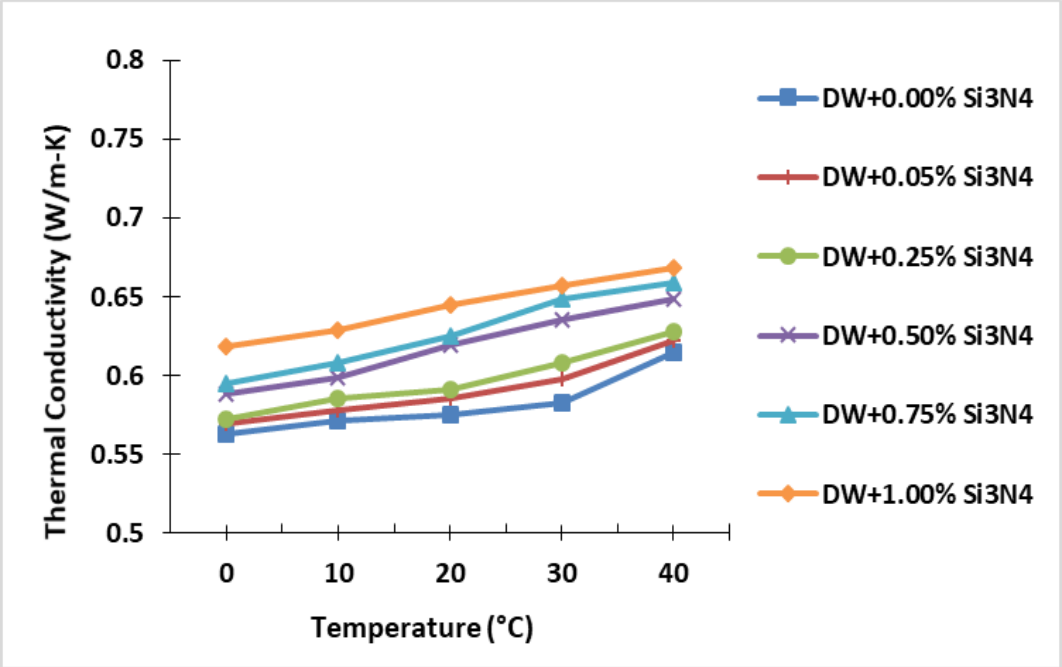

Fig. 4.2c Thermal Conductivity (W/m-k) vs temperature (°C) of Si_3N_4-DW-NePCM

Fig. 4.2c, indicates estimated marginal mean values of 'k' (dependent variable) of Si_3N_4-DW-NePCM as function of nanoparticle concentrations and temperatures at $p \leq 0.05$. The 'k' values in replications were analyzed statistically, at 0.00, 0.05, 0.25, 0.50, 0.75 and 1.00% of Si_3N_4 nanoparticles at 0, 10, 20, 30 and 40°C. The trends of 'k' enhancements rates in this case were also similar to that observed with CeO_2 and TiO_2 nanoparticles, however the magnitude of these enhancements were further less (restricted below 0.65 W/m-K) with Si_3N_4 nanoparticles in DW even after raising weight fractions of Si_3N_4 up to 1.00%. Therefore, it was inferred that 'k' enhancements with Si_3N_4 nanoparticles in DW were saturated earlier than TiO_2 and CeO_2 nanoparticles.

In any case (Fig. 4.2a-c), the enhancement rates in 'k' values were slower from 0 to 20°C, whereas rapid in 20 to 40°C temperature range. This could be attributed to augmentation in Brownian motions of nanoparticles, thereby micro-convection in the base fluid matrix.

Findings of the present study ('k' enhancements) were found in line with the reports published in literature by Liu *et al.* (2009) for TiO_2 nanoparticles dispersed into $BaCl_2$-salt eutectics, Żyła *et al.* (2018) for Si_3N_4 in EG and Keyvani *et al.* (2018) for CeO_2 in EG.

Thermal conductivities (k) of the base fluid 'DW+PG' (at 0.00% nanoparticle) and NePCM prepared in 'DW+PG', measured at different nanoparticle concentrations (0.00 to 1.00%) and different temperatures (0 to 40°C), were shown in Fig. 4.3(a-c).

Fig. 4.3a, indicates estimated marginal mean of measured values of 'k' of TiO_2-DW+PG-NePCM as function of nanoparticle concentrations and temperatures. The 'k' values in replications were measured at 0.00, 0.05, 0.25, 0.50, 0.75 and 1.00% concentration of TiO_2 nanoparticle at 0, 10, 20, 30 and 40°C.

It was observed that the enhancement rates in 'k' values with increasing nanoparticle concentrations and temperatures were similar to that in 'DW' based NePCMs, however, the magnitude of 'k' values at a given temperature and nanoparticle concentration, were less in DW+PG based NePCMs as compare to that in DW. It is evident from the plot that even at 1.00% weight fraction of TiO_2 in the base fluid (DW+PG), the 'k' values were up to 0.680 W/m-K, whereas at same concentration of TiO_2 in DW, it was nearly 0.750 W/m-K. Therefore, it was inferred that addition of PG into water negatively affected the thermal conductivity enhancements.

Fig. 4.3b, indicates estimated marginal mean of measured values of 'k' in CeO_2-DW+PG-NePCM as function of nanoparticle concentrations and temperatures. The 'k' values in replications were measured at 0.00, 0.05, 0.25, 0.50, 0.75 and 1.00% concentration of TiO_2 nanoparticle at 0, 10, 20, 30 and 40°C. It was observed that enhancement rates in 'k' values using CeO_2 nanoparticles in DW+PG base fluid were less than that with TiO_2 nanoparticles at a given temperature and weight fraction.

Fig. 4.3c, indicates estimated marginal mean of measured values of 'k' in Si_3N_4-DW+PG-NePCM as function of nanoparticle concentrations and temperatures. The 'k' values in replications were measured at 0.00, 0.05, 0.25, 0.50, 0.75 and 1.00% concentration of TiO_2 nanoparticle at 0, 10, 20, 30 and 40°C. It was observed that enhancement rates in 'k' values using Si_3N_4 nanoparticles in DW+PG base fluid were less than that with TiO_2 and CeO_2 nanoparticles at a given temperature and weight fraction.

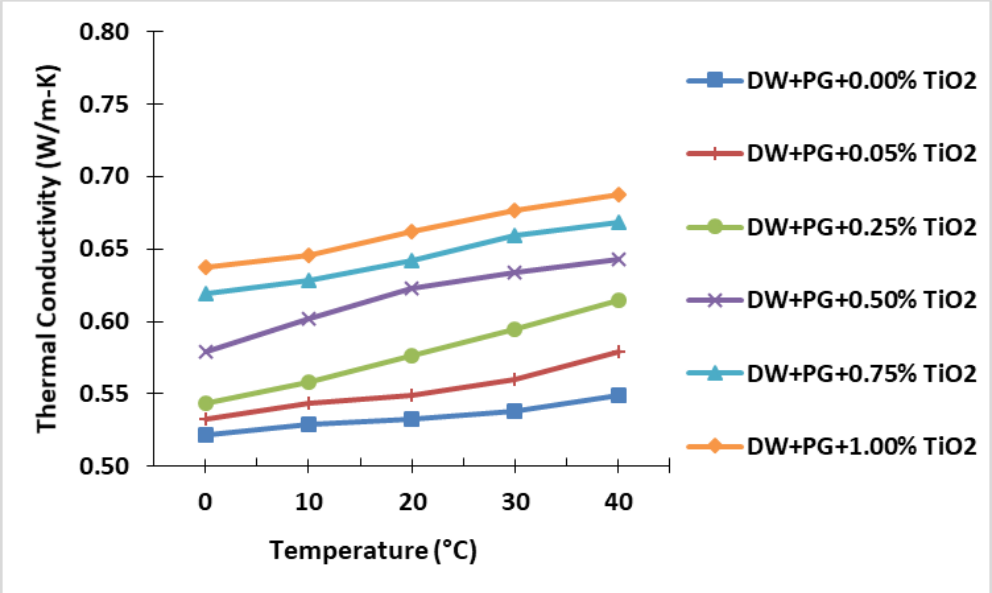

Fig. 4.3a Thermal Conductivity (W/m-k) vs temperature (°C) of TiO_2-DW+PG-NePCM

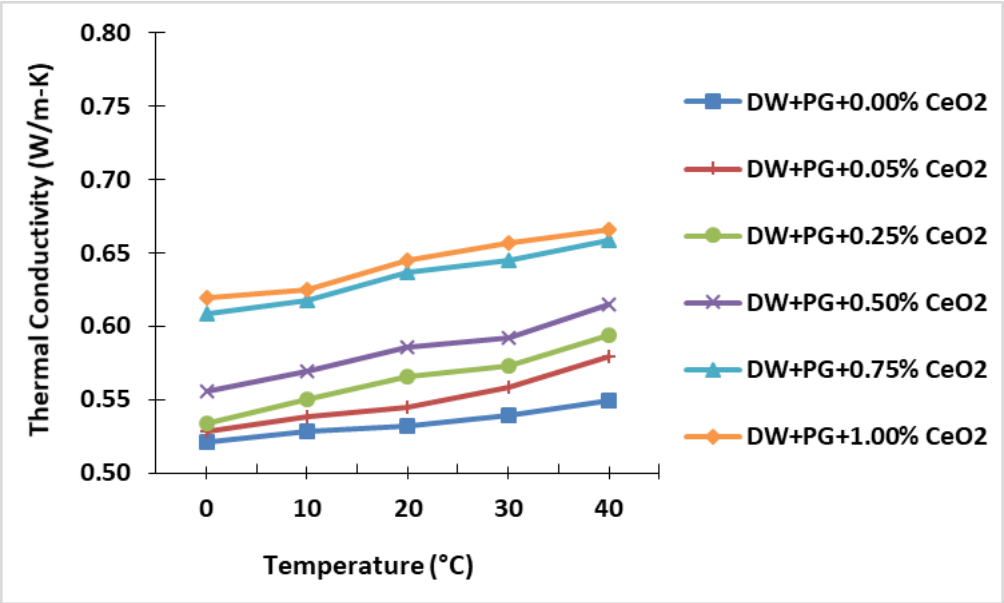

Fig. 4.3b Thermal Conductivity (W/m-k) vs temperature (°C) of CeO_2-DW+PG-NePCM

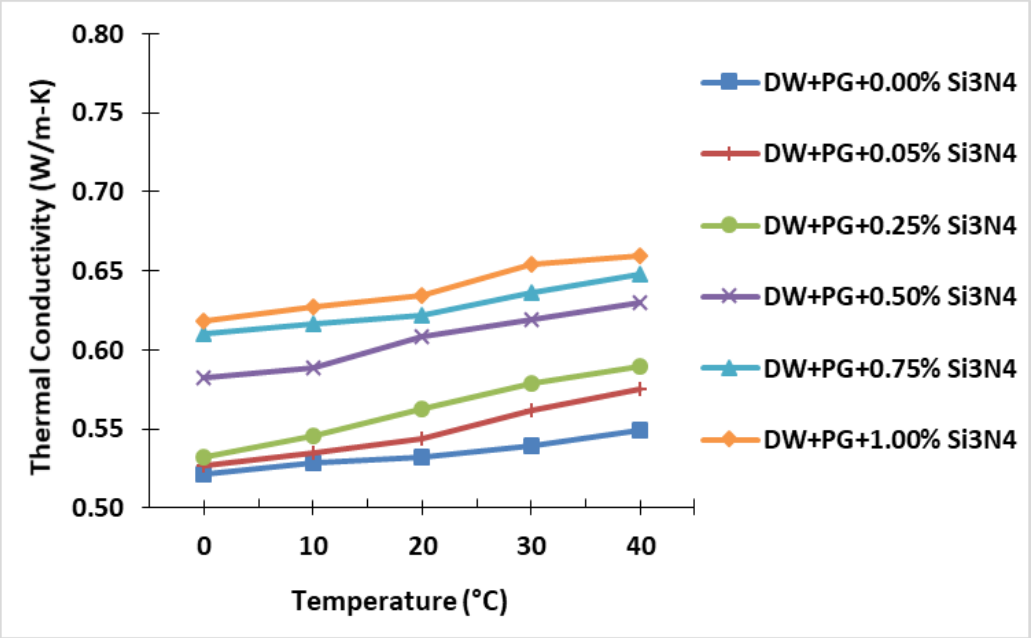

Fig. 4.3c Thermal Conductivity (W/m-k) vs temperature (°C) of Si_3N_4-DW+PG-NePCM

Thermal conductivities (k) of the base fluid 'DW+EG' (at 0.00% nanoparticle) and NePCM prepared in 'DW+EG', measured at different nanoparticle concentrations (0.00 to 1.00%) and different temperatures (0 to 40°C), were shown in Fig. 4.4 (a-c).

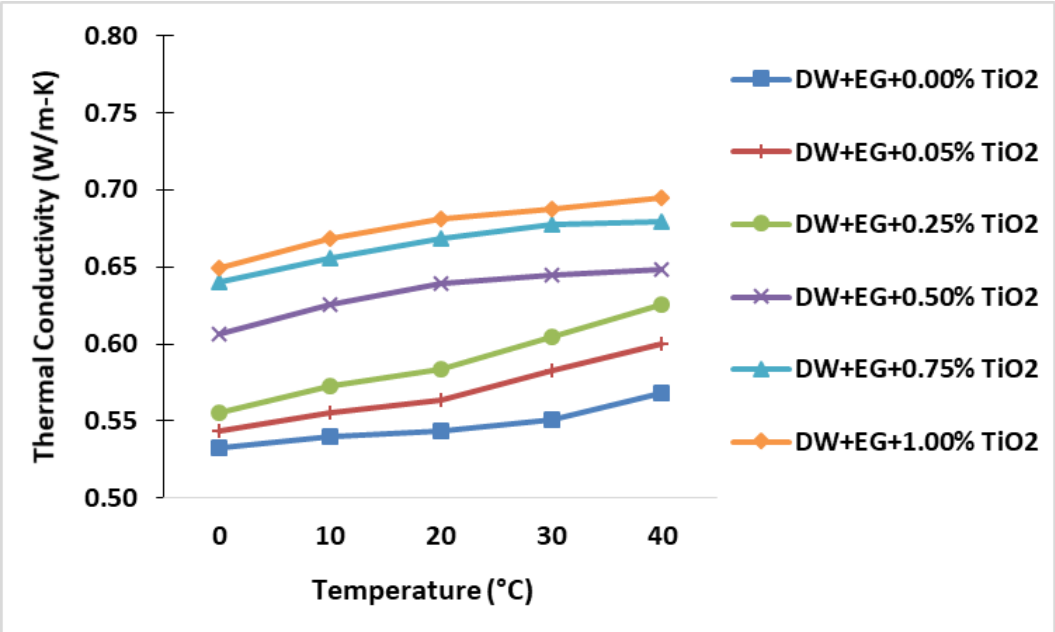

Fig. 4.4a Thermal Conductivity (W/m-k) vs temperature (°C) of TiO_2-DW+EG-NePCM

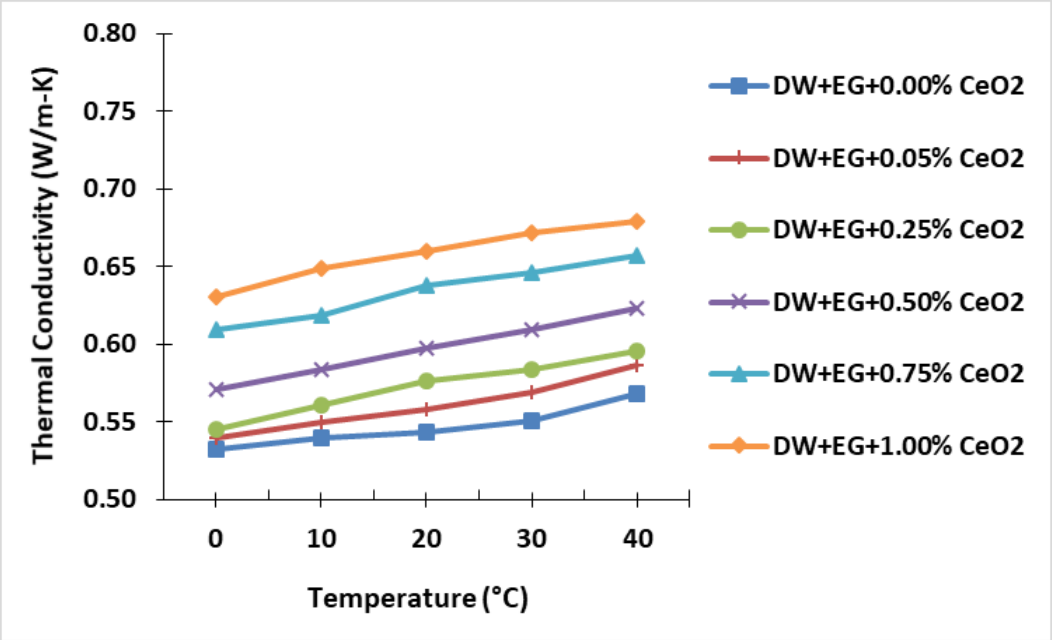

Fig. 4.4b Thermal Conductivity (W/m-k) vs temperature (°C) of CeO_2-DW+EG-NePCM

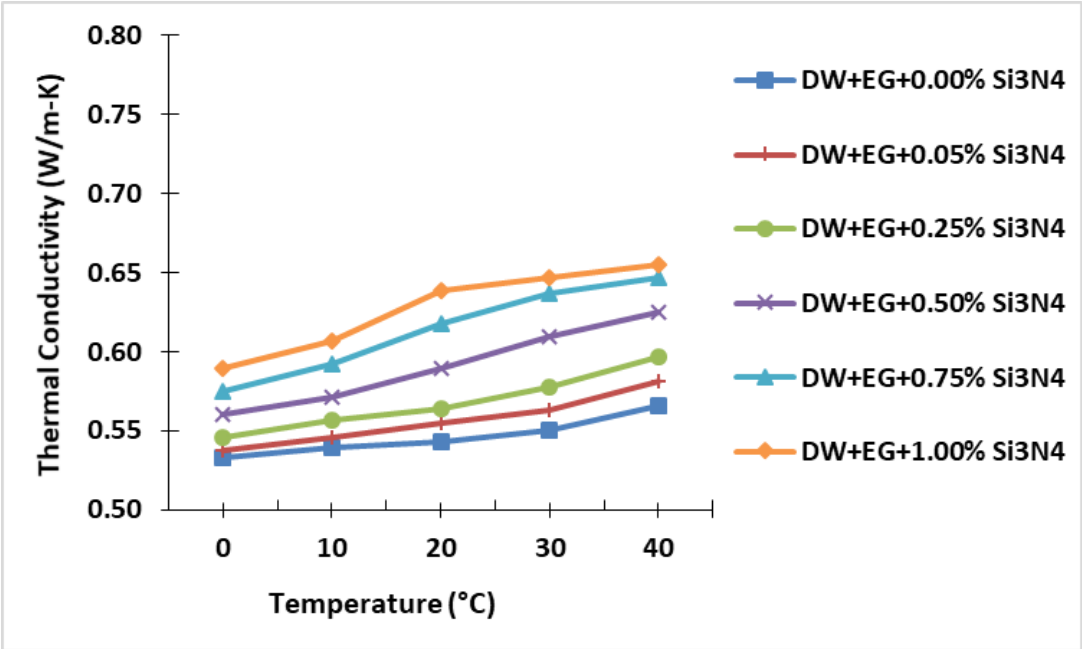

Fig. 4.4c Thermal Conductivity (W/m-k) vs temperature (°C) of Si_3N_4-DW+EG-NePCM

It was observed from, Fig. 4.4 (a-c), that the enhancement in 'k' values at a particular temperature and weight fraction of nanoparticles were as follows: TiO_2>CeO_2>Si_3N_4. The enhancement rates due to rise in temperature were more from 0-0.25% of nanoparticles, however, it was saturated in the range 0.50 to 1.00% of nanoparticles. In all cases, 1% level of nanoparticles enhanced the magnitude of 'k' by maximum values.

Thermal conductivities (k) of the base fluid 'DW+AgNP' (at 0.00% nanoparticle) and NePCM prepared in 'DW+AgNP', measured at different nanoparticle concentrations (0.00 to 1.00%) and different temperatures (0 to 40°C), were shown in Fig. 4.5 (a-c).

Fig. 4.5a, indicated that 'DW+AgNP' as a base fluid possessed highest thermal conductivity among all the other base fluids viz. DW, DW+PG, DW+EG. It was also noticed from slopes of thermal conductivity vs temperature curves that degree of saturation in 'k' enhancements were negligible up to 0.75% of TiO_2, however, it was slightly observed at 1.00% of TiO_2 between 30-40°C.

Fig. 4.5b, indicated that enhancements in 'k' values with CeO_2 nanoparticles were less in magnitude than TiO_2 nanoparticles at a particular temperature and weight fraction the base fluid 'DW+AgNP'. Saturation in 'k' enhancements were negligible up to 0.50 % weight fractions of nanoparticles and significant thereafter.

Fig. 4.5c, indicated that enhancements in 'k' values with Si_3N_4 nanoparticles were less in magnitude than TiO_2 and CeO_2 nanoparticles at a particular temperature and weight fraction the base fluid 'DW+AgNP'. Saturation in 'k' enhancements were negligible only up to 0.25% weight fractions of nanoparticles and significantly persisted thereafter.

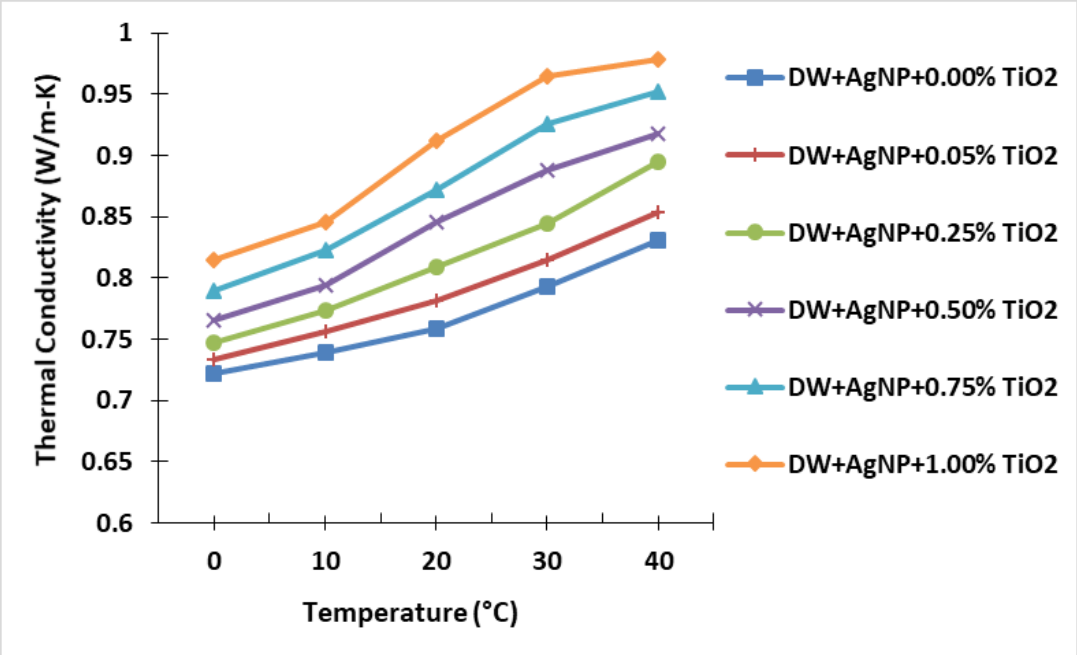

Fig. 4.5a Thermal Conductivity (W/m-k) vs temperature (°C) of TiO_2-DW+AgNP-NePCM

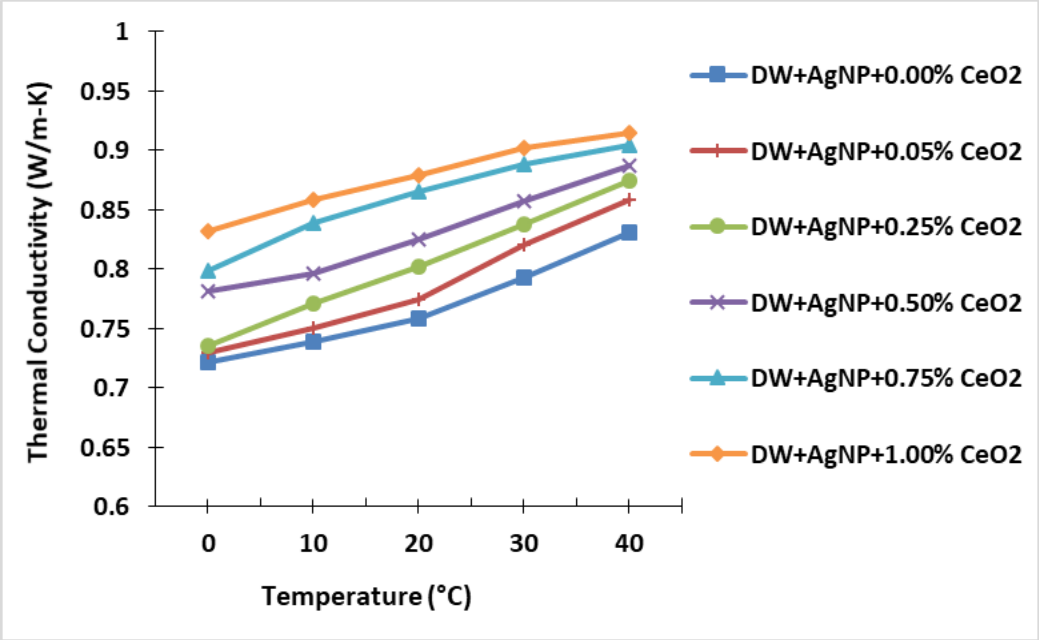

Fig. 4.5b Thermal Conductivity (W/m-k) vs temperature (°C) of CeO_2-DW+AgNP-NePCM

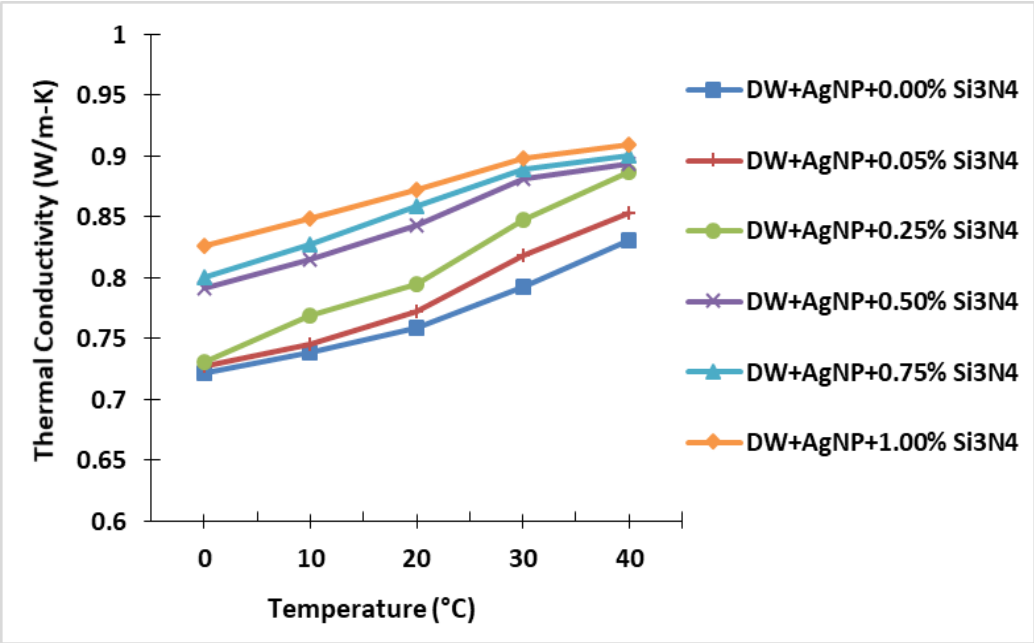

Fig. 4.5c Thermal Conductivity (W/m-k) vs temperature (°C) of Si_3N_4-DW+AgNP-NePCM

Therefore, based on thermal conductivity analysis of base fluids and NePCM, following points could be inferred:

- Thermal conductivity of base fluids: DW+AgNP > DW > DW+EG > DW+PG.
- Thermal conductivity enhancements by nanoparticles in a given base fluid: TiO_2 > CeO_2 > Si_3N_4.

- Saturation in 'k' enhancements due to rise in temperature : 0 to 30°C : negligible; 30-40°C: significant
- Saturation in 'k' enhancements due to rise in weight fraction of nanoparticles: 0 to 0.25%: negligible; 0.25 to 0.50%: moderate, 0.50 to 1.00%: significant.
- 1.00% weight fraction of nanoparticles exhibited maximum enhancement in 'k'.

4.1.3 Scanning Electron Microscopic (SEM) study of NePCM

Based on preceding observations in 'k' enhancements, SEM analysis of selected NePCM were carried out to understand the morphology and surface characteristics of nanoparticles in the PCM matrices.

Fig. 4.6 (a-c), indicated SEM-images of 0.25, 0.50 and 1.00% TiO_2 in DW-NePCM at 100 KX magnification. From comparative analysis SEM-micrographs, it was deduced that at low weight fraction of nanoparticles (say 0.25% TiO_2), the base matrix (i.e. base fluid network) consisted more empty/void space (due to less crowding) between subsequent nanoparticle clusters (Fig. 4.6a). This eased the free movement of nano-particles by Brownian motion in the base matrix network due to rise in temperature. This could be possible reason for higher enhancement rates in 'k' values at lower nanoparticle concentrations due to rise in temperature, as discussed in the previous sections.

However, at lower nanoparticle concentrations, the overall conduction effects might be low due to presence of voids. This could be the reason for lower magnitude of 'k' (of NePCM) at low weight fractions of nanoparticles. It was also noticed that at higher weight fractions (0.50 and 1.00%), TiO_2 nanoparticles were closely packed, minimizing the voids, thereby augmented 'k' (Fig. 4.6b-c) in magnitude. However, enhancement rates in 'k' due to rise in temperature were low, because of restricted mobility of nanoparticles (limited micro-convection) at higher concentrations.

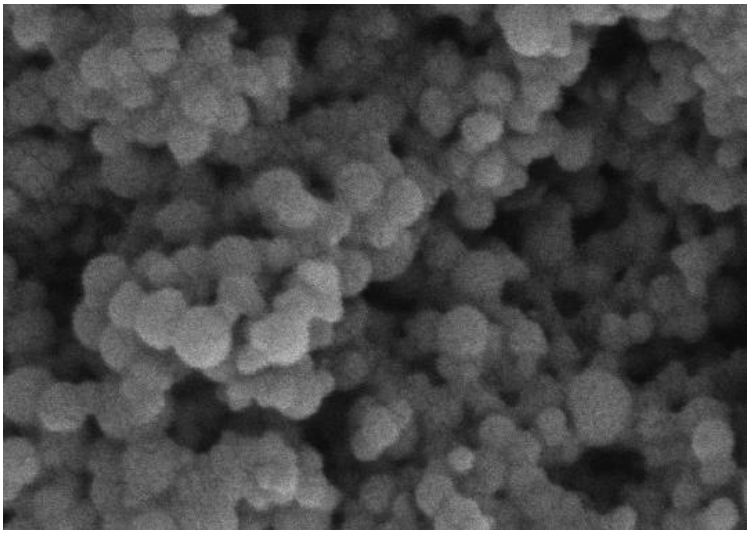

a. DW+0.25% TiO_2

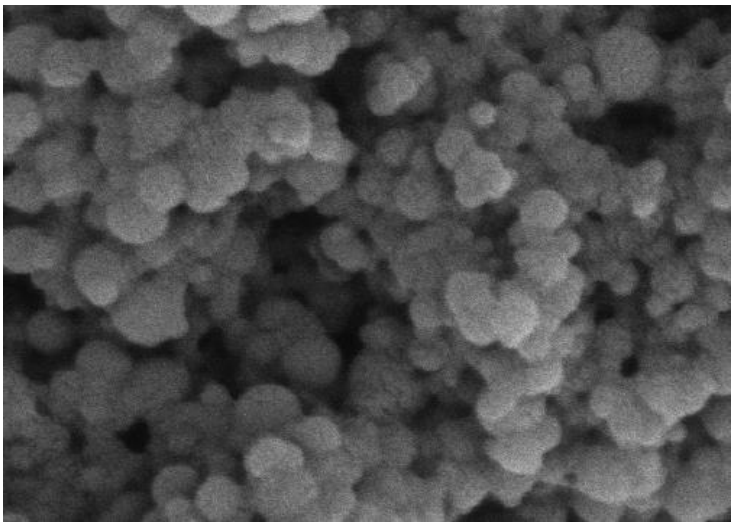

b. DW+0.50% TiO_2

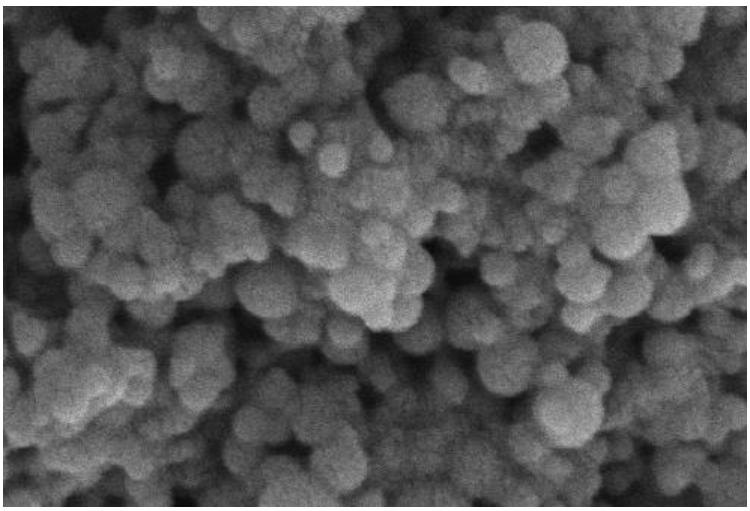

c. DW+1.00% TiO_2

Fig. 4.6(a-c) SEM images of 0.25, 0.50, 1% TiO_2 in DW NePCM at 100 KX

Fig. 4.7 (a-c), indicated SEM-images of 0.25, 0.50 and 1.00% TiO_2 in DW+PG, NePCM at 100 KX magnification. Comparative looks at the micrographs, revealed similar patterns of nanoparticle dispersions into the base fluid matrix as explained in the preceding paragraph. However, the surface characteristics of the nanoparticles in this case, as visualized from SEM-images, were not as smooth as the NePCM prepared into DW. It should be also pinged that the dispersion stability (i.e. separating out of dispersed particles from NePCM with time against gravity) measured in terms of Zeta-potential (discussed in coming para) and visual observations also indicated higher stability of NePCM prepared in PG or EG as compare to that in DW. The surface characteristics observed herewith could be the possible reason for higher dispersion stability.

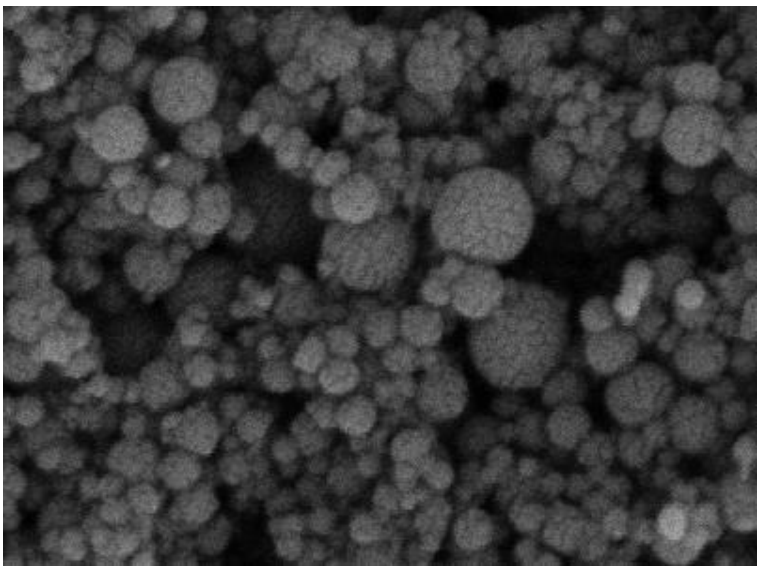

a. DW+PG+0.25% TiO_2

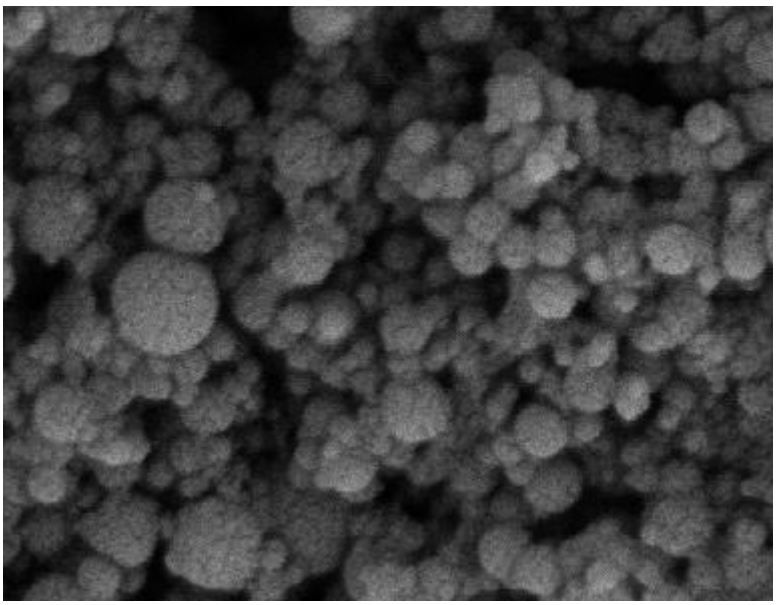

b. DW+PG+0.50% TiO_2

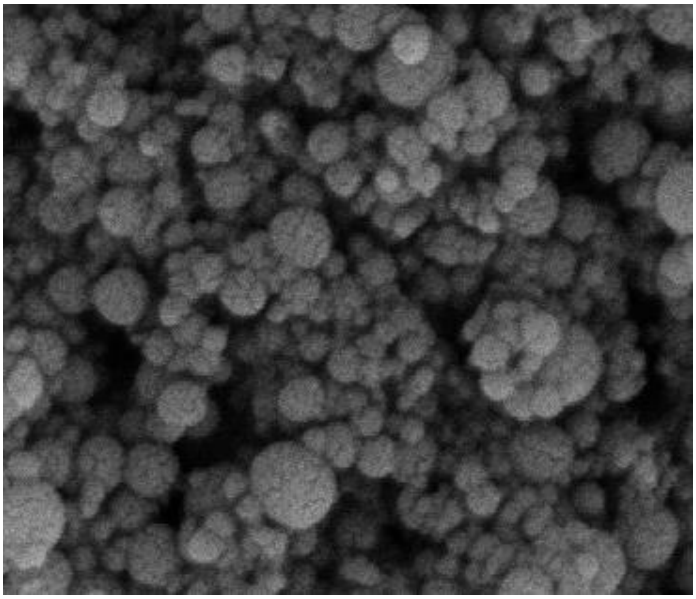

c. DW+PG+1.00% TiO_2

Fig. 4.7(a-c) SEM images of 0.25, 0.50, 1% TiO_2 in DW+PG NePCM at 100 KX

Fig. 4.8 (a-c), indicated SEM-images of 0.25, 0.50 and 1.00% TiO_2 in DW+EG, NePCM at 100 KX magnification. Similar trends of nanoparticle clustering and dispersion patterns were observed as in case of DW+PG.

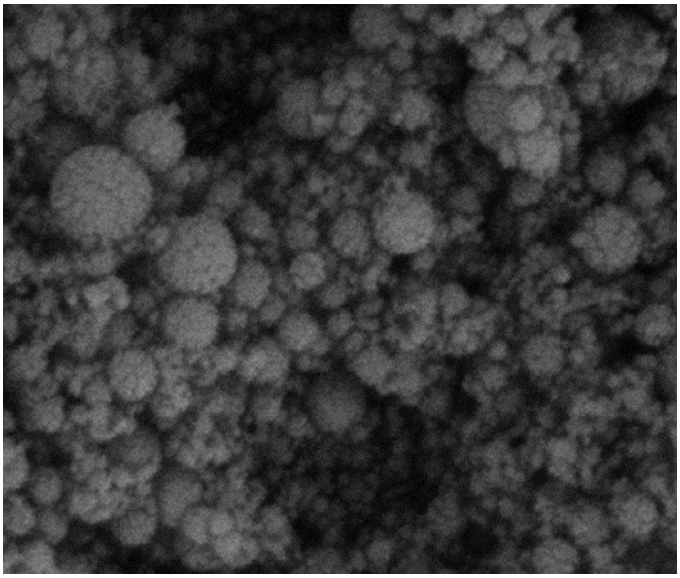

a. DW+EG+0.25% TiO_2

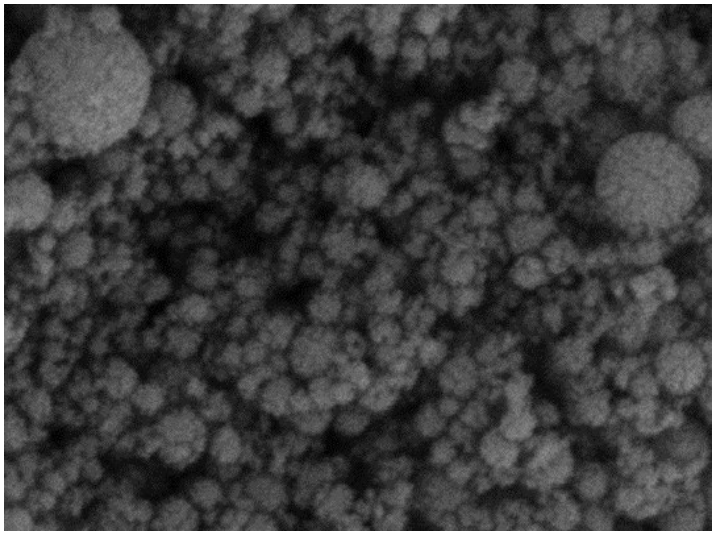

b. DW+EG+0.50% TiO_2

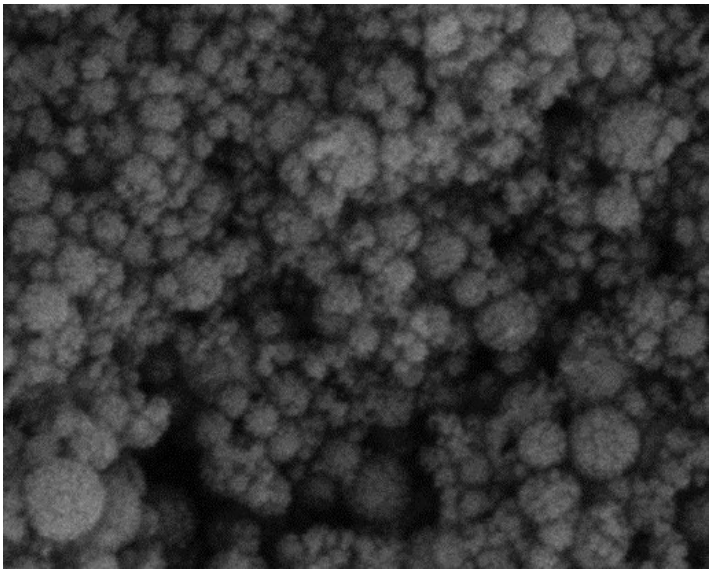

c. DW+EG+1.00% TiO_2

Fig. 4.8(a-c) SEM images of 0.25, 0.50, 1% TiO_2 in DW+EG NePCM at 100 KX

Fig. 4.9 (a-c), indicated SEM-images of 0.25, 0.50 and 1.00%TiO_2 in DW+AgNP, NePCM at 100 KX magnification. Similar patterns of nanoparticle clustering and distribution in the base fluid matrix were observed as earlier, however, nanoparticle clusters were visualized to be arranged in several chain-like patterns. This might have augmented overall heat conduction via chains, thereby effective thermal conductivity of the NePCM prepared in DW+AgNP also.

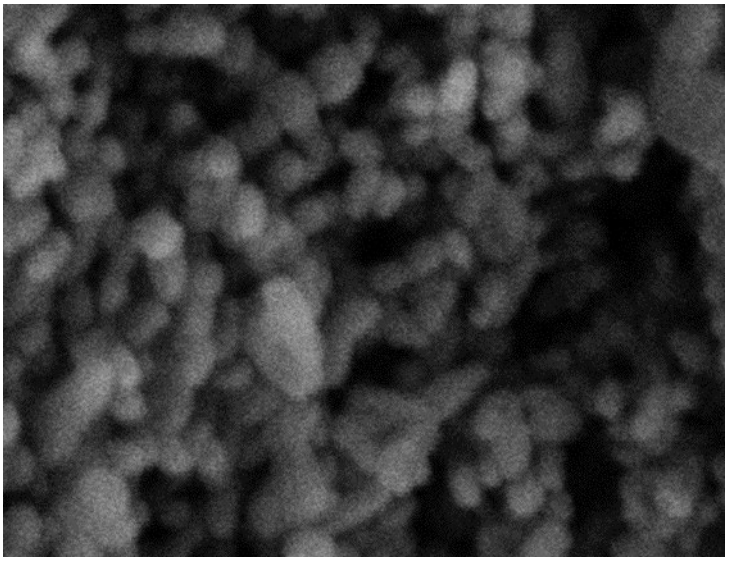

a. DW+AgNP+0.25% TiO_2

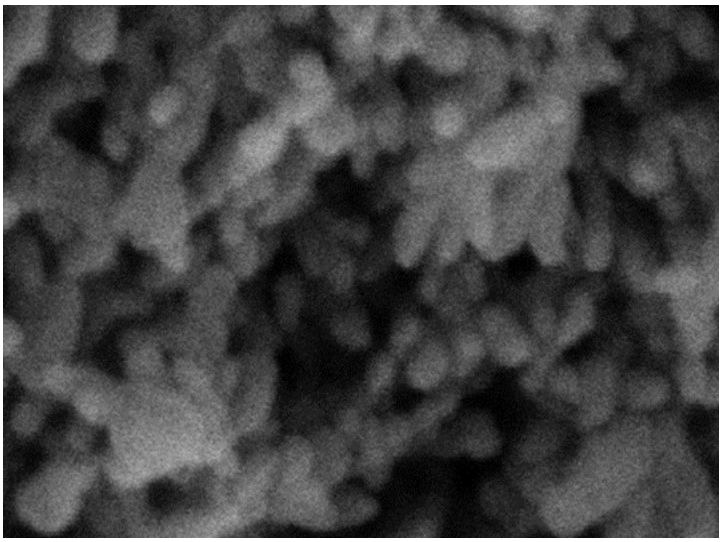

b. DW+AgNP+0.50% TiO_2

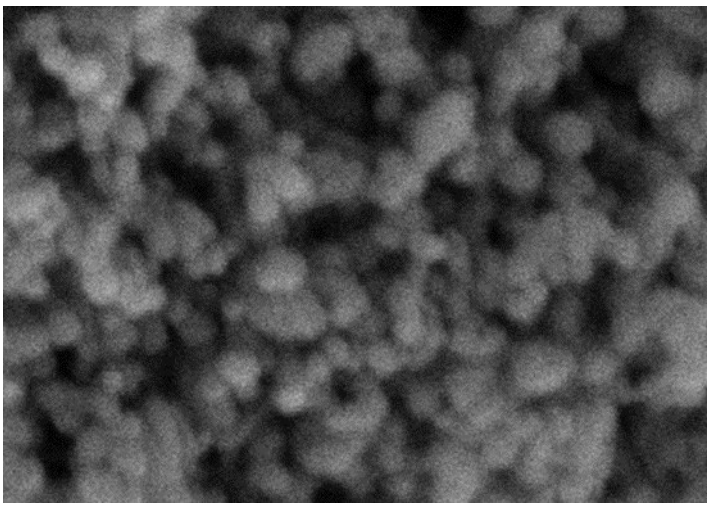

c. DW+AgNP+1.00% TiO_2

Fig. 4.9(a-c) SEM images of 0.25, 0.50, 1% TiO_2 in DW+AgNP NePCM at 100 KX

4.1.4 Differential Scanning Calorimetric (DSC) Analysis of NePCM

DSC analysis of selected NePCM (at 0.50 and 1.00% weight fractions), prepared from TiO_2, CeO_2 and Si_3N_4 nanoparticles, in DW, DW+PG and DW+EG, conducted to evaluate phase-transition as well as energy storage characteristics.

Fig. 4.10, indicate heat flow (J/g-°C) vs temperature (°C) curve of different NePCM, analyzed through DSC. It was noticed from the plot, that magnitudes of instantaneous heat-flow rates before melting (i.e. in frozen or solid state; indicated by nearly horizontal line at the bottom of left-half portion of the curve before the peak) were lower than those in the liquid states (indicated by bottom horizontal lines of right-half portion of the curve after the peak). Thus, it was deduced that magnitude of specific heats (C_p) were higher in the liquid states as compared to that in the solid states for a given NePCM. The phase-transition peaks of the curves were nearly close to the melting points, which indicated the properties of NePCM prepared were very close to the characteristics of the pure substances, i.e. nanoparticles least behaved like impurities affecting thermal behavior of a heat transfer fluids.

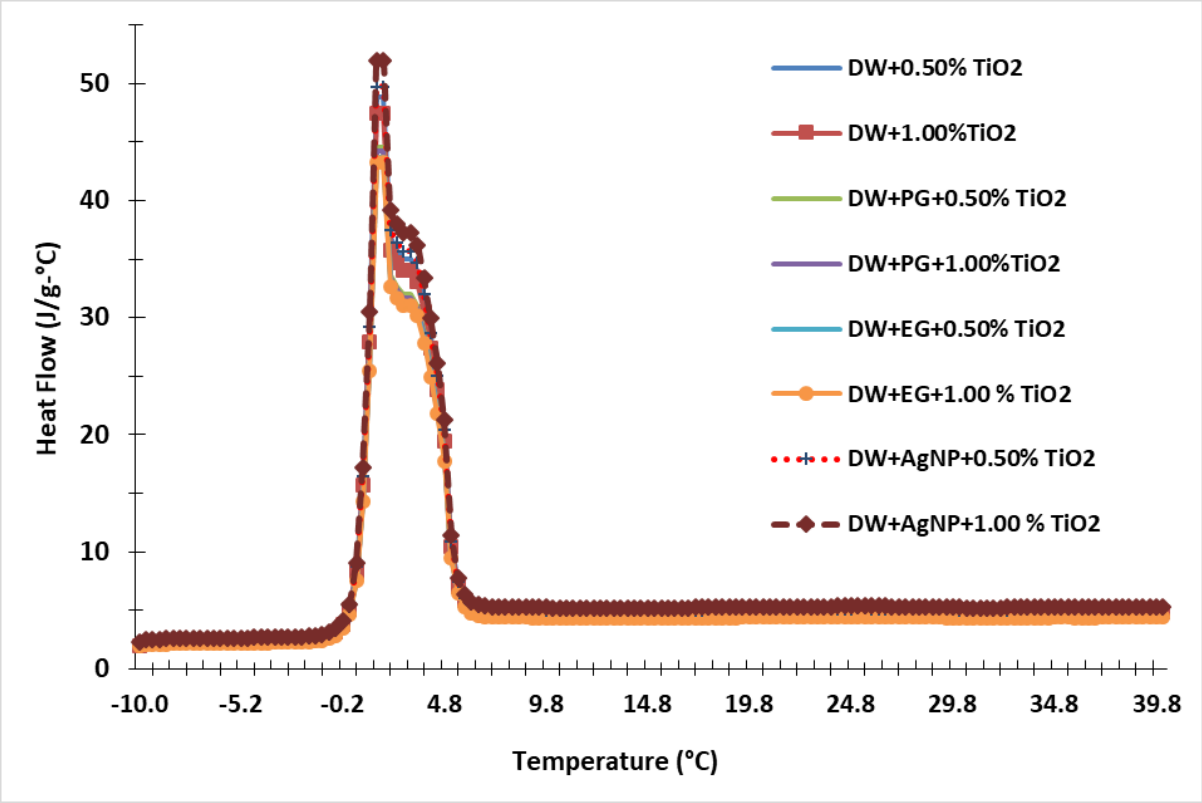

Fig. 4.10 DSC curve of 0.50, 1% TiO_2 in DW, DW+PG, DW+EG, DW+AgNP base fluids

The magnitude of $C_{p,}$ latent heat (ΔH), melting and freezing points, total energy stored (J/kg; computed as area under the heat-flow curve) were calculated using Universal Analysis 2000 software (*V3.7A*) of the TA instruments.

Fig 4.11, indicate the magnitude of energy stored (J/kg) in NePCM prepared from 0.50, and 1.00% TiO_2 in DW, DW+PG, DW+EG, DW+AgNP.

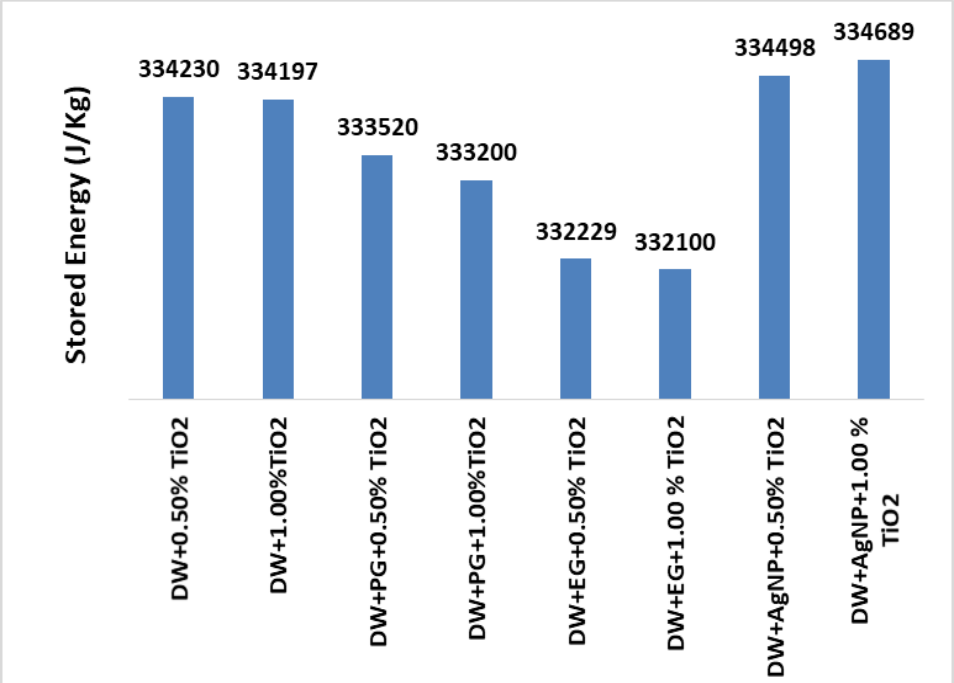

Fig. 4.11 Energy stored (J/kg) in NePCM

It was observed that energy stored in DW based NePCM were higher than that in DW+PG and it was lowest in DW+EG. It was due to inherently low thermal capacity of PG and EG materials. However, energy storability of DW+AgNP based NePCM were highest among the studied NePCMs. It was also noticed that increasing concentration of nanoparticles from 0.50 to 1.00 % reduced the magnitude of stored energy (but it was very less as compare to the enhancements in thermal conductivities at same concentration, therefore least affected the milk cooling performance discussed later). The trend observed in this study were in line with Khanafer and Vafai (2011), but contrary with Liu and Yang (2017), wherein an enhancement in C_p and ΔH up to 83.5 and 6.4% reported, respectively, using TiO_2 nanoparticles in eutectic hydrate salts. The phenomena was justified by explaining the prevalence of interfacial thermal resistance between base fluid and nanoparticles. However, Khanafer and Vafai (2011) considered the effective C_p of nanofluid to be an additive property furnished by individual components such as nanoparticles and the base fluids. Thus, results of present study could be justified based

on this explanation that DW inherently possess higher C_p and ΔH as compare to many metal oxides like TiO_2. Therefore, effective energy storage capacity of DW might have declined due to increase of TiO_2 concentrations. However, such negative effects were very little because nanoparticles were dispersed at most up to 1.00% to enhance 'k'.

Fig. 4.12, indicate minimum freezing temperature (solidus temperature: below which a NePCM is completely frozen to solid state) of NePCM. It could be observed that addition of PG or EG into DW (@10%) influenced freezing characteristics significantly. The depression in freezing points could be helpful in sensible cooling operations by increasing temperature difference between milk and coolants, but it was less useful in the present milk pail cum passive chiller design in which latent heat storage prevailed.

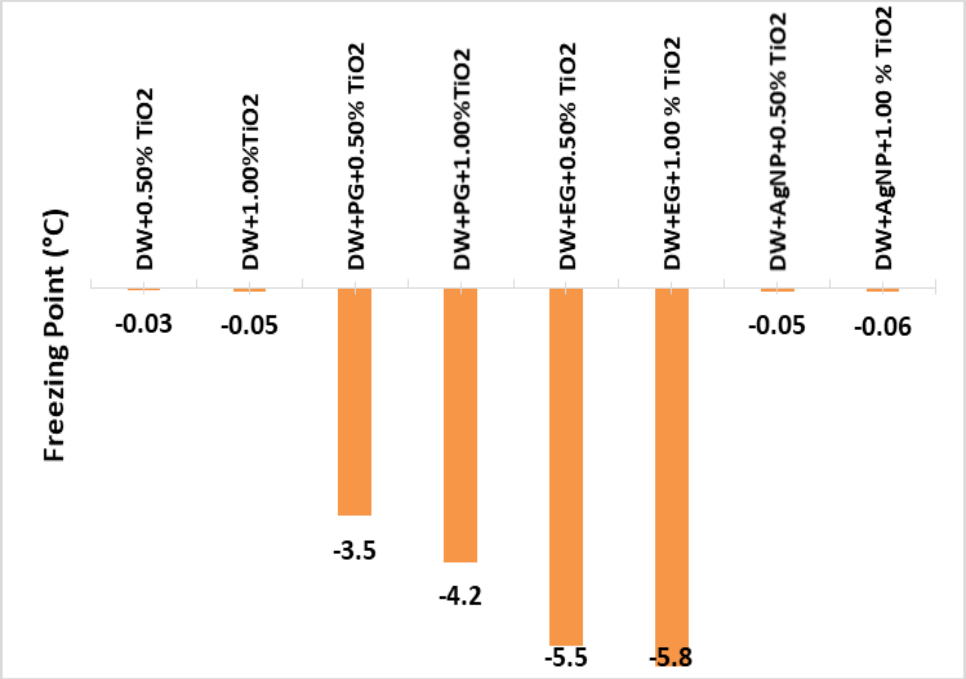

Fig. 4.12 Freezing Temperature (°C) of NePCM

4.1.5 Transmission Electron Microscopic (TEM) Analysis of NePCM

TEM analysis of selected NePCM (DW+AgNP; DW+AgNP+1.00 % TiO_2) were carried out to understand the 'k' enhancement, dispersion patterns and interactions among nano-particles as base fluid elements.

Fig. 4.13a-b, indicate the TEM-images of DW+AgNP (base fluid) and DW+AgNP+1.00% TiO_2 (NePCM). It was noticed from Fig. 4.13a, that silver ionic solution (DW+AgNP) contained ionic silver in water (the transparent crystals) and silver nanoparticles (the opaque crystals). Fig. 4.13b, revealed that ionic silver (transparent crystals) surrounded the dispersed nanoparticles (either TiO_2 or Ag; indicated by opaque

crystals) in the NePCM matrix in chain-like patterns. The self-assembly among crystals as visualized from TEM images, indicated some sort of affinity between the TiO_2 and ionic silver molecules, which could be responsible for 'k' enhancements.

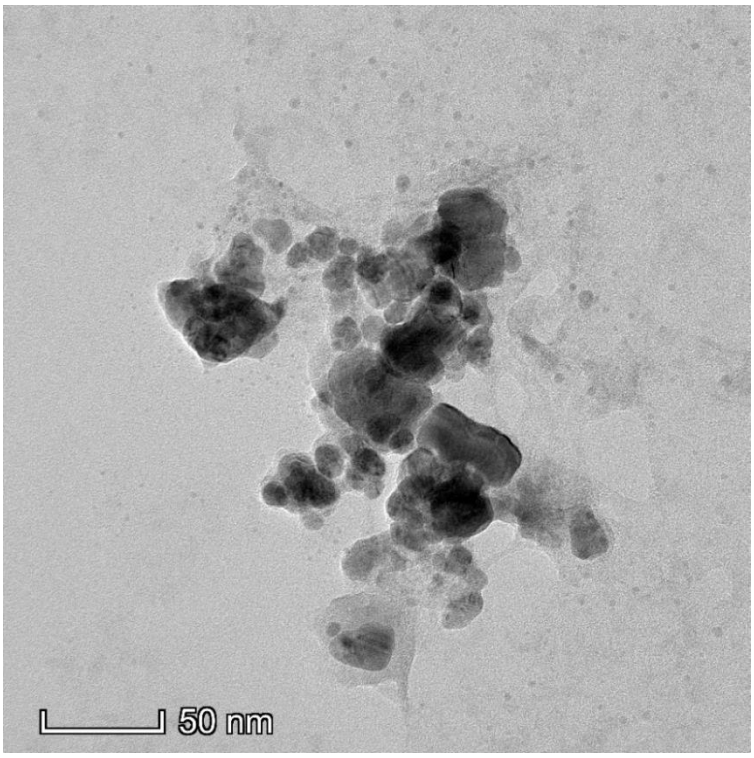

Fig. 4.13a TEM images of DW+AgNP (base fluid)

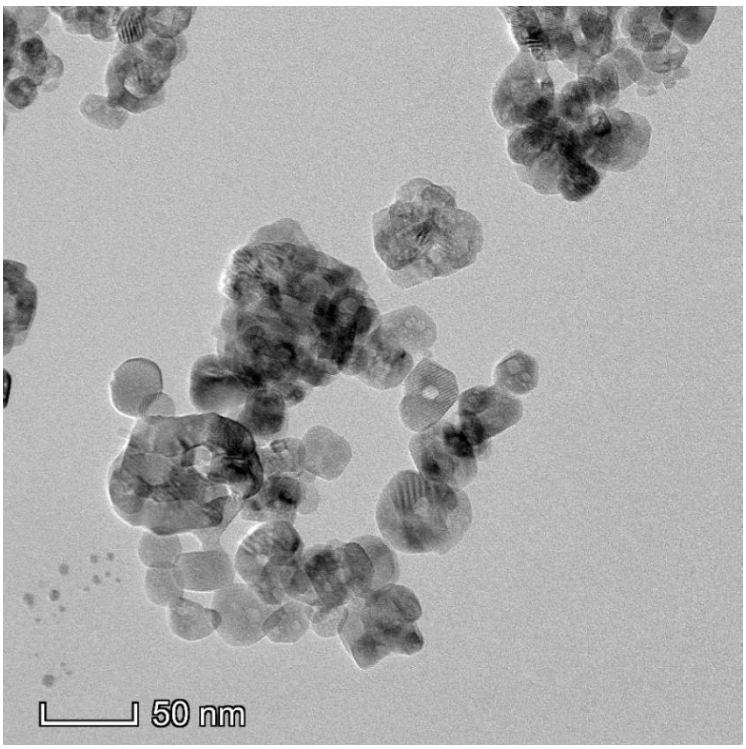

Fig. 4.13b TEM images of DW+AgNP+1.00% TiO_2 (NePCM)

4.1.6 Zeta Potential analysis of NePCM

Zeta potential (mV) as well as Zeta particle size analysis of selected NePCM (were carried out to understand the dispersion stability of nanoparticle dispersion into the base fluid matrix.

Fig. 4.14a-d, indicates zeta potential curves of DW+1.00 % TiO_2, DW+PG+1.00 % TiO_2, DW+EG+1.00% TiO_2 and DW+AgNP+1.00% TiO_2, NePCMs.

Brookhaven Instruments Corp.
PALS Zeta Potential Analyzer Ver. 5.60

Date: Dec 10, 2020
Time: 23:11:13
Batch: 0

Sample ID **NF 2 (Combined)**
Operator ID **Prathyusha**
Notes

Measurement Parameters:

Mean Zeta Potential	= 21.73 mV	Liquid	= Water
Zeta Potential Model	= Smoluchowski	Temperature	= 25.0 °C
Mean Mobility	= 1.70 (µ/s) / (V/cm)	Viscosity	= 0.890 cP
pH	= 7.00	Refractive Index	= 1.330
Conductance	= 8 µS	Dielectric Constant	= 78.54
Concentration	= 0.00 mg/mL	Particle Size	= 500.0 nm

Instrument Parameters:

Sample Count Rate	= 640 kcps	Voltage	= 4.00 volts
Ref. Count Rate	= 1309 kcps	Electric Field	= 10.60 V/cm
Wavelength	= 658.0 nm	User1	= 0.00
Field Frequency	= 2.00 Hz	User2	= 0.00
Cycles Per Run	= 30		

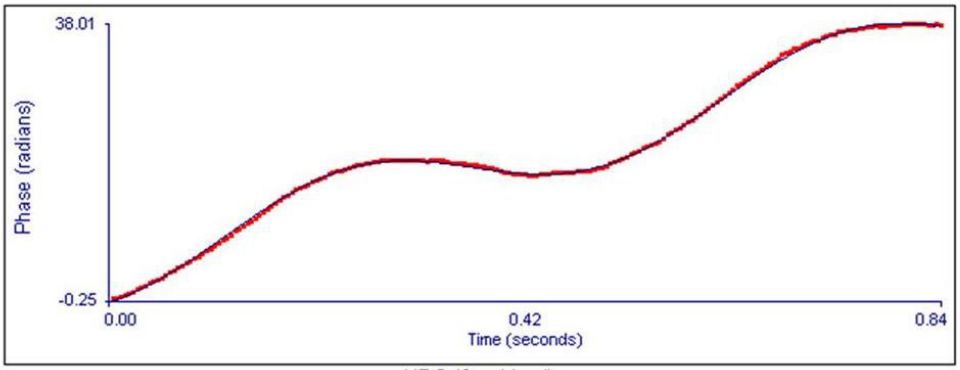

NF 2 (Combined)

Run	Mobility	Zeta Potential (mV)	Rel. Residual
1	1.84	23.57	0.0216
2	1.61	20.63	0.0151
3	1.64	20.97	0.0141
Mean	1.70	21.73	0.0169
Std. Error	0.07	0.93	0.0024
Combined	1.70	21.72	0.0104

Fig. 4.14a Zeta-Potential (mV) of DW+1.00% TiO_2 (NePCM)

Brookhaven Instruments Corp.
PALS Zeta Potential Analyzer Ver. 5.60

Date: Dec 10, 2020
Time: 23:50:13
Batch: 0

Sample ID **NF 26 (Combined)**
Operator ID **Prathyusha**
Notes

Measurement Parameters:

Mean Zeta Potential	= 24.27 mV	Liquid	= Water
Zeta Potential Model	= Smoluchowski	Temperature	= 25.0 °C
Mean Mobility	= 1.90 (μ/s) / (V/cm)	Viscosity	= 0.890 cP
pH	= 7.00	Refractive Index	= 1.330
Conductance	= 55 μS	Dielectric Constant	= 78.54
Concentration	= 0.00 mg/mL	Particle Size	= 500.0 nm

Instrument Parameters:

Sample Count Rate	= 473 kcps	Voltage	= 4.00 volts
Ref. Count Rate	= 1247 kcps	Electric Field	= 8.78 V/cm
Wavelength	= 658.0 nm	User1	= 0.00
Field Frequency	= 2.00 Hz	User2	= 0.00
Cycles Per Run	= 30		

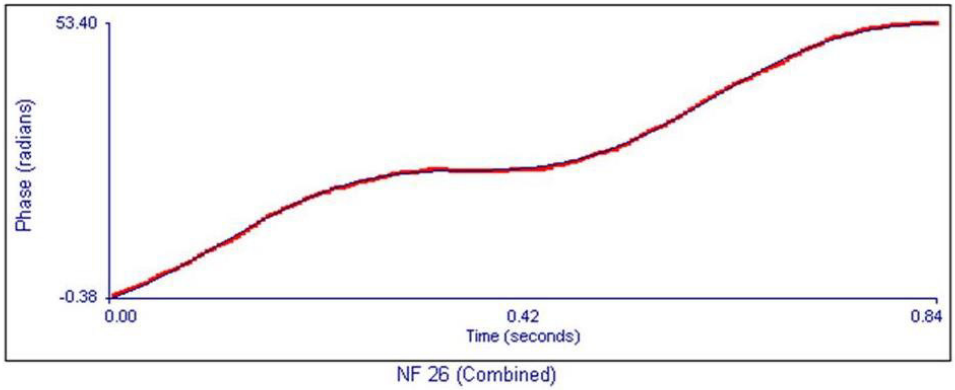

NF 26 (Combined)

Run	Mobility	Zeta Potential (mV)	Rel. Residual
1	1.39	17.82	0.0213
2	2.10	26.90	0.0235
3	2.19	28.08	0.0129
Mean	1.90	24.27	0.0192
Std. Error	0.25	3.24	0.0032
Combined	1.89	24.21	0.0108

Fig. 4.14b Zeta-Potential (mV) of DW+PG+1.00% TiO_2 (NePCM)

Brookhaven Instruments Corp.
PALS Zeta Potential Analyzer Ver. 5.60

Date: Dec 10, 2020
Time: 23:43:33
Batch: 0

Sample ID **NF 22 (Combined)**
Operator ID **Prathyusha**
Notes

Measurement Parameters:

Mean Zeta Potential	= 30.46 mV	Liquid	= Water
Zeta Potential Model	= Smoluchowski	Temperature	= 25.0 °C
Mean Mobility	= 2.38 (μ/s) / (V/cm)	Viscosity	= 0.890 cP
pH	= 7.00	Refractive Index	= 1.330
Conductance	= 31 μS	Dielectric Constant	= 78.54
Concentration	= 0.00 mg/mL	Particle Size	= 500.0 nm

Instrument Parameters:

Sample Count Rate	= 617 kcps	Voltage	= 4.00 volts
Ref. Count Rate	= 1381 kcps	Electric Field	= 9.65 V/cm
Wavelength	= 658.0 nm	User1	= 0.00
Field Frequency	= 2.00 Hz	User2	= 0.00
Cycles Per Run	= 30		

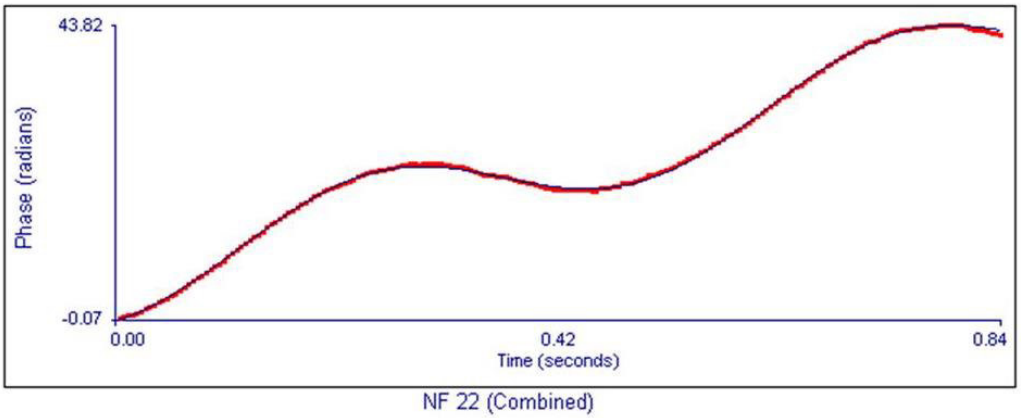

NF 22 (Combined)

Run	Mobility	Zeta Potential (mV)	Rel. Residual
1	2.05	26.19	0.0365
2	2.59	33.11	0.0336
3	2.51	32.07	0.0184
Mean	2.38	30.46	0.0295
Std. Error	0.17	2.16	0.0056
Combined	2.37	30.39	0.0097

Fig. 4.14c Zeta-Potential (mV) of DW+EG+1.00% TiO_2 (NePCM)

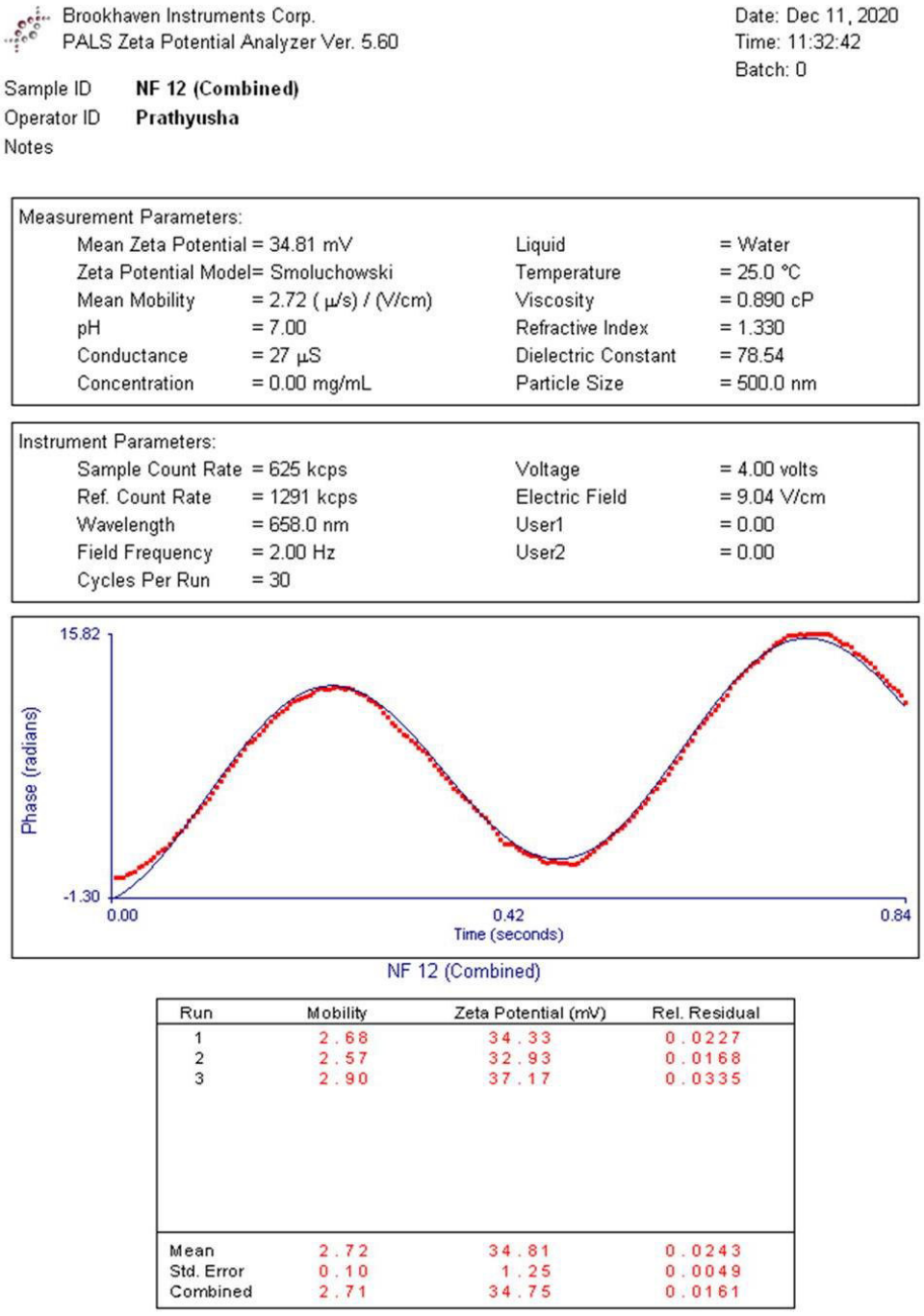

Fig. 4.14d Zeta-Potential (mV) of DW+AgNP+1.00% TiO_2 (NePCM)

Fig. 4.15a-d, indicates Zeta particle sizes of DW+1.00% TiO_2, DW+PG+1.00% TiO_2, DW+EG+1.00% TiO_2 and DW+AgNP+1.00% TiO_2; NePCMs.

Brookhaven Instruments Corp.
ZetaPALS Particle Sizing Software Ver. 5.23

Date: Dec 11, 2020
Time: 11:53:11
Batch: 0

Sample ID **NF 10 (Combined)**
Operator ID **Prathyusha**
Notes

Elapsed Time	00:03:00
Median Diam.	76.9 nm
Mean Diam.	86.1 nm
Polydispersity	0.275
GSD	1.637

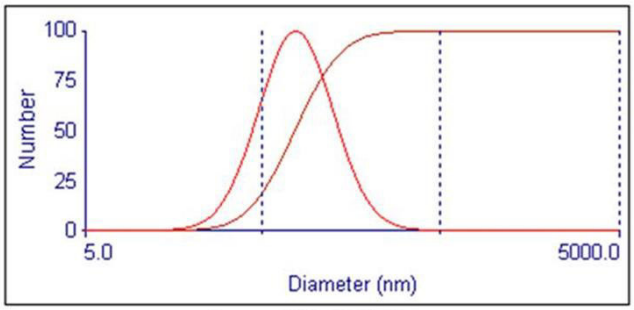

Lognormal Size Distribution

d(nm)	G(d)	C(d)	d(nm)	G(d)	C(d)	d(nm)	G(d)	C(d)
35.1	26	5	68.2	97	40	106.0	80	75
41.7	44	10	72.4	99	45	114.8	70	80
46.9	58	15	76.9	100	50	126.0	58	85
51.5	70	20	81.6	99	55	141.6	44	90
55.8	80	25	86.7	97	60	168.4	26	95
59.9	87	30	92.4	93	65			
64.0	93	35	98.7	87	70			

Fig. 4.15a Zeta-Particle size (nm) of DW+ 1.00% TiO_2 (NePCM)

Brookhaven Instruments Corp.
ZetaPALS Particle Sizing Software Ver. 5.23

Date: Dec 10, 2020
Time: 19:42:18
Batch: 0

Sample ID **NF 14 (Combined)**
Operator ID **Prathyusha**
Notes

Elapsed Time	00:03:00
Median Diam.	93.5 nm
Mean Diam.	105.4 nm
Polydispersity	0.292
GSD	1.658

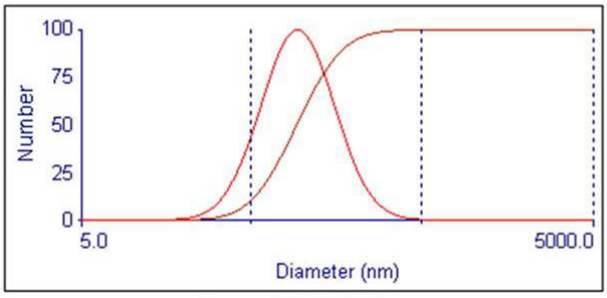

Lognormal Size Distribution

d(nm)	G(d)	C(d)	d(nm)	G(d)	C(d)	d(nm)	G(d)	C(d)
41.7	26	5	82.6	97	40	130.1	80	75
49.9	44	10	87.9	99	45	141.2	70	80
56.2	58	15	93.5	100	50	155.3	58	85
61.9	70	20	99.4	99	55	175.2	44	90
67.2	80	25	105.8	97	60	209.4	26	95
72.3	87	30	112.9	93	65			
77.4	93	35	120.8	87	70			

Fig. 4.15b Zeta-Particle size (nm) of DW+ PG+1.00% TiO_2 (NePCM)

Brookhaven Instruments Corp.
ZetaPALS Particle Sizing Software Ver. 5.23

Date: Dec 10, 2020
Time: 20:07:05
Batch: 0

Sample ID **NF 13 (Combined)**
Operator ID **Prathyusha**
Notes

Elapsed Time	00:03:00
Median Diam.	83.3 nm
Mean Diam.	94.9 nm
Polydispersity	0.319
GSD	1.693

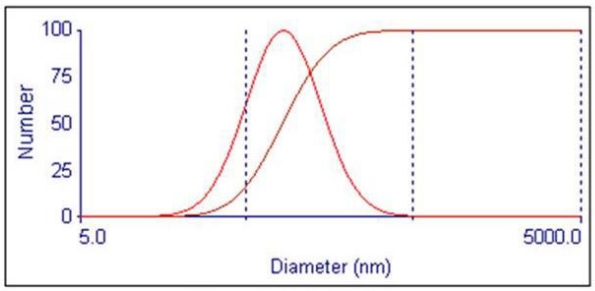

Lognormal Size Distribution

d(nm)	G(d)	C(d)	d(nm)	G(d)	C(d)	d(nm)	G(d)	C(d)
35.9	26	5	73.2	97	40	117.6	80	75
43.2	44	10	78.1	99	45	128.1	70	80
49.0	58	15	83.3	100	50	141.5	58	85
54.1	70	20	88.8	99	55	160.5	44	90
59.0	80	25	94.8	97	60	193.2	26	95
63.7	87	30	101.4	93	65			
68.4	93	35	108.9	87	70			

Fig. 4.15c Zeta-Particle size (nm) of DW+ EG+1.00% TiO_2 (NePCM)

Brookhaven Instruments Corp.
ZetaPALS Particle Sizing Software Ver. 5.23

Date: Dec 11, 2020
Time: 12:04:53
Batch: 0

Sample ID **NF 11 (Combined)**
Operator ID **Prathyusha**
Notes

Elapsed Time	00:03:00
Median Diam.	126.1 nm
Mean Diam.	139.0 nm
Polydispersity	0.234
GSD	1.582

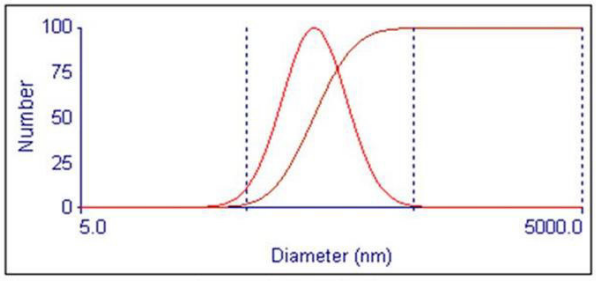

Lognormal Size Distribution

d(nm)	G(d)	C(d)	d(nm)	G(d)	C(d)	d(nm)	G(d)	C(d)
61.1	26	5	112.8	97	40	169.8	80	75
71.7	44	10	119.3	99	45	182.8	70	80
79.9	58	15	126.1	100	50	199.1	58	85
87.0	70	20	133.3	99	55	221.9	44	90
93.7	80	25	141.0	97	60	260.4	26	95
100.1	87	30	149.5	93	65			
106.5	93	35	158.9	87	70			

Fig. 4.15d Zeta-Particle size (nm) of DW+ AgNP+1.00% TiO_2 (NePCM)

Table 4.1, summarizes the outcomes of zeta-potential analysis as follows:

Table 4.1 Zeta-Potential (ξ; mV) and Mean Particle Diameter (nm) of NePCM

S. No	NePCM	ξ (mV)	Mean Particle Dia (nm)
1	DW+1.00% TiO_2	21.73	86.1
2	DW+PG+1.00% TiO_2	24.27	105.4
3	DW+EG+1.00% TiO_2	30.46	94.9
4	DW+AgNP+ 1.00% TiO_2	34.81	139.0

It was observed that all the NePCM had good dispersion stability, however, following trend of dispersion stability in terms of 'ξ' (mV) values can be deduced:

Mean particle sizes (nm) of the NePCM varied according to the extent of intra and intermolecular interactions and affinity among nanoparticles with nanoparticles and nanoparticles with base fluids. The highest values of mean particle dia. of DW+AgNP+TiO_2 nanoparticles, could be explained by the interactive effects among ionic silver molecules in DW, DW and TiO_2, as similar inferences were deduced from TEM analysis also.

4.2 Numerical and experimental study on thermal behavior of NePCM inside the spherical module

Based on preliminary trials on milk cooling as well as thermo-physical and morphological characterizations, TiO_2 nanoparticles were found better option among the selected nanoparticles. Before assimilating the developed NePCM into the jacketed milking pails, their milk cooling performance, charging and discharging behavior were numerically studied and validated with experiments by encapsulating into a spherical shaped enclosure, placed inside an ordinary insulated milk vessel. In this activity, TiO_2 nanoparticles at 0.05, 0.25, 0.50, 0.75 and 1.00% by weight, dispersed into DW to

expedite its energy storage, discharge and milk chilling performance. Transient energy exchange and phase-transition of the NePCM were numerically simulated using enthalpy-porosity model of computational fluid dynamics (CFD) technique. The simulated results were experimentally validated in an ordinary insulated milking vessel.

The experimentally measured and empirically calculated thermo-physical properties of the base fluid and the PCM used in this part of study, are presented in Table 4.2. These values were used as input parameters in CFD simulations from user defined functions (UDF).

Table 4.2 Thermo-physical properties of the NePCM studied in spherical module

Properties	**Temperature (°C)**	**% by *wt.* of nanoparticles**						
		0	0.05	0.25	0.50	0.75	1.00	Uncertainty (%)
k (W/m-K)	-10	2.281	2.321	2.392	2.461	2.50	2.553	±0.5%
	0	0.555	0.577	0.599	0.616	0.627	0.654	
	10	0.578	0.605	0.618	0.635	0.664	0.693	
	20	0.598	0.627	0.639	0.657	0.687	0.723	
	30	0.607	0.637	0.649	0.673	0.698	0.740	
	40	0.618	0.643	0.668	0.688	0.710	0.758	
μ(kg/m-s)	27	0.0008	0.0009	0.0011	0.0013	0.0015	0.0018	
C_p (j/kg-K)	-10	1998.4	1994.4	1990.5	1982.5	1974.5	1966.5	±0.1%
	0	4219.9	4181.1	4168.4	4138.2	4092.4	4056.7	
	10	4195.5	4171.2	4132.5	4111.5	4055.1	4006.5	
	20	4184.4	4162.3	4124.1	4099.6	4044.3	3998.6	
	30	4180.1	4155.1	4120.2	4098.5	4040.6	3994.5	
	40	4179.6	4150.5	4115.7	4092.2	4033.6	3985.6	
L (j/kg)	-	335000	334669	334598	334497	334330	334229	
ρ (kg/m^3)	27	1020.5	1032.6	1041.5	1054.5	1062.1	1070.5	
T_m (°C)	-	0	-0.05	-0.10	-0.15	-0.18	-0.20	

4.2.1 Transient temperature profiles and their comparison with computed predictions

4.2.1.1 Experimental temperature profile during charging

Fig. 4.16(a-b), demonstrate experimental plots of transient temperature profiles (at point 'C', located at the center of the module) of the PCM having different TiO_2 nanoparticles at different concentrations during charging.

It was observed that the sensible chilling of all the PCM from ambient to the phase-transition temperature took place at almost similar rates. However, considerable effects of dispersing nanoparticles into base fluid on supercooling degree, onset of phase-transition,

total phase-transition time and final temperature drop achieved in 9000s of fixed charging time, were observed.

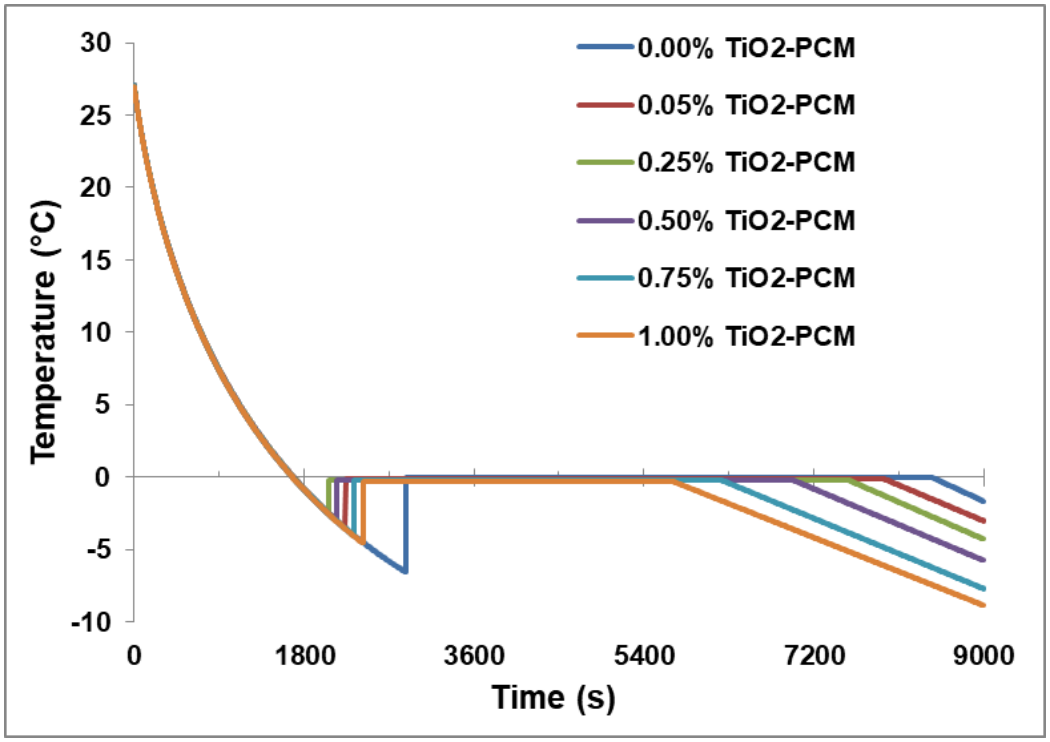

(a)

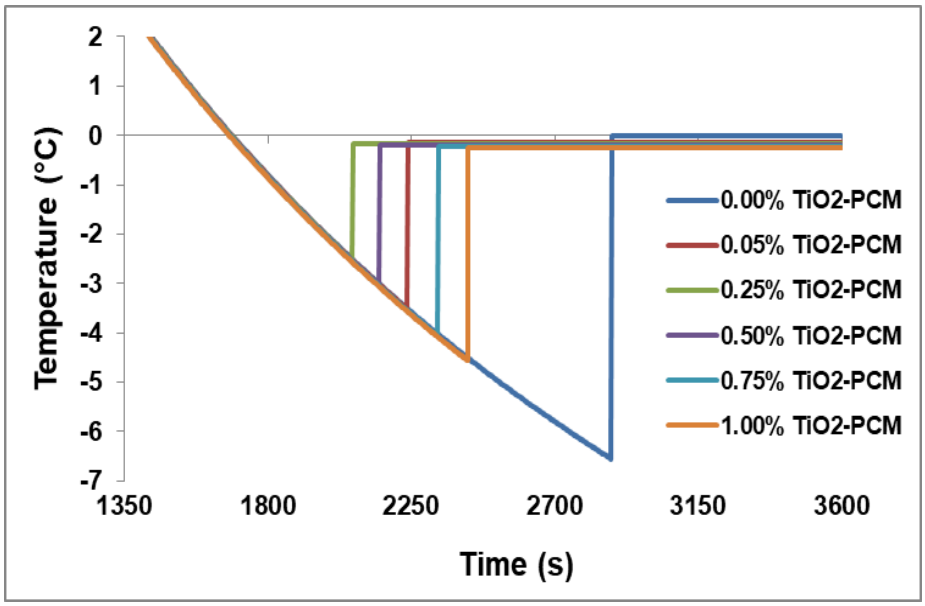

(b)

Fig. 4.16 Experimental transient temperature profiles (at point 'C', located at the center of the spherical module) at different nanoparticles concentrations **(a)** for entire charging duration **(b)** exploded view close to subcooling

It was also noticed that (Fig. 4.16b) supercooling degrees of -6.6, -3.5, -2.5, -3.0, -4.0 and -4.5°C and onsets of phase-transition were 2876, 2238, 2064, 2148, 2334 and 2428s at 0.00, 0.05, 0.25, 0.50, 0.75 and 1.00% TiO_2 nanoparticles concentrations, respectively. The total phase transition time were 8450, 7957, 7561, 6980, 6228 and 5693s and temperature drops finally achieved were up to -1.6, -3.0, -4.3, -5.7, -7.7 and -8.8°C for the said sequence of TiO_2 nanoparticle concentrations in 9000s of charging time (Fig. 4.16a). The total phase-transition time was reduced continuously with increasing nanoparticle concentrations and highest reduction was by 32.62% at 1.00% TiO_2 nanoparticle concentration. The results obtained herewith for charging durations were also supported by Liu *et al.* (2009) and Motahar *et al.* (2017), wherein TiO_2 nanoparticles were dispersed into saturated aqua-$BaCl_2$ salt blend and n-octadecane, respectively. However, contrary to their reports, in which supercooling degree decreased uninterruptedly, in the present work, it was noticed that the supercooling degree was reduced from -6.6 to -2.5 (by 62.12%) by increasing concentrations of nanoparticles only till 0.25%, and thereafter further addition of nanoparticles increased the supercooling degree. Such findings were alike to those reported on multi-walled carbon nanotubes in water by Kumaresan *et al.* (2013). The possible reason for this phenomena could be the sufficient assistance supplied by nanoparticles in freezing process only up to 0.25% of TiO_2 concentration. This helped in early start of the phase-transition process in the PCM during charging. However, after 0.25% of TiO_2 level, a considerable rise in viscosity of the liquid PCM and overloading/saturation of nanoparticles might have restricted the nucleation and micro-convections (free movement of nanoparticles in the base fluid matrix) in the PCM. This could be responsible for delayed freezing and higher supercooling degree, as supported in literature based on classical nucleation theory also (Colton and Suh, 1987).

4.2.1.2 Comparison of the experimental and CFD predicted transient temperature profiles during charging

Fig. 4.17 (a-c), elucidate the comparison of experimental and CFD predicted transient temperature profiles of the PCM (at 0.00 and 1.00% TiO_2 nanoparticles) at point 'A', 'B' and 'C' located inside the module during charging. Fig. 4.17a, indicated that at point 'A', the PCM were sensibly chilled from ambient to the phase-transition temperature, displayed negligible supercooling, while supercooling was pronounced at points 'B' and 'C' before the start of phase-transition process (Fig. 4.17b-c). It is evident that the supercooling degree was least at point 'A', moderate at 'B' and highest at 'C'.

This was because the continuous and rapid freezing proceeded from outer wall of the spherical module towards center and crossed the point 'A' more quickly by pushing unfrozen portion of the PCM towards center.

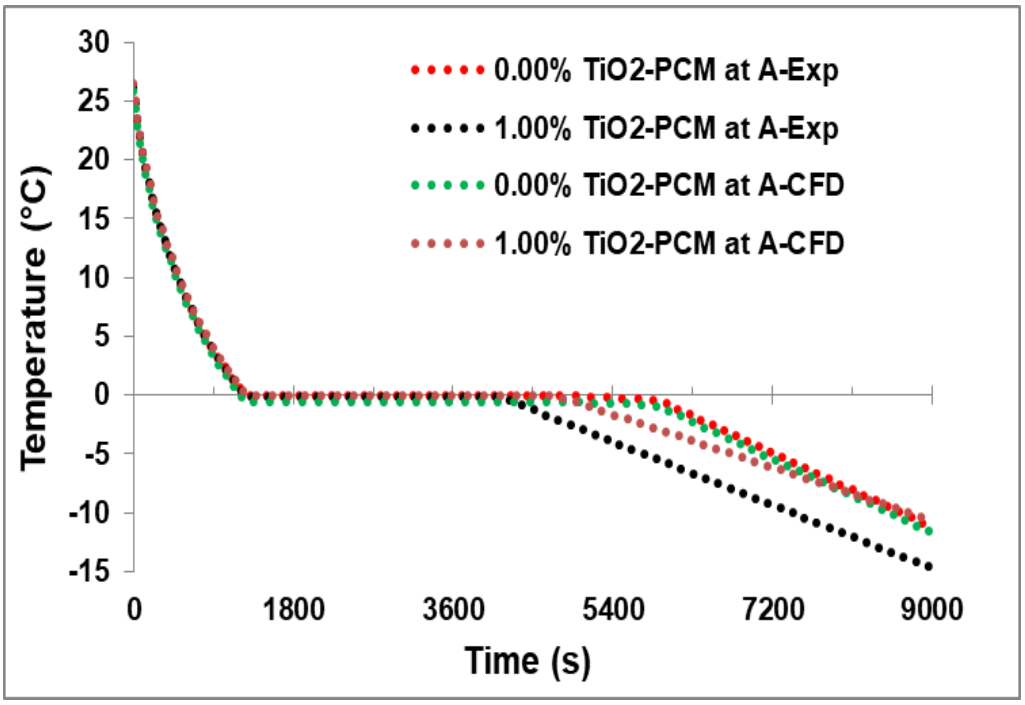

(a)

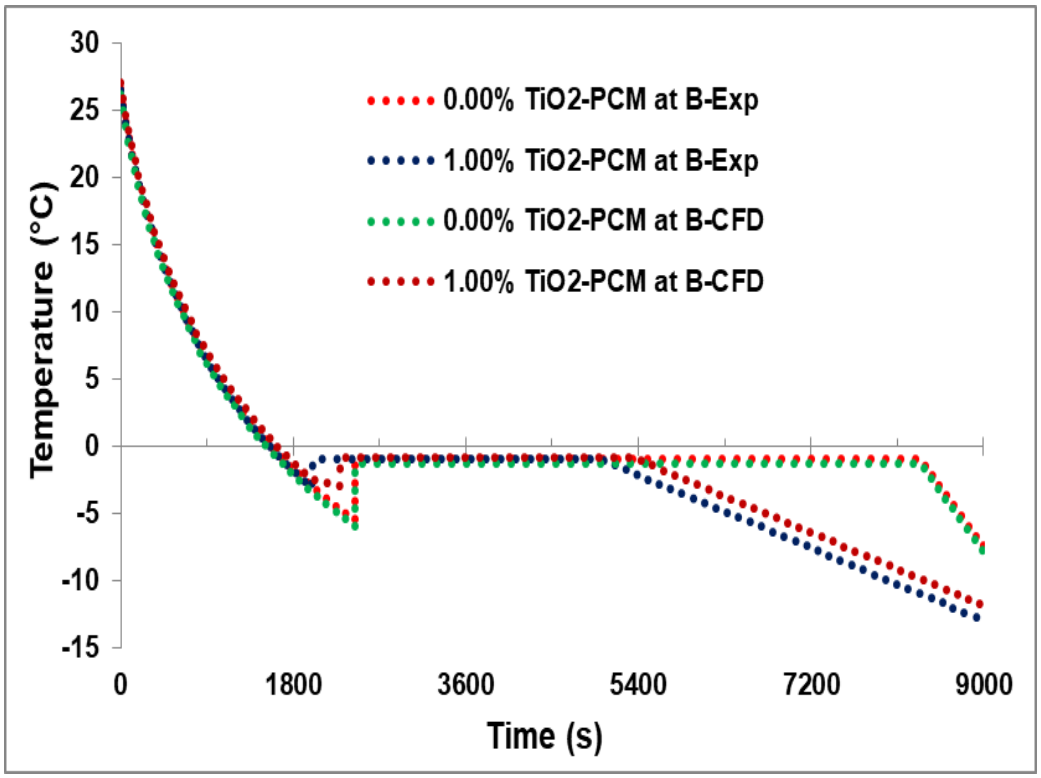

(b)

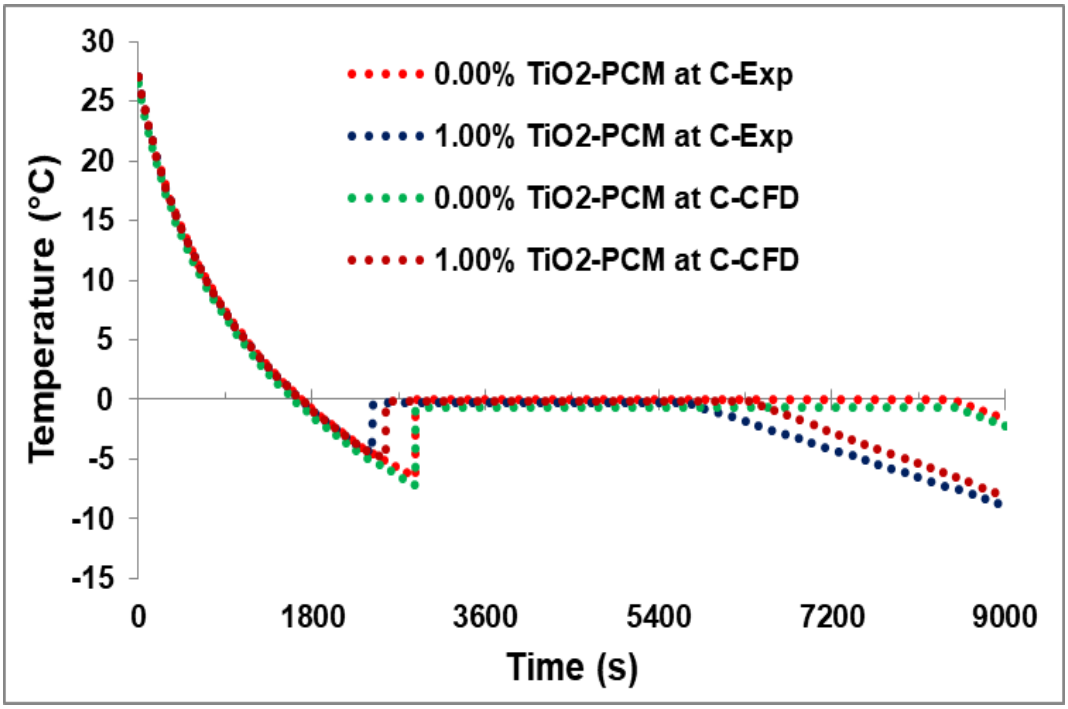

(c)

Fig. 4.17 (a-c) Experimental and CFD predicted transient temperature profiles of the PCM containing 0.00 and 1.00% TiO_2 nanoparticles, at point **(a)** 'A', **(b)** 'B' and **(c)** 'C' during charging

This was slower at points 'B' and 'C' as compared to 'A'. The differences in values of temperatures and degrees of supercooling at 'A' and 'B' were due to the location of points inside the module as well as the effects of gravity (observed in experimental as well as modelled curves). These factors might have resulted in accumulation of unfrozen PCM at 'B' during initial phases of charging process and at 'C' towards the end.

It was also noticed that the onset and end of the phase-transition appeared much earlier at point 'A', followed by 'B' and 'C'. For a 9000s of charging time, the net temperature drop achieved was highest at 'A' followed by 'B' and 'C'. In all the cases, CFD predicted data were in line with the experimental results with mean absolute percentage error (MAPE) within 1-3.5% (graph not shown). This was observed for the pre–freeze sensible cooling energy storage as well as in the solidification plateau region of the curve for both the base fluid and the PCM. However, deviation between experimental and simulated values of temperature were more significantly observed with late completions of phase-transition process in CFD predicted results, only in case of nanoparticle enhanced PCM at all three locations ('A', 'B' and 'C'). The possible reason for these differences could be that the simulations neglected the effects of nanoparticle assisted freezing which

generally takes account of the early nucleation and crystal growth (which are not simulated) in real-world situations.

4.2.1.3 Experimental transient temperature profiles during discharging

Fig. 4.18 (a-c), explicate the experimentally measured transient temperature profiles of the PCM (at different TiO_2 nanoparticles concentrations) during discharging and the consequent average chilled milk temperature. It was observed that the average milk chilling rates and phase-transition time during discharging were decreased with increasing concentrations of nanoparticles. The time required for milk to be chilled from 37 to just below 10°C were 7150, 6670, 5950, 5051, 4601 and 4115s by PCM (equivalent percentage reductions in milk chilling time were 6.71, 16.78, 29.35, 35.65 and 42.44 % as compared to control; control: 0.00% TiO_2 in base fluid) having 0.00, 0.05, 0.25, 0.50, 0.75 and 1.00% TiO_2 nanoparticles respectively. The observed percentage reduction in discharging time in this study were better than the data reported by Liu *et al.* (2009), who used 1.00% TiO_2 nanoparticles into saturated aqua-$BaCl_2$ salt blend. The results in this study were at par of the data reported by Harikrishnan *et al.* (2013), who used stearic acid as base fluid with TiO_2 nanoparticles. However, it was also comparatively analyzed that the stored energy density of these reported PCM were insufficient to be used for cooling milk below the critical limit as developed in this study.

Discharging of the pre-charged PCM in the spherical modules chilled the raw milk kept inside the milking vessel. Rapid milk chilling was observed by the PCM containing nanoparticles at higher concentrations. It could be credited to the two factors: **a.** higher initial temperature drops, achieved by the PCM having higher concentration of nanoparticles, during charging, thereby, during discharging, initial temperature differences between source (milk) and sink (PCM) were higher while using those PCMs; **b.** enhanced values of 'k' of the PCM of higher nanoparticle concentrations. Upon chilling milk inside the milking vessel by the spherical module, the maximum milk temperature drops achieved were 29, 29.2, 29.4, 29.5, 29.6 and 29.8°C; and these minimum values of milk temperatures reached were maintained for 1430, 2014, 2759, 4757, 5415, 6197s using the stored cooling energy in the PCM having 0.00, 0.05, 0.25, 0.50, 0.75 and 1.00% TiO_2 nanoparticles, respectively (Figure 4.18b). In this process, the phase-transition time during discharging of the PCM due to milk chilling were 5282, 3820, 3673, 3037, 2070, 1640s (Figure 4.18c), respectively. The quick temperature drops and long uphold of the chilled milk temperatures witnessed the improved thermal

properties of the PCM, because it enhanced the melting rate and rapid stored energy exchange into the milk volume.

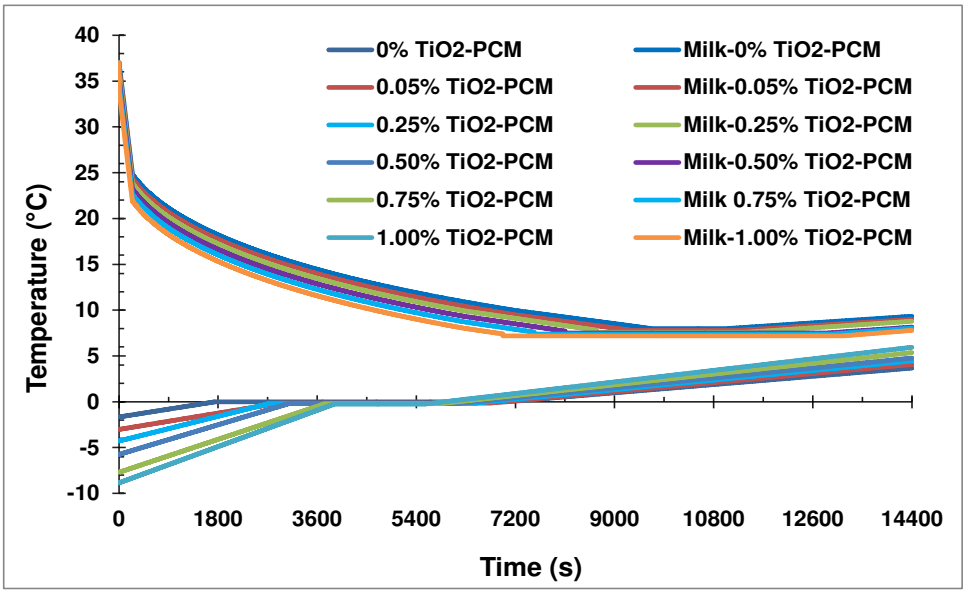

(a)

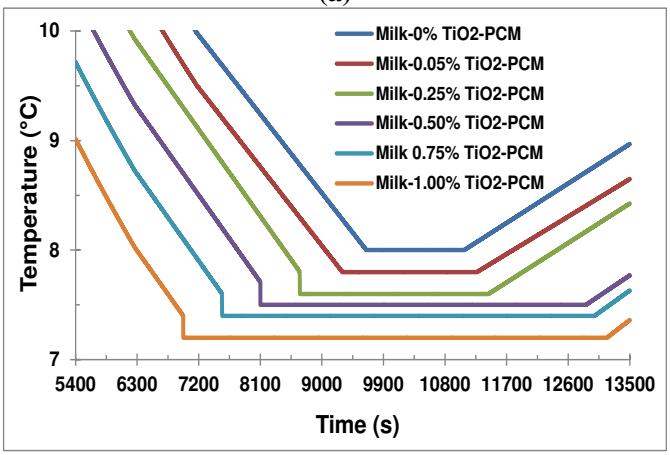

(b)

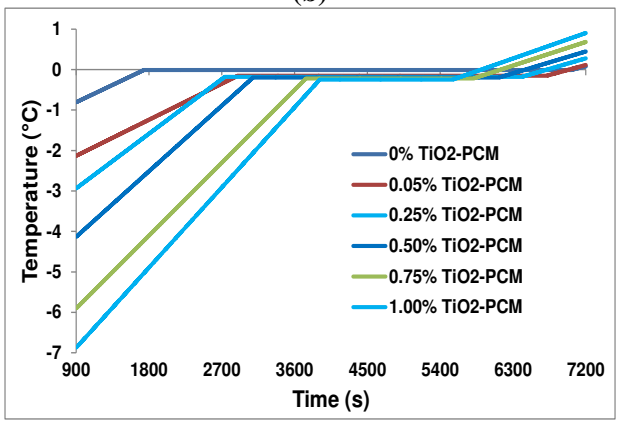

(c)

Fig. 4.18 (a-c) Experimental transient temperature profiles at point 'C' during discharging of the PCM, and the average milk temperature **(a)** for entire duration **(b)** exploded view near milk chilling range **(c)** exploded view near phase-transition range

4.2.1.4 Comparison of the experimental and CFD predicted transient temperature profiles during discharging

Fig. 4.19(a-c), depicts the comparison of experimental and CFD predicted transient temperature profiles of the PCM containing 0.00 and 1.00% TiO_2 at points 'A', 'B' and 'C' during discharging. It is evident from the plots that melting of the PCM started first, at point 'A' followed by 'B' and 'C' in the experimental as well as CFD simulation studies. The observed differences between temperature profiles at points 'A' and 'B' were due to downward flow of the melted PCM from top to bottom via circumference of the un-melted portion (as evident in the transient temperature field contours during discharging presented in Table 4.3), which resulted the presence of lower temperature zone near 'B' during experiments. It was also observed in CFD simulated predictions because effects of gravity were also modelled.

From Fig. 4.19a, it is evident that at point 'A', both the results (CFD predicted and experimental) followed almost similar trends before melting, but thereafter, rate of rise in experimental temperatures were much slower than the predicted results. This was due to inherently lower densities of the water based PCMs in solid state as compare to that in liquid state, which caused the free-floating of un-melted portion of the PCM over the melted pools during experiments, which resulted into persistent occurrence of solid-liquid mixture for longer duration at point 'A', and therefore it slowed down the temperature rising rates at 'A' as compared to 'B'. In case of CFD predicted results, the rate of rise in temperatures at 'A' were higher since floating phenomena (movement of cells) were not modelled (as it is also evident in the transient temperature field visualization and liquid fraction contours during discharging process as presented in the Table 4.3-4.4; which indicate immersed solid portion of PCM into the melted pool of PCM), therefore it neglected the presence of solid-liquid mixture at point 'A' during simulations. In support of the above findings, the differences in instantaneous temperatures at equidistant points from the periphery of a spherical capsule containing n-octadecane during unconstrained melting were reported in literature (Tan, 2008; Tan *et al.* 2009; Sattari *et al.* 2016), however, in the vertical plane inside the spherical capsule, the temperatures at upper points were higher than that at lower points (which is reversed in the present study). This was because the unfrozen PCM was settled down (in the reported studies cited), due to higher density of solid phase (therefore, not floated), at the bottom of the capsule inside the melted pool of PCM. At points 'B' and 'C', both the results (CFD simulated and experimental) followed almost similar trends (Fig. 4.19b-c).

The simulated average milk temperatures, achieved at a particular instant, due to milk being chilled by discharging of the PCM, trailed the experimental results with minor differences as shown in Fig. 4.19d. It could be due to some heat losses through the insulated walls (assumed as adiabatic walls in CFD modeling) of the milk vessel during the experiments.

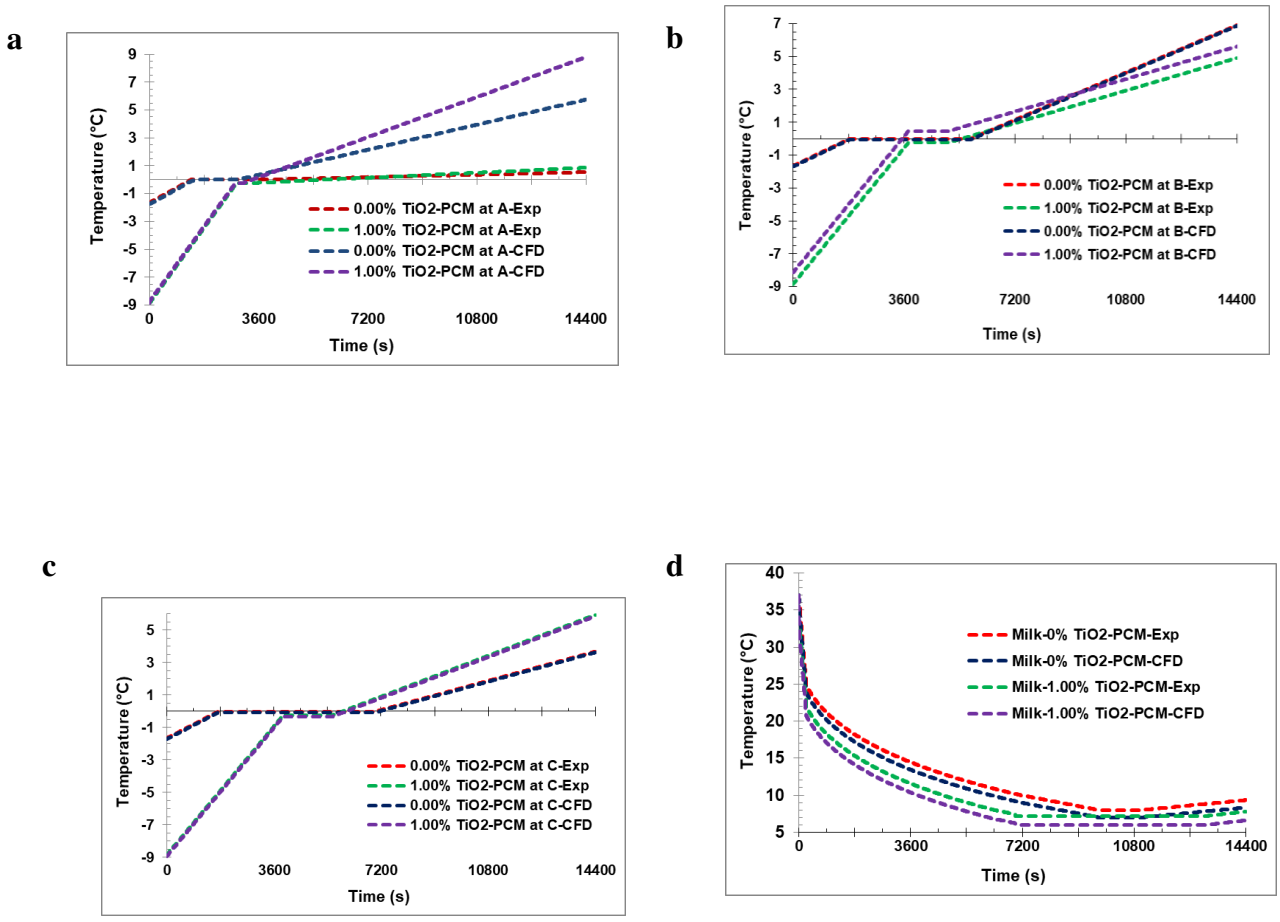

Fig. 4.19 Experimental and CFD predicted transient temperature profiles of the PCM containing 0.00 and 1.00% TiO_2 nanoparticles at point **(a)** 'A', **(b)** 'B', **(c)** 'C' during discharging; and **(d)** the consequent average milk temperature

4.2.1.5 CFD modeled transient temperature field contours

Table 4.3, expound the temperature field contours of the PCM, containing 0.00 and 1.00% TiO_2 during charging, discharging and the consequent milk chilling, recorded for 9000s.

Table 4.3. CFD simulated transient temperature field contours of the PCM containing 0.00 and 1.00% TiO_2 during charging, discharging and the consequent milk chilling

Time (s)	Charging		Discharging	
	0.00%TiO_2-PCM	1.00%TiO_2-PCM	0.00%TiO_2-PCM	1.00%TiO_2-PCM
300	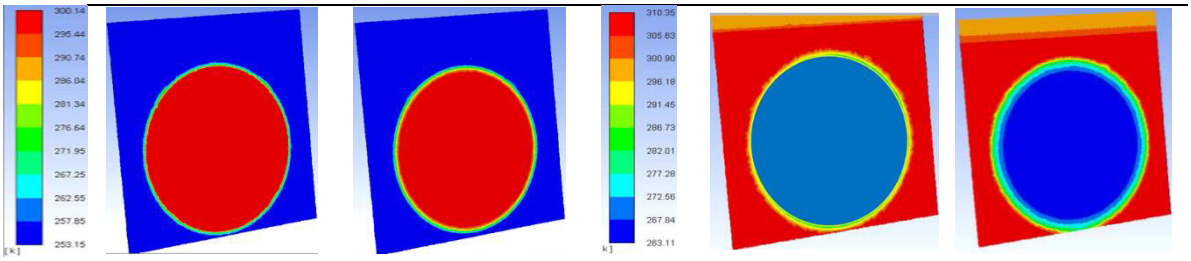			
1800	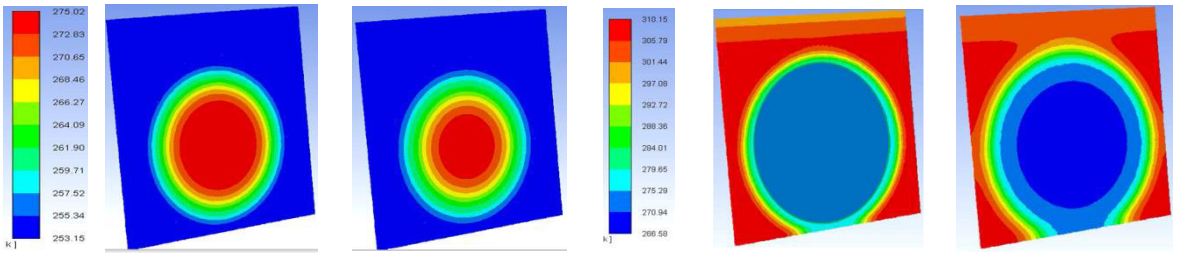			
3600	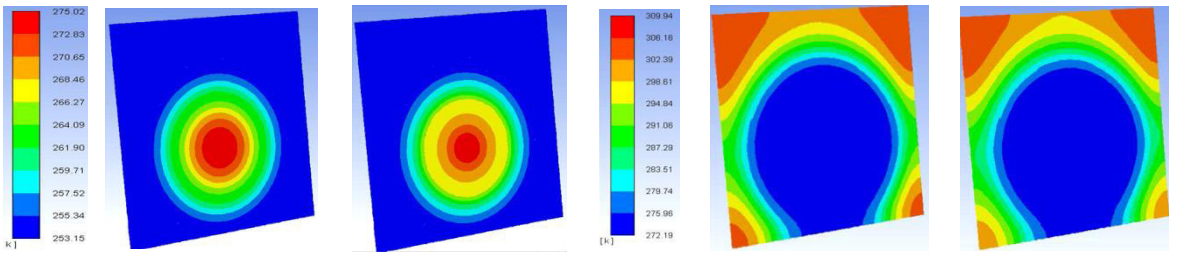			
5400	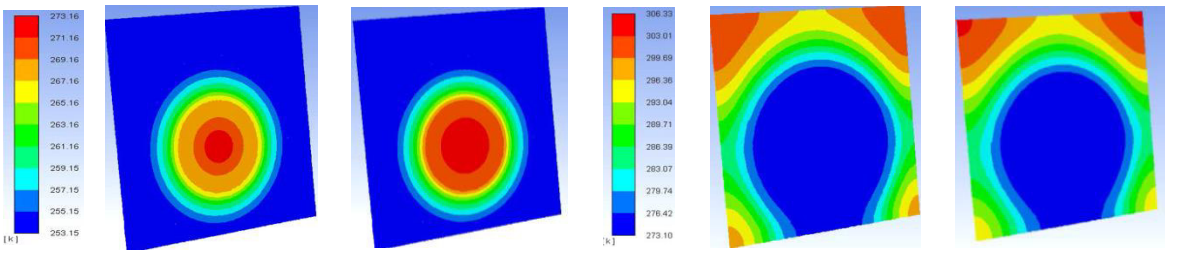			
7200	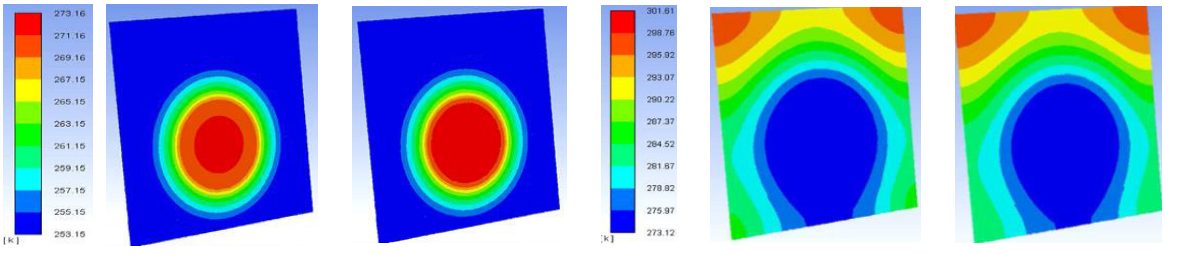			
9000	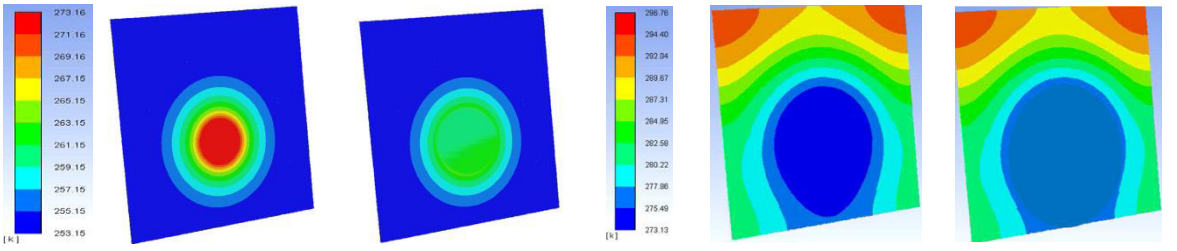			

It is evident that during charging, the hotter zone of the PCM (indicated by red band) was gradually diminished and the colder zone (indicated by blue band) developed parallelly from the periphery of spherical module towards its center radially, as time progressed. During discharging, the hotter zone (indicated by red band: initial milk temperature at around 37°C) was diminished with time which indicated milk cooling as shown by mixed bands at later stages outside the module within the milking vessel. The PCM confined inside the cooling module gained heat from milk and melted due to latent heat exchange, which could be visualized by diminishing dark blue region towards the center as the time progressed. It was also noticed that milk volume near the sides of the cuboidal vessel were chilled faster than those present in the corner pockets (indicated by leftover hotter zones in the corners). The charging, discharging and milk chilling rates of the developed PCM containing 1.00% TiO_2 nanoparticles were quite faster than those without nanoparticles (at 0.00% TiO_2).

4.2.2 Transient liquid fraction profiles and their comparison with computed predictions

4.2.2.1 CFD simulated transient liquid fraction profiles during charging

Fig. 4.20a, describes the CFD predicted volume average liquid fraction (β) data of the PCM at different nanoparticle concentrations. The spherical modules containing PCM were opaque; therefore no experimental comparisons were feasible for β during charging. Therefore, CFD predictions helped in estimating the instantaneous values of β with time. It is evident from plot that increase of nanoparticles concentrations in the base fluid enhanced the charging rate, thereby reduced total charging time (time required to reach β from 1 to 0). Reductions in total charging time were 2.12, 4.52, 8.28, 9.69 and 13.12% with 0.05, 0.25, 0.50, 0.75 and 1.00% TiO_2 nanoparticles as compared to base fluid.

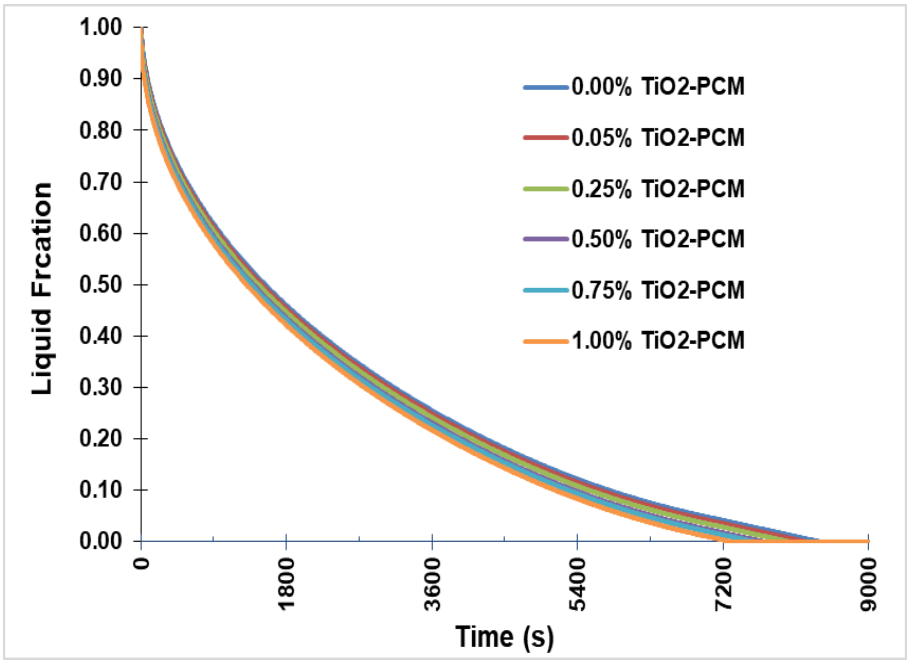

(a)

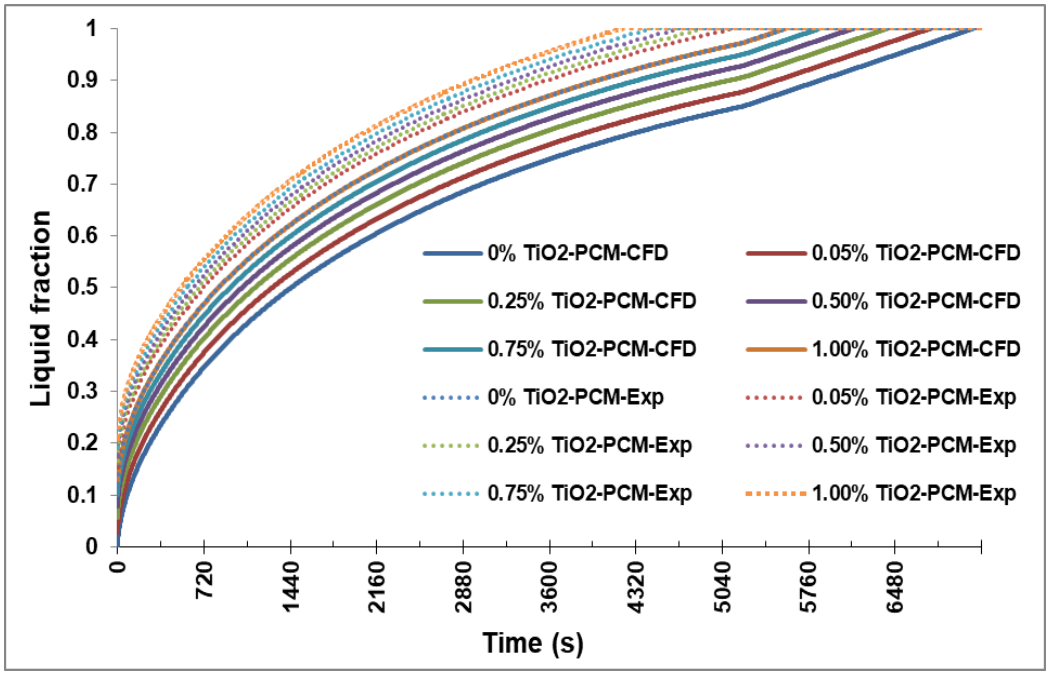

(b)

Fig. 4.20. **(a)** CFD predicted transient liquid fraction profiles of the PCM during charging; **(b)** Comparison of CFD predicted and experimental transient liquid fraction profiles of the PCM during discharging.

4.2.2.2 Comparison of CFD predicted and experimental transient liquid fraction profiles during discharging

Fig. 4.20b, indicate comparison of the CFD predicted and experimental transient liquid fractions of the PCM during discharging at different nanoparticle concentrations. It is

evident from the plots that increase of nanoparticles concentrations in the base fluid enhanced the discharging rate, thereby reduced total discharging time (time required to reach β from 0 to 1). This helped in rapid discharge of the stored cooling energy to milk during chilling, therefore milk was quickly chilled to a relatively lower temperature by the developed PCM as compared to the base fluid (control).

Reductions in simulated total discharging time were 4.95, 9.81, 13.85, 17.88 and 21.87%, whereas that in experiments were 7.90, 12.55, 16.00, 19.88 and 24.32% at 0.05, 0.25, 0.50, 0.75 and 1.00% TiO_2 nanoparticles as compared to the control. For opaque modules, experimental estimation of β during milk chilling was not feasible, therefore for comparison purpose, the modules were kept at surrounding temperatures, fixed at 37°C, inside a BOD incubator; and the melted liquid fractions of PCM collected into a measuring flask, were compared with the CFD predicted values of β. In CFD modelling, the values of β varied as function of chilled milk temperature but during experiments inside BOD incubator, the real-time boundary conditions were fixed at 37°C. This caused reasonable and comparable difference in β values obtained from experiments and the CFD simulated data.

4.2.2.3 CFD modelled liquid fraction contours

Table 4.4, illustrate the liquid fraction contours of the PCM containing 0.00 and 1.00% TiO_2 nanoparticles during charging, discharging and the consequent milk chilling recorded for 9000s. During charging, after t = 0s, the liquid PCM (i.e. β=1) is indicated by red zone inside the spherical module, which diminished as charging progressed and finally disappeared at the end of charging (i.e. β=0). During discharging, after t = 0s, the charged PCM (i.e. β=0) is indicated by dark blue region inside the module, which diminished with time due to discharging of PCM. The liquid milk and melted portion of the PCM were indicated in the contour by red band region (i.e. β=1) which progressed with time and covered the entire domain towards the end of discharging. This indicated the complete discharging of stored energy from the PCM in about 9000s during milk chilling. It was also marked that the charging and discharging rates of the PCM having nanoparticles were more rapid than base fluids without nanoparticles (i.e. at 0.00% TiO_2).

Table 4.4 Liquid fraction contours of PCM containing 0.00 and 1.00% TiO_2 during charging, discharging and the consequent milk chilling

Time (s)	Charging		Discharging	
	0% TiO_2 -PCM	1% TiO_2 -PCM	0% TiO_2 -PCM	1% TiO_2 -PCM
300	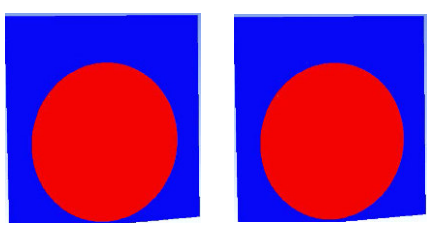		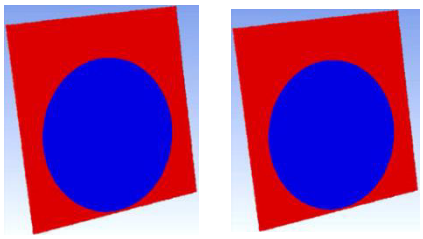	
1800	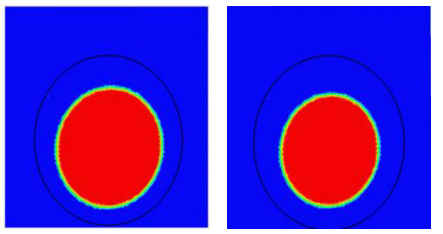		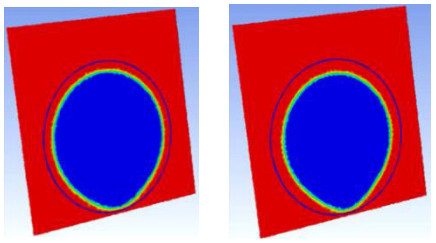	
3600	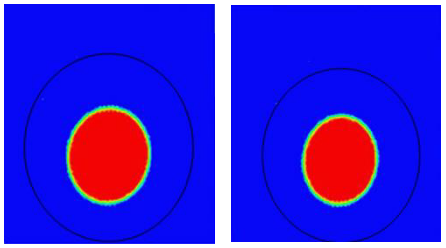		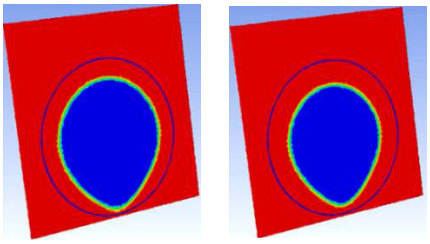	
5400	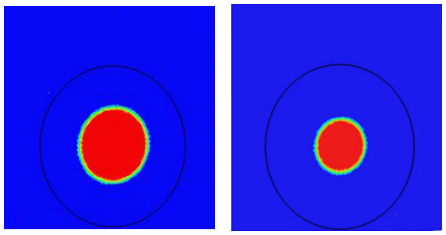		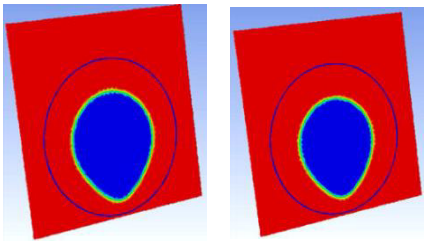	
7200	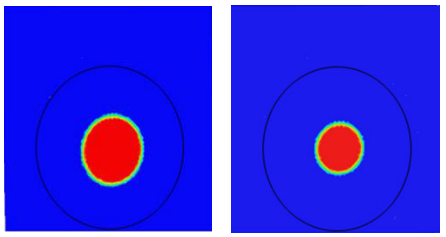		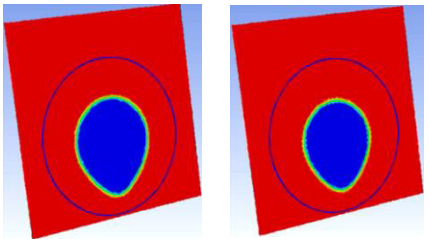	
9000	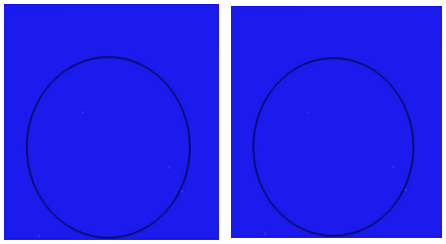		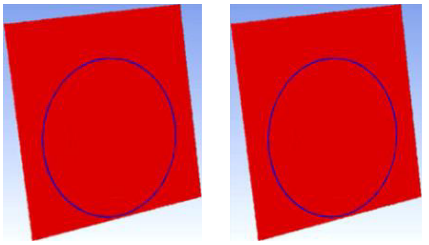	

4.2.3 Streamlines during charging, discharging and the consequent milk chilling

Table 4.5, illustrate the instantaneous streamlines contours representing convective diffusion currents of the melted PCM containing 0.00 and 1.00% TiO_2 during charging, discharging and the consequent milk chilling.

Table 4.5 Streamlines contours of PCM containing 0.00 and 1.00% TiO_2 during charging, discharging and the consequent milk chilling

Time (s)	PCM streamlines				Milk streamlines during chilling	
	Charging		Discharging			
	0% TiO_2 -PCM	1% TiO_2 -PCM	0% TiO_2 -PCM	1% TiO_2 -PCM	0% TiO_2 -PCM	1% TiO_2 –PCM
300	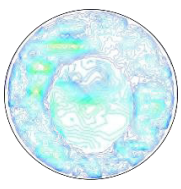	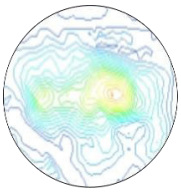	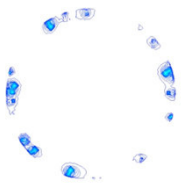		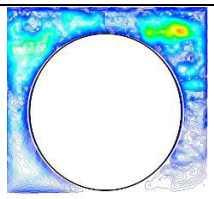	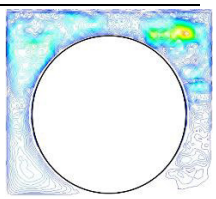
1800	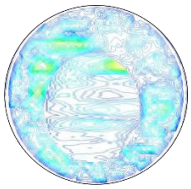	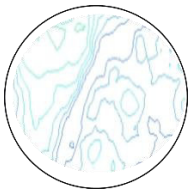		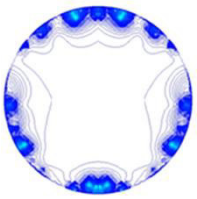	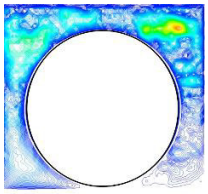	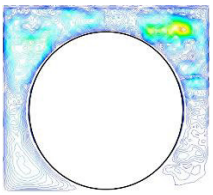
3600	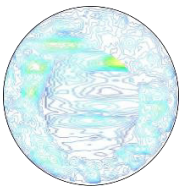	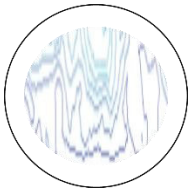			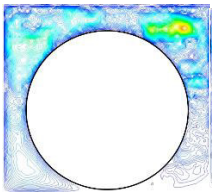	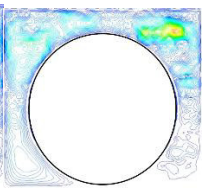
5400	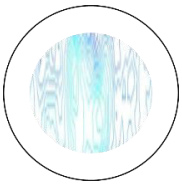	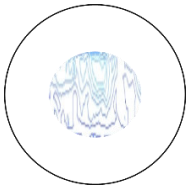	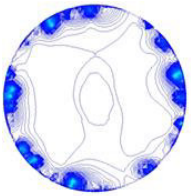	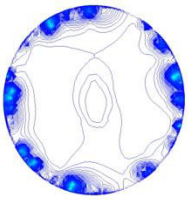	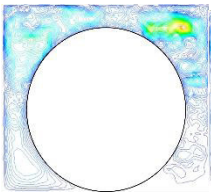	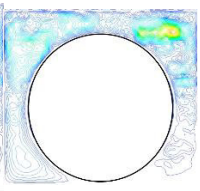
7200	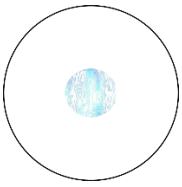	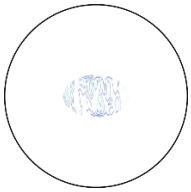	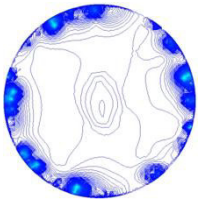	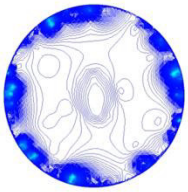	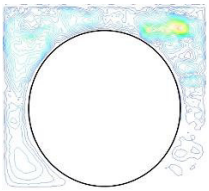	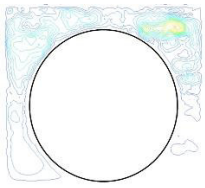
9000	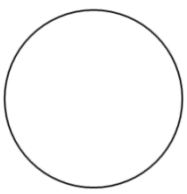	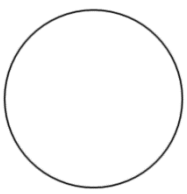	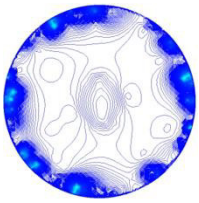	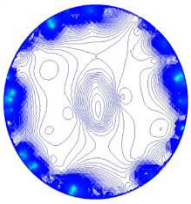	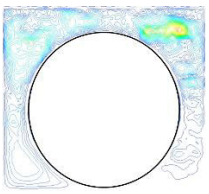	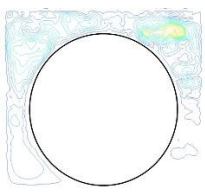

It was noticeable from charging streamline contours that at the start of the charging process, the magnitudes of natural convective currents throughout the PCM were dominant (at around 300s), however it started diminishing towards center of the module as the solidification progressed. Near the inner walls of the module, these currents ultimately disappeared in the solidified region of PCM at/around after 3600s. It could be noted that vanishings of the convective streams were more rapid in the PCM containing 1.00% TiO_2 nanoparticles as compared to the base fluid (having 0.00% TiO_2 nanoparticles; control). During discharging, as melting of the solidified PCM were commenced from inner walls of the module; therefore streamlines appeared initially near the inner walls and were built up throughout inside the melted volume of the PCM, as the melting progressed with time. During charging as well as discharging, streamlines indicated top to bottom thermally driven convective currents throughout its volume. This was due to difference in temperature at these points. In milk chilling contours, it was evident that the natural recirculating convective currents were more prominent during initial phases of milk chilling. As the chilling process progressed with time, due to reduction in temperature, thermally driven top to bottom convective and re-circulatory streams were slowly diminished, which ceased the heat exchange by convection and diffusion-driven molecular exchange continued. This ultimately, divided the hotter and colder milk layers into thermally stratified diffusing zones. Similar explanations pertaining to the heat-transfer mechanisms observed herewith were also elucidated for n-Octadecane PCM in literature (Tan *et al.*, 2009; Sattari *et al.* 2016). These zones were more projected and persistent in the contours towards the side walls and top of the milking vessel as compared to the bottom milk portions. Therefore, top layer milk portions and milk in the corners remained relatively hotter zones as compared to the bottom and side wall layers.

Therefore following points were inferred from testing of the PCM into the spherical module:

- CFD simulations revealed formation of a temporal thermal stratification in the chilled milk layers due to temperature variations in cuboidal geometry of milk vessel.
- The net phase-transition time were reduced by 5.83, 10.51, 16.90, 25.85 and 32.22% during charging, and 7.91, 12.55, 16.05, 20.11 and 24.32% during discharging, whereas total time required for milk chilling from 37 to below 10°C

were speeded-up by 6.71, 16.78, 29.35, 35.65 and 42.44% at 0.05, 0.25, 0.50, 0.75 and 1.00% TiO_2 nanoparticles in DW, respectively.

- Use of nanoparticles significantly influenced the reduction in supercooling degree of the base fluid, however the effects due to saturations at higher weight fractions of nanoparticles were also observed.
- Experimental results validating simulations, confirmed rapid milk chilling performance using NePCM in the module.

4.3 Numerical and experimental study on thermal behavior of NePCM inside the jacketed cylindrical milking pail module

After preliminary testing the NePCM in spherical module inside an ordinary milk vessel, it was intuited to develop a passive milk chilling, portable and handy container (resembling routinely used milking pails). An immediate container to hold milk after milking generally resembles a hollow cylinder with one end closed, either in household or at farm level. Thus, in this activity of the present investigation, TiO_2 nanoparticles were dispersed into DW at 0.20, 0.40 and 0.60% by weight (keeping cost, degree of saturation and cooling requirement in mind), to enhance its energy storage and milk chilling performance.

The NePCM were filled into the jackets of a cylindrical shape milk holding cum cooling module, taken as a test-rig for investigation. Transient charging, discharging and milk chilling behavior of NePCM were numerically simulated using computational fluid dynamics (CFD) technique and validated experimentally in the module.

The various thermo-physical properties of the base fluid and NePCM, measured experimentally and estimated empirically, required for numerical simulation in UDF, are presented in Table 4.6.

Table 4.6 Thermo-physical properties of the NePCM tested in jacketed cylindrical milking pail module

Properties	Temperature (°C)	% wt. of nanoparticles				Uncertainty (%)
		0	0.20	0.40	0.60	
k (W/m-K)	-10	2.279	2.385	2.459	2.497	±1%
	0	0.556	0.597	0.618	0.628	
	10	0.576	0.619	0.639	0.666	
	20	0.597	0.636	0.656	0.686	
	30	0.606	0.642	0.675	0.699	
	40	0.617	0.661	0.689	0.708	
μ(kg/m-s)	27	0.0008	0.0009	0.0011	0.0013	
C_p (j/kg-K)	-10	1995.3	1990.4	1981.8	1973.2	±0.5%
	0	4212.5	4162.3	4139.6	4091.5	
	10	4190.2	4131.4	4115.4	4054.7	
	20	4182.1	4122.1	4092.3	4043.2	
	30	4181.5	4122.1	4092.4	4039.2	
	40	4162.5	4116.5	4091.1	4032.7	
L (j/kg)	-	334997	334591	334486	334328	±0.5%
ρ (kg/m^3)	27	1020.5	1039.5	1053.2	1061.5	
T_m (°C)	-	0	-0.10	-0.14	-0.18	±0.5%

4.3.1 Experimental and CFD simulations studies

4.3.1.1 Charging

Charging (energy storage) studies of the NePCM inside the module were conducted for 120 min during simulation as well as experimental studies, since almost all liquid volumes were frozen within this timeframe.

4.3.1.1.1 Liquid fraction profile

Fig. 4.21a-b, describes the CFD predicted volume average liquid fraction (β) vs time of the NePCM at different nanoparticle concentrations. The experimental modules containing NePCM in the jackets were opaque; so, experimental estimations of β by image analysis or instantaneous drip collections were not feasible during charging. The CFD predicted values helped in approximating the instantaneous values of β. It is evident from exploded plot (Fig. 4.21b) that increase of nanoparticles concentrations from 0.00 to 0.60% in the base fluid enhanced the charging rate by reducing total charging time (i.e. time required to reach β from 1 to 0) from 110 to 85 min. Net reductions in total charging

time were 9.09, 16.36 and 22.72% at 0.20, 0.40 and 0.60% of TiO_2 nanoparticles as compared to the base fluid.

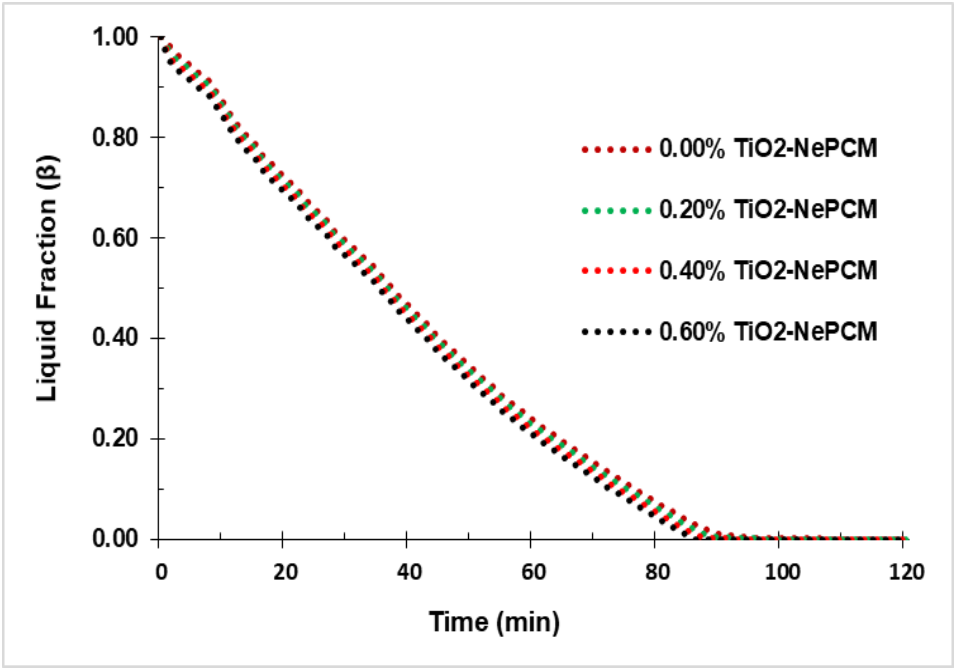

(a)

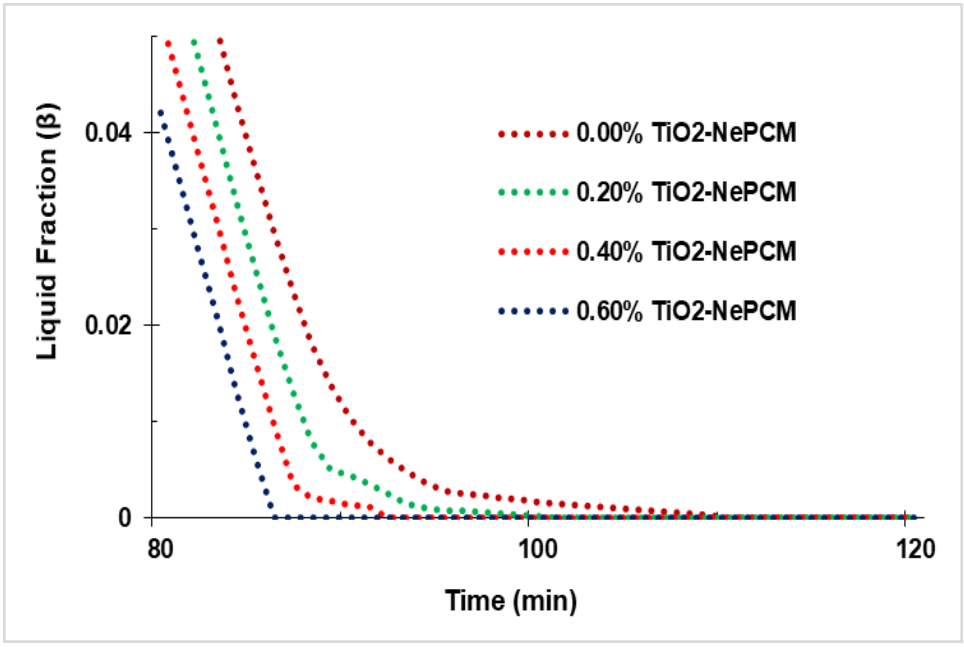

(b)

Fig. 4.21 CFD predicted transient liquid fraction profiles of the NePCM during charging inside jacketed cylindrical module for **(a)** entire duration **(b)** exploded view from 80-120 min

4.3.1.1.2 Temperature profile

Fig. 4.22, demonstrate comparisons of CFD predicted (i.e. instantaneous volume average values; dotted lines) and the experimental transient temperature profiles (average values of temperatures at points 'A' and 'B' (refer Fig. 3.17a) for points 'A' and 'B' inside the module; continuous lines) of the NePCM having TiO_2 nanoparticles from 0.00 to 0.60% by weight, during charging process.

It was observed from experiments that at t >0 min, sensible cooling rates of the NePCMs from ambient (around 27 °C) to their respective solidus temperatures were faster at higher nanoparticle concentrations. The total durations to reach the solidus points (i.e. starting of the freezing process) were 75, 63, 54 and 48 min at 0.00, 0.20, 0.40 and 0.60% nanoparticles respectively. The total freezing time (i.e. up to the end of freezing) was also reduced from 102 to 76 min upon increasing the nanoparticles concentration from 0.00 to 0.60%. Net percentage reductions in freezing time were 7.84, 18.62 and 25.49% at 0.20, 0.40 and 0.60% nanoparticles as compared to the base fluid. Similar studies depicting freezing time reductions for saturated aqua-$BaCl_2$ salt blends and n-octadecane, assisted by TiO_2 nanoparticles, were reported by Liu *et al.* (2009) and Motahar *et al.* (2017), respectively. Findings of the present study, indicated the possibilities of quickly finishing the charging process by use of nanoparticles and reduce the running hours of compressor or any other refrigeration set-up used in charging, thereby save electricity.

Quick completion of the charging process using nanoparticles could be attributed to two factors: **a.** enhanced 'k' of the NePCMs as compared to the base fluid, and, **b.** induced early nucleation in the energy storing media by nano-particles. Enhanced 'k' helped in rapid temperature reductions from ambient, whereas nanoparticles extended sites to initiate nucleation process, thereby reduced supercooling degrees. It is evident from the plot (Fig. 4.22), the supercooling degree was maximum at 0.00% (≈ -3.4°C) and minimum at 0.60% (≈ -1.8°C) of TiO_2 in NePCM. This helped in early start of the phase-transition process during charging.

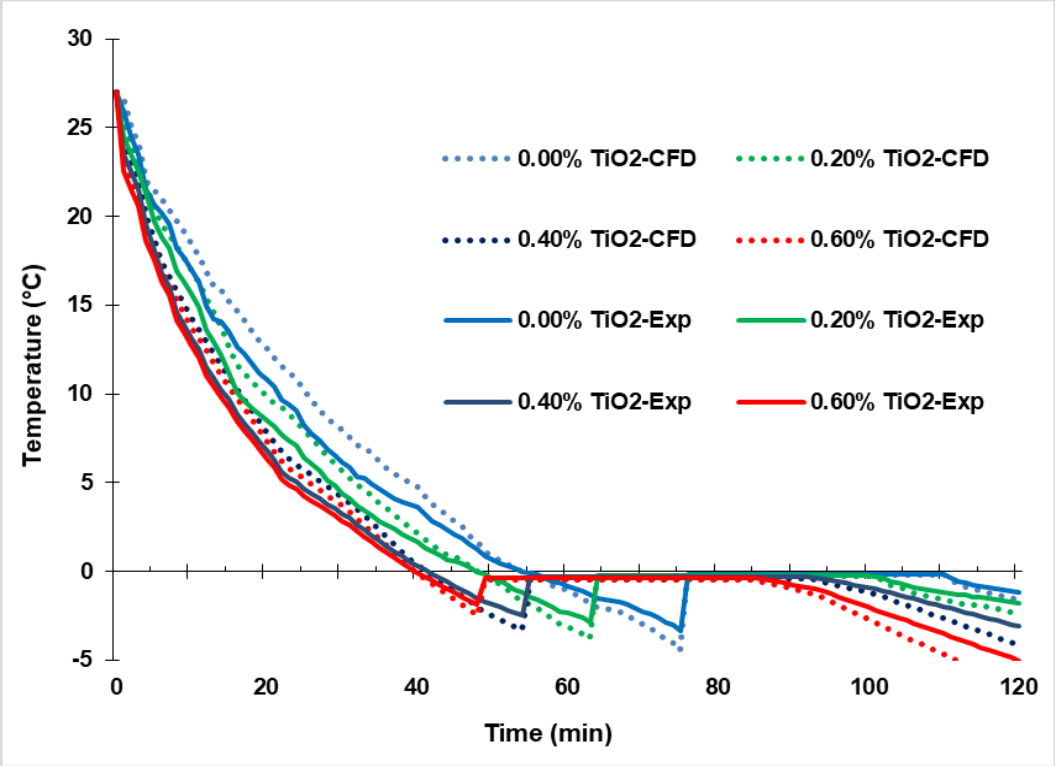

Fig. 4.22 CFD predicted and experimental transient temperature profiles of the NePCM during charging inside the jacketed cylindrical module

It is evident from the plot that, beginning from the ambient conditions, the net temperature drops in NePCMs, in a given charging duration of 120 min, were also more at higher level of nanoparticles. The final temperatures at the end of charging were -1.2, -1.8, -3.1, -5.0°C at 0.00, 0.20, 0.40 and 0.60% nanoparticles, respectively. This pointed to another advantage of using nanoparticles in achieving relatively lower temperatures of the NePCM as compared to the base fluid, at the end charging for a fixed duration. This facilitated higher temperature gradients during passive milk cooling by discharging of the same NePCM, thereby accelerated the milk chilling process (discussed later in discharging).

The CFD predicted values (represented by dotted lines) plotted in Fig. 4.22, were comparable and followed similar trends with the experimental results. This showed the robustness of simulations physics. But, CFD predicted results of net freezing time were somewhat lagging behind the experimental results, because the nucleation assisted freezing were not modelled in the CFD tools (involved complex modelling), rather NePCM was assumed as a homogeneous medium of enhanced 'k'. Though, this included the effects of enhanced 'k' by use of nanoparticles, but neglected the effects of early nucleation and supercooling reductions, which actually existed in the experiments.

Therefore, observed degrees of supercooling were more in the CFD predicted results as compared to the experimental results for a given concentration of nanoparticles and charging duration.

4.3.1.1.3 Comparing temperature profiles at 'A' and 'B'

Fig. 4.23a-b, represent plots comparing the transient temperature profiles of 0.60% TiO_2 NePCM at points 'A' and 'B'. In CFD predicted results, it was observed that the rate of cooling (i.e. charging or energy storage) at point 'A' was faster as compared to 'B' (Fig. 4.23a), whereas in experimental results, it was reversed (i.e. charging rate at point 'B' was faster than at 'A'; Fig. 4.23b).

The faster rate of charging at 'A' in numerically predicted trials, were due to its location, situated at the middle of two heat exchanging walls maintained at fixed charging temperature. But, point 'B' was located in the corner of the cylindrical geometry, which delayed the energy exchange process at 'B', by lengthening the effective distance between source (local centroid of the cells near 'B' holding NePCM) and sink (heat absorbing walls).

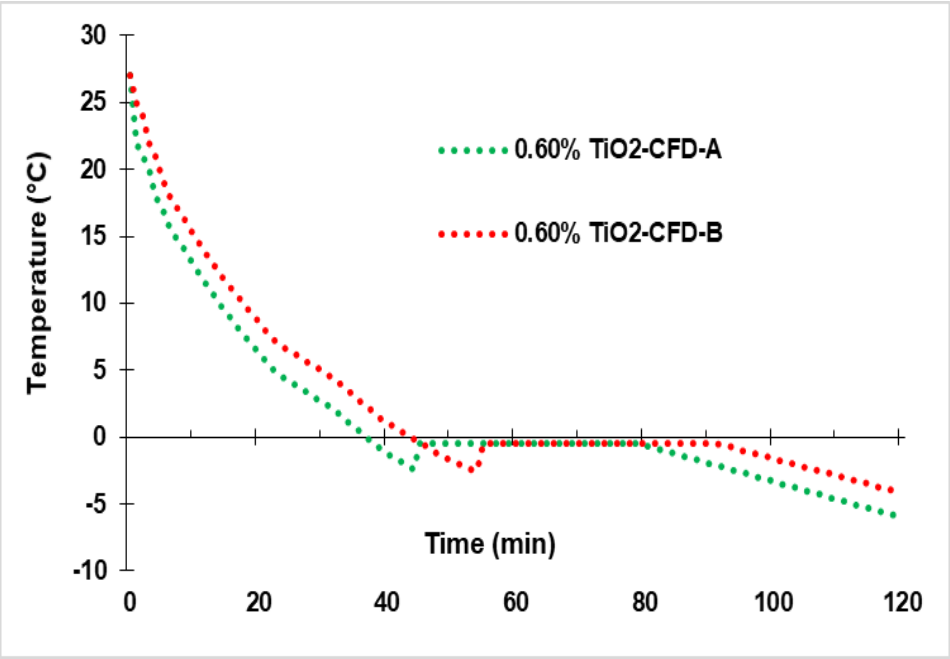

(a)

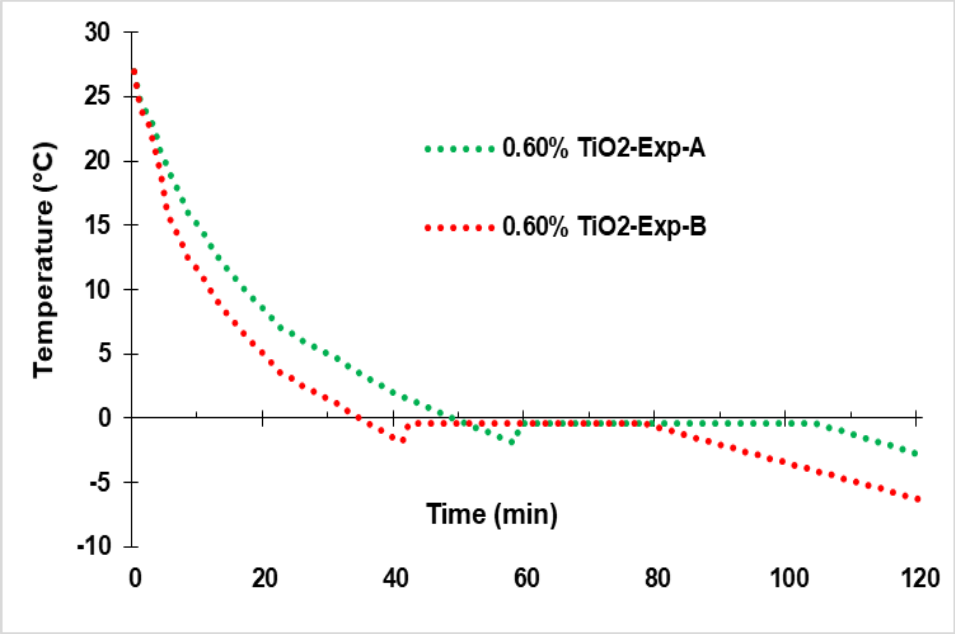

(b)

Fig. 4.23 **(a)** CFD predicted; **(b)** experimental transient temperature profiles of 0.6% TiO_2 NePCM at 'A' and 'B' during charging inside jacketed cylindrical module

During experimental trials, the point 'B' was located more towards the bottom of charging slot (the practically colder zone inside charger) as compared to 'A'. Thus, a temperature gradient along the heat exchanging charging walls (confining the NePCM), from bottom to top, was observed for a considerable period (which was assumed fixed in the modelling). This delayed the charging process at 'A' during the experiments and reversed the observed trends of temperature profiles.

4.3.1.1.4 Temperature field and liquid fraction contours during charging

Table 4.7, indicates the CFD modelled transient temperature fields (T,°C) and liquid fraction (β) contours of the NePCM at 0.00 and 0.60 % TiO_2 during charging inside the module.

The effects of dispersing nanoparticles into the base fluid (0.00% TiO_2) on charging rate is evident from the contours plots. It is clear from T-contours that the NePCM (initially at ambient temperature) located inside the jacket of the module (indicated by reddish band) was diminishing as the time progressed. It was consequently converted into the yellowish, greenish and bluish bands, indicating reduction in temperature of the NePCM due to charging. However, the charging rates were quite faster in 0.60%, as compared with 0.00% TiO_2 NePCM, as shown in the second row of T-contours. At the end of t = 120

min, clear differences in NePCM temperatures at these nanoparticle fractions are detectible by the color bands. Cooling rates at the cells of domain located between the parallel vertical walls of the jacket were higher than those at the corners. This clearly visualized the differences in temperatures at points 'A' and 'B' during charging.

β-contours indicated rate of solidification of the NePCM inside the module from completely liquid (β = 1, indicated by red bands) to mixture (solid+liquid: 0<β<1; indicated by light red, yellow, green and light blue bands), to completely solid (β = 0, indicated by dark blue bands). Trends of liquid fraction variation were similar to that of temperatures in different zones. The solidification rates of 0.60% TiO_2 NePCM were higher as compared to that of 0.00, and the slower charging zones (i.e. corners) showed relatively slower rate of β converting to '0', as compared to the parallel vertical zones in the jacket, as visualized from the contours.

Table 4.7 CFD modelled transient temperature field (T,°C) and liquid fractions (β) contours of the NePCM (at 0.00 and 0.60% TiO_2) during charging

Time (min)		20	40	60	80	100	120
T (°C)	0.00 %TiO_2	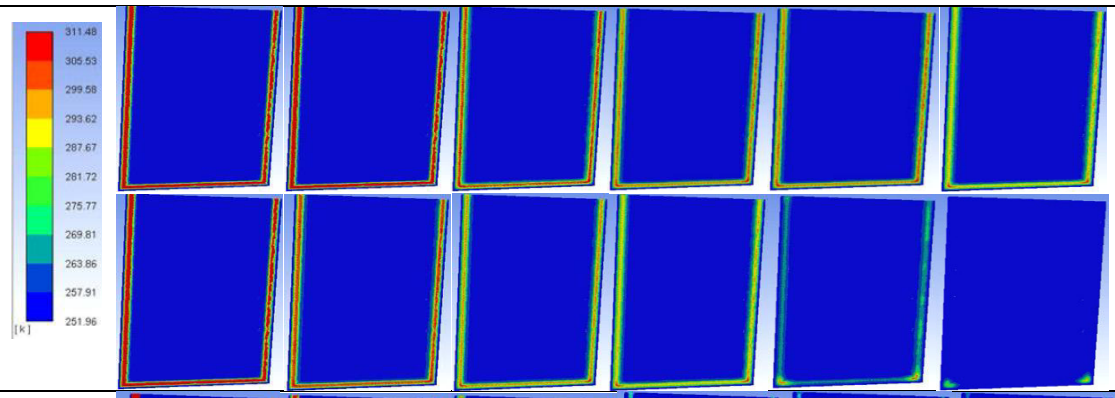					
	0.60 %TiO_2						
β	0.00 %TiO_2	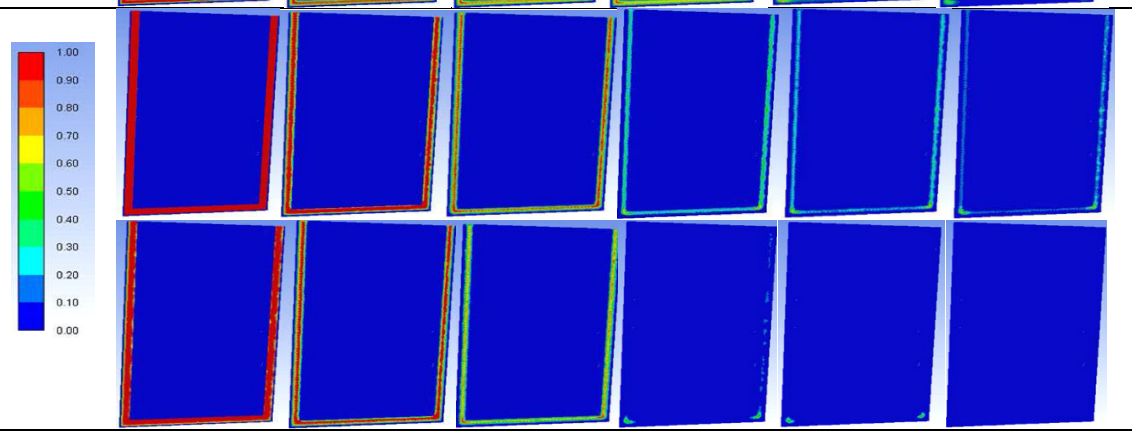					
	0.60 %TiO_2						

4.3.1.2 Discharging and Passive milk chilling

Discharging (energy release) of the NePCM inside the module due to passive milk chilling were studied for 240 min during simulation as well as experiments, since almost

all the charged NePCM (solid volumes) were converted into liquids, and milk temperature also started slowly rising after reaching a minimum value.

4.3.1.2.1 Liquid fraction profile

Fig. 4.24, indicated a comparison of CFD predicted and experimentally observed transient liquid fraction (β) profiles during discharging of the NePCM (at different nanoparticle concentrations). The CFD predicted values of β (indicated by dotted lines) were obtained from simulating the passive milk cooling conditions in the study.

It was observed that the time required to completely melt (β = 1) the charged NePCM (discharging time) was reduced from 235 to 134 min, as the nanoparticle concentrations were increased from 0.00 to 0.60%. Percentage reductions in discharging time were 8.51, 33.6 and 42.9% at 0.20, 0.40 and 0.60% TiO_2 nanoparticles. This revealed that NePCM released the stored energy quickly due to enhanced 'k', into the milk being passively chilled. Thus, it would be advantageous to use the developed NePCM over base fluid, for milk chilling, where original milk quality is a function of time required for chilling it below the safe limit.

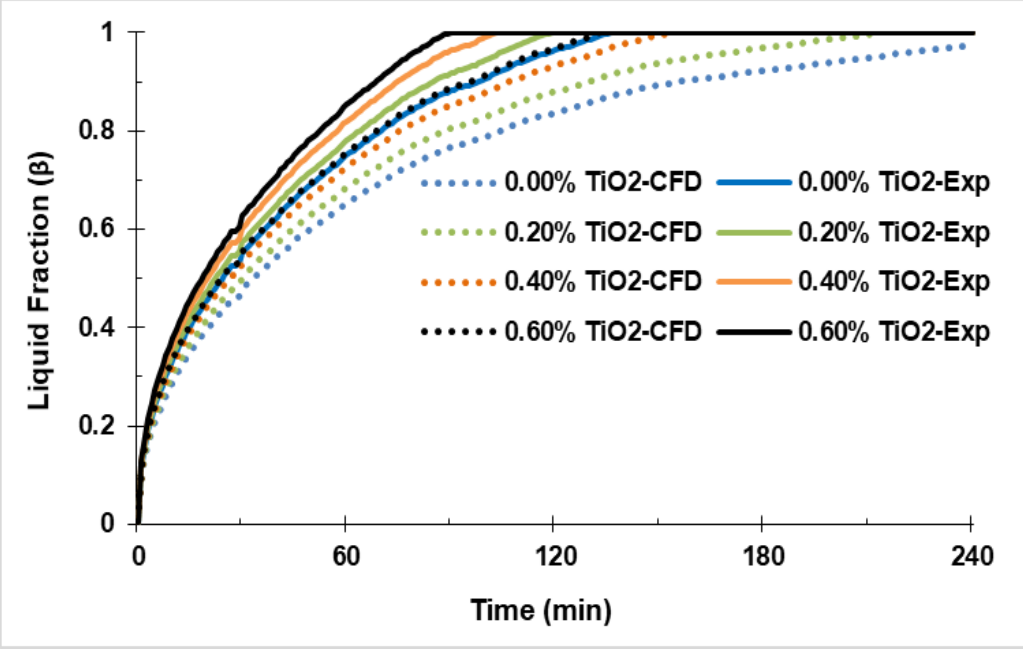

Fig. 4.24 CFD predicted and experimental transient liquid fraction profiles of the NePCM at different nanoparticle concentrations during discharging

The experimental values of β (indicated by continuous lines) with time were obtained from measuring volumes of the melted fractions collected from the module kept inverted inside a BOD incubator fixed at 37°C.

The melting rates were faster as compared to simulations, because the heat exchanging boundary conditions were fixed in the experiments, but varied during simulations (with milk temperature). But effects of nanoparticle enhancements on melting rates were evident in these studies also. Percentage reductions in discharging time were 11.7, 25.0 and 33.8% at 0.20, 0.40 and 0.60% TiO_2 nanoparticles.

4.3.1.2.2 Temperature profile

Fig. 4.25, demonstrate comparisons of CFD predicted (i.e. instantaneous volume average values; plotted as dotted lines) and the experimental transient temperature profiles (average values of temperatures at points 'A' and 'B' (refer Fig. 3.17b for 'A' and 'B' inside the module); shown as continuous lines) of the NePCM having TiO_2 nanoparticles from 0.00 to 0.60% by weight, during discharging process. In this plot, the consequent temperature profiles of milk being passively chilled inside the module by discharging of the NePCM represented by dotted lines (CFD-predicted volume average values) and continuous lines (experimental values: average of temperatues at points 'C', 'D' and 'E'; refer Fig. 3.17b for these points).

In experimental trails, milk inside the module was passively chilled from 37 to a minimum temperature of 18.8, 16.3, 14.1 and 9.5°C by NePCM having 0.00, 0.20, 0.40 and 0.60% nanoparticles, respectively. Therefore, NePCM with 0.60%TiO_2 nanoparticles was best for milk chilling, inside the module, below the safe limit of quality deteriorations. After reaching these minimum values, the milk temperatures were maintained for 40, 50, 70 and 92 min, for respective concentrations of nanoparticles, and rose slowly thereafter at constant rates. The final temperatures of milk after 240 min, at respective nanoparticle fractions, were 20.2, 17.5, 15.3 and 10.5°C, respectively. The CFD simulated values followed almost similar trend with the experiments with MAPE at most 2.00%.

The higher temperature drop in milk chilled by 0.60%TiO_2-NePCM were achieved because of enhanced phase-transition rates (i.e. reduced discharging time), which enabled quicker release of stored cooling energy (in the form of latent heat) by absorbing heat from milk.

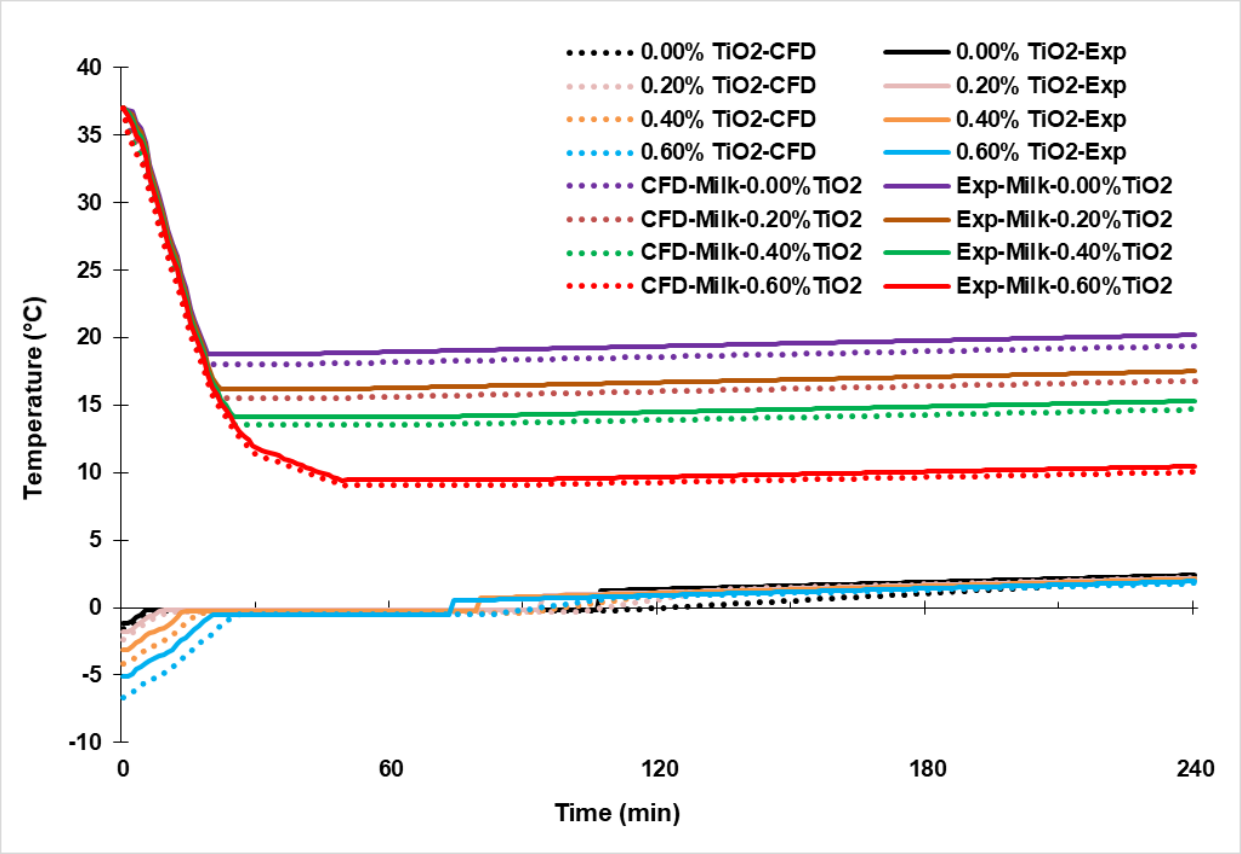

Fig. 4.25 CFD predicted and experimental transient temperature profiles milk chilling and discharging NePCM at different nanoparticle concentrations

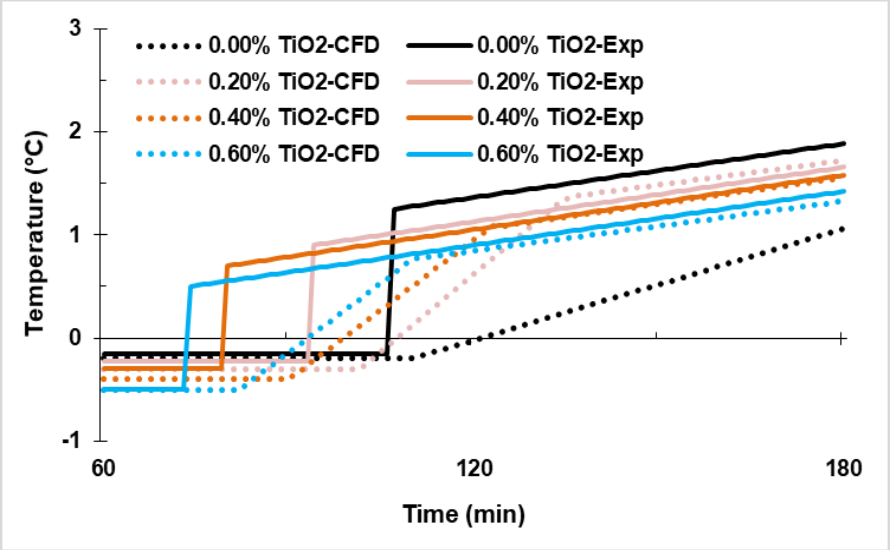

Fig. 4.26 Exploded view (60-180 min: phase-transition range) of CFD predicted and experimental transient temperature profiles of discharging NePCM

However, the rising rates in milk temperatures, thereafter, controlled by insulated housing, were almost same irrespective of nanoparticle concentrations. Since, higher milk temperature drops were achieved in the beginning phase itself, therefore it helped in

maintaining fresh raw milk at relatively lower temperature for longer duration by use of 0.60%TiO_2-NePCM.

In experimental studies (Fig. 4.25) on NePCM discharging, it was observed that the NePCMs pre-charged up to -1.2, -1.8, -3.1 and -5.1°C, started energy exchange with milk at t > 0 min, completed phase-transitions (according to temperature profile) within 106, 93, 79 and 74 min at 0.00, 0.20, 0.40 and 0.60% TiO_2 in NePCM (Fig. 4.26). The reductions in phase-transition time were due to enhanced 'k', which brought rapidity in the melting process. Fig. 4.26, explicitly describe an exploded view of the melting profile near phase-transition ranges of the NePCMs. It is evident that at the end of melting, there are sudden early rises in temperatures of the NePCMs in experimental results, but late and slowly progressive rises in the CFD predicted values. This might be due to real-time presence of solid-liquid mixture inside the partly melted NePCM volume, during experiments, which partly controlled the rise of average temperatures during phase-transitions. However, as the floating volume of un-melted NePCM inside the melted liquid diminished, it suddenly rose the average experimental temperatures much earlier than CFD-predictions (where complex phenomena related to movement of cells were not modelled).

4.3.1.2.3 Comparing temperature profiles at 'A', 'B', 'C', 'D' and 'E'

Fig. 4.27, shows a comparison of temperature variations of the discharging 0.60%TiO_2-NePCM at 'A' and 'B' and of chilled milk at 'C', 'D' and 'E' located inside the module. It was observed from Fig. 4.27a, instantaneous temperatures at 'A' were higher than 'B' throughout the experiments as well as CFD-predictions. It was due to locations of the points; as the effective distance of heat source (milk) from 'A' was less than 'B', therefore 'B' remained in relatively colder zones inside the module.

Fig. 4.27b, indicated that trends of instantaneous temperatures at 'C', 'D' and 'E' during experiments were D>C>E; whereas, that during simulations as C>D>E. Since, milk cooling proceeded from sides and bottom, so, the hotter zones of milk were confined near the center (close to 'C'), therefore 'C' remained hottest zone in the simulations. However, during real-time testing, the relatively hotter milk volumes at center slowly rose towards 'D' due to local convection. Therefore, point 'D' remained hottest during experiments. Point 'E' remained coldest in both type of studies due to its location near the bottom.

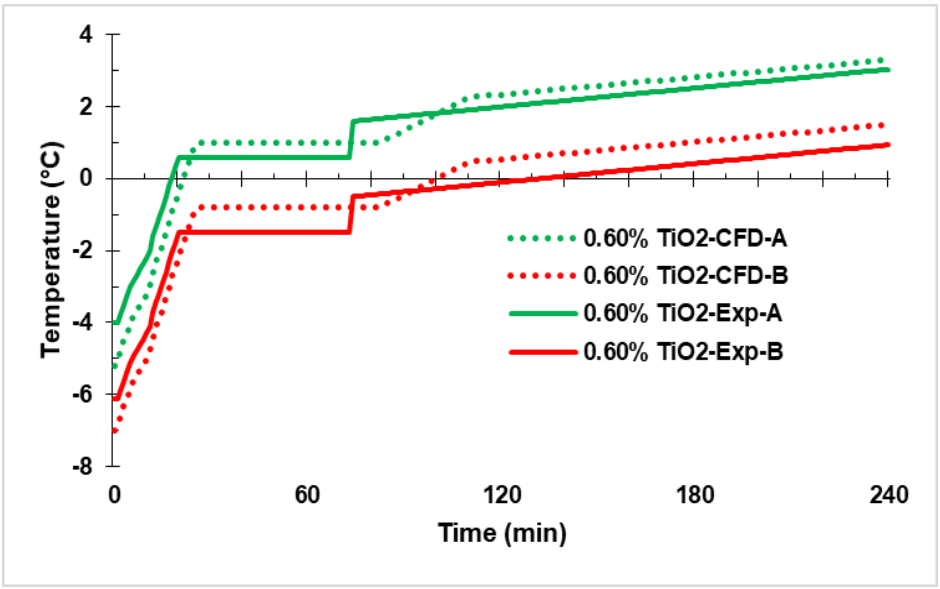

(a)

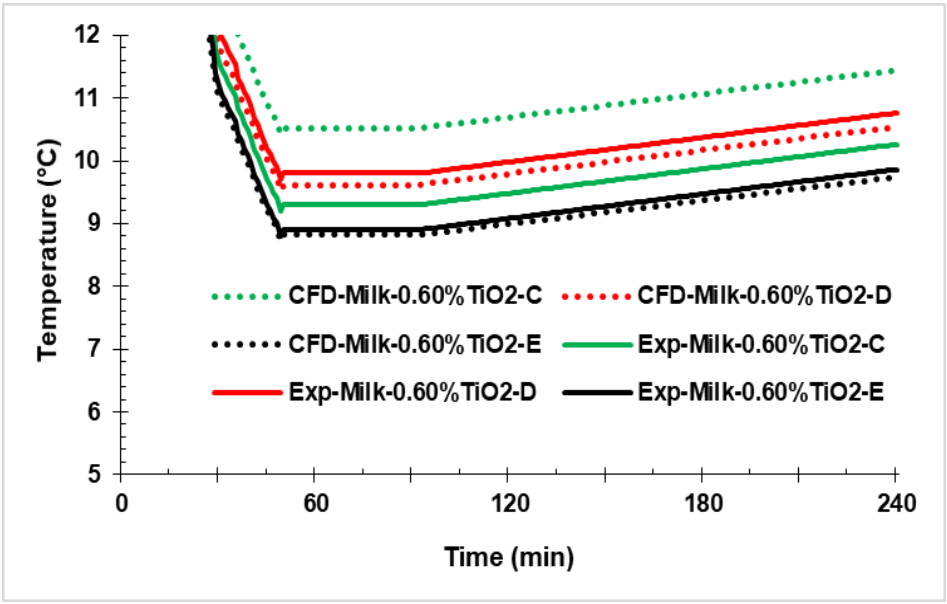

(b)

Fig. 4.27 Temperature profile of **(a)** NePCM at 'A' and 'B'; **(b)** milk at 'C', 'D' and 'E' (exploded view from 0-12°C) during discharging and passive milk chilling

4.3.1.2.4 Temperature field and liquid fraction contours during discharging and passive milk chilling

Table 4.8, elaborates on CFD modeled transient temperature field (T,°C) and liquid fractions (β) contours of the NePCM (at 0.00 and 0.60 % TiO_2) during discharging and consequent passive milk chilling for 120 min.

The enhancement effects due to nanoparticles in the NePCM as compared to the base fluid (0.00% TiO_2) on discharging as well as milk chilling rate are evident from the

contours plots. It was noticed from the T-contours that the NePCM (initially at pre-charged temperatures) located inside the jacket of the module (indicated by deep bluish bands) was diminishing as the time progressed. The volume of milk (initially at around milking temperature, 37°C) indicated by reddish zone, was slowly diminishing towards the center of the module, as cooling progressed. The various temperature zones inside the module were indicated by intermediary color bands such as yellow, light greenish, light bluish etc., indicating reduction in milk temperature. The differences in temperatures at points 'C', 'D' and 'E', as discussed before, could be justified by the developing temperature zones of colder milk from sides and bottom, as visible in the contours. The overall discharging as well as milk cooling rates were quite faster in 0.60%, as compared to 0.00% TiO_2 NePCM, as visualized in the second row of T-contours. At the end of t = 120 min, clear differences in NePCM as well as milk temperatures with and without nanoparticles are detectible by the color bands. Heat exchanging rates at the cells of the domain located between the parallel vertical walls of the jacket (near point 'A') were higher than those at the corners (point 'B'), therefore 'B' remained colder as compared to 'A'.

β-contours indicated rate of melting of the NePCM inside the module from completely solid ($\beta = 0$, indicated by deep bluish bands) to mixture (solid+liquid: $0<\beta<1$; indicated by light green yellow, reddish and light blue bands), to completely liquid ($\beta = 1$, indicated by red bands). Instantaneous liquid fractions varied as per the temperatures rising zones inside the domain. The discharging rates of 0.60% TiO_2 NePCM were higher as compared to that of 0.00, and the colder zones (i.e. corners) showed relatively slower rate of melting, (i.e. some solid fractions remained even up to the end of discharging process) than the readily heat exchanging zones near the parallel vertical walls of the jacketed cylindrical module.

Table 4.8 CFD modeled transient temperature field (T,°C) and liquid fractions (β) contours of the NePCM (at 0.00 and 0.60% TiO_2) during discharging and that of passive milk cooling

Time (min)		20	40	60	80	100	120
T (°C)	0.00 %TiO_2	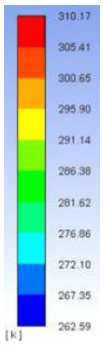					
	0.60 %TiO_2						
β	0.00 %TiO_2	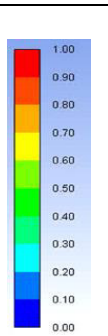					
	0.60 %TiO_2						

Therefore following points were inferred from testing of the NePCM into the jacketed cylindrical milking pail module:

- CFD simulations validated with experiments revealed the existence of relatively hotter and colder points in the module during milk chilling.
- Net reductions in total charging time were 9.09, 16.36 and 22.72 % at 0.20, 0.40 and 0.60 % of TiO_2 nanoparticles as compared to the base fluid.
- The final temperatures reached by a PCM at the end of charging were significantly influenced by level of nanoparticles i.e. -1.2, -1.8, -3.1, -5.0 °C at 0.00, 0.20, 0.40 and 0.60% nanoparticles, respectively.
- The charging, discharging and milk chilling rates were quite faster with NePCM having 0.60% TiO_2, as compared to 0.00% TiO_2 NePCM.
- Percentage reductions in discharging time were 8.51, 33.6 and 42.9% at 0.20, 0.40 and 0.60 % TiO_2 nanoparticles.

4.4 Numerical and experimental study on thermal behaviour of NePCM inside the jacketed cylindrical milking pail module with and without agitator

Considering the findings of preceding activity under this project, it was hypothesized that a provision of agitating the chilled milk, would not only augment the heat transfer co-efficient by disturbing the stagnant milk layers, but also be helpful in eliminating the differences between hotter and colder zones inside the milking pail being developed. In general, agitation at slower speed during milk chilling halts separating out of the different phases without incorporating surrounding air and rupturing of the fat globules. Thus, in this activity of the investigation, TiO_2 nanoparticles at 0.00, 0.50, and 1.00% by weight, were used for preparing NePCM into DW, to arrive a comparative figure depicting the effects hypothesized. The NePCM were assimilated into the jackets of a cylindrical shape, portable, milk chilling container module having top mounted agitator at the center, taken as a test-rig in the investigation. Time dependent, unsteady state discharging of the NePCM were simulated using enthalpy-porosity models. The impeller rotations (the rotating frame) and milk flow patterns (the stationary frame) were simulated using multiple reference frame (MRF) technique.

Table 4.9. Thermo-physical properties of the NePCM for simulating milking pail with agitator

Properties	**Temperature (°C)**	**% by *wt.* of nanoparticles**			**Uncertainty (%)**
		0	0.50	1.00	
k (W/m-K)	-10	2.277	2.458	2.555	±1%
	0	0.552	0.612	0.651	
	10	0.571	0.633	0.692	
	20	0.595	0.655	0.722	
	30	0.604	0.671	0.738	
	40	0.616	0.685	0.756	
μ(kg/m-s)	27	0.0007	0.0011	0.0016	
C_p (j/kg-K)	-10	1995.1	1981.4	1963.4	±0.5%
	0	4212.2	4137.1	4055.8	
	10	4189.2	4110.9	4007.3	
	20	4181.7	4097.3	3989.7	
	30	4180.9	4097.2	3986.3	
	40	4160.8	4091.8	3981.9	
L (j/kg)	-	334988	334389	334112	±0.5%
ρ (kg/m^3)	27	1020.4	1052.4	1068.4	
T_m (°C)	-	0	-0.16	-0.20	±0.5%

Milk flow patterns were modelled using Laminar (≤ 30 rpm) and Transition Shear-Stress-Transport (SST)-models (≥ 50 rpm) of CFD at 0, 30, 50, 70 and 100 rpm. The various

thermo-physical properties of the base fluid and NePCM, used in numerical simulation as UDF, measured experimentally and estimated empirically, are presented in Table 4.9.

4.4.1 Experimental and CFD simulations studies in milking pail module with agitator

Simulations pertaining to the charging process (energy storing) of the NePCM inside a similar container module as discussed in the previous section, were conducted (data not shown) and validated with experiments, for a fixed charging duration of 120 min using a matching capacity freezing chamber maintained at -20°C. It was anticipated that effects on energy exchange due to milk agitation would be noticeable only during milk chilling and energy discharging, therefore charging processes were studied only in background. It was observed that the final temperatures achieved by charging of the NePCMs for 120 min, were significantly influenced by different nanoparticle concentrations dispersed into the base fluid matrix. The final mean temperatures (of replicative trials) at the end of charging (for 120 min) were -2.1, -4.5, -6.2°C at 0.00, 0.50 and 1.00% nanoparticles, respectively. This pointed out an advantage of using nanoparticles in achieving relatively lower temperatures of the pre-charged NePCM for given energy consumption. This facilitated higher temperature gradients during passive milk cooling inside the container by discharging of the pre-charged NePCM, thereby accelerated the milk chilling process. Energy discharging trials of the pre-charged NePCM inside the module due to passive milk chilling were conducted for 240 min during simulation as well as experiments, since almost all the charged NePCM (solid volumes) were converted into liquids, and milk temperature also started slowly rising after reaching a minimum value.

4.4.1.1 Liquid fraction profile

Fig. 4.28, indicated a comparison of CFD simulated and experimentally observed transient liquid fraction (β) profiles during discharging of the NePCM (at different nanoparticle concentrations) at different rpm of the agitator. The CFD predicted values of β (indicated by dotted lines) were obtained from simulating the passive milk cooling conditions in the study. It was observed from Fig. 4.28a, that the time required to completely melt (β=1) the charged NePCM (discharging time) was reduced from 236 to 194 min, at 0.00% nanoparticle concentrations, as the agitator speed was increased from 0 (control) to 100 rpm. The percentage reductions in discharging time due to agitator

speed were 3.81, 10.16, 13.98 and 17.79% at 30, 50, 70 and 100 rpm, respectively, as compared to control.

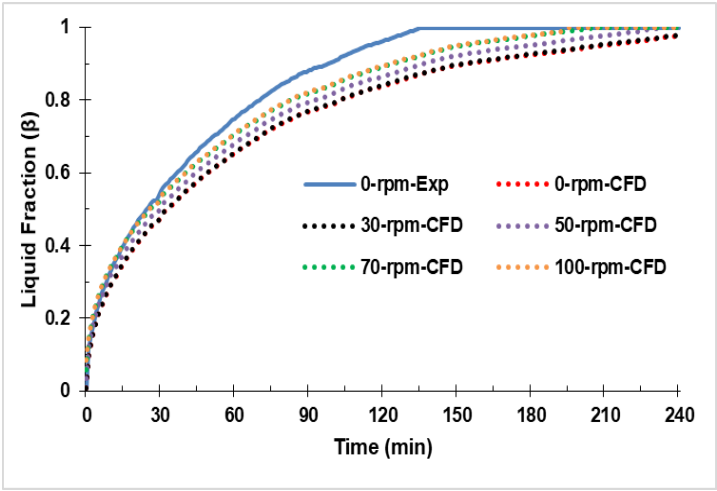

(a) For 0.00 % TiO_2 –NePCM

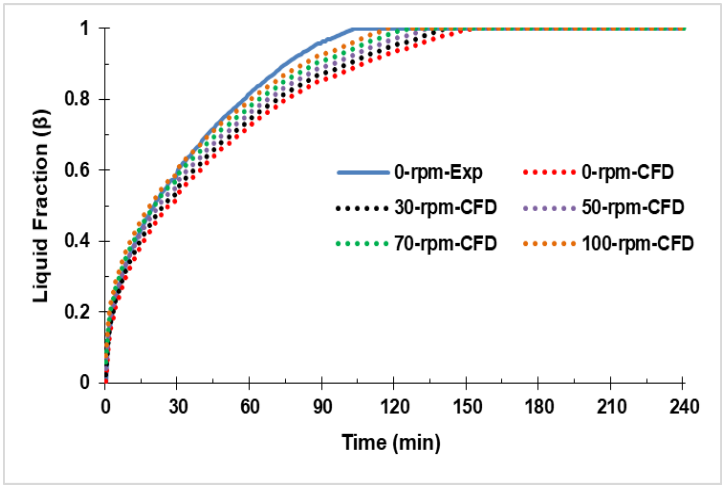

(b) 0.50 % TiO_2 –NePCM

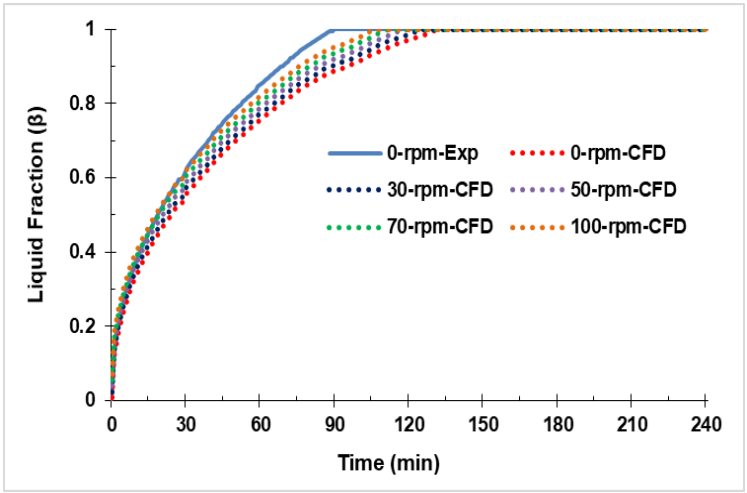

(c) 1.00 % TiO_2 –NePCM

Fig. 4.28 CFD predicted and experimental transient liquid fraction profiles of the NePCM at different rpm of agitator during energy discharging

Fig. 4.28b, indicated these reductions by 7.69, 12.82, 17.94 and 23.07% at similar sequence of speeds at 0.50% nanoparticle concentrations; whereas Fig. 4.28c, indicated further reductions in these values by 6.67, 13.44, 16.29 and 20.00% at same sequence of speeds at 1.00% nanoparticle concentrations. Thus, it was inferred that energy discharging process was expedited by both the factors viz. increased level of nanoparticles as well as the agitator speed. Increased level of nanoparticles enhanced the rate of energy exchange by augmenting thermal conductivities, therefore, NePCM quickly released the stored cooling energy into milk. Increased speed of agitation from 0 to 100 rpm, augmented the effective number of milk cell volumes in physical domain of simulation (which are relatively hot) coming in contact with the heat sink (i.e. NePCM-wall) per unit time. This improved the heat-convections within milk as well as overall heat transfer co-efficient on heat exchanging walls (by disturbing the stagnant milk layer). The synergic effects of agitator speed and level of nanoparticles indicated net reductions in discharging time by 54.23%. This opined the advantages of using the developed NePCM and the container module for energy efficient milk chilling in villages. Uniformly cooled milk not only maintains good quality parameters but also eases the sampling process for quality evaluations and pricing.

The experimental transient values of β (indicated by continuous lines) as shown in Fig. 4.28a-c, were obtained from measuring volumes of the melted fractions of NePCM, collected from the module kept inverted inside a BOD incubator fixed at 37°C. Therefore, the effects of milk agitation were not included in these trials, only the values at 0-rpm at different nanoparticle concentrations were plotted and compared. The observed melting rates herewith were faster as compared to simulations, because the heat exchanging boundary conditions were fixed in the experiments (37°C), but varied during simulations (with milk temperature and time). However, effects of increasing the level of nanoparticles in NePCM were noticeable as the energy discharging rates were expedited by 24.46 and 33.8% at 0.50 and 1.00% of nanoparticles as compared to same at 0.00%.

4.4.1.2 Temperature profile

Fig. 4.29a-f, demonstrate comparisons of CFD predicted (i.e. instantaneous volume average values; shown by dotted lines) and the experimental transient temperature profiles (average values of temperatures at points ‘A’ and ‘B’ (refer Fig. 3.18a; for points ‘A’ and ‘B’) inside the module; plotted as continuous lines) of the

NePCM having TiO_2 nanoparticles at 0.00, 0.50 and 1.00% by weight, at 0, 30, 50, 70 and 100 rpm of agitator, during discharging and milk chilling process. In these plots, the consequent temperature profiles of milk being passively chilled inside the module by discharging of the NePCM represented by dotted lines (CFD-predicted volume average values) and continuous lines (experimental values: average of temperatures at points 'C', 'D' and 'E'; refer Fig. 3.18a; for points 'C', 'D' and 'E').

Fig. 4.29a-b, indicates that pre-charged 0.00% TiO_2-NePCM passively chilled the raw milk inside the container from 37 to 18.1, 16.5, 15.7, 14.8 and 15.2°C at 0, 30, 50, 70 and 100 rpm of agitator, in 25, 23, 21, 20 and 18 min (estimated marginal mean of 3 replications), respectively. It was observed that as the speed of agitator increased from 0 to 100 rpm, net milk temperature drop from 37 to a minimum value (as reported above), was increased by 15.34%.

An exploded view of the temperature profiles with time near the phase-transition ranges of 0.00% TiO_2-NePCM, were shown in Fig. 4.29b, which revealed that energy discharging and phase-change processes were accomplished in 110, 101, 92, 85 and 78 min, at 0 (control), 30, 50, 70 and 100 rpm of agitator, respectively. In this way, the total energy exchange time for milk cooling was expedited by 8.18, 16.36, 22.72 and 29.09%, respectively at 30, 50, 70 and 100 rpm, as compared to control.

Fig. 4.29c-d, indicates pre-charged 0.50% TiO_2-NePCM passively chilled fresh raw milk inside the container from 37 to 13.5, 12.7, 11.9, 10.8 and 9.8°C at 0, 30, 50, 70 and 100 rpm of agitator, in 28, 26, 24, 22 and 21 min, respectively. It was observed that as the speed of agitator increased from 0 to 100 rpm, net milk temperature drop from 37 to a minimum value, was increased by 15.74%.

An exploded view of the temperature profiles with time near the phase-transition ranges of 0.50% TiO_2-NePCM, were shown in Fig. 4.29d, which revealed that energy discharging and phase-change process was accomplished in 90, 83, 72, 64 and 61 min; at 0 (control), 30, 50, 70 and 100 rpm of agitator, respectively. In this way, the total energy exchange time for milk cooling was expedited by 7.77, 20.00, 28.88 and 32.22%, respectively; at 30, 50, 70 and 100 rpm, as compared to control.

Fig. 4.29e-f, indicates pre-charged 1.00% TiO_2-NePCM passively chilled fresh raw milk inside the container from 37 to 9.1, 8.5, 8.2, 7.6 and 7.2°C at 0, 30, 50, 70 and 100 rpm of agitator; in 53, 48, 44, 42 and 40 min, respectively. It was observed that as the speed of agitator increased from 0 to 100 rpm, net milk temperature drop from 37 to a minimum value, was increased by 6.81%.

An exploded view of the temperature profiles with time near the phase-transition ranges of 1.00% TiO_2-NePCM, were shown in Fig. 4.29f, which revealed that energy discharging and phase-change process was accomplished in 75, 69, 61, 56 and 52 min; at 0 (control), 30, 50, 70 and 100 rpm of agitator, respectively. In this way, the total energy exchange time for milk cooling was expedited by 8.00, 18.67, 25.33 and 30.67%, respectively at 30, 50, 70 and 100 rpm, as compared to control.

From above plots, it was also inferred that upon increasing nanoparticles concentrations from 0.00 to 1.00% and agitator speed from 0 to 100 rpm, synergic effect on milk cooling time to reach a temperature below the critical limit were significant. The NePCM also released the stored energy quickly at higher nanoparticle concentrations and high speeds of agitator. Therefore, considering gentle handling of milk during cooling process, a speed ranging between 50-100 rpm, for given size of passive cooling container in this study, may be recommended. It would help in shortening the cooling time as well as homogeneous temperature distribution in milk.

The CFD-predicted values almost reported nearby the experimentally observed values. The sources of slight differences could be attributed to the minor heat losses to the surroundings during real-time observations.

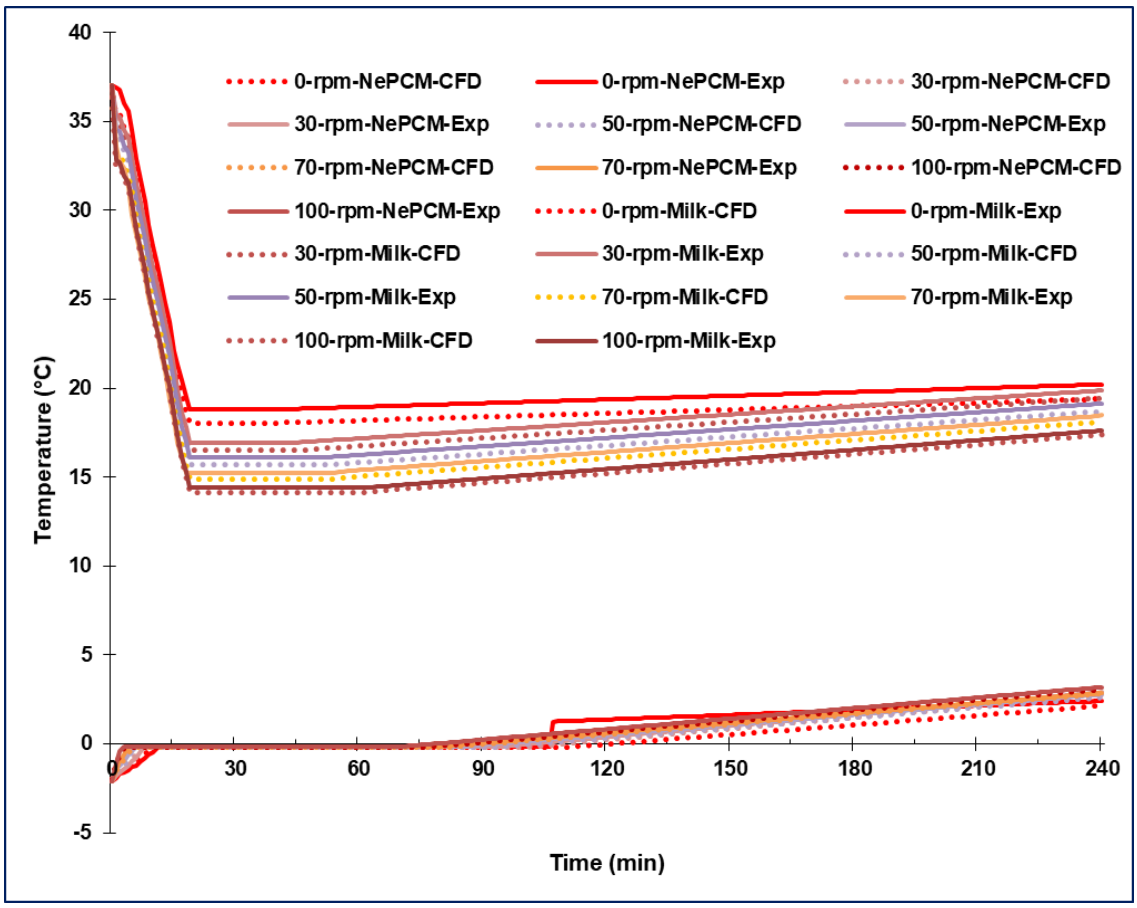

(a) For 0.00% TiO_2 –NePCM (entire range of milk cooling)

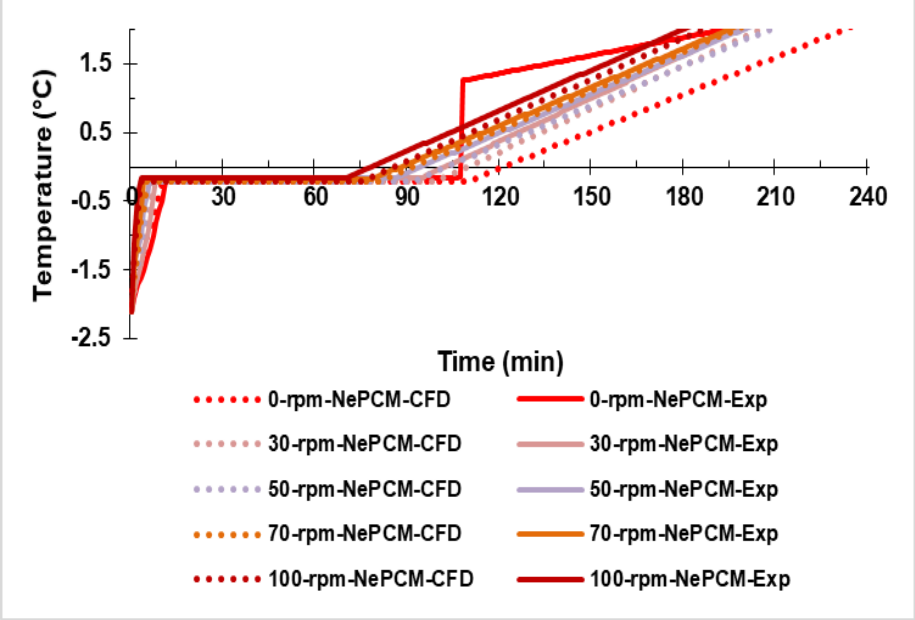

(b) For 0.00% TiO_2 –NePCM (exploded view near phase-transition)

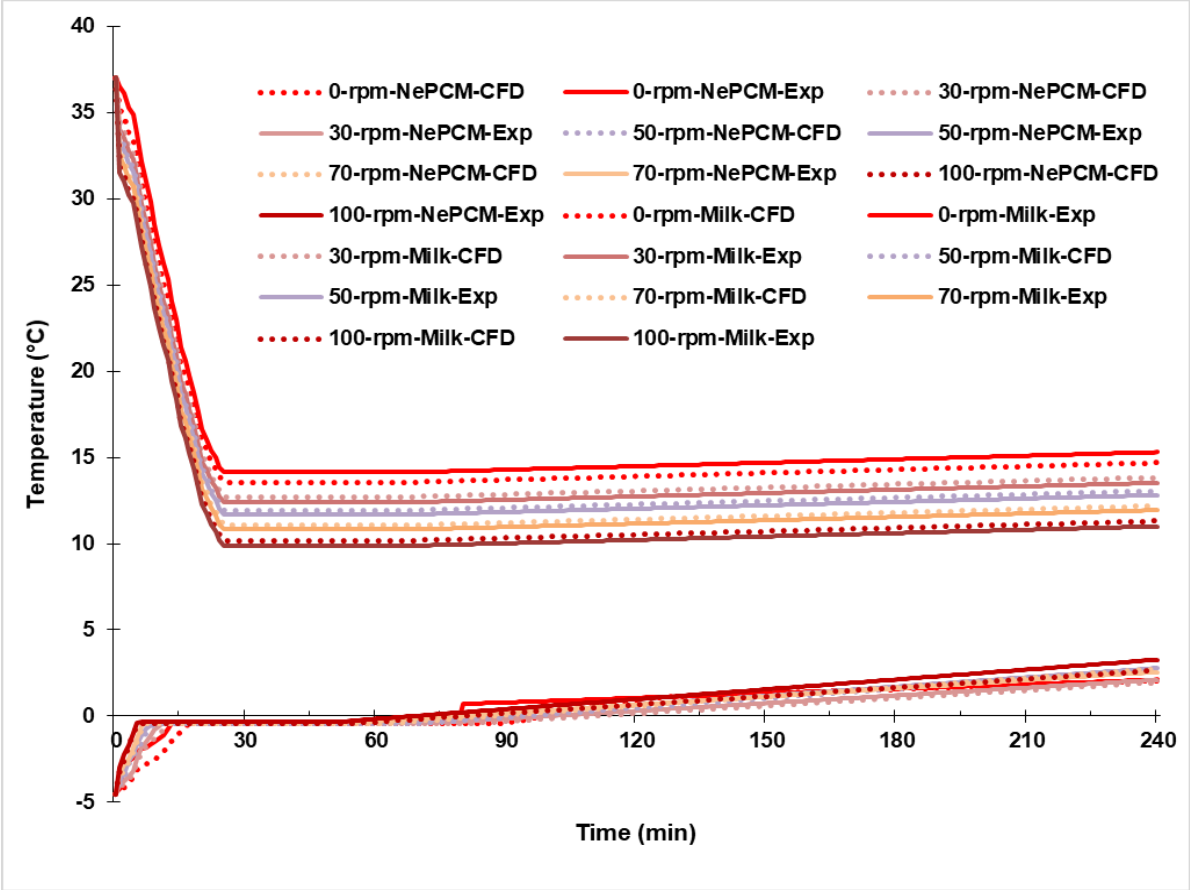

(c) 0.50 % TiO_2 –NePCM (entitre range of milk chilling)

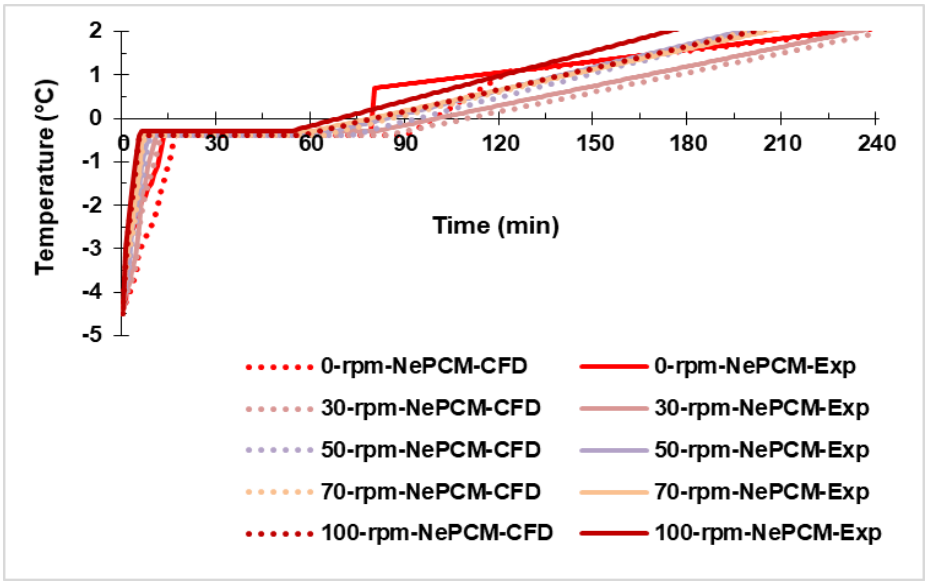

(d) 0.50% TiO_2 –NePCM (exploded view near phase-transition range)

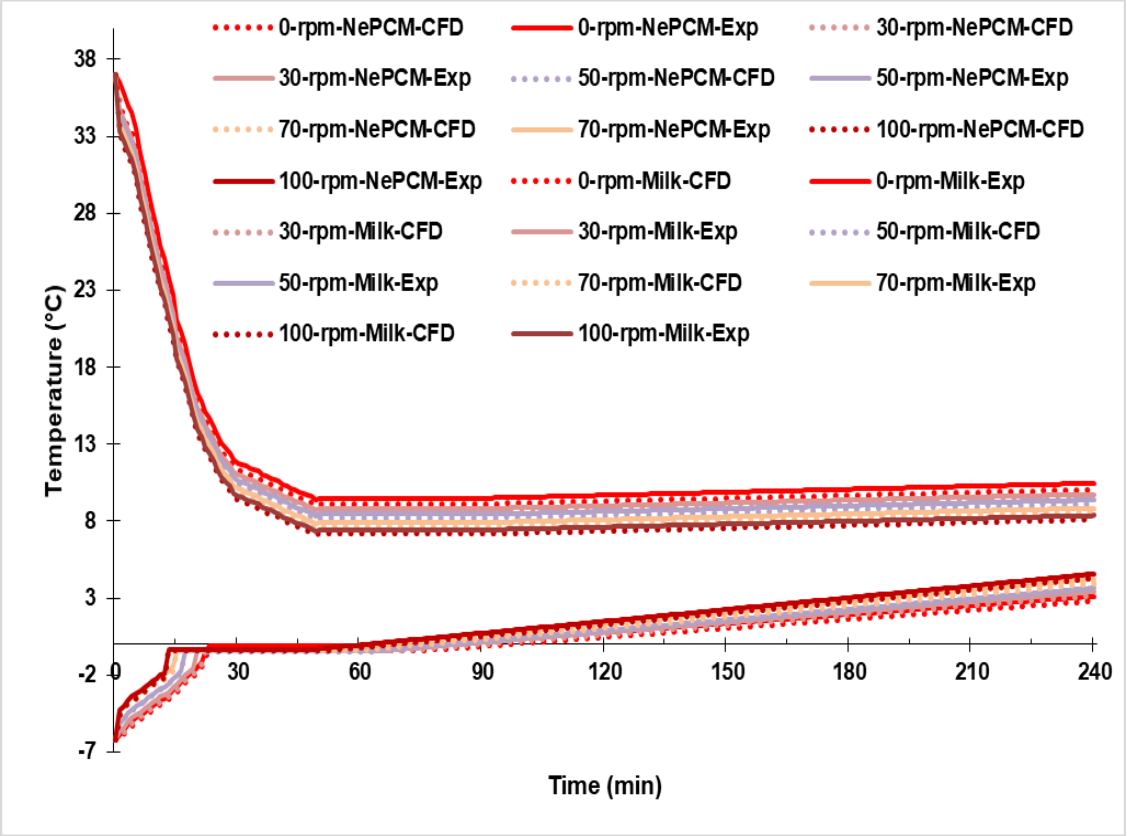

(e) 1.00 % TiO_2 –NePCM (entire range of milk chilling)

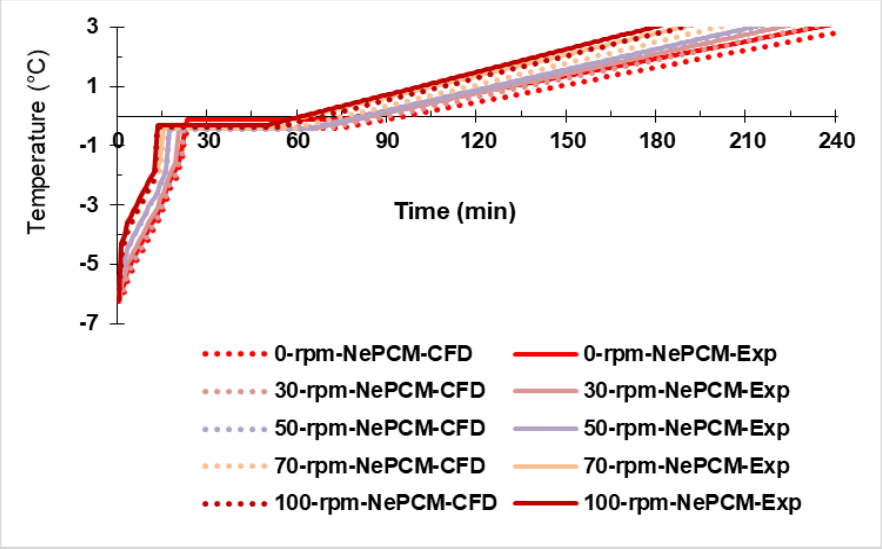

(f) 1.00 % TiO_2-NePCM (exploded view near phase-transition)

Fig. 4.29 (a-f) CFD predicted and experimental transient temperature profiles of milk chilling and discharging of NePCM at different nanoparticle concentrations and agitator speeds.

4.4.1.3 Comparing temperature profiles at 'A', 'B', 'C', 'D' and 'E'

In order to understand the hotter and colder zones or points inside the container module, the temperatures at 'A', 'B', 'C', 'D' and 'E', were calculated from simulated data and validated with experiments.

Fig. 4.30(a-c), shows a comparison of temperature variations of the discharging 0.50% TiO_2 NePCM at 'A' and 'B' and of chilled milk at 'C', 'D' and 'E' located inside the module. It was observed from Fig. 4.30a, instantaneous PCM temperatures at 'A' were higher than 'B' throughout the experiments as well as CFD-predictions at 50 rpm. It was due to locations of the points, the effective distance of heat source (milk) from 'A' was less than 'B', therefore 'B' remained in relatively colder zones. Moreover, point 'A' was located near the agitator shaft (which pushed the agitated milk towards this point), so the heat-exchange rates were more at 'A'. Thus, stored energy was quickly released from 'A' whereas these reasons were not persisted at 'B'. Similar trends were observed at all other rpm and nanoparticle weight fractions (data not shown) as indicated for 50 rpm herewith.

Fig. 4.30b, indicated that trends of instantaneous milk temperatures at 'C', 'D' and 'E' during experiments were D>C>E, whereas, that during simulations as C>D>E, at 30 rpm. Similar trends were observed at 0 rpm also (data not shown). Since, milk cooling proceeded from sides and bottom, so, the hotter zones of milk were confined near the center (closer to 'C'), therefore 'C' remained hottest zone in the simulations. However, during real-time testing, the relatively hotter milk volumes at center slowly rose towards 'D' (vertically upper point from 'C') due to local convection. Therefore, point 'D' remained hottest during experiments. Point 'E' remained coldest in both type of studies due to its location near the bottom. The difference in temperatures at 'C', 'D' and 'E' were due to inefficient mixing of chilled milk at low rpm.

Fig. 4.30c, indicated that trends of instantaneous temperatures at 'C', 'D' and 'E' during experiments as well as simulations were almost D≈C≈E, at 50 rpm. Similar trends were observed for 70 and 100 rpm also (data not shown). This indicated well and gentle mixing of milk throughout, which shows homogeneity in temperature distributions.

Therefore, from these observations, it could be inferred that at any rpm below 30, the temperature distributions in chilled milk were not uniform, whereas the same turned uniform after an rpm equal to or above 50. Therefore, for the size of modular unit in this study, at least 50 rpm of agitation would be sufficient to maintain homogeneity of temperatures.

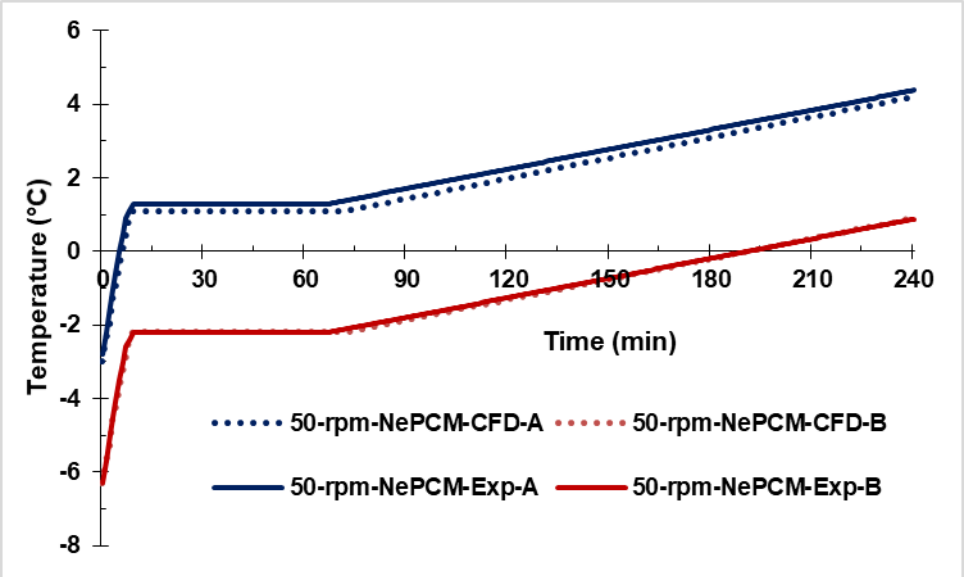

(a) Temperature profiles of 0.50%-TiO_2-NePCM at 'A' and 'B' at 50 rpm

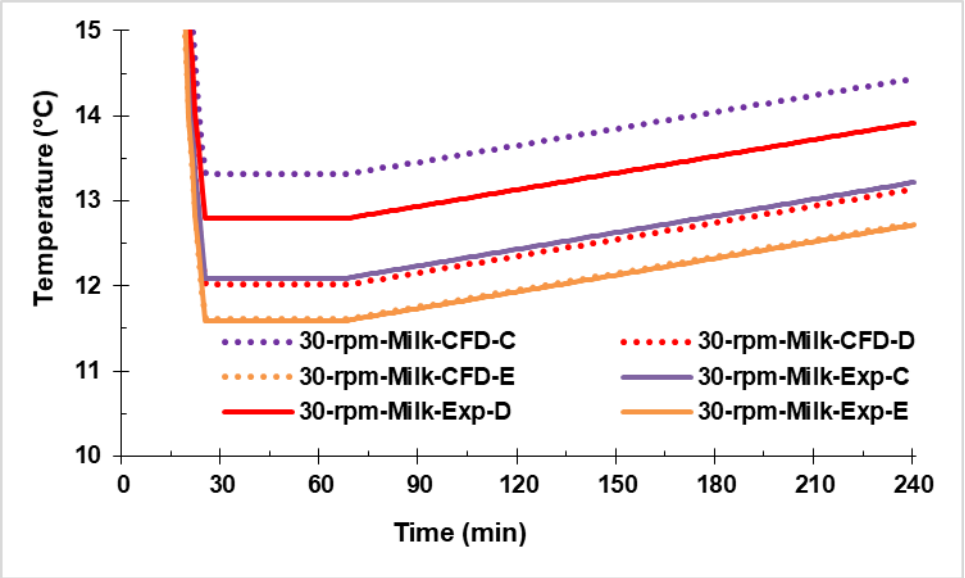

(b) Temperature profiles of milk, chilled by 0.50%-TiO_2-NePCM, at 'C', 'D' and 'E' at 30 rpm.

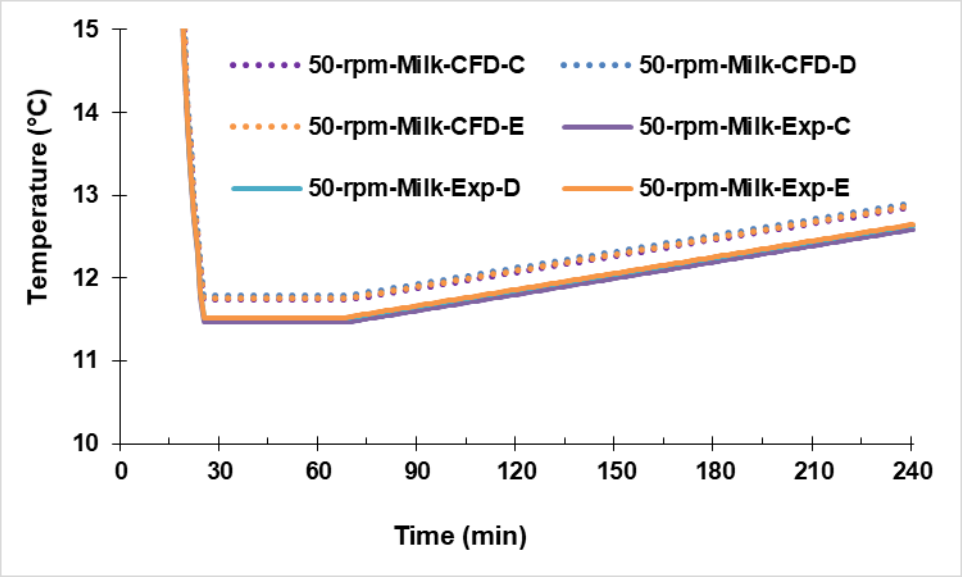

(c) Temperature profiles of milk, chilled by 0.50%-TiO_2-NePCM, at 'C', 'D' and 'E' at 50 rpm.

Fig. 4.30 (a-c) CFD predicted and experimental transient temperature profiles of 0.50%-NePCM at 'A' and 'B'; and of milk being chilled at 'C', 'D' and 'E' at different agitator speeds

4.4.1.4 Temperature field and liquid fraction contours during discharging and passive milk chilling

Table 4.10, elaborates on CFD modeled transient temperature field (T,°C) and liquid fractions (β) contours of the NePCM (at 0.50 % TiO_2) during discharging and consequent passive milk chilling at 30 and 50 rpm.

The effects of increasing rpm of agitator on discharging rates of NePCM as well as milk chilling rates are evident from the temperature and liquid fraction contours plots. It was noticed in the T-contours that the NePCM (initially at pre-charged temperatures) located inside the jacket of the module (indicated by deep bluish bands) was discharged (indicated by diminishing blue bands) as the time progressed. But, the rate of diminishing of this band were faster at 50 rpm as compared to that at 30 rpm. The hotter volume of milk (initially at around milking temperature, 37°C) indicated by reddish zone, was slowly diminishing towards the center of the module, as cooling progressed. The various intermediate temperature zones inside the module were indicated by intermediary color bands such as yellow, light greenish, light bluish etc., indicating reduction in milk temperature.

The effects of agitation and subsequent uniformity in temperature distributions of milk were more evident and faster at 50 rpm as compare to that at 30 rpm. The differences in

temperatures at points 'C', 'D' and 'E', were clearly visible in the contours at 30 rpm, since top to bottom mixing was poor. But these differences were almost nullified at 50 rpm due to well mixing and uniform top to bottom temperature distribution. The overall discharging as well as milk cooling rates were quite faster at 50 rpm as compared to same at 30 rpm, as visualized in the T-contours. At the end of t = 180 min, clear differences in NePCM as well as milk temperatures at 30 and 50 rpm can be detectible by the color bands. Heat exchanging rates at the cells of the virtual domain located between the parallel vertical walls of the jacket (near point 'A') were higher than those at the corners (point 'B'), therefore 'B' remained colder spot as compared to 'A'.

Table 4.10 CFD modeled transient temperature field (T,°C) and liquid fractions (β) contours of the NePCM (at 0.50 % TiO_2) during discharging and that of passive milk cooling at 30 and 50 rpm of agitation

Time (min)		30	60	90	120	150	180
T (°C)	30 rpm	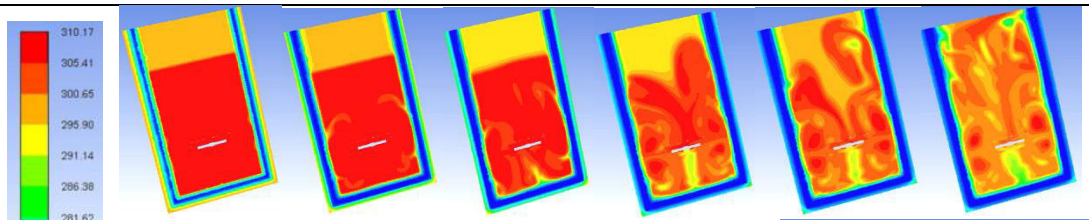					
	50 rpm	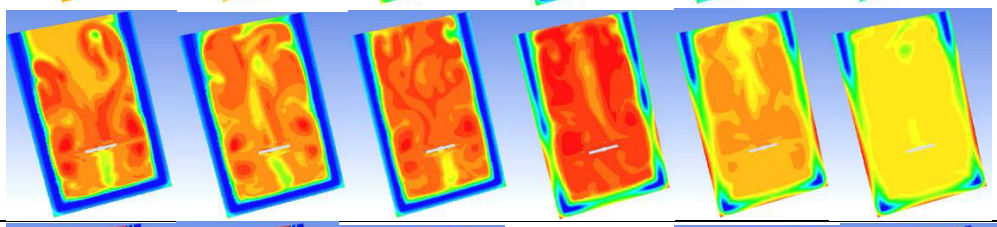					
β	30 rpm	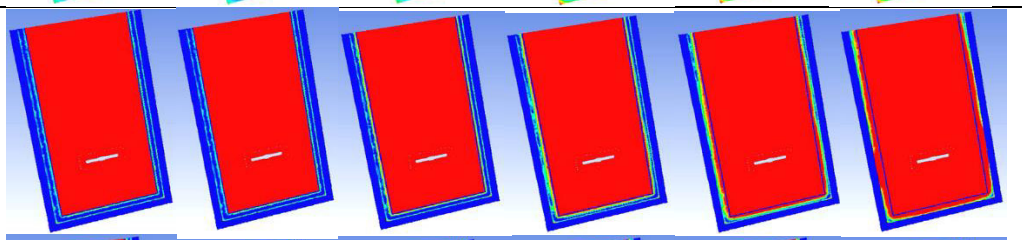					
	50 rpm	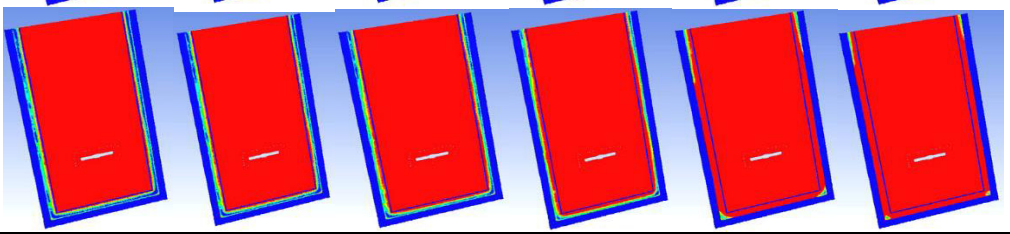					

β-contours indicated rate of melting of the NePCM inside the module from completely solid (β=0, indicated by deep bluish bands) to mixture (solid+liquid: 0<β<1; indicated by light green yellow, reddish and light blue bands), to completely liquid (β=1, indicated by

red bands). Instantaneous liquid fractions varied as per the temperatures rising zones inside the domain. The discharging rates (changing of β) of NePCM were higher at 50 rpm as compared to that at 30 rpm, and the colder zones (i.e. corners) showed relatively slower rate of melting, (i.e. some solid fractions remained even up to the end of 180 min of discharging period recorded), than the readily heat exchanging zones near the parallel vertical walls (near 'A') of the container module in the present study.

4.4.1.5 Velocity field contours during agitation of chilled milk

Table 4.11, indicates the CFD modeled transient velocity fields (v, m/s) contours of the chilled milk by 0.50%-NePCM at 30 and 50 rpm agitation.

Table 4.11 CFD modeled transient velocity field (v, m/s) contours of chilled milk by 0.50%-NePCM at 30 and 50 rpm of agitation

Time (min)		30	60	90	120	150	180
V_v, (m/s)	30 rpm	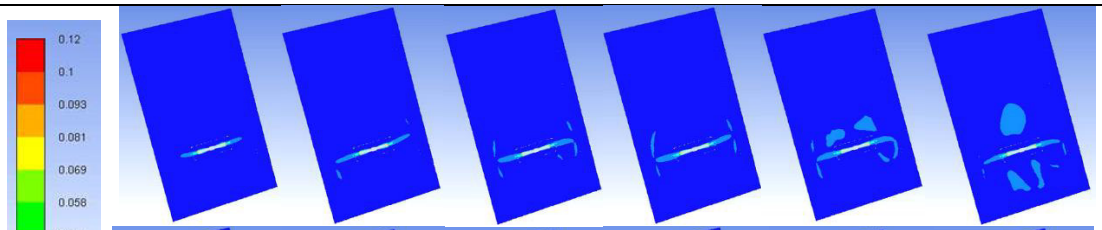					
	50 rpm	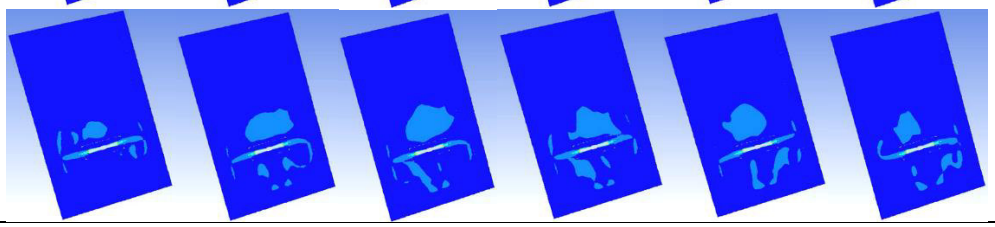					
V_h, (m/s)	30 rpm	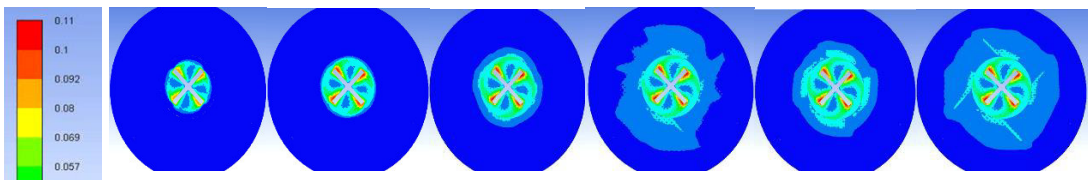					
	50 rpm	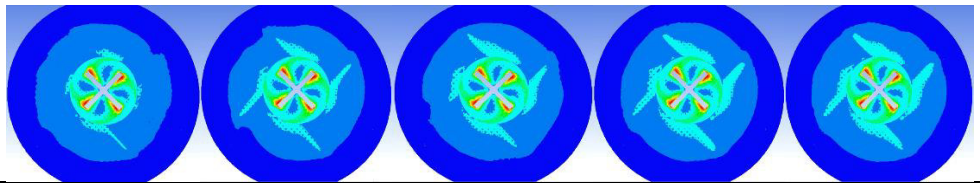					

v_v : velocity in vertical plane
v_h : velocity in horizontal plane

The top to bottom (v_v: velocity in vertical plane) and center to wall (v_h: velocity in horizontal plane) displacement of milk cell volumes with time, due to rotation of agitator, were visualized as shown in the table. It was observed that at 30 rpm, the milk flow rate

was at very slow, and therefore could not cover the entire domain of physical model under study so as to achieve the uniform convection throughout the milk volume. But, at 50 rpm, in both the cases either horizontal or vertical, the flow was fully developed and covered the entire domain to uniformly convect the cooling effect throughout the milk volumes. The similar trends were observed for a speed of agitator higher than 50 rpm (data not shown).

Table 4.12 CFD modeled transient velocity vector (v, m/s) contours of chilled milk by 0.50%-NePCM at 30 and 50 rpm of agitation

Time (min)		**60**	**120**	**180**
V_v, (m/s)	**30 rpm**	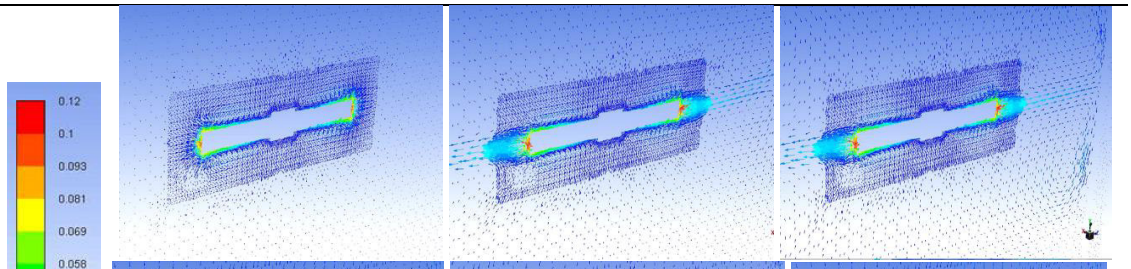		
	50 rpm	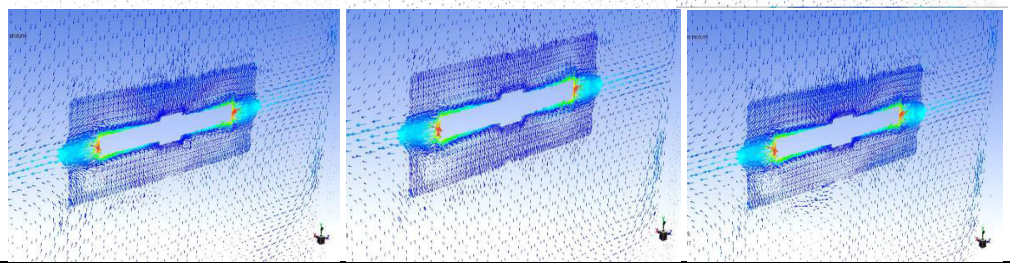		
V_h, (m/s)	**30 rpm**	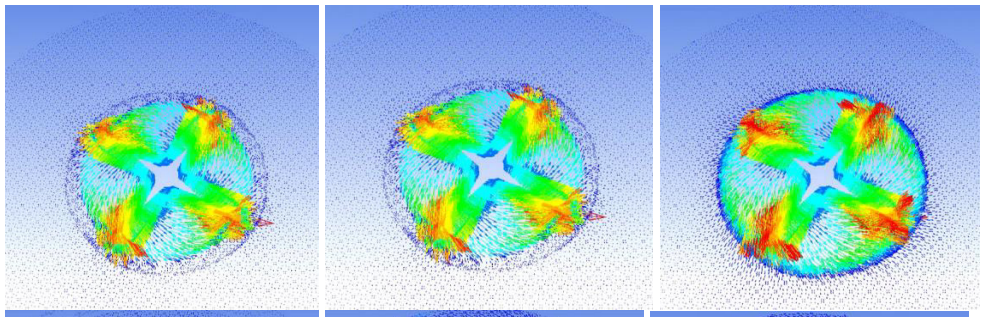		
	50 rpm	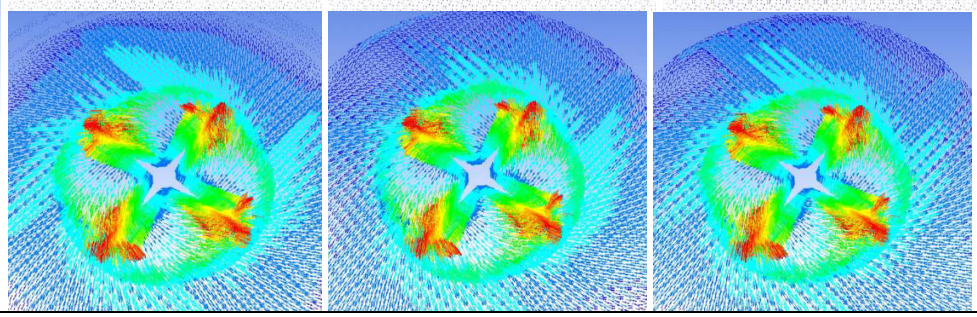		

v_v : velocity in vertical plane
v_h : velocity in horizontal plane

Table 4.12, indicates the CFD modeled transient velocity vectors (*v*, m/s) contours of the chilled milk by 0.50%-NePCM at 30 and 50 rpm of agitation. The velocity vectors clearly indicate the flow patterns in the regime at different rpms. At 30 rpm, the flow pattern either top to bottom (v_v: velocity in vertical plane) and center to wall (v_h: velocity in horizontal plane) were just disturbing the stationary frame (milk) but eddies were not observed. But, at 50 rpm, the flow pattern clearly indicated the top to bottom as well as side to center movement of milk volumes being agitated. The eddies with regular velocity patterns, formed due to reversal of flows from stationary walls and returned flows towards the center, as these are visualized in the contours at 50 rpm.

Therefore following points were inferred from testing of the NePCM into the jacketed cylindrical milking pail module with agitator:

- The percentage reductions in discharging time due to agitator speed were 3.81, 10.16, 13.98 and 17.79% at 30, 50, 70 and 100 rpm, respectively, as compared to control (0 rpm).
- Energy discharging process was expedited by both the factors viz. increased level of nanoparticles as well as the agitator speed.
- The synergic effects of agitator speed and level of nanoparticles indicated net reductions in discharging time up to 54.23%.
- The total energy exchange time for milk cooling was expedited by 8.00, 18.67, 25.33 and 30.67%, respectively at 30, 50, 70 and 100 rpm, as compared to control (0 rpm) at 1.00% of TiO_2 nanoparticles in NePCM.
- At any rpm below 30, the temperature distributions in chilled milk were not uniform, whereas the same turned uniform after an rpm equal to or above 50.

4.5 On-farm testing of performance of the milking pail module

4.5.1 Milk chilling performance

On-farm testing of the developed milking pail modular unit was conducted at Livestock Research Centre (LRC) of SRS of ICAR-NDRI, Bengaluru. Based on the studies conducted so far, two NePCMs were selected for on-farm testing viz. DW+1.00% TiO_2 (read as NePCM1, henceforth) and DW+AgNP+1.00% TiO_2 (read as NePCM2, henceforth).

Fig. 4.31, indicated the temperature profile (mean of 3 replications) of milk chilled in the developed pail using NePCM1 and NePCM2. It was observed that fresh raw milk was

passively chilled from milking temperature (37±1°C) to below 10°C (critical limit for milk quality) in about average 30-40 minutes. It was also observed that NePCM2 performed better as compared to NePCM1 for milk chilling performance. The chilled milk temperature was maintained below the critical limit inside the developed pail for at least 4h counted since milking. After directly milking the adequate (4.5-5L) quantity of milk, the container was kept inside a BOD incubator, at fixed temperature 40°C, to simulate summer field conditions inside the laboratory. The key precautions should be undertaken to close the lid quickly after milking and not to leave the charged container just open in idle state for any fraction of time. This may allow heat gain from atmosphere and cause losses of stored cooling energy from the pail.

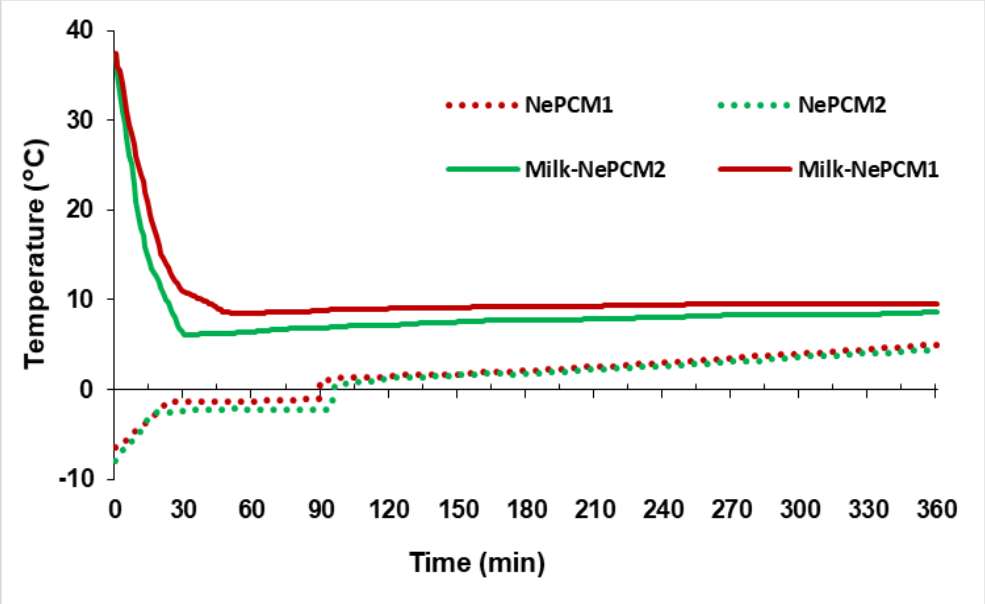

Fig. 4.31 On-farm milk chilling performance of NePCM

4.5.2 Thermal Cyclic Performance of the NePCM

Fig. 4.32a-b, indicated the temperature profiles of milk chilled by NePCM2 in subsequent thermal cycles of charging and discharging. It also indicated the variation of PCM temperature profiles with time after n^{th} ($0 \leq n \leq 1000$) cycle of charging and discharging.

It was observed that the developed PCM was thermally stable, having temperature profiles varied within ±1°C in due to charging and discharging cyclic effects studied up to 1000 cycles.

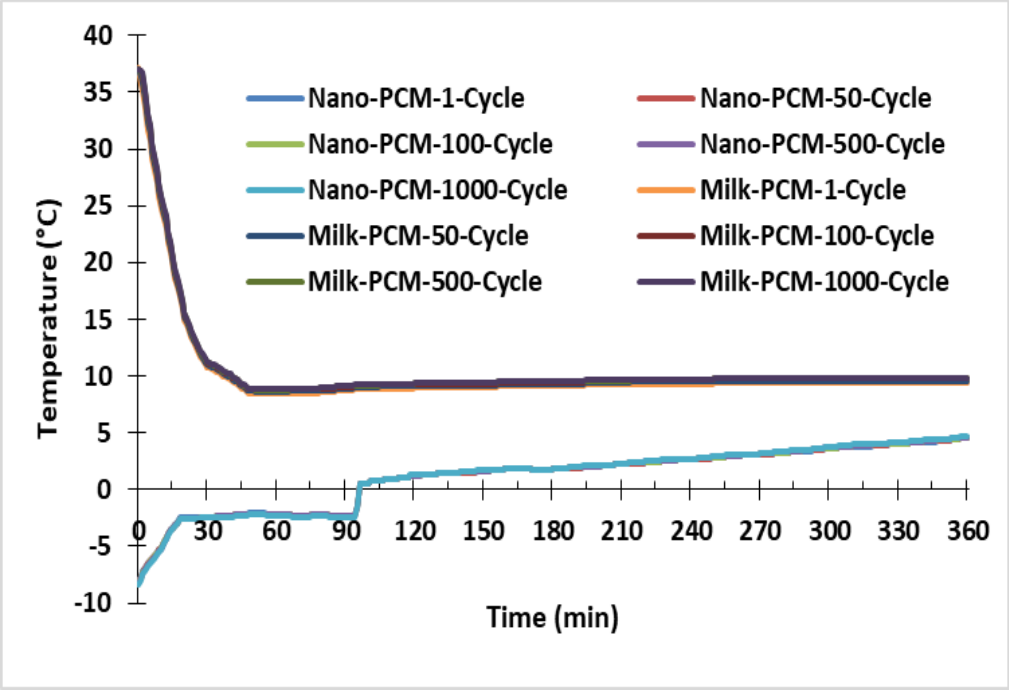

(a) Thermal cyclic test of NePCM2 (for entire range)

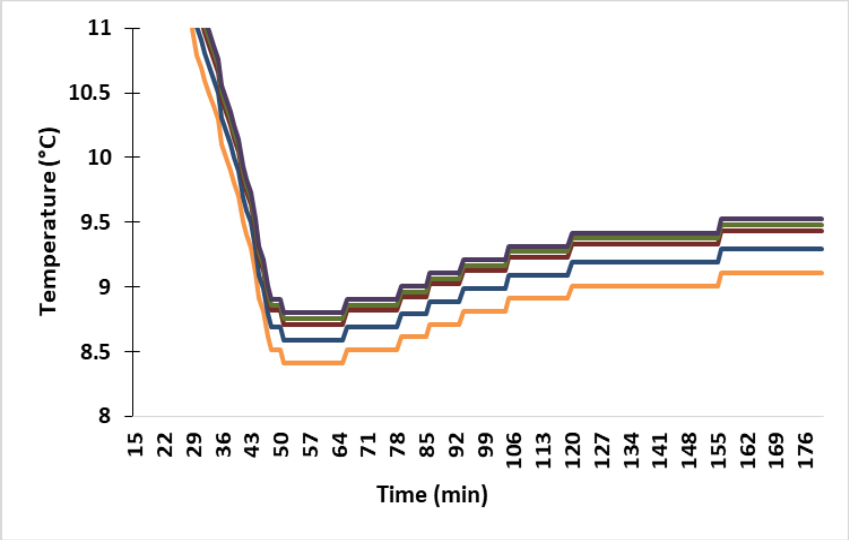

(b) Exploded view of milk chilling curves

Fig. 4.32 (a-b) Thermal cyclic performance of NePCM2

4.5.3 Co-efficient of performance (COP) of the charger unit of the developed milking pail unit

Fig. 4.33, indicate COP, units of electricity consumed (kWh), and refrigeration effect gained (energy stored in the PCM) per unit time, of the refrigeration cum charger unit of developed milking pail operated for 10h. It was observed that COP ranged from 1.9 to 2.4 kWh consumed in subsequent hours of operation ranged from 0.28 to 0.22. It was noticed that in the beginning of operation, the COP was less, improved slowly up to 1 to 2h and remained constant till 10h. It was because the kWh consumed for charging same amount

of PCM in the first pails were higher than that in the subsequent pails, since the charger took some time to equalize the effect.

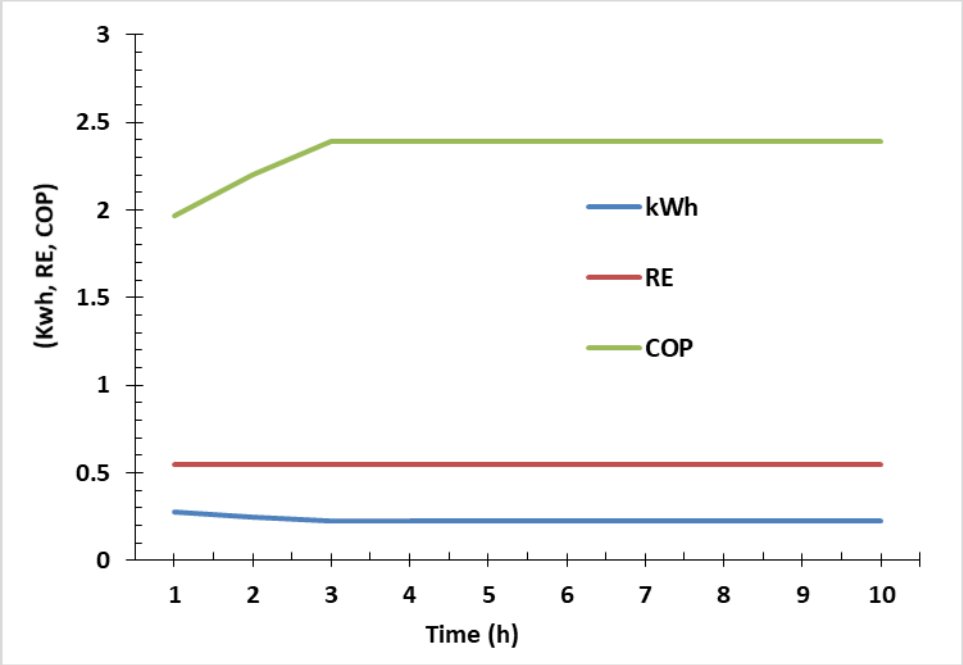

Fig. 4.33 COP, kWh and RE of the charger unit for the milking pail module

4.5.4 Quality evaluation of chilled milk

Milk qualities in terms of methylene blue dye reduction time (MBRT), total bacterial counts (TBC), pH and titratable acidity (TA) were evaluated for raw milk cooled by the developed milking pail modules, as well as of control (raw milk kept in an ordinary milk pail for 6h at ambient temperature 40°C, after milking). Before, taking samples for microbiological analysis, it was ensured that the animal milked was healthy (particularly free from mastitis) as well as containers were pre-sterilized.

Fig. 4.34a-b, indicate TBC and MBRT of control and chilled milk by the developed milk chilling pail. It was observed that the effects due to chilling milk immediately after production, and subsequent storing it inside the developed pail (at below the safe temperature), on raw milk quality, were significant as compared to the control. The differences in TBC and MBRT between control and chilled milk samples were in order of 2-3 log cycles and 3-4.5h respectively.

The pH values of chilled milk were 6.66-6.67 and that of control after 6h were 6.20 to 6.25. The differences in TA were observed in ranges of ±0.055. The TA of chilled milk

were in the range of 0.12 to 0.14% of lactic acid (LA) and that of control (after 6h) were 0.18 to 0.19% of LA.The microbiological and chemical analysis of milk chilled and stored in the developed pails indicated very good quality preservation of raw milk after harvesting.

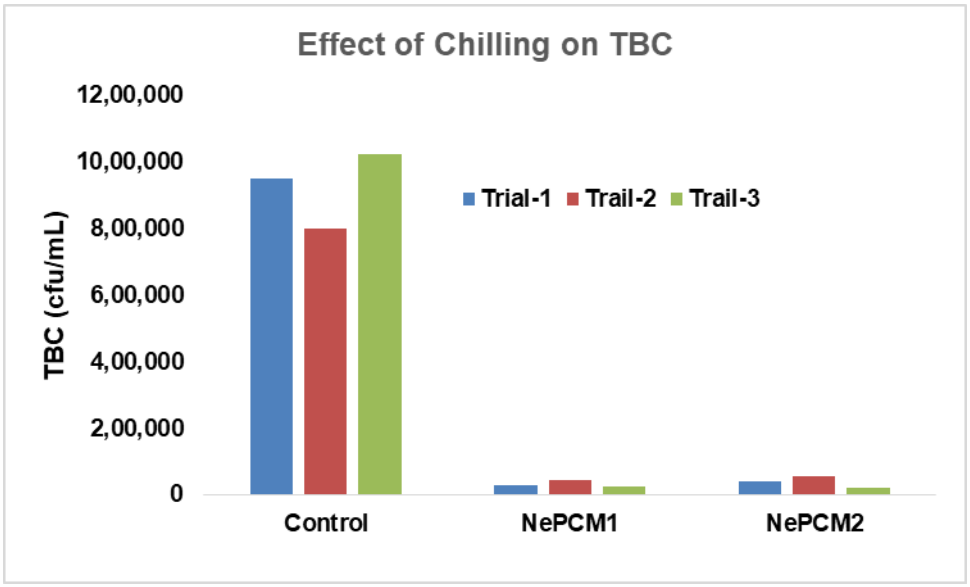

(a)

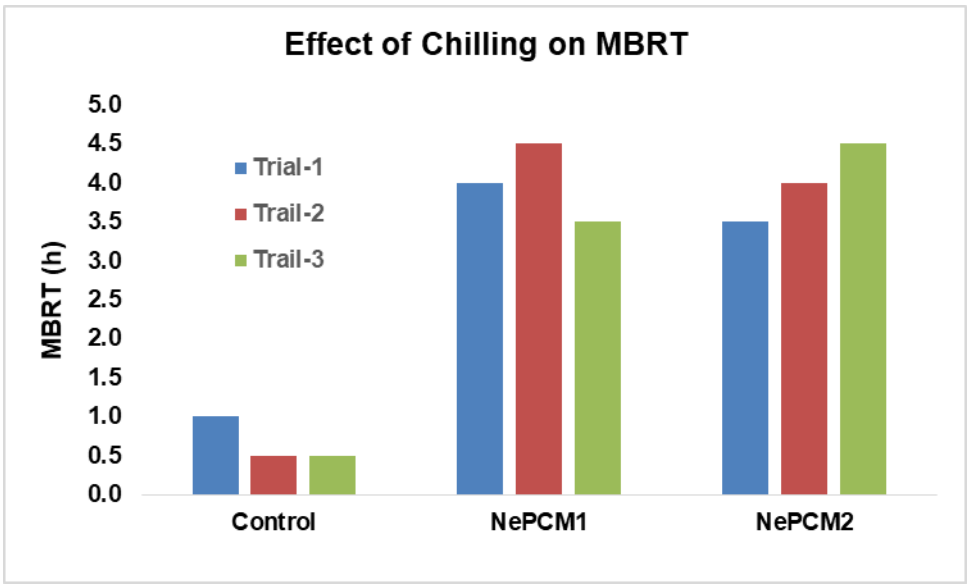

(b)

Fig. 4.34(a-b), Effect of chilling and storing fresh raw milk inside the milking pail module on **(a)** TBC; **(b)** MBRT

CHAPTER-5

SUMMARY AND CONCLUSION

Milk at its drawing temperature (37°C) serves as an ideal substrate for microbial growth and chemical deterioration. Such deteriorative reactions follow first order kinetics, in which rate of reaction depends directly on total microbial count at a particular instant, which increases logarithmically above the critical temperature (10°C). Therefore, it is imperative to immediately cool milk from 37 to below 10°C in order to preserve the safety and quality of fresh raw milk and thereby, its derived products. In developed and large-scale commercial dairy enterprise, this critical step to bring down temperature below the limit in post-production processing of milk is achieved by integrating the milking machine with chilling unit accessorized with suitable piping and storage tanks. However, in a country like India, where most of the dairy farmers belong to a class of millions of scattered small scale producers (0.5-10L per head; ≈ 17 million registered dairy farmers across 1,90,516 dairy cooperative societies in India (NDDB, 2019-20)), such sophistications remained impractical and uneconomical at the field level. It is to be emphasized that it is the major contribution of these small to marginal dairy farmers (70-80%) whose pooled efforts brought India to achieve its status as the world leading producer of milk (198.4 MT, NDDB, 2020).

Presently, the individual farmers pool their milk at a village or society level wherein it is cooled using chilling units or bulk milk coolers. Such interventions are useful for larger volumes of milk (minimum of 500L) and takes at least 3-4h to cool the raw milk below critical limit. The dairy industry faces huge loss in terms of product quality and almost 3% of total milk pooled at various dairies across the country wasted annually (IBEF, 2019), particularly due to poor cold-chain facilities and larger time gap (practically 5-6h) between point of production and cooling of milk below critical limit.

Over the years, several approaches and cooling systems viz., hydro-vac cooler, surface cooler, sprinkler cooler, tub cooler, mechanical cooler, ice bank coolers, bulk milk coolers, refrigerated tank cooling, cooling rings, ice cones, instant chillers, churn cooling, direct expansion cooling and rural-air-cum-milk-can-cooler have been developed to cool and/or chill fresh raw milk, but they are not very practical and economical for small and scattered production of milk.

Therefore, a need to develop a system/device that could instantly cool small volumes of milk at the on-farm level, preferably simultaneous to the milking process, was realized. This work was aimed at addressing the issue by developing a phase change material (PCM) based milking cum cooling pail to be used at the farm level/by individual farmer to cool milk from its drawing temperature to below 10°C immediately after milking.

Under these considerations, the present study was proposed with the following objectives:

1. To evaluate and select suitable phase change material for rapid cooling of milk.
2. To design and fabricate a milking cum cooling pail based on selected phase change material.
3. To evaluate the performance of the developed pail.

The developed unit intended for milk cooling is in the shape of an ordinary milking pail commonly used by farmers, a jacketed vessel design made of stainless steel 304 (SS 304), filled with developed PCM into the jacket adequately and appropriately. The entire unit is housed by a detachable and matching shape insulated container to avoid heat gain from surrounding. A de-attachable refrigeration cum charger unit for re-charging the milking pails was also designed and developed. Different base fluids viz., distilled water (DW), distilled water+propylene glycol (DW+PG), distilled water+ethylene glycol (DW+EG) and distilled water+silver nano-ionic solution (DW+AgNP) were used as dispersing media for TiO_2, CeO_2 and Si_3N_4 nanoparticles during PCM formulation.

The developed base fluids and PCMs were tested for thermo-physical, charging, discharging and milk cooling behavior to arrive best base fluids and nanoparticle combination and composition. The selected nanoparticle enhanced PCM (NePCM) were preliminary tested in a spherical shaped enclosure and then filled into the jackets of the cylindrical container. The developed units were tested for on farm milk cooling performance at Livestock Research Centre (LRC) of SRS, ICAR-NDRI, Bengaluru. The milk cooling performance was reported in terms of net temperature drop, rapidity of milk cooling, methylene blue dye reduction time (MBRT), total bacterial counts (TBC), pH and titratable acidity.

Based on thermal property analysis of base fluids and NePCM, the following points could be inferred:

- Thermal conductivity of base fluids: DW+AgNP > DW > DW+EG > DW+PG.
- Thermal conductivity enhancements by nanoparticles in a given base fluid: TiO_2 > CeO_2 > Si_3N_4.
- Saturation in 'k' enhancements due to rise in temperature : 0 to 30°C : negligible; 30-40°C: significant
- Saturation in 'k' enhancements due to rise in weight fraction of nanoparticles: 0 to 0.25%: negligible; 0.25 to 0.50%: moderate, 0.50 to 1.00%: significant.
- 1.00% weight fraction of nanoparticles exhibited maximum enhancement in 'k'.

The morphological analysis with SEM, revealed the dispersion pattern and mechanisms behind thermal property enhancements due to nanoparticles at different levels.

Zeta-potential analysis confirmed the order of dispersion stability of NePCM as follows:

(DW+AgNP+1.00 % TiO_2) > (DW+EG+1.00 % TiO_2) > (DW+PG+1.00 % TiO_2) > (DW+1.00 % TiO_2)

The following points were inferred from testing of the NePCM into the spherical module:

- CFD simulations revealed formation of a temporal thermal stratification in the chilled milk layers due to temperature variations in cuboidal geometry of milk vessel.
- The net phase-transition time were reduced by 5.83, 10.51, 16.90, 25.85 and 32.22% during charging, and 7.91, 12.55, 16.05, 20.11 and 24.32% during discharging, whereas total time required for milk chilling from 37 to below 10°C were speeded-up by 6.71, 16.78, 29.35, 35.65 and 42.44% at 0.05, 0.25, 0.50, 0.75 and 1.00% TiO_2 nanoparticles in DW, respectively.
- Use of nanoparticles significantly influenced the reduction in supercooling degree of the base fluid, however the effects due to saturations at higher weight fractions of nanoparticles were also observed.

The following points were inferred from testing the NePCM into the jacketed cylindrical milking pail module:

- CFD simulations validated with experiments revealed the existence of relatively hotter and colder points in the module during milk chilling.
- Net reductions in total charging time were 9.09, 16.36 and 22.72% at 0.20, 0.40 and 0.60% of TiO_2 nanoparticles as compared to the base fluid.
- The final temperatures reached by a PCM at the end of charging were significantly influenced by level of nanoparticles i.e. -1.2, -1.8, -3.1, -5.0°C at 0.00, 0.20, 0.40 and 0.60% nanoparticles, respectively.
- The charging, discharging and milk chilling rates were quite faster with NePCM having 0.60% TiO_2, as compared to 0.00% TiO_2 NePCM.
- Percentage reductions in discharging time were 8.51, 33.6 and 42.9% at 0.20, 0.40 and 0.60% TiO_2 nanoparticles.

The following points were inferred from testing the NePCM into the jacketed cylindrical milking pail module with agitator:

- The percentage reductions in discharging time due to agitator speed were 3.81, 10.16, 13.98 and 17.79% at 30, 50, 70 and 100 rpm, respectively, as compared to control (0 rpm).
- Energy discharging process was expedited by both the factors viz. increased level of nanoparticles as well as the agitator speed.
- The synergic effects of agitator speed and level of nanoparticles indicated net reductions in discharging time up to 54.23%.
- The total energy exchange time for milk cooling was expedited by 8.00, 18.67, 25.33 and 30.67%, respectively at 30, 50, 70 and 100 rpm, as compared to control (0 rpm) at 1.00% of TiO_2 nanoparticles in NePCM.
- At any rpm below 30, the temperature distributions in chilled milk were not uniform, whereas the same turned uniform after an rpm equal to or above 50.

The following conclusions were drawn based the results obtained during the study

- A two-step protocol was standardised to prepare nanoparticle enhanced PCMs using ultra-sonication of the selected base fluid and nanoparticles.
- TiO_2 at 1.00% by *wt.* was observed to perform better than CeO_2 and Si_3N_4, while DW+AgNP performed better than DW and DW + EG/PG as the base fluid, in terms of the thermal properties and stability of the NePCMs.
- The physical domain of the developed milking cum cooling pail was successfully translated in to a meshed computational domain using Ansys-ICEM-CFD ver. 19.0.
- The performance of the developed pail was simulated, using pressure based solver for transient, gravity-enabled, laminar, incompressible and three-dimensional multiphase model, to describe the temperature profile of the raw milk and PCM in the pail.
- Experimental validation of the simulated results depicted a close agreement confirming the robustness of the simulation.
- A milking cum cooling pail based on developed PCM was successfully designed, fabricated and tested to cool milk from 37 to below 10°C in 30-40 min.
- The PCM in the developed pail maintained the chilled temperature of the raw milk for at least 4h when exposed to an environmental temperature of 40°C.
- The quality of the milk chilled and stored in the developed pail was better than conventional milking pail/storage vessel in terms of its microbial count and MBRT.
- The PCM formulated with enhanced thermal performances assimilated into the developed milking cum cooling pail efficiently cooled fresh raw milk from the point of production to below the critical temperature, which could help preserve the quality of the raw milk in the primary tier of the supply chain.

SUGGESTIONS FOR FUTURE RESEARCH WORK

1. Further investigations may be taken up to enhance the energy efficiency, convenience and ergonomic features of the present design of modular milking cum cooling pails to be more adaptable by milk farmers.

2. Possible investigation on enhancing energy storability, thermal and dispersion stability, and chilling performance may be explored.

3. Scope of integrating the developed units with renewable energy resources could be a step towards sustainability in rural areas of developing nations.

4. Scope of deploying a community set-up for charging the multiple pails at a central place in villages may reduce the electricity/energy cost for milk chilling.

BIBLIOGRAPHY

Andersen K. (1970). Refrigerated tanks on dairy farm. XVIII International Dairy Congress. 1E: 654. (Cited in Dairy Science. Abstract, **32** (11): 4712).

Anonymous (2009) Fact sheet. United States environment protection agency, DC, USA. pp: 1-4.

ANSYS (2013). Fluent Theory Guide, 15.0, ANSYS, Inc., 2013, Ch.2, Flows with Moving Reference Frames, pages 17-32.

ANSYS (2015). Fluent Theory Guide, 15.0, ANSYS, Inc., 2015.

Arias J. and Lundqvist P. (2005). Modelling supermarkets energy usage. IIF/IIR, Commercial Refrigeration, Vicenza.

Badoo N.R. (2008). Stainless steel in construction: a review of research, applications, challenges and opportunities. Journal of Constructional Steel Research **64**(11):1199-1206. doi: 10.1016/j.jcsr.2008.07.011.

Bailey A. E. (1950). Melting and Solidification of Fats. New York USA, Wiley Interscience.

Barba A., Spiga M. (2003). Discharge mode for encapsulated PCMs in storage tanks. Solar Energy, **74**(2), 141-148.

Bhavadasan M.K., Abraham M.J. and Ganguli N.C. (1982). Influence of Agitation on Milk Lipolysis and Release of Membrane-Bound Xanthine Oxidase, Journal of Dairy Science, **65**(9):1692-1695.

Bi S., Shi L. and Zhang L. (2008) Application of nanoparticles in domestic refrigerators. Applied Thermal Engineering, **28**, 1834–1843.

Cabaleiro D., Gracia-Fernández C., Legido J.L. and Lugo L. (2015). Specific heat of metal oxide nanofluids at high concentrations for heat transfer. International Journal of Heat and Mass Transfer. **88**:872–79.

Cabeza L. F., Gutierrez A., Barreneche C., Ushak S., Fernandez, A. G., Fernádez, A. I., Grágeda M. (2015). Lithium in Thermal Energy Storage: A State-of-the-art Review. Renewable and Sustainable Energy Reviews, **42**, 1106-1112.

Charbgoo F., Ahmad M. B. and Darroudi M. (2017). Cerium oxide nanoparticles: green synthesis and biological applications. International Journal of Nanomedicine, **12**: 1401–1413.

Chew T.S., Daik R. and Hamid M.A. Abdul. (2015). Thermal conductivity and specific Heat capacity of Dodecylbenzenesulfonic acid-doped polyaniline particles—water based nanofluid. Polymers. **7**: 1221-1231.

Chieruzzi M., Gian F.C., Miliozzi A. and Kenny J.M. (2013). Effect of nanoparticles on heat capacity of nanofluids based on molten salts as PCM for thermal energy storage. Nanoscale Research Letters. **8**:448.

Colton J.S., Suh N.P. (1987). The nucleation of microcellular thermoplastic foam with additives: Part II: Experimental results and discussion, Polymer Engineering and Science, **27**: 493-9.

Conde M.R. (2004). Properties of aqueous solutions of lithium and calcium chlorides: formulations for use in air conditioning equipment design, International Journal of Thermal Sciences, **43**:367-383.

Dabas J.K., Dodeja A.K., Kumar S. and Kasana K.S. (2011) Performance characteristics of "Vapour Compression Refrigeration System" under real transient conditions. **2** (4): 584-593.

Darshan G.B. (2015). Design and development of eutectic module for raw milk cooling. M. Tech. Thesis, submitted to SRS of ICAR-NDRI, Bengaluru.

Deeth H.C. and Fitz-Gerald H.C. (1977). Effects of mechanical agitation of raw milk on the milk-fat globule in relation to the level of induced lipolysis, Journal of Dairy Research, **44,** 569-583.

Demirbas M. F. (2006). Thermal Energy Storage and Phase Change Materials: An Overview. Energy Sources Part B, **1**: 85-95.

Dincer I. and Rosen M. A. (2002). Thermal Energy Storage: Systems and Applications. Chichester, England, Wiley.

El-Dessouky H. and Al-Juwayhel F. (1997). Effectiveness of a Thermal Energy Storage System using Phase-Change-Materials. Energy Conversion and Management, **38**: 601-617.

FAO (1989), cited from http://www.fao.org/docrep/006/y5013e/y5013e08.htm.

Fedele L., Colla L. and Bobbo S. (2012). Viscosity and thermal conductivity measurements of water-based nanofluids containing titanium oxide nanoparticles. International Journal of Refrigeration. **35**(5):1359–66.

Feldman D., Shapiro M. M., Banu D. and Fuck C. J. (1989). Fatty Acids and Their Mixtures as Phase Change Materials for Thermal Energy Storage. Solar Energy Materials, **18**: 201-216.

Ferrer G., Sole A., Barreneche C., Martorell I. and Cabeza L. F. (2015). Review on Methodology Used in Thermal Stability Characterization of Phase Change Materials. Renewable and Sustainable Energy Reviews, **50:** 665-685.

FICCI, (2020). FICCI Paper on Development of Dairy Sector in India, July 2020.

Flejtuch K. (2004). Badnie Przemian Fazowych Ukladow Polieterow Pod Katem Akumulacji Energii Cieplnej. *PhD Thesis,* Cracow University of Technology, Cracow.

Fox P.F., Uniacke-Lowe T., McSweeney P.L.H., O'Mahony J.A. (2015). Physical Properties of Milk. In: Dairy Chemistry and Biochemistry. Springer, Cham. https://doi.org/10.1007/978-3-319-14892-2_8.

Gamble J A. (1918). Cooling milk and cream on the farm. U.S. Department of agricultural farmers, Bulletin – 976.

Granryd E. and Melinder Å. (2005). Secondary refrigerants for indirect systems. Refrigerating Engineering, Granryd, KTH, Stockholm. **6**: 2-6.

Gunther R.C. (1957). Refrigeration air conditioning and cold storage, ch.13, pp.767.

Harikrishnan S., Magesh S., Kalaiselvam. (2013). Preparation and thermal energy storage behaviour of stearic acid-TiO_2 nanofluid as a Phase change material for solar heating system. Thermochmica Acta, **565:** 137-145.

He B., Gustafsson E. M., Setterwall F. (1999). Tetradecane and Hexadecane Binary Mixture as Phase Change Materials (PCMs) for Cool Storage in District Cooling System. Energy, **24**: 1015-1028.

Heckenkamp J. and Baumann, H. (1997). Sonderdruck aus Nachrichten. Latent Warme Speicher, **11**: 1075-1081.

Hegde V., Bhattacharya A., Srikari S. (2014). Design of mobile raw milk chilling unit for rural areas. SAS Tech Journal. **13**(1): 31-38.

Hesaraki A., Holmberg S. and Haghighat F. (2015). Seasonal Thermal Storage with Heat Pumps and Low Temperature in Building Projects-A Comparative Review. Renewable and Sustainable Energy Reviews, **43:** 1199-1213.

Hillerns F. (2001). Thermophysical properties and corrosion behavior of secondary coolants. ASHRAE winter meeting, seminar 19 – secondary fluids and systems, Atlanta, GA, Jan 27-31.

Holman J. D. Experimental methods for engineers, 5th ed. New York, McGrow-Hill; 1989.

IBEF; https://www.ibef.org/blogs/digitalisation-of-india-s-dairy-farming.

International Stainless Steel Forum. (2010). Stainless Steel in the Dairy Industry: A Sustainable Solution for Human Diet. pp 3-6.

Iten M. and Liu S. A. (2014). Work Procedure of Utilizing PCMs as Thermal Storage Systems Based on Air-TES Systems. Energy Conversion and Management, **77**: 608-627.

Jamotte P. (1968). Refrigerated cooling of milk on the farm. Publs Stnlait. Etat, Gembloux.**3** 34pp. (Cited in Dairy Science, Abstract, **32** (4): 1509).

Jiang W., Ding G. and Peng H. (2009) Measurement and model on thermal conductivities of carbon nanotube nanorefrigerants. International Journal of Thermal Sciences, **48**: 1108–1115.

Johnston J. H., Grindrod J. E., Dodds M., Schimitschek K. (2008). Composite Nano-structured Calcium Silicate Phase Change Materials for Thermal Buffering in Food Packaging. Current Applied Physics, **8** (3-4): 508-511.

Karakoti A.S., Munusamy P., Hostetler K., Kodali V., Kuchibhatla S., Orr G., Pounds J. G., Teeguarden G., Thrall B. D., Baer D. R. (2012). Preparation and characterization challenges to understanding environmental and biological impacts of Ceria nanoparticles, Surface and Interface Analysis. **44**:882– 889.

Keles S., Kaygusuz K., Sari A. (2005). Lauric and Myristic Acids Eutectic Mixture as Phase Change Materials for Low-Temperature Heating Applications. International Journal of Energy Research, **29**: 857-870.

Keyvani M., Afrand M., Toghraie D. and Reiszadeh M. (2018). An experimental study on the thermal conductivity of cerium oxide/ethylene glycol nanofluid: developing

a new correlation, Journal of Molecular Liquids, doi:10.1016/ j.molliq.2018.06.010.

Khanafer K. and Vafai K. (2011). A critical synthesis of thermophysical characteristics of nanofluids. International Journal of Heat and Mass Transfer, **54**(19–20):4410–4428.

Khudhair A. M. and Farid M. M. (2004). A Review on Energy Conservation in Building Applications with Thermal Storage by Latent Heat using Phase Change Materials. Energy Conversion and Management, **45**: 263-275.

Kim P., Shi L., Majumdar A. and McEuen P. L. (2001). Thermal transport measurements of individual multiwalled nanotubes. Physical Review Letters, 87(**21**): 5502–5514.

Kruse H. (2005). Commercial refrigeration–on the way to sustainability. IIF/IIR, Commercial refrigeration, Vicenza.**4**.

Kumar S.R. and Dodeja A.K. (2005). Development of intermittent vapour absorption refrigeration system for cooling milk, Indian Journal of Dairy Science, **58**(1): 17-22.

Kumaresan V., Chandrasekaran P., Nanda M., Maini A.K. and Velraj R. (2013) Role of PCM based nanofluids for energy efficient cool thermal storage system. International Journal of Refrigeration. **36:** 1641-47.

Lancaster T. (1983). Generalized residuals and heterogeneous duration models: the exponential case. Bulletin of Economic Research, **35**(2): 0307-3378.

Langtry R.B., Menter F.R., Likki S.R., Suzen Y.B., Huang P.G. and Völker S. (2006). A correlation-based transition model using local variables—Part II: Test cases and industrial applications. Journal of Turbomachinary. **128**:423-434.

Leducq D., Doye F.T. and Alvarez F.G. (2015). Phase Change Material for the Thermal Protection of Ice-cream during Storage and Transportation. 24ième Congrès International du Froid ICR, Yokohama, Japan. 6 p. ffhal-01548813f.

Liu Y. and Yang Y. (2017). Investigation of specific heat and latent heat enhancement in hydrate salt based TiO_2 nanofluid phase change material. Applied Thermal Engineering. **124**: 533-538.

Liu Y. D., Zhou Y.G., Tong M.W., Zhou X.S. (2009). Experimental Study of Thermal Conductivity and Phase Change Performance of Nanofluids PCMs. Microfluidics and Nanofluidics. **7**(4): 579–584.

Liu Y., Li Xin, Hu P. and Hu G. (2015). Study on the supercooling degree and nucleation behavior of water-based graphene oxide nanofluids PCM. International Journal of Refrigeration. **50**: 80-86.

Lu M.C. and Huang C. (2013). Specific heat capacity of molten salt-based alumina nanofluid. Nanoscale Research Letters. **8**:292.

Lu W. and Tassou S.A. (2013). Characterization and Experimental Investigation of Phase Change Materials for Chilled Food Refrigerated Cabinet Applications. Applied Energy, **112** (c): 1376–1382.

Lu Y. L., Zhang W. H., Yuan P., Xue M. D., Qua Z.G., Tao W.Q. (2010). Experimental Study of Heat Transfer Intensification by using a Novel Combined Shelf in Food Refrigerated Display Cabinets (Experimental Study of a Novel Cabinets). Applied Thermal Engineering, **30** (2-3): 85-91.

Lundqvist P.G. (2000). Recent refrigeration equipment trends in supermarkets: Energy efficiency as leading edge. The International Institute of Refrigeration, IIR, Paris.**5**.

Luo J. Y., Issa R. I., and Gosman A. D. (1994). Prediction of Impeller-Induced Flows in Mixing Vessels Using Multiple Frames of Reference. In IChemE Symposium Series. **136**: 549–556.

Mahajani and Joshi (2003). Process equipment design. Macmillan India Limited, First edition, New Delhi, India.

Majewski T. (1975) Effect of milking and storage conditions on psychrotrophic and mesophilic bacterium content in milk. Academiai Kiado, 453-456. (Cited in Dairy Science, Abstract, 1978, **40**: 5983).

Melinder Å. (1998). Thermophysical properties of liquid secondary refrigerants. A critical review on literature references and laboratory measurements, Tekn. Lic. Thesis. KTH, Stockholm.

Menter F.R., Langtry R.B., Likki S.R., Suzen Y.B., Huang P.G., Völker S. (2006). A correlation-based transition model using local variables — Part I: Model formulation. Journal of Turbomachinary. **128**:413-422.

Motahar S., Alemrajabi A.A. and Khodabandeh R. (2017). Experimental study on solidification process of a phase change material containing TiO_2 nanoparticle for thermal energy storage. Energy Conservation and Management. **138**: 162-70.

Mueller (1982). U.S. Patent No. 4, 351,271, issued Sep. 28, 1982.

Must E.I. (1969). Effect of cooling and handling of milk on the farm on its microflora. Moloch. Prom. **30** (8):36-37. (Cited in Dairy Science, Abstract, **32** (2): 735).

Nagano K., Mochida T., Takeda S., Domanski R., Rebow M. (2003). Thermal Characteristics of Manganese (II) Nitrate Hexahydrate as a Phase Change Material for Cooling Systems. Applied Thermal Engineering, **23**: 229-241.

NDDB (2019-20). Annual report, National Dairy Development Board, Anand, India.

NDDB (2020). Statistic of milk production of India, Department of Animal Husbandry Dairying and Fisheries, Ministry of Agriculture, Government of India. Cited from http://www.nddb.org/information/stats/milkprodindia.

Oro E., de Gracia A., Castell A., Farid M. M. and Cabeza L. F. (2012). Review on Phase Change Materials (PCMs) for Cold Thermal Energy Storage Applications. Applied Energy, **99** (c): 513–533.

Pantzali M. N., Mouza A. A., Paras S. V. (2009). Investigating the efficacy of nanofluids as coolants in plate heat exchangers (PHE). Chemical Engineering Science. **64**: 3290—3300.

Paris J., Falardeau M., Villeneuve C. (1993). Thermal Storage by Latent Heat: A Viable Option for Energy Conservation in Buildings. Energy Sources, **15**: 85-93.

Patankar S. V. (1980). Numerical Heat Transfer and Fluid Flow. Hemisphere, Washington, DC.

Peng S., Fuchs A. and Wirts R. (2004). Polymeric Phase Change Composites for Thermal Energy Storage. Journal of Applied Polymer Science, **93:** 1240-1251.

Perrella M., Meldrum R., Moos M. T. and Young I. (2017). The effectiveness of common methods of cold-holding on the temperature of milk. EHR Vol. **60** (4):98–103.

Perullini M., Sara A., Bilmes A. and Jobbágy M. (2013). R. Brayner (Eds.), Cerium Oxide Nanoparticles: Structure, Applications, Reactivity, and Eco-Toxicology. Nanomaterials: A Danger or a Promise?, DOI: 10.1007/978-1-4471-4213-3_12, Springer-Verlag London.

Pielichowski K. and Flejtuch K. (2003 A). Binary Blends of Polyethers with Fatty Acids: A Thermal Characterization of the Phase Transitions. Journal of Applied Polymer Science, **90:** 861-870.

Pielichowski K. and Flejtuch K. (2003 B). Differential Scanning Calorimetry Study of Blends of Poly (Ethylene Glycol) with Selected Fatty Acids. Macromolecular Materials and Engineering, **288:** 259-264.

Pielichowski K. and Flejtuch K. (2005). Recent Developments in Polymeric Phase Change Materials for Energy Storage: Poly (Ethylene Oxide)/Stearic Acid Blends. Polymers for Advanced Technologies, **16:** 127-133.

Pintaldi S., Perfumo C., Sethuvenkatraman S., White S. and Rosengarten G. (2015). A Review of Thermal Energy Storage Technologies and Control Approaches for Solar Cooling. Renewable and Sustainable Energy Reviews, **41**: 975-995.

Prakash R. (2016). Development of Nanofluid Based Cooling Module for Raw Milk Cooling. M.Tech. Thesis, Submitted to SRS, ICAR-NDRI, Bengaluru, India.

Prakash R., Ravindra M.R. (2021). Energy Storage using Phase Change Materials: Principles, Methods, Numerical Simulations, and Applications in Food Processing, Handbook of Research on Food Processing and Preservation Technologies, Apple Academic Press, FL, USA, **3** : 12-22.

Rasic J., Vujicic V. and Lazic P. (1968) Effect of farm cooling on bacteriological quality of milk. Mljekarstvo. **18** (10): 224-233.

Robberts J. and Larson G.H. (1941). Milk cooling on Kansas farms. Historical document of agricultural experiment station, Kansas state college of agriculture and applied science, Manhattan, Kansas. Bulletin-**295**:1-39.

Roy S. K. and Sengupta S. (1989). Melting of a free solid in a spherical enclosure: effects of subcooling. Journal of Solar Energy Engineering. **111**:32–36.

Roy S. K. and Sengupta S. (1990). Gravity-assisted melting in a spherical enclosure: effects of natural convection. International Journal of Heat and Mass Transfer **33**:1135–47.

Saidur R., Leong K.Y. and Mohammad H.A. (2011) A review on applications and challenges of nanofluids. Renewable and Sustainable Energy Review, **15**(3): 1646–1668.

Sari A. (2003). Thermal Characteristics of a Eutectic Mixture of Myristic and Palmitic Acids as Phase Change Materials for Heating Applications. Applied Thermal Engineering, **23**: 1005-1017.

Sari A. (2005). Eutectic Mixture of some Fatty Acids for Low Temperature Solar Heating Applications: Thermal Properties and Thermal Reliability. Applied Thermal Engineering, **25:** 2100-2107.

Sari A. and Karaipekli A. (2008). Preparation and Thermal Properties of Capric Acid/Palmitic Acid Eutectic Mixture as a Phase Change Energy Storage Material. Materials Letters, **62,** 903-906.

Sari A. and Kaygusuz K. (2002 A). Thermal and Heat Transfer Characteristics in a Latent Heat Storage System using Lauric Acid. Energy Conversion and Management, **43**: 2493-2507.

Sari A. and Kaygusuz K. (2002 B). Thermal Performance of a Eutectic Mixture of Lauric and Stearic Acids as PCM Encapsulated in the Annulus of Two Concentric Pipes. Solar Energy, **72:** 493-504.

Sattari H., Mohebbi A., Afsahi M.M. and Yancheshme A.A. (2016). CFD simulation of melting process of phase change materials (PCMs) in a spherical capsule, International Journal of Refrigeration, **73**:209-18.

Sharma A., Tyagi V. V., Chen C. R. and Buddhi D. (2009). Review on Thermal Energy Storage with Phase Change Materials and Applications. Renewable and Sustainable Energy Reviews, **13**: 318-345.

Shin D. and Banerjee D. (2010). Enhancement of specific heat capacity of high-temperature silica-nanofluids synthesized in alkali chloride salt eutectics for solar thermal-energy storage applications. International Journal of Heat and Mass Transfer. **54**: 1064–1070.

Spoorthy G.S. (2010). Development and performance evaluation of rural air-cum-milk can cooler. M. Tech. Thesis, IGKV Raipur.

Stenson J.P. (1970) Improved method and means for cooling milk. Br. Pat. **1** 196 291. (Cited in Dairy Science, Abstract, **32** (9): 3702).

Stinson G.E., Studman C.J. and Warburton D.J. (1987) The performance and economics of a dairy refrigeration heat recovery unit. Journal of Agricultural Engineering Research. **36**: 287-300.

Sult G. M. (1978). U.S. Patent. No. 4,130,996, issued Dec. 26, 1978.

Tan F.L. (2008). Constrained and unconstrained melting inside a sphere. International Communication in Heat and Mass Transfer. **35**:466–75.

Tan F.L., Hosseinizadeh S.F., Khodadadi J.M. and Fan L. (2009). Experimental and computational study of constrained melting of phase change materials (PCM) inside a spherical capsule. **52**: 3464–72.

Tatsidjodoung P., Le-Pierres N., Luo L. (2013). A Review of Potential Materials for Thermal Energy Storage in Building Applications. Renewable and Sustainable Energy Reviews, 2013, **18**: 327-349.

Vajjha R.S. and Das D.K. (2009). Specific heat measurement of three nanofluids and development of new correlations. Journal of Heat Transfer, **131**(7): 071601.

Vegter J.E., Brouwer J., Vries T. D. and Verheij C.P. (1969). Testing a refrigerated farm milk tank, manufactured by Holvrieka, Utrecht. Rapp. ned. Inst. Zuivelanderz.**78** 40 pp. (Cited in Dairy Sci., Abstract, **31** (5): 1803).

Vogelauer R. (1969). Test report on Alfa Laval Universal immersion cooler, type KJ 610 C. Milchw. Ber. Wolfpassing u. Rotholz, No. **21**: 85-86.(Cited in Dairy Sci., Abstract, **32** (5): 1959).

Voller V., Prakash C. (1987). A fixed grid numerical modeling methodology for convection-diffusion mushy region phase-change problems. International Journal of Heat and Mass Transfer, **30**:1709–19.

Volovirta I. and Vinha J. (2004). Water vapour permeability and thermal conductivity as a function of temperature and relative humidity. ASHARE, USA.

Wang B.X., Zhou, L.P. and Peng X.F. (2006). Surface and size effects on the specific heat capacity of nanoparticles. International Journal of Thermophysics, **27**(1): 139–151.

Wang X., Djakovica U., BaobJuan H. and Torresa F. (2021). Experimental evaluation of heat transfer performance under natural and forced convection around a phase change material encapsulated in various shapes. Sustainable Energy Technologies and Assessments. **44:** 101025.

Waqas A. and Ud-Din Z. (2013). Phase Change Material (PCM) Storage for Free Cooling of Buildings-A Review. Renewable and Sustainable Energy Reviews, **18:** 607-625.

Wilster G.H., Hoffmann H. and Price F.E. (1934). Comparative efficiency of farm milk coolers. Agricultural Experiment station, Oregon state agricultural college, Corvallis. Station Bulletin – **332**: 1-42.

Wu S., Zhu D., Zhang X., and Huang J. (2010). Preparation and melting/freezing characteristics of Cu/paraffin nanofluid as phase-change material (PCM). Energy and Fuels. **24**(3):1894–1898.

Yang L. and Hu Y. (2017). Toward TiO_2 nanofluid-part1: preparation and properties. Nanoscale Research Letters, **12**: 417-22.

Younsi Z. and Naji H. (2017). A numerical investigation of melting phase change process via the enthalpy-porosity approach: Application to hydrated salts. International Communications in Heat and Mass Transfer. **86:** 12-24.

Zeneli M., Nikolopoulos A., Karellas S. and Nikolopoulos N. (2021). Numerical methods for solid-liquid phase-change problems, in Ultra-High Temperature Thermal Energy Storage, Transfer and Conversion, 1 Elsevier Ltd., ch7, DOI: https://doi.org/10.1016/B978-0-12-819955-8.00007-7, pp 165-199.

Zhou L.P., Wang B., Xuan X.F., Xiao Z. and Yong P.Y. (2010). On the specific heat capacity of CuO nanofluid. Advances in Mechanical Engineering, Article ID 172085, **4** pages.

Zhou S. and Ni R. (2008). Measurement of the specific heat capacity of water-based Al_2O_3nanofluid. Applied physics letters. **92**(9): 3123.

Żyła G., Fal J., Bikić S. and Wanic M. (2018). Ethylene glycol based silicon nitride nanofluids: An experimental study on their thermophysical, electrical and optical properties, Physica E: Low-dimensional Systems and Nanostructures. doi: 10.1016/j.physe.2018.07.023.